Removal of NH_3 and H_2S from Biomass Gasification Producer Gas

---

A thesis submitted in fulfilment of the requirements for

the Degree of Doctor of Philosophy

in Chemical and Process Engineering

at the University of Canterbury

by Janjira Hongrapipat

University of Canterbury

2014

Table of Contents

List of Figures

List of Tables

Acknowledgments

First of all, I would like to express my deepest appreciation to my principal supervisor, Professor Shusheng Pang, for the scholarship in the PhD research in biomass gasification process given to me. This is a great opportunity as it is a subject in my dream that I would like to be part of. I would also like to thank him for his invaluable guidance and support throughout this journey.

I would like to thank to my supervisory team, Dr. Aaron Marshall, Dr. Alex Yip, and Dr Woei-Lean Saw, for their patience, motivation, and infightful guidance and comments.

I am thankful to all the technical staff at the Department of Chemical and Process Engineering, Leigh Richardson, Glenn Wilson, Tim Moore, Stephen Beuzenberg, Michael Sandridge, Tony Allen, Frank Weerts, and Stephen Hood. Without their support, my research would not go this far.

My sincere thanks also go to the technical staff at the other departments, to Rob McGregor from the Glass Workshop at the Department of Chemistry for building quartz reactors and fittings – whose assistance for the reactor setup is invaluable, and to Stephen Brown from the Department of Geological Science for the sand sample analysis.

Thanks to all of my friends from the Department of Chemical and Process Engineering and the other departments, as well as the friends outside the University, for the good time spent with me, especially Matthew Currie, Diandree Padayachee, and Nargess Puladian: to Matt for all the support and special time sharing with me, and to Diandree and Nargess, your friendship is very important to me.

Last but not least, I would like to thank my family, relatives, and friends back home for their love and everything they have done for me.

Abstract

Biomass gasification is a promising technology for conversion of various biomass feedstocks to producer gas for subsequent production of fuels and chemicals. A dual fluidised bed (DFB) steam gasifier is used in the present research to produce the producer gas for Fischer-Tropsch (FT) liquid fuel synthesis. However, NH_3 and H_2S gases in the producer gas remain an issue to be resolved because they are poisonous to the catalysts employed in the FT reactor. To remove NH_3 and H_2S, two methods were investigated in this research: (1) primary measures which were employed in the DFB steam gasifier including process optimisation and application of bed materials for catalytic NH_3 decomposition and H_2S adsorption; and (2) secondary measures or downstream cleaning methods after the gasifier. The combination of the primary measures and the secondary measures is an effective way to remove the NH_3 and H_2S in the producer gas from gasification process.

Studies on the primary measures were divided into two parts. In the first part, in situ reduction of NH_3 and H_2S in biomass producer gas from the DFB steam gasifier was performed. The primary measures consisted of optimisation of operation conditions and application of bed materials. The main operation conditions in the DFB steam gasifier studied were gasification temperature, steam to fuel (S/F) ratio, and mean gas residence time (τ_f). The bed materials tested include silica sand, iron sand (ilmenite), and calcined olivine sand. For the second part of the primary measures, an influence of the lignite to fuel (L/F) ratio on NH_3 and H_2S concentrations and conversions in co-gasification of blended lignite and wood pellets in the DFB steam gasifier was investigated. Experiments were performed in the DFB steam gasifier at 800°C with blended lignite and radiata pine wood with the L/F ratio ranging from 0% to 100%. It was found that all of the studied parameters including gasification temperature, S/F ratio, τ_f, bed material, and L/F ratio significantly influenced the NH_3 and H_2S concentrations and conversions in the producer gas.

For the secondary measures, a novel hot catalytic reactor and adsorber was developed in the present research for the simultaneous removal of NH_3 and H_2S. In a hot gas reactor operated at 500-800°C and under atmospheric pressure, titanomagnetite was tested for NH_3 and H_2S removal by hot catalytic NH_3 decomposition and H_2S adsorption reactions.

Titanomagnetite was tested with three different gas streams including 2,000 ppmv NH_3 in Ar, 2,000 ppmv NH_3 and 230 ppmv H_2S in Ar, and 2,000 ppmv NH_3 and 230 ppmv H_2S in simulated biomass producer gas. From the experimental results, it was discovered that ferrite (α-Fe) readily formed by the H_2 reduction of titanomagnetite has shown almost complete NH_3 decomposition (100%) in Ar gas at 700 and 800°C. The presence of H_2S in the gas mixture of NH_3 and Ar slightly reduced the catalytic activity for NH_3 decomposition at 700 and 800°C (>96%) and H_2S adsorption of more than 98% could be achieved at the same temperature range. However, in the test with simulated biomass producer gas, 60% NH_3 decomposition and 9% H_2S adsorption were obtained at 800°C, whereas 40% NH_3 decomposition and 80% H_2S adsorption were obtained at 500°C. The decrease of NH_3 decomposition and H_2S adsorption at 800°C in simulated biomass producer gas could be due to the high content of H_2 (45 vol%) in the feed gas that favours the reverse reactions of NH_3 decomposition and H_2S adsorption, the increased surface coverage of the active α-Fe phase by adsorbed hydrogen, and the competition of α-Fe for the reverse water-gas shift reaction. Besides, it was discovered that the temperature significantly affected the removal of NH_3 and H_2S in simulated biomass producer gas and thus it needs to be optimised.

Glossary

Ar	Archimedes number, dimensionless
A_t	cross-sectional area of the bed (m^2)
C_D	drag coefficient, dimensionless
d_p	particle diameter based on screen analysis (m)
d_p^*	dimensionless measure of particle diameter
d_t	bed or column diameter (m, cm)
g	acceleration of gravity (= 9.8 m/s^2)
g_c	conversion factor (= 1 $kg \cdot m/N \cdot s^2$)
L_m	height of fixed-bed (m)
L_{mf}	height of bed at minimum fluidisation (m)
L_f	height of bubbling fluidised bed (m)
Δp_b	pressure drop across the bed (Pa)
Δp_{fr}	frictional pressure (Pa)
Q	gas flow rate (m^3/s)
$Q_{20°C}$	gas flow rate at 20°C (m^3/s)
$Q_{800°C}$	gas flow rate at 800°C (m^3/s)
Re_p	particle Reynolds number (= $d_p u_o \rho_g / \mu$), dimensionless
$Re_{p,mf}$	particle Reynolds number at minimum fluidisation (= $d_p u_{mf} \rho_g / \mu$), dimensionless
$Re_{p,c}$	particle Reynolds number at transition to turbulent fluidisation (= $d_p u_c \rho_g / \mu$), dimensionless
u^*	dimensionless measure of gas velocity
u_c	turbulent transition velocity (m/s)
u_{mb}	minimum bubbling velocity (m/s)
u_{mf}	minimum fluidisation velocity (m/s)
u_{ms}	minimum slugging velocity (m/s)
u_{se}	critical velocity, which indicates the onset of fast fluidisation (m/s)
u_o	superficial gas velocity (based on an empty vessel basis) through a bed of solids (m/s)
u_t	particle terminal velocity (m/s)

W	mass of solid (kg)
z_s	height of bed at which slugging sets in (cm)
ε_m	voidage or void fraction in a fixed-bed
ε_{mf}	voidage or void fraction in a bed at minimum fluidisation
μ	viscosity of gas (kg/m·s)
ρ_{bu}	bulk density of the solid (kg/m^3)
ρ_g	gas density (kg/m^3)
ρ_s	particle density of the solid (kg/m^3)
$\emptyset_s$	sphericity of the particle
τ	mean gas residence time (s)

BFB	bubbling fluidised bed
CAPE	Department of Chemical and Process Engineering, University of Canterbury
CFB	circulating fluidised bed
DFB	dual fluidised bed
DSRP	direct sulphur recovery process
ER	equivalence ratio
FFB	fast fluidised bed
FT	Fischer-Tropsch
GC	gas chromatography
IGCC	integrated gasification combined cycle
IGFC	integrated gasification fuel cell
L/F	lignite to fuel ratio
PAFC	phosphoric acid fuel cell
PEMFC	proton exchange membrane fuel cell
S/B	steam to biomass ratio
S/F	steam to fuel ratio
XRD	x-ray powder diffraction

1. Introduction

1.1 Introduction

A dual fluidised bed (DFB) steam gasifier operated at atmospheric pressure and temperature from 700 to 850°C has been developed and extensive experiments have been conducted at the Department of Chemical and Process Engineering (CAPE), University of Canterbury. The DFB steam gasifier consists of a fast fluidised bed (FFB) reactor and a bubbling fluidised bed (BFB) reactor. The BFB reactor is for gasification where solid fuel is fed to the bed and the gasification agent, steam, is injected from the bottom. The FFB reactor combusts the solid char, which is transferred from the BFB reactor with circulating bed material to the FFB reactor, to provide the energy carried by the bed material for the endothermic gasification reactions in the BFB reactor. The DFB steam gasifier has shown its advantages of producing hydrogen-rich producer gas with high heating value (11.5-14.0 MJ/Nm^3) for heat and power generation and potential for commercialisation in New Zealand [1]. Additionally, the producer gas containing high H_2 and CO contents with the optimum H_2/CO molar ratio of 2 for FT liquid fuel synthesis has been achieved with the application of the DFB steam gasifier [2, 3].

The gasification producer gas from the DFB steam gasifier comprises hydrogen (H_2), carbon monoxide (CO), carbon dioxide (CO_2), methane (CH_4) and other hydrocarbon gases (HCs), as well as a trace amount of other impurities. This gas can be utilised in a variety of applications: in gas turbines or engines for power generation, and for further production of hydrogen gas, synthetic natural gas, and transportation fuels (e.g. Fischer-Tropsch liquid fuel).

The Fischer-Tropsch (FT) liquid fuel synthesis for diesel production from the biomass gasification producer gas is high-quality liquid fuel as it is cleaner than the petroleum-based liquid fuels, i.e. lower sulphur and aromatic hydrocarbons [4]. The FT liquid fuel can directly be utilised in current diesel engines and facilities [4]. The FT liquid fuel synthesis is a series of catalytic reactions of CO and H_2 to form major amount of paraffin straight-chain hydrocarbons (C_xH_{2x}) in a FT reactor, which is typically operated at the temperature of 200-250°C and the pressure of 25-60 bar [4]. The ideal molar ratio of H_2/CO for stoichiometric requirement is 2 [4].

The common catalysts used in the FT reactors are iron or cobalt based, which are easily poisoned by even a very low content of impurities, e.g. condensable organic hydrocarbons known as tars, and inorganic sulphur and nitrogen compounds. With the poisoning, the catalysts will lose their activity and selectivity. Therefore, the feed gas specifications for FT liquid fuel synthesis are very stringent. For example, the amount of particulates should be completely removed, tars should be essentially below their dew point, and total nitrogen compounds (NH_3 + HCN) and total sulphur compounds (H_2S + COS + CS_2) should be below 1 ppmv [4].

Under these strict feed gas requirements for the FT reactor, the gas cleaning system for removal of tars, nitrogen compounds, and sulphur compounds has been extensively studied and developed. For the tar removal from the producer gas, an organic solvent scrubber using biodiesel to scrub tars has been built and investigated at CAPE. The biodiesel scrubber has been successfully removed tars with the efficiency of more than 99% [5]. However, at current stage, nitrogen compounds and sulphur compounds in the producer gas, mainly NH_3 and H_2S, still remain the main technical challenges for the FT liquid fuel synthesis.

Formation of NH_3 and H_2S is inevitable as they are mainly generated from N and S in the biomass feedstock [6, 7]. The concentrations of NH_3 and H_2S produced from the gasification depend on several factors, including N and S contents in the feedstock, gasifier operation conditions, gasifier types, types of gasifying agent, N- and S-binding structures of the feedstock, and mineral matter present in the fuel feedstock [8, 9]. In the producer gas from gasification of woody biomass, which commonly has the N content below 0.5 wt%, NH_3 concentration ranges from 100 to 2,000 ppmv [10]. Content of S in woody biomass and in herbaceous crops is typically less than 0.1 wt% and between 0.3 and 0.4 wt%, respectively [11], and H_2S concentration in the biomass producer gas varies from 20 to 230 ppmv [12]. Although H_2S is produced from biomass gasification in a very low amount, its concentration is still higher than the requirement for the FT liquid fuel synthesis, which is extremely low at 1 ppmv. Therefore, the removal of H_2S is necessary to reduce H_2S to be below 1 ppmv.

In order to reduce the NH_3 and H_2S concentrations in the producer gas, there are several methods that can be effectively used for the DFB steam gasifier system. These methods include (1) primary measures: methods employed in the DFB steam gasifier including process optimisation (i.e. optimising the operation conditions affecting the NH_3 and H_2S concentrations), and application of bed materials for catalytic NH_3 decomposition and H_2S adsorption; and (2) secondary measures or downstream cleaning methods after the gasifier (e.g. hot catalytic NH_3 decomposition and H_2S adsorption).

In order to clarify the overall gas cleaning system for the integration of the DFB steam biomass gasification for the FT liquid fuel synthesis, the proposed system line-up is shown in Figure 1.1. Firstly, particulates can be removed by available mature technologies which are cyclones and filters (e.g. metal or ceramic candle filters) [11, 13]. Next, tars are scrubbed in the solvent scrubber and the tar-loaded solvent can be recovered by the use of hot air [5]. Finally, the hot gas reactor is used to remove NH_3 and H_2S.

The aim of this research, therefore, is to remove NH_3 and H_2S in the producer gas from the DFB steam gasifier for feeding into the FT liquid fuel reactor. In this research, the combination of all these specified removal technologies has been investigated including (1) the process optimisation of the DFB steam gasifier; (2) the application of bed materials in the DFB steam gasifier for catalytic NH_3 decomposition and H_2S adsorption; and (3) the downstream cleaning methods by hot catalytic NH_3 decomposition and H_2S adsorption.

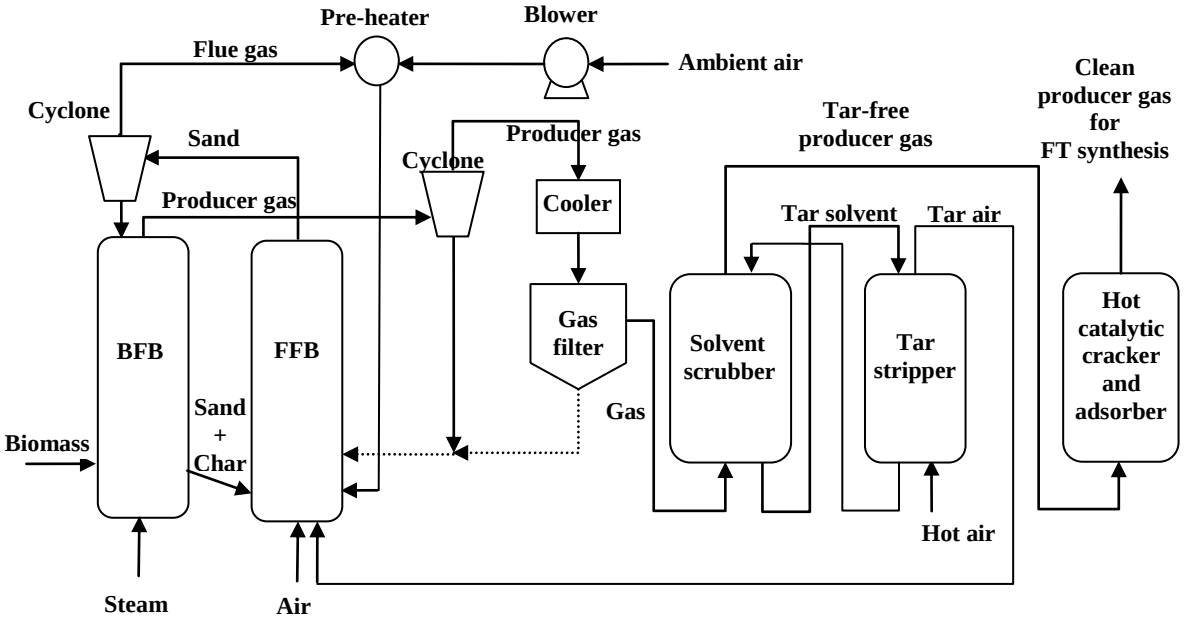

Figure 1.1 Schematic process of the DFB steam biomass gasification integrated with gas cleaning system for FT liquid fuel synthesis

1.2 Thesis scope and outline

A literature review will be summarised in Chapter 2. The literature review will first provide the background and understanding of biomass and woody biomass in New Zealand, biomass conversion technologies, biomass gasification process, and FT liquid fuel synthesis. The obstacles to the application of biomass producer gas for FT liquid fuel, which are NH_3 and H_2S presented in the producer gas, are highlighted and discussed. This leads to the options and discussion of the possible and effective measures to solve the problems including the primary and secondary measures.

Based on the comprehensive literature review, the primary measures will be investigated using process optimisation and the application of bed materials for NH_3 and H_2S removal in the DFB steam gasifier. As the primary measures cannot achieve the required cleanness, the secondary measures using hot catalytic NH_3 decomposition and H_2S adsorption have been chosen for the removal of NH_3 and H_2S in this research. From the literature review study, a review paper has been published on the removal of NH_3 from the producer gas in biomass gasification using the primary and secondary measures [10].

For the study of hot catalytic NH_3 decomposition and H_2S adsorption, a lab-scale reactor and system has been designed and developed, which is described in Chapter 3. In addition, the reactor testing as well as preliminary experiments have been conducted and the results of these investigations are also provided.

In order to examine the removal of NH_3 and H_2S in the DFB steam gasifier and in the lab-scale reactor, the measurement of NH_3 and H_2S concentrations in the producer gas is necessary, and it is described in Chapter 4 and published in Fuel [14]. The sampling and analysis of NH_3 and H_2S has been used in Chapters 5-7.

In Chapter 5, the experiments on the secondary measures using hot catalytic NH_3 decomposition and H_2S adsorption have been conducted. It presents the investigation of simultaneous removal of NH_3 and H_2S by titanomagnetite in the lab-scale reactor. The work in this chapter has recently been published in Fuel [15].

Chapter 6 presents the experiments on the primary measures for removal of NH_3 and H_2S in the DFB steam gasifier by optimisation of operation conditions and application of bed materials. The work in this chapter is currently in the progress for submission to a journal.

Another set of experiments on the primary measure on the co-gasification of coal and biomass in the DFB steam gasifier is presented in Chapter 7. Co-gasification of coal and biomass has potential to offer combined benefits of coal for high energy density and biomass for clean and renewable resources. Economic returns of biomass gasification can be improved by addition of coal into the biomass feedstock, and thus a feasible scale of biomass energy plant can be realised [3]. It was also found that co-gasification provides the adjustment of H_2/CO ratio in the producer gas to meet the requirement of downstream applications [3, 16-18]. In the present study, the influence of lignite to fuel ratio on the NH_3 and H_2S concentrations and conversions in co-gasification of blended lignite and wood pellets has been studied. The work in this chapter is published in Fuel [14].

Finally, Chapter 8 is the conclusions of the research and the recommendations on the future work.

1.3 References

[1] D. Bull, Performance improvements to a fast internally circulating fluidized bed (FICFB) biomass gasifier for combined heat and power plants, in: the Department of Chemical and Process Engineering, University of Canterbury, 2008.

[2] W.L. Saw, S. Pang, The influence of calcite loading on producer gas composition and tar concentration of radiata pine pellets in a dual fluidised bed steam gasifier, Fuel, 102 (2012) 445-452.

[3] W.L. Saw, S. Pang, Co-gasification of blended lignite and wood pellets in a 100 kW dual fluidised bed steam gasifier: The influence of lignite ratio on producer gas composition and tar content, Fuel, 112 (2013) 117-124.

[4] H. Boerrigter, H.P. Calis, D.J. Slort, H. Bodenstaff, A.J. Kaandorp, H. den Uil, L.P.L.M. Rabou, Gas cleaning for integrated biomass gasification (BG) and Fischer-Tropsch (FT) systems: Experimental demonstration of two BG-FT systems ("Proof-of-Principle"), in: the Energy research Centre of the Netherlands (ECN), the Netherlands, report no: ECN-C--04-056, 2004.

[5] G. Mwandila, Determination of design parameters and investigation on operation performance for an integrated gas cleaning system to remove tars from biomass gasification producer gas, in: the Department of Chemical and Process Engineering, University of Canterbury, 2010.

[6] M. Dias, I. Gulyurtlu, H_2S and HCl formation during RDF and coal co-gasification: a comparison between the predictions and experimental results, in: Proceedings of the biomass gasification technologies workshop MRC Gebze Campus-Türkiye, 2008.

[7] S.H. Aljbour, K. Kawamoto, Bench-scale gasification of cedar wood – Part II: Effect of operational conditions on contaminant release, Chemosphere, 90 (2013) 1501-1507.

[8] J. Leppälahti, T. Koljonen, Nitrogen evolution from coal, peat and wood during gasification: literature review, Fuel Processing Technology, 43 (1995) 1-45.

[9] A. Attar, Chemistry, thermodynamics and kinetics of reactions of sulphur in coal-gas reactions: A review, Fuel, 57 (1978) 201-212.

[10] J. Hongrapipat, W.-L. Saw, S. Pang, Removal of ammonia from producer gas in biomass gasification: integration of gasification optimisation and hot catalytic gas cleaning, Biomass Conversion and Biorefinery, 2 (2012) 327-348.

[11] D.J. Stevens, Hot gas conditioning: Recent progress with larger-scale biomass gasification systems, in: National Renewable Energy Laboratory, the U.S. Department of Energy Laboratory, report no: NREL/SR-510-29952, 2001.

[12] S. Cheah, D.L. Carpenter, K.A. Magrini-Bair, Review of mid-to high-temperature sulfur sorbents for desulfurization of biomass- and coal-derived syngas, Energy & Fuels, 23 (2009) 5291-5307.

[13] R.W.R. Zwart, Gas cleaning downstream biomass gasification: Status report 2009, in: the Energy research Centre of the Netherlands (ECN), the Netherlands, report no: ECN-E--08-078, 2009.

[14] J. Hongrapipat, W.L. Saw, S. Pang, Co-gasification of blended lignite and wood pellets in a dual fluidized bed steam gasifier: The influence of lignite to fuel ratio on NH_3 and H_2S concentrations in the producer gas, Fuel, 139 (2014) 494-501.

[15] J. Hongrapipat, A.C.K. Yip, A.T. Marshall, W.L. Saw, S. Pang, Investigation of simultaneous removal of ammonia and hydrogen sulphide from producer gas in biomass gasification by titanomagnetite, Fuel, 135 (2014) 235-242.

[16] J.J. Hernández, G. Aranda-Almansa, C. Serrano, Co-gasification of biomass wastes and coal−coke blends in an entrained flow gasifier: An experimental study, Energy & Fuels, 24 (2010) 2479-2488.

[17] I. Aigner, C. Pfeifer, H. Hofbauer, Co-gasification of coal and wood in a dual fluidized bed gasifier, Fuel, 90 (2011) 2404-2412.

[18] K. Kumabe, T. Hanaoka, S. Fujimoto, T. Minowa, K. Sakanishi, Co-gasification of woody biomass and coal with air and steam, Fuel, 86 (2007) 684-689.

2. Literature review

2.1 Biomass

Biomass is an organic material derived from living organisms, or more specifically, from plants and animals [1]. Biomass is a carbon-based material and consists of a mixture of organic molecules containing hydrogen, oxygen, nitrogen, sulphur, and trace amounts of other elements such as alkali, alkaline earth, and heavy metals. Biomass feedstocks can be divided into several categories such as wood residues from forestry or from wood processing, agricultural residues from agriculture harvesting or processing, energy crops or high yield crops grown specifically for energy applications, food wastes, and industrial wastes [1].

Biomass is a clean renewable and sustainable energy resource that can be replenished. Biomass has gained attention worldwide due to the rapid increase in energy consumption, environmental concerns, and an international agreement on climate change. According to the U.S. Energy Information Administration [2], the world marketed energy consumption increased from 355×10^{15} British thermal units (Btu) in 1990 to 524×10^{15} Btu in 2010. Although the world's economy is still recovering from the 2008-2009 global recession, the energy consumption is estimated to grow to 630×10^{15} Btu in 2020 and to 820×10^{15} Btu in 2040 due to economic growth in developing countries [2]. In order to meet the tremendous energy requirements, fossil fuels such as coal, oil, and natural gas have mostly been utilised. However, burning coal and other fossil fuels to generate heat and electricity produces greenhouse gases, and this is a major cause of air pollution in the Earth's atmosphere. These air pollution emissions lead to climate change and global warming. An increase in worldwide awareness of climate change has led to an international agreement or the so-called Kyoto Protocol linked to the United Nations Framework Convention on Climate Change (UNFCCC). In the first commitment period (2008-2012), the Kyoto Protocol set compulsory objectives for 37 industrialised countries and the European Communities to decrease their emission of greenhouse gases to an average of 5% below the 1990 levels. During the second commitment period (2013-2020), the target is a further reduction of greenhouse gases by at least 18% below the 1990 levels [3]. Therefore, to fulfill the requirements for energy consumption and international agreement, the use of

biomass has significantly increased because it is considered as one of the most important renewable energy resources for this century.

2.2 Woody biomass availability in New Zealand

In New Zealand, exotic plantation forest covers 1.75 million hectares or approximately 7% of New Zealand's land area [4]. For the exotic planted forest, radiata pine (*Pinus radiata*) is the most important species; it shares 1.58 million hectares or 90% of the total planted forest area. Other planted species making up another 10% are Douglas fir (6%), eucalyptus and other softwood and hardwood species [4]. Statistics show that total harvested logs from plantation forests amounted to 27.4 million m^3/year in 2012, of which 50% were processed in New Zealand and the rest were exported [5]. The harvested logs are used in New Zealand as a raw material for the production of several kinds of products such as logs, sawn timber, pulp and paper, plywood, and reconstituted panels.

Two major potential sources of wood waste for use in energy production include forest residues arising from log extraction in the forest and wood process residues generated in the wood processing industry. The total forest residue volume in New Zealand was predicted to increase from 4.0 million m^3/year in 2000 to about 4.4 and 4.6 million m^3/year in 2010 and 2020, respectively [6]. Forest residues that can be collected for reuse were estimated to be 0.6 and 1.1 million m^3/year in 2000 and 2010 and to increase slightly to 1.2 million m^3/year in 2020 [6].

In wood processing industries, residues or by-products from sawmills such as bark, sawdust, and chips, are currently utilised as a raw material and as a boiler fuel and pellets. The total wood process residues were approximately 23% of the total harvested log volume or about 4.0 million m^3/year in 2000 and forecasted to reach 6.7 million m^3/year in 2010 [6]. However, more than 50% volume of these wood process residues is currently reused in the wood processing industry and is not available for energy production. Therefore, the estimated wood process residues available for energy production were forecasted to be 1.3, 2.0, and 2.1 million m^3 in 2000, 2010, and 2020, respectively [6].

From the above-mentioned statistics, the approximate quantity of woody biomass residues from both the forest and wood process was 3.1 million m^3/year in 2010 and increasing to

3.3 million m^3/year in 2020. These woody biomass residues would equate to around 31×10^{15} and 33×10^{15} joule total potential primary energy in the respective years of 2010 and 2020. Therefore, a large quantity of woody biomass residues, which is readily available in New Zealand, can be potentially used for alternative energy production.

2.3 Biomass conversion technologies

Biomass can be converted into various forms of energy via a number of conversion processes. The main products from biomass conversion comprise power/heat generation, transportation fuels, and chemical feedstocks. The most suitable option for the biomass conversion process depends on several factors including the available types and quantities of biomass feedstocks, the final forms of the energy required, environmental standards, project plant economics, and project specific factors [7].

The three main current biomass conversion technologies include thermo-chemical, bio-chemical/biological, and mechanical processes [7]. For the thermo-chemical process, combustion, gasification, and pyrolysis are the major conversion processes for energy production. Each of these three technologies generates several types of intermediate energy carriers and final energy products which are shown in Figure 2.1. In Figure 2.1, it indicates that, via gasification and pyrolysis processes, biomass can be converted into synthetic liquid fuel.

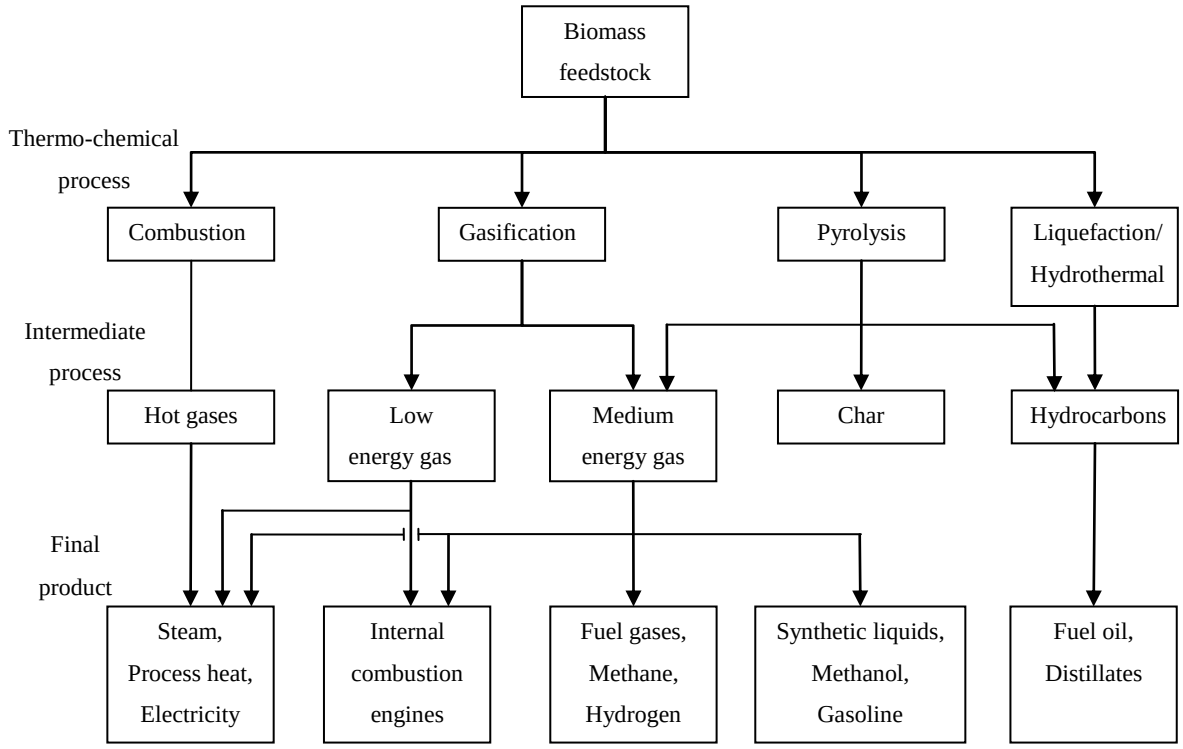

Figure 2.1 Main processes, intermediate energy carriers, and final energy products from the thermo-chemical conversion of biomass [7]

2.4 Biomass gasification process

2.4.1 Biomass gasification

Gasification is the thermo-chemical conversion of any carbonaceous fuel to a combustible gas, where the fuel can be in the form of solid, liquid, and gaseous feedstocks such as coals, biomass residues, oils, and natural gases [8]. Gasification is a partial oxidation process which applies heat to the feedstock at sub-stoichiometric levels of oxygen to that required for complete oxidation. The oxidant used can be oxygen, air, steam, or a mixture of these.

Biomass gasification is the thermo-chemical conversion of biomass to produce combustible gas or producer gas mainly comprising hydrogen (H_2), carbon monoxide (CO), carbon dioxide (CO_2), methane (CH_4), and other hydrocarbon gases. The producer gas can be utilised to further produce electricity through integrated gasification combined cycle (IGCC) or integrated gasification fuel cell (IGFC) technology, as well as liquid fuel by Fischer-Tropsch (FT) synthesis, and other chemical products [8, 9]. Due to the flexibility of the applications of biomass producer gas, biomass gasification has been considered as the

basis for biomass conversion that provides a variety of energy and chemical products. However, in the biomass gasification, minor gas contaminants are also generated such as tars, volatile inorganic metals, nitrogen-containing compounds, sulphur-containing compounds, and halogens [9-12]. These contaminants in the producer gas are undesirable in the downstream applications of the producer gas. Details and definition of undesirable products or contaminants are given in Section 2.4.4.

2.4.2 Biomass properties related to gasification

Each type of biomass has its own specific properties. Therefore, the evaluation of a particular type of biomass as a potential resource for gasification necessitates the determination of its properties related to gasification. The proximate analysis, ultimate analysis, heat of combustion, and ash analysis of the biomass provide important information on its volatility, elemental composition, heat content, and potential for slagging and fouling, respectively [13].

2.4.2.1 Proximate analysis

Proximate analysis determines the content (percent mass basis) of various products obtained from heating material under controlled conditions [14]. Proximate analysis reports the properties of fuel in terms of the content of moisture, volatile matter, fixed carbon and ash. Proximate analysis of some selected biomass is given in Table 2.1. Information from proximate analysis is important in the development of the gasification process as discussed below.

Moisture content of biomass is the content of water in the material representing only physically bound water, whereas water released from chemical reactions in pyrolysis is classified as being part of the volatiles [13]. Moisture content of biomass can be easily determined by gravimetric method, where biomass is weighed, and then heated at 100°C and reweighed [14]. For biomass gasification, biomass with a low moisture content is generally required because it produces higher quality producer gas, i.e. higher heating value and higher gas efficiency [15].

Volatile matter is the material in biomass that decomposes and releases as gases upon heating in an inert gas atmosphere at a moderate temperature (400°C) [14]. The volatile matter is related to the yield of volatile compounds produced during pyrolysis, which is explained in details in Section 2.4.3.2. Due to the high quantity of volatile matter in biomass (70-80 wt%) compared with coal (30-40 wt%) and the higher reactivity of its char, biomass is a high potential resource for the gasification process [14].

Ash content is the amount of mineral matter or inorganic compounds in biomass. Ash content is determined by driving off the volatiles and fixed carbon or solid carbon in combustion process at high temperature, which results in only the ash remaining [14]. Ash content in different biomass feedstocks varies widely from about 0.1% in wood to about 15% for some agricultural products. The ash content influences the design of the gasifier, particularly the ash removal system [15].

Finally, fixed carbon or solid carbon content is calculated from the mass balance. The fixed carbon and ash content from proximate analysis can be used to estimate the char yield in the pyrolysis process (Section 2.4.3.2).

Table 2.1 Proximate analysis of some selected biomass feedstocks

Biomass	**Proximate analysis (wt% as-received basis)**				**Reference**
	Moisture	**Volatile matter**	**Fixed carbon**	**Ash**	
Pinus pinaster	12.0	71.5	16.0	0.5	[16]
Holm-oak	9.5	70.2	17.8	2.4	
Eucalyptus	10.6	74.8	13.9	0.7	
Radiata pine	8.0	77.4	14.2	0.4	[17]
Willow	8	69.8	20.1	2.52	[18]
Corn straw	6.17	75.95	13.75	5.93	[19]
Seed corn	15.01	66.43	17.15	1.4	[20]
Oak + Maple	6.25	75.11	16.81	1.83	

2.4.2.2 Ultimate analysis

Ultimate analysis or elemental analysis reports the major elemental composition of the fuel on a mass percent basis, which comprises C, H, O, N, S, and Cl along with moisture and ash [14]. Ultimate analysis can be presented on an as-received, dry, or dry and ash free (daf) basis. Information from ultimate analysis is important as it can be used to perform the mass balance of each element in the gasification process and to indicate possible pollutants emitted such as N, S, and Cl compounds. Ultimate analysis of some selected biomass is given in Table 2.2.

Table 2.2 Ultimate analysis of some selected biomass feedstocks

Biomass	**Ultimate analysis (wt% dry and ash free)**					**Reference**
	C	**H**	**N**	**S**	**O**	
Pinus pinaster	51.6	4.9	0.9	n.d.[a]	42.6	[16]
Holm-oak	51.1	5.3	0.9	n.d.[a]	42.7	
Eucalyptus	52.8	6.4	0.4	n.d.[a]	40.4	
Radiata pine	51.5	5.9	0.2	<0.1	42.3	[17]
Willow	50.3	6.17	0.69	0.002	37.4	[18]
Corn straw	43.83	5.95	0.97	0.13	45.01	[19]
Seed corn	40.07	7.1	1.4	0.17	50.5	[20]
Oak + Maple	46.56	6.24	0.14	0.02	46.13	

[a] Not detected

2.4.2.3 Heat of combustion or Heating value

Apart from proximate and ultimate analyses, heat of combustion or heating value is also important in the gasification process. The heating value gives information on the amount of heat released during combustion under isothermal conditions. Heating value is classified as higher heating value (gross calorific value) and lower heating value (net calorific value). The higher heating value (HHV) is the total amount of energy obtained from fuel combustion, in which the water vapour in combustion products is condensed to liquid and the latent heat of condensation of water vapuor is recovered. The amount of energy released during combustion that does not include the latent heat of condensation of water vapour is

called the lower heating value (LHV). The HHV of fuel can be measured with oxygen in a bomb calorimeter or simply estimated from the C wt% value in the ultimate analysis on a dry basis by using Equation 2.1 [15]. The HHV or LHV is necessary for calculation of the energy efficiency of the gasification process.

$$\text{HHV in MJ/dry kg} = 0.4571 \times (\text{wt\% C on dry basis}) - 2.70 \quad (2.1)$$

2.4.2.4 Ash analysis

Ash analysis reports the amount of mineral matter or inorganic compounds in the biomass which remain after complete combustion. Ash analysis normally detects Si, Al, Fe, Ca, Mg, Na, K, Ti, and P and reports them in the highest oxide forms as SiO_2, Al_2O_3, Fe_2O_3, CaO, MgO, Na_2O, K_2O, TiO_2, and P_2O_5, respectively. Ash composition is important because it affects the melting point of the ash and the consequent control of the maximum temperature that can be operated in the gasifier, due to slagging and fouling [14, 15]. Ash melting can cause slagging which is the partial or complete melting of ash, and fouling which is the accumulation of sticky ash particles on the surfaces [14]. K in combination with Si is of particular concern because they can form low melting point compounds at gasification temperature [13]. Moreover, mineral matter in the ash such as Fe, Ca, and/or Mg was found to have the catalytic effect on tar cracking [12, 21, 22], NH_3 decomposition [21, 23, 24] and desulphurisation or adsorption reaction for H_2S removal [12, 25, 26].

2.4.3 Thermo-chemical processes and reactions in biomass gasification

Thermo-chemical processes and reactions in the gasification of biomass and coal can be sequenced into four main steps: heating and drying, pyrolysis or devolatilisation, char-gas reactions, and gas phase reactions, as shown in Figure 2.2.

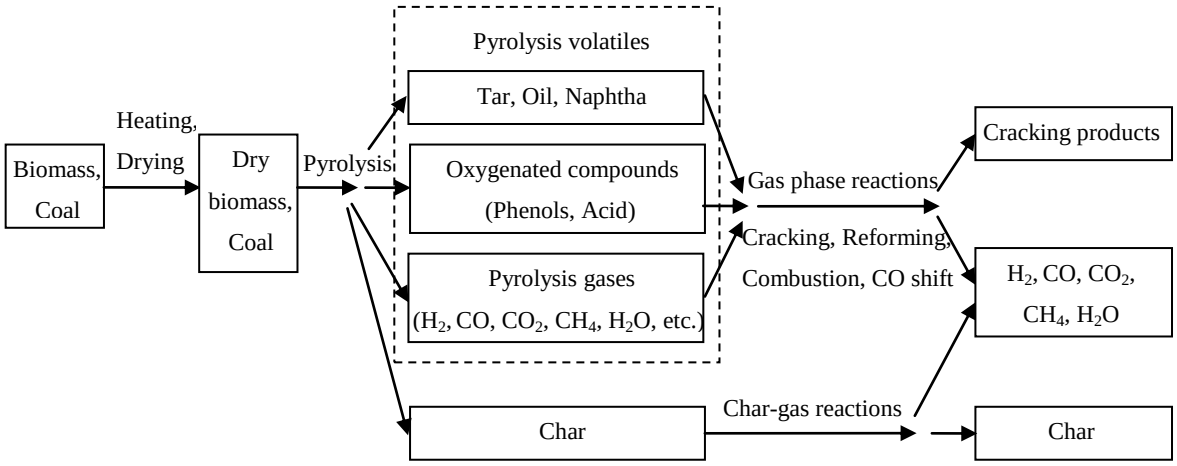

Figure 2.2 Reaction sequence for gasification of biomass or coal (adapted from [8])

2.4.3.1 Heating and drying

Heating and drying are endothermic processes which require a source of heat supplied by an external source or by the partial oxidation of fuel. Heating and drying of fuel particles takes place in the first step, where moisture in the solid fuel evaporates at a temperature of about 150°C and higher [27]. Figure 2.3 shows a schematic diagram of the heating and drying of a fuel particle. When heat is supplied, a thermal front forms on the outside surface ,which then penetrates into the centre of the fuel particle. Moisture is driven from the particle and the temperature of the particle increases high enough to initiate pyrolysis [14]. Since the temperature at the centre of the fuel particle is lagging behind the outer surface, the heating and drying process through to the centre of the particle takes longer for larger fuel particles. In other words, the heating rate is slower for larger fuel particles [13].

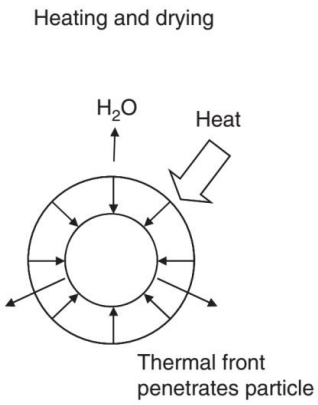

Figure 2.3 Heating and drying of a fuel particle [14]

2.4.3.2 Pyrolysis or devolatilisation

The pyrolysis or devolatilisation process is a complex series of thermal decomposition and chemical reactions of fuel particles which yields a porous carbonaceous solid or char, as well as volatiles comprising permanent gases (mainly H_2, CO, CO_2, CH_4, and other light hydrocarbons) and condensable vapours (water, methanol, acetic acid, acetone, and heavy hydrocarbons or tars) [13, 14]. Pyrolysis takes place at 350-800°C in parallel with the heating up of the fuel particle [8]. Pyrolysis begins slowly at a low temperature of 350°C and accelerates to a very high rate above 700°C [27]. A schematic diagram of pyrolysis of a fuel particle is shown in Figure 2.4. Pyrolysis follows the thermal front through the fuel particle, releasing volatile compounds and generating porous solid char containing residual carbon (C) and inorganic compounds (ash) [13, 14].

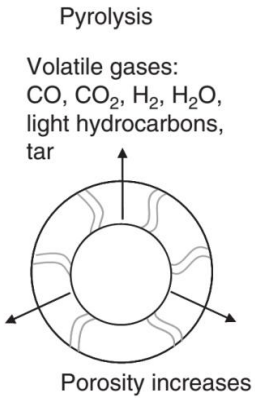

Figure 2.4 Pyrolysis of a fuel particle [14]

The product distribution of the pyrolysis process depends mainly on fuel chemical composition, a heating rate of the fuel particles, and temperature achieved in the reactor [8, 14]. The total yield of pyrolysis products can be roughly estimated from the proximate analysis of the fuel. Volatile matter in the fuel can be used to estimate the yield of volatiles, whereas fixed carbon and ash content roughly correspond to the char yield [14]. Due to the high volatile matter in biomass (70-80 wt%), up to 80% wt of the biomass can be converted into volatile compounds (gases and vapours) during pyrolysis [13].

The heating rate of the fuel particles influences the interplay between pyrolysis and gasification reactions and thus the product distribution of the pyrolysis process [8]. The

heating rate is classified as slow or fast. The pyrolysis and gasification reaction paths occurring at slow and fast heating rates are shown in Figure 2.5. At a slow heating rate, the pyrolysis reactions set in at 350°C, but gasification reactions of both volatile gases and char with a gasifying agent are very slow at this temperature. This leads to a rapid increase in the concentrations of volatiles building up outside the particle. Therefore, the gasification reactions start only after pyrolysis is complete [8]. The high concentrations of volatiles (tars) produced at a slow heating rate can be removed unreacted from a reactor by the producer gas. In contrast to a slow heating rate, both pyrolysis and gasification reactions take place simultaneously at a fast heating rate, which results in low concentrations of volatiles (tars) and cleaner producer gas being obtained [8]. Moreover, the particle size of the fuel affects the heating rate, which in turn influences the way the pyrolysis takes place and the production distribution from the pyrolysis.

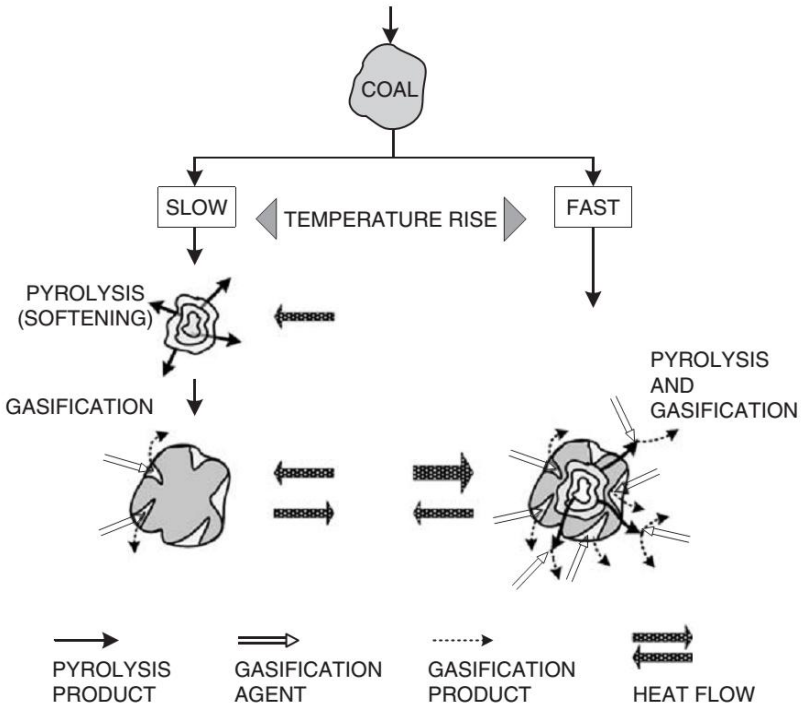

Figure 2.5 Influence of the heating rate on pyrolysis and gasification reactions [8]

2.4.3.3 Char-gas reactions or solid-gas reactions

The third step of the gasification process is char-gas reactions or solid-gas reactions which follow pyrolysis. Char-gas reactions are the reactions between the residual char and volatile

compounds (gases and vapours) released from the pyrolysis process, as well as a gasifying agent (oxygen and steam) injected into the reactor [13]. The char-gas reactions are the slowest reactions, and therefore they govern the overall conversion rate in the gasification process [8]. Four main char-gas reactions that convert solid carbon (C) in the char into gaseous CO, H_2, and CH_4 are shown in Equations 2.2-2.5 [13, 14]:

Carbon-oxygen reaction:	$C + \frac{1}{2} O_2 \leftrightarrow CO$	$\Delta H^{\circ}_{298°C}$ = -110 kJ/mol	(2.2)
Hydrogenation reaction:	$C + 2H_2 \leftrightarrow CH_4$	$\Delta H^{\circ}_{298°C}$ = -75 kJ/mol	(2.3)
Reverse Boudouard reaction:	$C + CO_2 \leftrightarrow 2CO$	$\Delta H^{\circ}_{298°C}$ = 172 kJ/mol	(2.4)
Carbon-water reaction:	$C + H_2O \leftrightarrow H_2 + CO$	$\Delta H^{\circ}_{298°C}$ = 131 kJ/mol	(2.5)

Some researchers also proposed two more char-gas reactions apart from those four reactions and they are as follows (Equations 2.6 and 2.7) [16]:

Carbon-oxygen reaction:	$C + O_2 \leftrightarrow CO_2$	$\Delta H^{\circ}_{298°C}$ = -393 kJ/mol	(2.6)
Carbon-water reaction:	$C + 2H_2O \leftrightarrow 2H_2 + CO_2$	$\Delta H^{\circ}_{298°C}$ = 90 kJ/mol	(2.7)

The exothermic carbon-oxygen and hydrogenation reactions supply the thermal energy required for the heating and drying, pyrolysis, and endothermic reverse Boudouard and carbon-water reactions. The reverse Boudouard and carbon-water reactions are important in the gasification process as they convert C into useful gaseous CO and H_2 [13]. At the chemical equilibrium state, all of the carbon in the char from pyrolysis is completely reacted through char-gas reactions into gases. However, the contact time between char and gases is typically insufficient to reach equilibrium at high temperature in gasification process, and thus up to 10 wt% of biomass is left as unreacted char [13].

2.4.3.4 Gas-phase reactions

Gas-phase reactions are more rapid than the char-gas reactions and they normally take place simultaneously with the char-gas reactions. Gas-phase reactions involve the reactions of all gases in the system including volatiles released from pyrolysis, gases produced from char-gas reactions, and oxygen and/or steam introduced into the gasifier as a gasifying agent [13, 16]. Two main gas-phase reactions are the water-gas shift reaction (or called CO shift

reaction) and the steam-methane reforming reaction, and they determine the final composition of the gaseous products [13, 14].

Water-gas shift reaction: $CO + H_2O \leftrightarrow H_2 + CO_2$ $\Delta H^{\circ}_{298°C} = -41$ kJ/mol (2.8)

Steam-methane reforming: $CH_4 + H_2O \leftrightarrow 3H_2 + CO$ $\Delta H^{\circ}_{298°C} = 206$ kJ/mol (2.9)

The final gas composition from gasification depends significantly on the oxygen and steam contents introduced into the gasifier as well as on reaction temperature and time [14]. With a sufficiently long reaction time, a chemical equilibrium state can be attained and the products are only light gases including H_2, CO, CO_2, and CH_4. From the thermodynamic analysis of the six gasification reactions (Equations 2.2-2.5 and 2.8-2.9), it was found that high temperatures and low pressures favour the production of H_2 and CO, whereas low temperatures and high pressures favour the production of CH_4 [14]. In practice, chemical equilibrium is not attained due to the short reaction time, and therefore light hydrocarbons such as ethane (C_2H_6), ethylene (C_2H_4), and acetylene (C_2H_2) as well as heavy hydrocarbons or tars are formed in the producer gas [14].

2.4.4 Main and contaminant gases from biomass gasification

The composition of the gas from biomass gasification is dependent on the type of gasification process, type and amount of gasifying agent, type of biomass feedstock and its properties, and gasification operation parameters. Gas typically produced from the biomass gasification process can be classified into main permanent gases or so-called producer gas and a lesser amount of other undesired products or contaminants as listed below.

Main permanent gases (producer gas):

- Hydrogen (H_2)
- Carbon monoxide (CO)
- Carbon dioxide (CO_2)
- Methane (CH_4)
- Aliphatic hydrocarbons (C_xH_y) larger than methane, with a majority of them being ethylene (C_2H_4)
- Water vapour (H_2O)

Undesirable products or contaminants [9]:

- Particulates, e.g. dust, soot, char, and ash
- Volatile inorganic metals, e.g. alkali and alkaline earth metal compounds.
- Aromatic hydrocarbon, e.g. benzene
- Tars, i.e. condensable organic hydrocarbons with a molecular weight higher than benzene
- Nitrogen-containing compounds, e.g. mainly ammonia (NH_3) and traces of hydrogen cyanide (HCN) and nitrogen oxide (NO_x)
- Sulphur-containing compounds, e.g. hydrogen sulphide (H_2S), carbonyl sulphide (COS), and other organic sulphur compounds such as carbon disulphide (CS_2), mercaptans (RSH), thiophene (C_4H_4S), thiols (CH_4S, C_2H_5SH), thiophenol (C_6H_6S), and benzothiophene (C_8H_6S)
- Halogens, e.g. hydrogen chloride (HCl), hydrogen bromide (HBr), and hydrogen fluoride (HF)

The requirements of the producer gas depend on the end-use application of the gas. In this research, the producer gas generated from the DFB steam gasifier is to be used for the liquid fuel production in the FT synthesis reactor. The specifications and requirements of the producer gas for the FT liquid fuel synthesis are provided and discussed in Section 2.6.2.

Comprehensive details on the definition and formation of nitrogen- and sulphur-containing compounds, which are the main focus of this research, are presented below. However, for particulates and tars, their definitions are also given.

2.4.4.1 Particulates

Particulates, which are defined as any solid particles carried in the raw producer gas exiting the gasifier, include inorganic ash, unconverted char, and entrained catalytic or circulating bed material [10]. Fine inorganic ash comes from mineral matter in the biomass feedstock, and it is either entrained in the producer gas or retained in the gasifier bed. The amount of fly ash entrained in the producer gas depends on the gasifier design and configurations and the concentrations of minerals in the biomass, where clean wood contains about 1-2 dry

wt%, herbaceous biomass has about 10 dry wt%, and straw or rice hulls contain 15-20 dry wt% mineral [10].

Organic char is the unconverted biomass originating from incomplete gasification reactions. Char is a light particle which is easily blown away from the gasifier bed with the producer gas, particularly in the turbulent regimes such as the circulating fluidised bed regime. As char represents incomplete gasified biomass, higher char content in the producer gas means lower carbon conversion efficiency. The separation of char from the producer gas and recirculation back to the gasifier can therefore improve overall gasification efficiency [10].

The other solid particle carried over in the producer gas is the bed material, which is either inert or catalytic matter, used as bubbling or circulating bed material in the gasifier. When this bed material encounters the turbulent flow of fluidising agents in the reactor, it undergoes attrition and generates fine particles that are blown out with the producer gas. The amount of fine bed material could be large in the case of soft bed material being used in the circulating fluidised bed reactor, which creates the loss of bed material, and it needs to be refilled into the gasifier.

2.4.4.2 Tars

According to the tar definition set by Energy research Centre of the Netherlands (ECN), tars are defined as all organic components with molecular weight higher than benzene [28]. Benzene is excluded from tars. Tars can be classified into six classes as shown in Table 2.3.

Table 2.3 Tar classification system [28]

Class	Type	Examples
1	GC undetectable tars.	biomass fragments, heaviest tars (pitch)
2	Heterocyclic compounds. These are components that generally exhibit high water solubility.	phenol, cresol, quinoline, pyridine
3	Aromatic components. Light hydrocarbons, which are important from the point view of tar reaction pathways, but not in particular towards condensation and solubility.	toluene, xylenes, ethylbenzene (excluding benzene)
4	Light polyaromatic hydrocarbons (2-3 rings PAHs). These components condense at relatively high concentrations and intermediate temperatures.	naphthalene, indene, biphenyl, antracene
5	Heavy polyaromatic hydrocarbons (≥4-rings PAHs). These components condense at relatively high temperatures and at low concentrations.	fluoranthene, pyrene, crysene
6	GC detectable, unidentified compounds.	unknowns

2.4.4.3 Nitrogen-containing compounds

In biomass gasification, most of the nitrogen (N) in the feedstock is converted to N-containing compound gases and the remaining is retained in unreacted solid char [29-31]. Figure 2.6 shows the formation and liberation of N-containing compounds in biomass gasification which is similar to the reaction sequence for gasification of biomass shown in Figure 2.2. From Figure 2.6, it can be seen that N in the biomass is liberated into volatile-N compounds including N-gases and N-containing aromatic hydrocarbons (N-tar compounds) and into N-solid char during initial pyrolysis reactions [29]. The N in N-tar compounds and N-solid char is released when the decomposition of N-tar compounds or char-gas reactions occur in the subsequent gasification reactions [24, 29, 32].

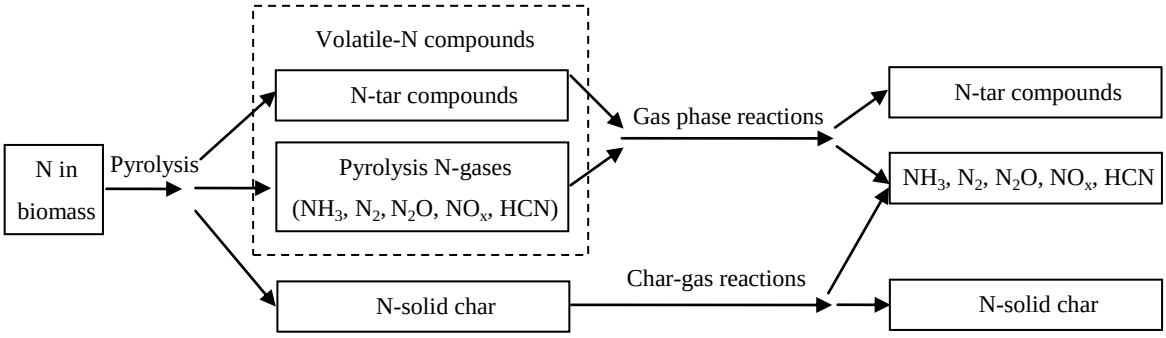

Figure 2.6 Formation and liberation of N-containing compounds in biomass gasification [33]

The N-containing gases from the biomass gasification process include ammonia (NH_3), molecular nitrogen (N_2), nitrogen oxides (NO_x), cyanides (-C≡N), thiocyanates $(SCN)^-$ and various N-tar compounds [29, 34]. The major N-containing compound in the producer gas is NH_3 [31, 34-38], however, Torres et al. [21] and Zhou et al. [30] reported that N_2 is also a major component, while the contents of hydrogen cyanide (HCN) and NO_x are much lower. The concentrations of each gas contaminant in the biomass gasification producer gas are summarised in Table 2.4 from previous studies for various biomass and different gasifier types. The NH_3 concentration in the producer gas from gasification of wood, with N content approximately below 0.5 wt%, generally ranges between 100 to 2,000 ppmv, whereas gasification of some other biomass feedstocks with high N content generates much higher NH_3 concentration reaching over ten thousand ppmv (Table 2.4).

From Table 2.4, it can be clearly seen that the NH_3 concentration in the producer gas from an updraft fixed-bed gasifier is lower than those from fluidised bed gasifiers including bubbling fluidised bed (BFB), circulating fluidised bed (CFB) and dual fluidised bed (DFB). The above observation has also been found in peat gasification by Leppälahti et al. [32], who reported that a significant proportion of N in the feedstock is bound in the N-tar compounds in the producer gas using an updraft gasifier. However, for fluidised bed gasifiers operated at a significant higher temperature, the N-tar compounds are decomposed and liberated to form NH_3, HCN and N_2 [32]. In the same type of the gasifier, the amount of the total N-containing compounds generated in the gasification process depends

dominantly on the N content in the biomass and the gasification operation conditions [21, 29-31, 39-44].

According to Zhou et al. [30], NH_3 and N_2 are the major species evolved from fuel-bound N in biomass during oxygen-blown gasification, whereas HCN and NO are produced at very low concentrations. In this study, more than 90% of the N in the biomass is transformed into NH_3 and N_2, where N_2 is proposed to be converted primarily from the thermo-chemical conversion of NH_3 [30]. In a separate study [38], it is reported that 60-80% of the biomass-bound N is converted to NH_3.

Compared to the NH_3 concentration, the HCN concentration is much lower in the biomass gasification producer gas [21, 29, 30, 34, 38, 45]. The concentration of NH_3 in the producer gas from a bench-scale oxygen-blown fluidised bed gasifier was found to be 2-3 orders of magnitude higher than that of HCN [30]. However, the concentration of NH_3 was measured to be about 30 times higher than HCN in a small pressurised fluidised bed gasifier with air and steam as the gasifying agents [35]. For air-blown biomass gasification, the concentration of NH_3 in the Lurgi atmospheric pressure CFB gasifier was found to be about 25 times higher than that of HCN [46].

Finally, for N-tar compounds, they were found in extremely low concentrations in the biomass producer gas [47-49]. N-tar compounds that have been reported in the literature include pyridine (C_5H_5N), pyrrole (C_4H_5N), quinoline (C_9H_7N), quinazoline ($C_8H_6N_2$), isoquinoline (C_9H_7N), benzoquinoline ($C_{13}H_9N$), indole (C_8H_7N), 2-methylpyridine (C_6H_7N), 3-methylpyridine (C_6H_7N), and 4-methylpyridine (C_6H_7N) [12, 29, 47-49].

Table 2.4 Measured N-containing gases in biomass producer gas from various biomass feedstocks and different gasification processes

Gasifier type	**Updraft fixed-bed**	**Downdraft fixed-bed**	**Bubbling fluidised bed (BFB)**						**Pressurised fluidised bed**
Gasifier size	n.r.[a]	Pilot-scale (120 kWth)	Small-scale pilot plant			Pilot-scale (800 kWth)		Bench-scale	Bench-scale	Small-scale (400 kWth)
Biomass type	Wood	Wood and almond shells	Mixture of residue from olive oil production and small pine wood chips			Corn	Switchgrass	Leucaena, sawdust, bagasse and banagrass	Leguminous tree	Pine sawdust
Bed material	-	-	Raw olivine	Dolomite	Ni-olivine	n.r.[a]		Alumina beads	Alumina beads	n.r.[a]
Gasification pressure (MPa)	0.1	n.r.[a]	0.1			0.1		Exceeds atmospheric	0.1	0.4
Gasification temperature (°C)	n.r.[a]	850	827-879			735-790	735	700-950	800	745-815
Gasification agent	Air and steam	Air	Air			n.r.[a]		Oxygen	Steam and N_2	Air and steam
N in biomass (wt%)	0.1[b]	0.1-0.4	0.10-0.30[b] for wood chips, 1.1-1.5[b] for olive oil residue			1.0[c]	0.5[c]	0.03-2.51[b]	0.31[b]	0.1[b]
NH_3 (ppmv)	120-160	200-800 mg/L	910-1,200	2,490-3,200	1,975	3,200-5,500 µg/L	1,400 µg/L	400-31,240	2,662 ± 484[e] (N_2 free)	450-950
HCN (ppmv)	210-500	0-600 mg/L	n.r.[a]			n.r.[a]		30-55	n.r.[a]	10-30
N_2 (vol%)	n.r.[a]	n.r.[a]	n.r.[a]			n.r.[a]		0.95-1.67	n.r.[a]	n.r.[a]
NO_x (ppmv)	n.r.[a]	n.r.[a]	n.r.[a]			n.r.[a]		NO = 5-150	NO = 8.3	n.r.[a]
Reference	[29]	[50]	[51]			[52]		[30]	[48, 53]	[34, 35, 54]

Table 2.4 (continued)

Gasifier type	**Circulating fluidised bed (CFB)**								**Dual fluidised bed (DFB)**			
Gasifier size	Pilot plant (2 MWth)	Small-scale pilot plant			Bench-scale (500 kWth)				Demonstration plant (8 MWth)			Lab-scale MILENA (25 kWth)
Biomass type	Wood chips	Mixture of residue from olive oil production and small pine wood chips			Willow	Demolition wood	Park and public garden wood	Park wood (bio-dried)	Wood pellets		Untreated wood chips	Wood
Bed material	n.r.[a]	Sintered olivine	Raw olivine	Dolomite	Sand				Olivine	Calcite	n.r.[a]	n.r.[a]
Gasification pressure (MPa)	0.1	0.1			0.1				Closes to atmospheric		Closes to atmospheric	n.r.[a]
Gasification temperature (°C)	700-820	850-855			827	847	861	805	841	645	850-900	800
Gasification agent	Air	Air			Air				Steam		Steam	Steam
N in biomass (wt%)	0.1[d]	0.10-0.30[b] for wood chips, 1.1-1.5[b] for olive oil residue			0.88[b]	0.46[b]	0.26[b]	1.16[b]	0.12[b]		0.22[b]	n.r.[a]
NH_3 (ppmv)	26[e]	2,370-5,000	460-1,650	1,950-2,275	1,800[e]	2,100[e]	1,300[e]	3,100[e]	882	789	1,100-1,700[e]	500-1,000[e]
HCN (ppmv)	1[e]	n.r.[a]			n.r.[a]				n.r.[a]		n.r.[a]	n.r.[a]
N_2 (vol%)	47.7[e]	n.r.[a]			n.r.[a]				n.r.[a]		1.2-2.0[e]	1-4[e]
NO_x (ppmv)	n.r.[a]	n.r.[a]			n.r.[a]				n.r.[a]		n.r.[a]	n.r.[a]
Reference	[46]	[51]			[55]				[56]		[57, 58]	[9, 59]

[a] Not reported, [b] Dry basis, [c] As-received basis, [d] Dry ash free basis, [e] Dry gas basis

2.4.4.4 Sulphur-containing compounds

In the gasification process, sulphur in the feedstock is converted to mainly H_2S and to minor quantities of carbonyl sulphide (COS), carbon disulphide (CS_2), S-containing aromatic hydrocarbons (S-tar compounds), and S-solid char [11, 12, 48]. Sulphur content in woody biomass and in herbaceous crops is typically less than 0.1 wt% and between 0.3 and 0.4 wt%, respectively [10]. The H_2S concentration in the producer gas from most biomass feedstocks is on the order of 100 ppmv [21, 25].

The concentration of H_2S in the range of 20-230 ppmv was found in the producer gas from gasification of four different biomass types in a 500 kW_{th} atmospheric air-blown CFB gasifier [55]. In a 8 MW_{th} DFB steam gasifier in Guessing, Austria, H_2S concentration from gasification of untreated wood chips was measured to be about 130-170 ppmv [58]. Furthermore, H_2S of 40-100 ppmv was measured in the producer gas from wood gasification from a so-called MILENA biomass gasification technology, developed by the Energy research Centre of the Netherlands (ECN) [9]. In the producer gas from gasification of various woody biomass types, H_2S concentration generally varied from 20 to 230 ppmv [26]. The H_2S concentration produced in the gasification process depends on feedstock types, gasifier design parameters, and process operation conditions [26]. Pinto et al. [60, 61] studied co-gasification of coal and two different biomass wastes (pine wood and olive oil bagasse) with a mixture of steam and oxygen or steam and air in a BFB gasifier operated at 850-900°C and atmospheric pressure. They found that, regardless of the types of tested feedstocks, H_2S release was dependent on the S content in which the feedstock with higher S led to higher concentration of H_2S [60, 61]. Additionally, S-tar compounds such as thiophene (C_4H_4S), benzothiophene (C_8H_6S), and dibenzothiophene ($C_{12}H_8S$) were found only in small amounts [12, 48].

2.4.5 Types of gasifiers

The biomass gasification process is operated in a gasification reactor or a gasifier. Types of gasifiers can be categorised based on (1) gasifying agent; (2) heat for gasification; (3) gasifier pressure; (4) ash production; and (5) reactor design [15]. These are described below.

Gasifier type based on gasifying agent:

- Air-blown gasifier
- Oxygen-blown gasifier
- Steam gasifier

Gasifier type based on heat for gasification:

- Autothermal or direct gasifier - heat is supplied by partial combustion of the biomass
- Allothermal or indirect gasifier - heat is supplied via external heat exchanger or circulating bed materials between combustion and gasification zones.

Gasifier type based on gasification pressure:

- Atmospheric
- Pressurised

Gasifier based on ash production:

- Slagging
- Non-slagging

Gasifier based on reactor design (schematic diagrams of different gasifiers are shown in Figure 2.7):

- Fixed-bed
- Fluidised bed
- Circulating fluidised bed
- Entrained flow

More details of gasifiers based on reactor design can be found in the literature on biomass and coal gasification [8, 15, 62]. In this research project, a dual fluidised bed (DFB) steam gasifier was used in the experimentation on biomass gasification, and therefore basic concept and comprehensive details of the DFB steam gasifier are given in Section 2.5.

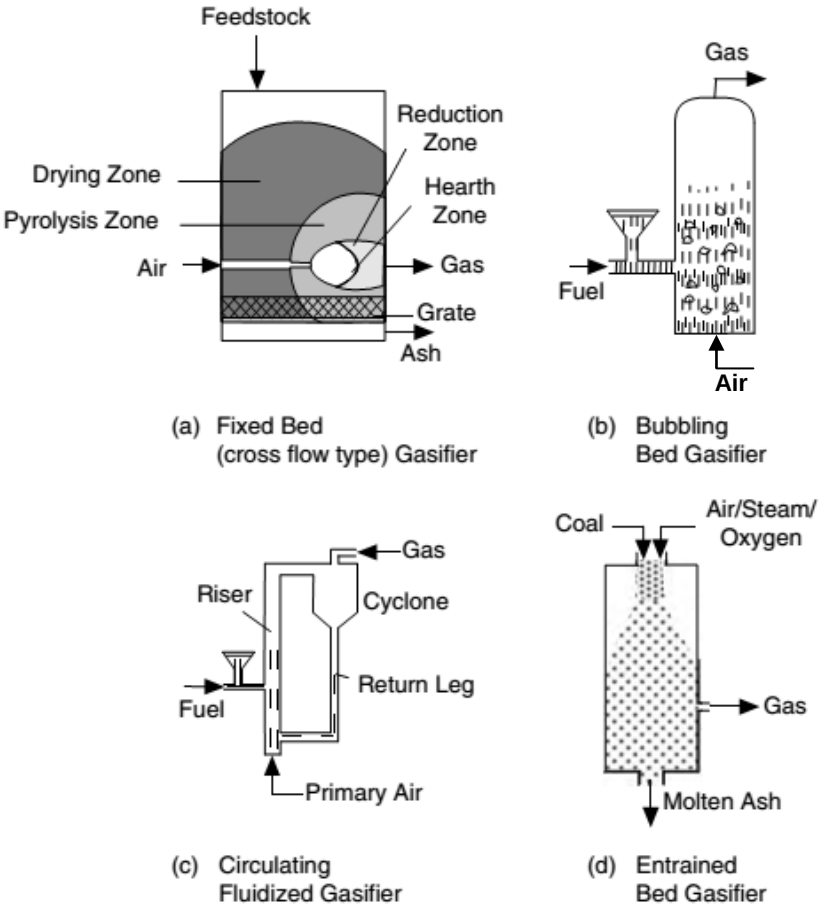

Figure 2.7 Different gasifier types based on reactor design [27]

2.5 Dual fluidised bed steam gasifier at University of Canterbury

The dual fluidised bed (DFB) steam gasifier, also known as a Fast Internally Circulating Fluidised Bed (FICFB) gasifier, developed at the Department of Chemical and Process Engneering (CAPE) at the University of Canterbury, is used in this research for the production of producer gas for FT liquid fuel synthesis. The DFB steam gasifier is operated at high temperature and atmospheric pressure.

CAPE's DFB steam gasifier consists of two main parts: a fast fluidised bed (FFB) chamber for combustion of solid char and a bubbling fluidised bed (BFB) chamber for actual gasifying of the feed biomass (the so-called gasification zone). The basic concept of the DFB steam gasifier is shown graphically in Figure 2.8. The exothermic reactions in the combustion zone provide the energy for the endothermic gasification reactions with steam

by the circulation of a heat-carrying bed material [57, 63, 64]. The bed material with a high heat capacity (typically silica sand) acts as a heat-transfer material and is circulated between these two chambers for supplying heat from the combustion of the solid char and specified grade of liquid petroleum gas (LPG) in the FFB combustion reactor to the BFB gasification reactor. Therefore, the bed material at the exit of the combustion zone has higher temperature than at the entrance. The flue gas from combustion and the producer gas from gasification are separated by a siphon and a chute, where a barrier is created by the bed material flow. Instead of inert material like silica sand, a catalytic bed material can also be used to transfer heat while simultaneously stimulating steam gasification reactions and reforming methane and tars to modify the compositional ratio of the producer gas (H_2/CO). With this concept, high-quality producer gas free of nitrogen can be produced without the use of pure oxygen. Details of the DFB steam gasifier's design, construction, modification, and operating instructions can be found from Bull [65] and McKinnon [66].

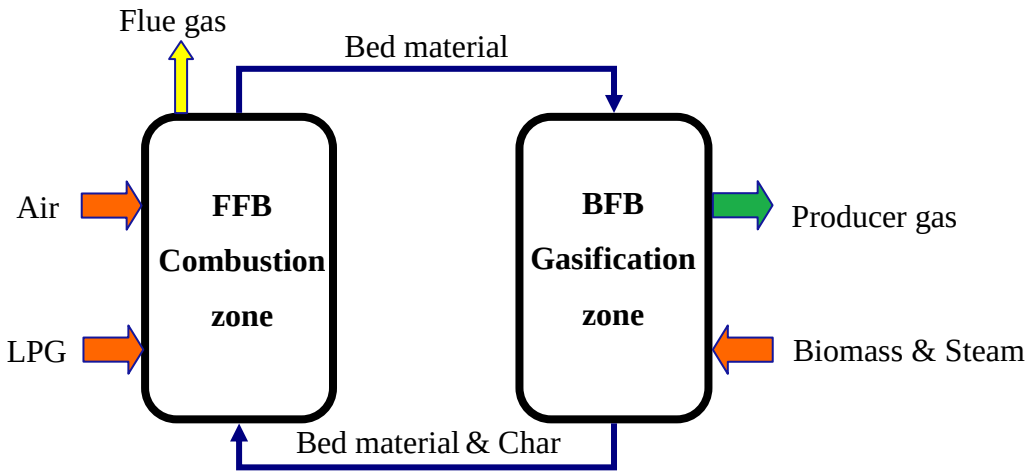

Figure 2.8 Basic concept of the DFB steam gasifier (reproduced from [57, 63, 64])

2.6 Fischer-Tropsch liquid fuel synthesis

This section gives the background to the FT liquid fuel synthesis, the feed gas requirements and specifications for the FT liquid fuel synthesis, which will lead to the gas cleaning technology presented in Sections 2.7 to 2.9. Gas cleaning technology is required for purification of the biomass producer gas to match the gas specifications for the FT liquid fuel synthesis.

2.6.1 Background of Fischer-Tropsch synthesis

FT liquid fuel synthesis was originally discovered in the 1920's by the German scientists Franz Fischer and Hans Tropsch. FT liquid fuel synthesis is a collection of catalytic reactions that converts a mixture of H_2 and CO (ideally H_2/CO molar ratio of 2) into long chain liquid hydrocarbons. The reactions occurred in the FT reactor are complex, but they can be simplified as the following chemical reactions (Equations 2.10-2.13) [67, 68]:

Paraffin production:	$(2n+1)H_2 + nCO \rightarrow C_nH_{2n+2} + nH_2O$	(2.10)
Olefin production:	$2nH_2 + nCO \rightarrow CH_3[(CH_2)_{n-3}]CH=CH_2 + nH_2O$	(2.11)
Alcohol production:	$2nH_2 + nCO \rightarrow C_nH_{2n+2}O + (n-1)H_2O$	(2.12)
Water-gas shift reaction:	$CO + H_2O \leftrightarrow CO_2 + H_2$	(2.13)

The products of the catalytic FT liquid fuel synthesis are mainly paraffin straight-chain hydrocarbons with minor amounts of branched and unsaturated hydrocarbons, and primary alcohols. The FT products can be also classified based on the number of C atoms as: light hydrocarbons (C1-C2); LPG (C3-C4); naphtha (C5-C11); diesel (C12-C20); and wax (>C20) fractions [11]. Therefore, Equation 2.10 is the main reaction required for liquid diesel synthesis.

The FT reactor is typically operated at 200-250°C and 25-60 bar, and it requires the use of a catalyst to enhance the chemical reaction rates [11]. Various catalysts have been researched for the FT liquid fuel synthesis such as nickel (Ni), ruthenium (Ru), palladium (Pd), cobalt (Co), and iron (Fe)-based catalysts. However, only Fe and Co catalysts are feasible and applied at commercial scales [67]. Properties of the Fe and Co catalysts are compared and summarised in Table 2.5. In general, Co catalysts are more active and give higher conversion rates than Fe catalysts [11, 67]. The FT products from Co catalysts contain less unsaturated hydrocarbons and alcohols compared to Fe catalysts. Co catalysts have a long lifetime of more than five years, whereas Fe catalysts are generally limited to eight weeks in commercial installations [11]. However, under the circumstances of feed gas with high sulphur concentrations and low H_2/CO molar ratio, Fe catalysts can be more attractive as they are less sensitive to sulphur poisoning and they catalyse the water-gas shift reaction (Equation 2.13) to produce more H_2. Besides, Fe catalysts are much cheaper than Co

catalysts, and therefore the Fe catalysts can be replaced regularly when they are deactivated by sulphur [11, 67].

Table 2.5 Comparison of advantages and disadvantages between Fe and Co catalysts

Properties	**Fe catalysts**	**Co catalysts**
Catalytic conversion rate	Lower conversion rate	Higher conversion rate
Catalyst lifetime	Shorter	Longer
Tolerance to sulphur poisoning	Higher tolerance	Less tolerance
Cost of catalysts	Cheaper	More expensive
Catalytic activity for water-gas shift reaction	Active for water-gas shift reaction	No catalytic activity for water-gas shift reaction

2.6.2 Gas requirements for Fischer-Tropsch synthesis

Gas contaminants in the producer gas cause problems with downstream equipment such as blockage of pipelines and vessels, catalyst deactivation, and side reactions in the synthesis reactors. For the utilisation of producer gas, contaminants must be removed to match with the feed gas specifications of the downstream applications. In FT liquid fuel synthesis, the catalysts are intrinsically very sensitive to small amounts of contaminants which cause catalyst deactivation or poisoning. According to the feed gas specifications for FT liquid fuel synthesis (Table 2.6), the producer gas requires the removal of at least the primary contaminants including particulates, tars, nitrogen-containing compounds, sulphur-containing compounds, halogens, and alkali metal compounds.

Particulates or solids consisting of soot, dust, and ash must be purified essentially completely to prevent plugging and fouling of pipes, tubes, and other equipment [11]. Concentrations of organic constituents or tars are not limited regarding the deactivation of the FT synthesis catalysts, but tar concentrations must be below the dew point at FT synthesis pressure (25-60 bar) to prevent tar condensation and fouling. However, class 2 tars with S or N hetero atoms such as thiophene (C_4H_4S) and pyridine (C_5H_5N) must be removed to below 1 ppmv because they intrinsically poison the FT synthesis catalysts [11].

For total N- or S-compounds, their limits of no more than 1 ppmv are recommended due to catalyst deactivation. As the acceptable concentrations of N-containing compounds (mainly NH_3) and S-containing compounds (mainly H_2S) in the FT liquid fuel synthesis are much lower than those in the raw producer gas, the NH_3 and H_2S must be removed from the producer gas before feeding into the FT synthesis reactor. Finally, total alkaline metal compounds and halogen compounds should be less than 10 ppbv [11].

Table 2.6 Fischer-Tropsch feed gas specifications [11]

Impurity	**Removal level**
Total nitrogen compounds (NH_3 + HCN)	< 1 ppmv
Total sulphur compounds (H_2S + COS + CS_2)	< 1 ppmv
Total halogen compounds (HCl + HBr + HF)	< 10 ppbv
Alkaline metals	< 10 ppbv
Solids (soot, dust, ash)	essentially completely
Organic compounds[a] (tars)	Below dew point
Class 2[b] (hetero atoms)	< 1 ppmv
CO_2, N_2, CH_4, and larger HCs (= inert)	< 15%vol

[a] Organic compounds include also benzene, toluene, and xylene (BTX)

[b] Class 2 tars comprise phenol, pyridine, and thiophene

There are some other undesired products in the producer gas that need to be removed for FT liquid fuel synthesis including CO_2, N_2, CH_4, aliphatic hydrocarbons (C_xH_y) larger than methane, and benzene. Considering the economic issues, the maximum total concentration of CO_2, N_2, CH_4, and larger hydrocarbons, considered as inert gases in the FT liquid fuel synthesis, is suggested to be 15 vol% [11].

The presence of inert gases requires larger reactors and higher total gas pressures leading to higher overall costs [11]. Moreover, these inert gases reduce overall conversion efficiencies for the FT liquid fuel synthesis [10]. The removal of CO_2 can be conducted by standard technologies, but the removal of N_2 and light hydrocarbons cannot be operated at reasonable costs. Therefore, high concentrations of N_2 and light hydrocarbons in the producer gas should be avoided, especially the unsaturated (olefin) hydrocarbons [11].

Ethylene, an unsaturated (olefin) hydrocarbon which could be present in significant concentration, is considered as a very active component. Ethylene might be hydrogenated or re-inserted on the catalyst surface to react further in the FT chain-growth reactions, resulting in a slightly different product distribution and hydrogen consumption compared to typical feed gas suitable for FT liquid fuel synthesis [11].

2.7 Concept of primary and secondary measures for NH_3 and H_2S removal

This section provides a review of the gas removal technologies used for elimination or removal of NH_3 and H_2S in the biomass gasification process for FT liquid fuel synthesis. NH_3 and H_2S can be removed from the biomass gasification process by primary and secondary measures, which is a similar approach as for tar removal from the producer gas proposed by Devi et al. [69] and Kiel et al. [70]. The concept of primary and secondary measures is given in Figure 2.9. The primary measures are methods employed in the gasifier to reduce NH_3 and H_2S concentrations or convert NH_3 and H_2S to other less harmful gases and the secondary measures are downstream treatment methods after the gasifier to reduce or clean up NH_3 and H_2S from the producer gas.

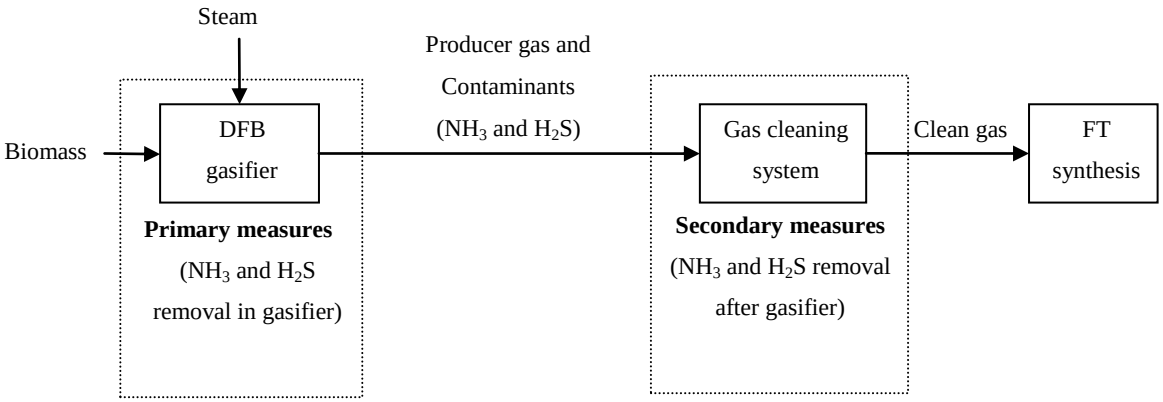

Figure 2.9 Diagram of the primary and secondary measures for removal of contaminants in biomass producer gas (adapted from [69])

2.8 Primary measures for NH_3 and H_2S removal

The primary measures undertaken in the gasification process for reduction of NH_3 and H_2S include:

(1) Optimisation of the gasification operation parameters, which can influence the NH_3 concentration in the producer gas, and these parameters are:
(a) gasifier bed temperature in fluidised bed gasification;
(b) freeboard temperature in fluidised bed gasification;
(c) operation temperature in entrained flow gasification;
(d) operation pressure;
(e) steam to fuel (S/F) ratio in steam gasification;
(f) equivalence ratio (ER) and gasification ratio; and
(g) biomass type.

(2) Application of catalytic bed materials in the fluidised bed gasifier.

2.8.1 Optimisation of the gasification operation parameters for NH_3 removal

Several key operation parameters in biomass gasification have been studied for their influence on the NH_3 formation and NH_3 concentration in the producer gas. These operation parameters include gasifier bed temperature and freeboard temperature in fluidised bed gasification, operation temperature in entrained flow gasification, operation pressure, S/F ratio in steam gasification, ER, gasification ratio and biomass type. A summary of the influence of gasification operation parameters on NH_3 concentration in the producer gas from published research is shown in Table 2.7.

2.8.1.1 Gasifier bed temperature in fluidised bed gasification

Gasifier bed temperature in a bench-scale indirectly-heated fluidised bed gasifier strongly affects the NH_3 concentration in the producer gas from oxygen-blown gasification of two types of biomass feedstocks (leucaena and sawdust) [30]. It was found that the increase of gasifier bed temperature resulted in reduction of NH_3 concentration in the producer gas. For example, in the gasification of sawdust containing 0.03 wt% N, the concentration of NH_3 was decreased from 950 to 400 ppmv as the gasifier bed temperature was increased from

700 to 900°C [30]. The same trend has also been reported with leucaena as a biomass feedstock, which has a much higher N content of 2.51 wt%. The NH_3 concentration decreased sharply from 31,240 ppmv at 750°C to 6,060 ppmv at 900°C [30]. However, Farzam et al. [71] reported that the effect of bed temperature over the range of 795 to 980°C on the NH_3 production rate was insignificant in the steam-oxygen pressurised gasification of lignite and subbituminous coal in a pilot-scale fluidised bed gasifier. Furthermore, Vriesman et al. [72] found that in an air-blown atmospheric pressure fluidised bed gasifier, the conversion of fuel-bound N in the biomass to NH_3 increased when temperature increased from 700 to 800°C, but the influence was insignificant and only limited data were reported.

2.8.1.2 Freeboard temperature in fluidised bed gasification

Freeboard height is defined as the distance between the top of the fluid bed and the gas-exit position in a bubbling- or turbulent-fluidised bed unit, where the solid particles disengage from the gas [8, 73]. This term has been adopted in the fluidised bed gasifier. Freeboard temperature in fluidised bed gasification can be increased by the addition of secondary air introduced above the fluidised bed in air gasification [34, 49]. Kurkela and Ståhlberg [34] and Leppälahti and Kurkela [49] have reported that the freeboard temperature slightly influenced the NH_3 concentration in the producer gas.

The concentration of NH_3 in the producer gas increased when the freeboard temperature was increased from 820°C to 940°C in an air-blown atmospheric pressure fluidised bed gasifier for gasification of crushed peat pellets [49]. However, the effect of the freeboard temperature on NH_3 concentration was insignificant [29, 49]. In another study of Kurkela and Ståhlberg [34] on gasification of various fuel feedstocks of pine sawdust, crushed peat pellets, and brown coal in a small pilot air-blown pressurised fluidised bed gasifier, the freeboard temperature was increased from 800°C up to 1,000°C. The NH_3 concentration was found to decrease slightly with increasing freeboard temperature for all the fuel feedstocks tested [34]. The contrary results are believed to be due to the effect of operation pressure, which will be discussed in Section 2.8.1.4. In addition, the effect of the freeboard temperature is a complex process. With the increase in freeboard temperature in a pressurised fluidised bed gasifier, the conversion of N in the biomass into N-tar compounds

and N-solid char decreased, while the conversion into HCN increased. The increase in the HCN content was believed to be contributed to the gas phase reactions of NH_3 or the release of N-solid char [34]. Moreover, from the results of Kurkela and Ståhlberg [34], it is found that N-tar compounds were decreased while the HCN content was increased. The increase in the HCN content is believed to be from the cracking of N-tar compounds.

Wang et al. [39] conducted experimental studies at a pilot-scale air-blown fluidised bed gasifier under the pressure of 0.5-2.0 MPa, and they found that the conversion of N-bound biomass to NH_3 was low at high freeboard temperature. Therefore, for pressurised gasification, higher freeboard temperature resulted in lower NH_3 concentration in the producer gas.

The effect of freeboard temperature on the N conversion has been investigated based on fundamental kinetics of gas-phase reactions, from which the rate of NH_3 decomposition in the gasifier is found to be negligible at a high temperature of 1,200°C [35]. It was, therefore, believed that the influence of temperature on NH_3 conversion could be due to the heterogeneous reactions, where char particles in the gasifier may act as catalyst for the decomposition of NH_3 [35].

There was an opposite trend on the influence of freeboard temperature between air-blown fluidised bed gasification at atmospheric pressure and at high pressure. At atmospheric pressure, the increase of the freeboard temperature would lead to a slight increase in NH_3 concentration in the producer gas. However, for pressurised gasification, the high freeboard temperature in the gasifier reduces the NH_3 concentration in the producer gas, to a certain extent. Due to the limited publications on this topic, further investigation is needed to confirm and explain the effect of the freeboard temperature.

2.8.1.3 Operation temperature in entrained flow gasification

In pressurised entrained flow air gasification of various types of coal, it was reported that the high operation temperature used resulted in lower conversion of N-bound fuel to NH_3 [35]. At gas temperature above 1,100°C, the conversion of N-bound fuel to NH_3 was below 20% [35]. Operation temperature higher than 900°C is commonly applied in entrained flow

and downdraft gasifiers, but the higher operation temperature is expected to reduce the concentration of NH_3 further in the producer gas. The effect of high temperature on NH_3 reduction probably attributes to the thermal decomposition of NH_3.

2.8.1.4 Operation Pressure

In the report of Kurkela and Ståhlberg [34], higher conversion of N in peat to NH_3 was found in pressurised gasification than at atmospheric pressure with the similar N content in the feedstocks. This finding was confirmed by separate studies, in which NH_3 concentration in peat gasification producer gas from an air-blown pressurised fluidised bed gasifier (0.5 MPa) was found to be higher than those from an air-blown atmospheric pressure fluidised bed gasifier [24, 32, 49]. In contrast to NH_3 concentration, the HCN concentration was found to be lower in pressurised gasification than in atmospheric pressure gasification [34]. The reason for these findings is still unclear [34, 49]. However, in some cases, the effect of pressure is insignificant over the range of 0.4 to 1.0 MPa. For example, in the study of Farzam et al. [71] with steam-oxygen pressurised gasification of lignite and subbituminous coal in a pilot-scale fluidised bed gasifier, it was found that pressure had no measureable effect on the production rates of NH_3 over the range from 0.77 to 0.83 MPa. Another study conducted by Kurkela and Ståhlberg [34] also proved that the pressure level did not show significant influence on the NH_3 concentration in the producer gas with varying pressure in the range of 0.4 to 1.0 MPa in air-blown gasification of peat or brown coal.

2.8.1.5 Steam to fuel ratio in steam gasification

In steam gasification, the S/F ratio in a pressurised fluidised bed gasifier seemed to have no measureable effect on the NH_3 concentration in the producer gas from gasification of sawdust, peat, or coal [29, 34, 71]. In a study on steam-oxygen pressurised gasification of lignite and coal, it was found that the molar ratio of steam to carbon feed within a range of 0.99 to 2.27 had insignificant effect on the NH_3 concentration [71]. In another study on the steam-air gasification of sawdust, varying the weight ratio of steam to dry ash free sawdust between 0.08-0.34 resulted in no measureable effect on the NH_3 concentration [29, 34]. From the above studies, no consistent correlation was obtained between S/F ratio and the NH_3 concentration in the producer gas.

2.8.1.6 Equivalence ratio and gasification ratio

The ER is defined as the fed oxygen-to-fuel ratio (mass basis) in the air or oxygen gasification process divided by the stoichiometric oxygen-to-fuel ratio for complete combustion [30, 74]. Previous studies tend to suggest that the NH_3 concentration in the biomass gasification producer gas increased with the ER [31, 41, 50, 72]. Vriesman et al. [72] and Berg et al. [31] found that the increase of the ER from 0.1 to 0.3 in the air-blown atmospheric pressure fluidised bed gasifier at temperatures of 700-800°C increased the conversion of fuel-bound N in the biomass to NH_3. Furthermore, Wang et al. [41] reported that the high ER increased the fuel-bound N conversion and subsequently increased the NH_3 concentration in an air-blown pressurised fluidised bed gasifier. However, experiments by Zhou et al. [30] in an oxygen-blown gasifier operated at above 800°C have shown that the influence of the ER varying from 0.18 to 0.32 had insignificant influence on the NH_3 concentration in the producer gas.

A study conducted by De Bari et al. [50] found that the NH_3 concentration in the producer gas was dependent on gasification ratio (air-to-fuel ratio), which is the relative amount of air injected into the gasifier with respect to the loaded biomass [50]. Within the gasification ratio from about 1.3 to 2.5 Nm^3/kg investigated for air-blown gasification at 850°C in a downdraft fixed-bed gasifier, the NH_3 concentration in the producer gas increased from 250 to 500 mg/L for woody biomass and from 400 to 800 mg/L for almond shells. In the same study of De Bari et al. [50], when the gasification ratio increased from about 1.3 to 2.5 Nm^3/kg, the HCN concentration decreased from 300 mg/L (woody biomass) and 600 mg/L (almond shells) to non-detectable level, which was in comparable value for the increase of NH_3 [50]. This behaviour was proposed to be due to the oxidation of cyanide by oxygen in air followed by the generation of NH_3 [50].

2.8.1.7 Biomass type

The type of fuel feedstock for the gasification, or more specifically the N content of the feedstock, has a strong impact on the concentration of NH_3 in the producer gas [30, 39, 41, 44, 50]. As shown in Figure 2.10, the concentration of NH_3 in the producer gas from an air-blown atmospheric pressure fluidised bed gasification increased from 900 ppmv with

bagasse as the gasification feedstock (0.12 wt% N, dry basis) to 1,700 ppmv for treated banagrass as the gasification feedstock (0.44 wt% N, dry basis) [44].

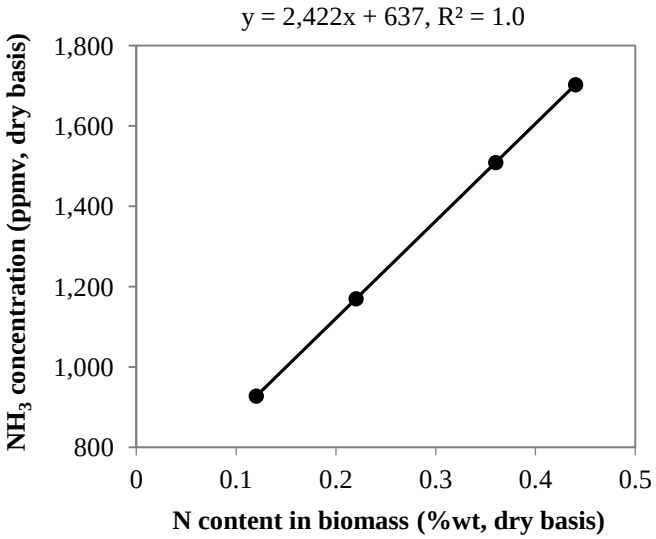

Figure 2.10 NH_3 concentration in the producer gas from air gasification of various biomass feedstocks with different N contents [44]

In a similar study on oxygen-blown fluidised bed gasification, Zhou et al. [30] reported that the NH_3 concentration in the producer gas increased from about 400 ppmv for gasification of sawdust (0.03 wt% N, dry basis) to about 18,000 ppmv for gasification of leucaena (2.51 wt% N, dry basis). The results from the study of Zhou et al. [30] are shown in Figure 2.11, which are consistent with the results presented in Figure 2.10.

Furthermore, Wang and Olofsson [41] and Wang et al. [39] performed experimental studies in a pilot-scale air-blown pressurised fluidised bed gasifier for gasification of sawdust and blends of sawdust and solid waste. They found that the NH_3 concentration in the producer gas from gasification of sawdust (with a low N content of 0.2 wt%) was 300 to 400 ppmv, which was much lower than that (6,000 ppmv) from gasification of blends of sawdust and solid waste, which had N content of 1.5 wt%. Finally, De Bari et al. [50] found that at the same gasification condition operated in an air-blown downdraft gasifier, the NH_3 concentration for almond shells was almost 2-fold of that for woody biomass, in which the N content in almond shells (0.4 wt%) was 4-fold of that in woody biomass (0.1 wt%).

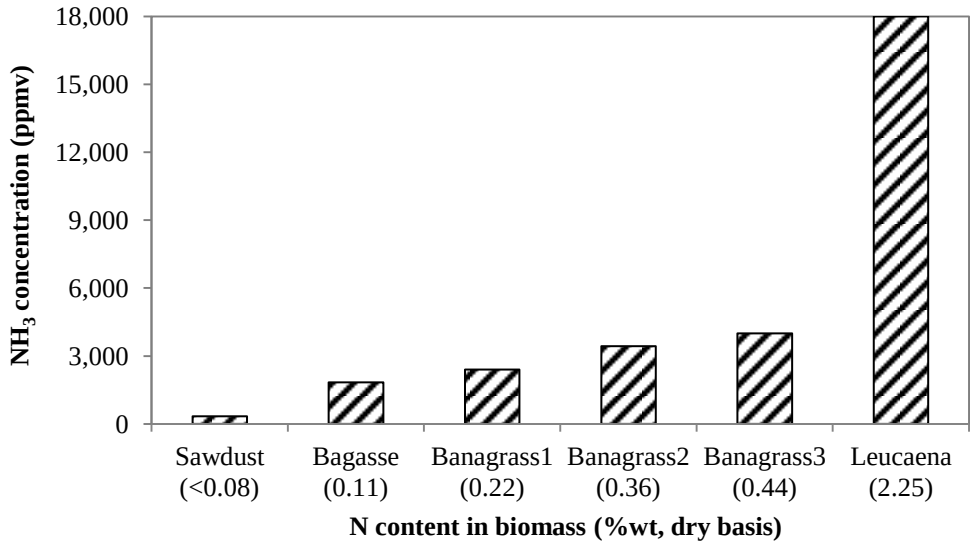

Figure 2.11 NH_3 concentration in the producer gas from air gasification of various biomass feedstocks with different N contents [30]

In the summary as shown in Table 2.7, in order to reduce the NH_3 concentration in the producer gas from biomass gasification, the gasifier should be operated at a high bed temperature of more than 900°C at atmospheric pressure. For pressurised gasification, high free board temperature is necessary and the increase in the operation pressure does not appear to affect the NH_3 concentration. Moreover, it seems that S/F ratio in steam gasification has no significant influences on the NH_3 concentration. However, the increase in the ER and the gasification ratio for air gasification tends to increase the NH_3 concentration in the producer gas. All of the reviewed studies show that the NH_3 concentration in the producer gas is positively related to the amount of N in the feedstock. Therefore, the biomass feedstock with higher N content generates more NH_3 in the producer gas.

Table 2.7 Summary of the influence of gasification operation parameters on NH_3 concentration in the producer gas [33]

With increase of these gasification operation parameters	**Steam-oxygen pressurised gasification**	**Air-blown atmospheric pressure gasification**	**Air-blown pressurised gasification**	**Oxygen-blown atmospheric pressure gasification**
Gasifier bed temperature in fluidised bed gasification	Insignificant influence	Insignificant influence	Not available	Reduce NH_3
Freeboard temperature in fluidised bed gasification	Not available	Insignificant influence	Reduce NH_3	Not available
Gasifier temperature in entrained bed gasification	Not available	Not available	Reduce NH_3	Not available
Operation pressure	Insignificant influence	-	Insignificant influence	-
S/F ratio in steam gasification	Insignificant influence	-	-	-
ER and gasification ratio	-	Increase NH_3	Increase NH_3	Insignificant influence
Fuel-bound N content in Biomass	Not available	Increase NH_3	Increase NH_3	Increase NH_3

2.8.2 Optimisation of the gasification operation parameters for H_2S removal

Main operation parameters that have been found to influence the H_2S formation and concentration in the producer gas include gasifier temperature, S/F ratio in steam gasification, and ER.

2.8.2.1 Gasifier bed temperature in fluidised bed gasification

In the study of Meng et al. [18], it was found that temperature in a CFB gasifier did not affect the H_2S concentration in the gasification of an agricultural residue with steam and oxygen. The residue (Dry Distiller's Grains with Solubles: DDGS) used in the study was a dry-grind process to produce ethanol from wheat, and it contained 0.76 wt% S [18]. H_2S concentration of about 200-225 ppmv was obtained when temperature was increased from 790 to 820°C [18]. Similarly, conversion (wt%) of fuel-S in cedar wood into H_2S was

found to be constant at 88% in a temperature range of 750-850°C. The cedar wood was gasified in a bench-scale externally heated updraft gasifier [75].

However, H_2S concentration and conversion increased with an increase of temperature from 720 to 850°C in co-gasification of coal (30 wt%) and refuse derived fuel (RDF) in a BFB gasifier with steam and oxygen as a gasifying agent [76]. The experimental results also showed that higher S content in the char was obtained at lower temperature. Therefore, it was concluded that higher temperature led to an increase release of volatiles and thus producing more H_2S in the producer gas and less S content in the solid fraction [76].

In thermodynamic equilibrium calculations performed by Kuramochi et al. [77], H_2S concentration at equilibrium was found to increase with temperature from 400 to 850°C. However, H_2S concentration in the biomass producer gas was stable when temperature was above 850°C, and it was proportional to the S content in the feedstock [77]. They also reported that metal sulphides such as FeS, ZnS, MnS, PbS, Ni_3S_2, and Cu_2S, were formed from the reactions of metal in the ash with S-compounds at low temperatures (400-850°C) [77]. The amount of metal sulphides was decreased with increasing temperature from 400 to 850°C, leading to higher H_2S concentration as more S was available for H_2S formation.

2.8.2.2 Steam to fuel ratio in steam gasification

Meng et al. [18] studied an effect of S/F ratio in a CFB gasifier for gasification of the DDGS agricultural residue with steam and oxygen using Austrian olivines (pre-treated and untreated olivines). They discovered that higher S/F ratio led to a significant decrease in H_2S concentration [18]. When pre-treated Austrian olivine was used as a circulating material, H_2S decreased from 2,700 to 1,800 ppmv with increasing S/F ratio from about 1.0 to 1.1 [18]. The same trend was also reported in a gasification of corn straw in a downdraft fixed-bed gasifier [19]. With an increase of S/F ratio from 0.8 to 1.6, H_2S concentration decreased gradually [19].

.

However, in an updraft gasifier operated at 850°C, conversion (wt%) of fuel-S in cedar wood into H_2S increased linearly as the steam to carbon ratio was increased from 0 to 2 [75]. However, conversion of fuel-S into COS decreased with increasing the steam to

carbon ratio. Therefore, it was postulated that an increase of H_2S conversion with the steam to carbon ratio was due to the reaction of COS with H_2O and COS with H_2 to produce H_2S, as shown in Equations 2.14 and 2.15.

$$COS + H_2O \rightarrow H_2S + CO_2 \quad (2.14)$$

$$COS + H_2 \rightarrow H_2S + CO \quad (2.15)$$

2.8.2.3 Equivalence ratio

Higher ER led to lower H_2S concentration when DDGS agricultural residue was gasified in a CFB gasifier with steam and oxygen [18]. However, in a separate study, stable concentration of H_2S (35-39 ppmv) was observed with ER between 0 and 0.3 in cedar wood gasification in an updraft gasifier [75]. Although the H_2S concentration was steady, the conversion of fuel-S to H_2S increased linearly from 81 to 92 wt% when ER was raised from 0 to 0.3 [75].

An increase of ER from 0 to 0.4 led to an increase of H_2S concentration (from 672 to 1,204 ppmv) and conversion and a decrease of S content in the solid char in co-gasification of coal (30 wt%) and RDF in a BFB gasifier with steam and oxygen at 850°C [76]. It was inferred that an increment of oxygen would lead to an increase of degradation of the solid matrix of the char from partial combustion reactions and thus S was more accessible to the H radicals generated from the presence of steam [76].

In the study of Gai et al. [19], who examined the effect of ER on the gasifier of corn straw in a downdraft fixed-bed gasifier, they reported that increasing ER led to an increase of temperature and influenced the H_2S concentration. With an increase of ER from 0.2 to 0.4, temperature was increased from 900 to 1,080°C, whereas H_2S concentration increased and dropped at any levels of S/F ratio [19]. They inferred from the study of Kuramochi et al. [77] for the explanation of the increase of H_2S concentration with increasing temperature at a lower temperature range as mentioned in Section 2.8.2.1. In contrast, the reduction of H_2S concentration with increasing the temperature in a higher temperature range was attributed to the neutralisation reactions between H_2S and alkali metals in the ash, as well as the

reactions shown in of Equations 2.16-2.18 [19]. Equations 2.16 and 2.17 are the reverse reactions of Equations 2.14 and 2.15, respectively.

$$H_2S + CO_2 \rightarrow COS + H_2O \quad (2.16)$$

$$H_2S + CO \rightarrow COS + H_2 \quad (2.17)$$

$$H_2S + 3/2O_2 \rightarrow SO_2 + H_2O \quad (2.18)$$

2.8.3 Application of in-bed catalytic decomposition of NH_3

Due to the high activation energy (385 kJ/mol) required for NH_3 decomposition reaction to its elements, N_2 and H_2 [78, 79], thermal decomposition of NH_3 is inefficient at typical operation temperatures of fluidised bed gasification, ranging from 800 to 950°C [34, 49]. Moreover, the rate of thermal decomposition of NH_3 is very slow at typical gasification conditions, although the equilibrium value of NH_3 is low [30, 35]. With the employment of suitable catalysts in the bed of the gasifier, the activation energy for NH_3 decomposition will be lowered, and therefore NH_3 can be decomposed at lower temperatures.

Extensive studies have been conducted to investigate the impact of adding various catalytic bed materials in the fluidised bed biomass gasifier on the NH_3 concentration in the producer gas [34, 49, 51]. The bed materials tested inside the gasifier include raw olivine ($(Mg, Fe)_2SiO_4$), sintered olivine (calcined at 1,500°C), calcined dolomite ($CaO{\cdot}MgO$) which was calcined at 900°C, Ni-olivine [51], raw dolomite ($CaCO_3{\cdot}MgCO_3$) [34, 49], and raw limestone ($CaCO_3$) [34].

Raw olivine was proven to have a higher catalytic activity for NH_3 reduction than calcined dolomite, which was pretreated in an oven for one hour at 900°C in an environment of absence of CO_2 [51, 80]. In the biomass gasification in a small-scale air-blown CFB gasifier, three bed materials (raw olivine, calcined dolomite, and sintered olivine) were tested at 850°C. The raw olivine was the most active followed by calcined dolomite and then by sintered olivine in regard to the NH_3 reduction in the producer gas [51]. In the same study conducted by Corella et al. [51], raw olivine, Ni-olivine (3.7 wt% Ni) and calcined dolomite were also compared as the bed materials in a small-scale air-blown BFB gasifier. The results showed that the raw olivine was the most active and the calcined dolomite was

the least active, while the Ni-olivine fell in the middle based on the NH_3 reduction in the producer gas.

To understand the catalytic effect of the bed materials, Corella et al. [51] suggested that the iron oxide (Fe_2O_3) content in the bed materials was not a determining parameter in the NH_3 concentration in the producer gas from biomass gasification [51]. This is because Fe_2O_3 catalysed the reaction of N_2 and H_2 to produce NH_3, but the calcined dolomite had much lower Fe_2O_3 content (0.12 wt%) than the raw olivine (7.5-8.5 wt%). In attempt to explain the experimental results, Corella et al. [51] suggested that the calcined dolomite was more active in cracking N-tar compounds than the raw olivine in the biomass gasification, resulting in more NH_3 from the N-tar compounds. This explanation is in accordance with the results of Leppälahti et al. [32], who stated that active catalysts for the tar removal such as dolomite and limestone can simultaneously liberate more NH_3 from cracking of N-tar compounds.

The experimental results showed that the calcined dolomite was less effective as a catalytic bed material for NH_3 reduction in the gasifier, which was confirmed by a separate study of Leppälahti and Kurkela [49]. In the study of Leppälahti and Kurkela [49], the raw dolomite was applied as the bed material and calcination was taken place in the bed of an air-blown atmospheric pressure fluidised bed gasifier for gasification of peat pellets. It was found that the NH_3 concentration in the producer gas was significantly increased, but the HCN content was reduced compared with no addition of dolomite. The increase of NH_3 concentration with application of the calcined dolomite may be explained by the following reactions (Equations 2.19 and 2.20), although these reactions need to be experimentally verified [49]:

$$CaO + 2HCN \rightarrow CaCN_2 + CO + H_2 \quad (2.19)$$

$$CaCN_2 + H_2O + 2H_2 + CO_2 \rightarrow CaO + 2NH_3 + 2CO \quad (2.20)$$

Another research by Kurkela and Ståhlberg [34] showed that neither dolomite nor limestone had noticeable effects on the NH_3 reduction for gasification of peat in a pressurised fluidised bed gasifier. In this study, raw dolomite and raw limestone were added into the bed at loadings of 2.5-3.5 wt% of the peat feed. The mixture of air and steam was used as the gasification agent.

In summary, olivine is a promising catalytic bed material in the fluidised bed gasifier as it showed higher catalytic activity for NH_3 reduction than calcined dolomite and limestone. Moreover, the olivine has a favourable property of more abrasion resistance and high hardness compared to calcined dolomite and limestone [51, 81]. Due to the turbulent nature in the fludised bed gasifier, the high hardness of the bed material is important to avoid the generation of fine particulates from the abrasion of and breaking down of the added catalytic bed material.

From the above discussion, the primary measures, the application of the optimisation of the operation conditions and the employment of catalytic bed materials can be implemented in the biomass gasifier to reduce NH_3 concentration in the producer gas. However, the primary measures may not be sufficient to reduce NH_3 concentration to a level which is complied with feed gas specifications for IGCC system [34, 41] and other downstream applications. The applications of the producer gas in FT liquid fuel synthesis and IGFC system require even lower levels of NH_3 concentration. Therefore, the development of the secondary measures for gas cleaning technologies is necessary, which are based on hot catalytic gas cleaning to decompose the NH_3 in the producer gas.

2.8.4 Application of in-bed desulphurisation of H_2S

The in-bed desulphurisation or adsorption of H_2S can be applied in the fluidised bed gasifier by the use of Ca-based adsorbents or sorbents, mainly limestone or dolomite [25, 82]. There are also some commercial Ca-based sorbents such as calcium acetate and calcium magnesium acetate that were found to have high desulphurisation efficiency [25]. The desulphurisation or sulphidation reactions involved limestone ($CaCO_3$) and dolomite ($CaCO_3{\cdot}MgCO_3$) are as follows:

Sulphidation reaction: $CaO + H_2S \leftrightarrow CaS + H_2O$ (2.21)

Sulphidation reaction: $CaO{\cdot}MgO + H_2S \leftrightarrow CaS{\cdot}MgO + H_2O$ (2.22)

Direct sulphidation reaction $CaCO_3 + H_2S \leftrightarrow CaS + CO_2 + H_2O$ (2.23)

Direct sulphidation reaction: $CaCO_3{\cdot}MgO + H_2S \leftrightarrow CaS{\cdot}MgO + CO_2 + H_2O$ (2.24)

Limestone ($CaCO_3$) is calcined to form CaO or remains uncalcined in the gasifier depending on the partial pressure of CO_2 [82]. As shown in Equations 2.22 and 2.24, with the use of dolomite ($CaCO_3{\cdot}MgCO_3$), $MgCO_3$ is calcined to MgO under gasification conditions, but the MgO does not react in the sulphidation reaction because MgS is an unstable compound under gasification conditions [25, 82-84]. Dolomite was found to have high desulphurisation efficiency in co-gasification of coal and wastes in a BFB gasifier using steam and oxygen as a gasifying agent at 850°C [61]. Comparing with various sorbents, dolomite showed the highest desulphurisation efficiency in the order of dolomite > Ni-dolomite > calcined olivine > natural olivine [61].

Limestone or dolomite is normally used in fluidised bed gasifiers in a once-through mode due to the fact that: (1) they are cheap and abundantly available; (2) they are relatively soft and easily broken up; and (3) they tend to form a stable sulphate layer during the regeneration process [25, 26]. Therefore, they require stabilisation and disposal of a large amount of $CaSO_4$. The Ca-based sorbents can remove only about 90% of sulphur in a reducing gas atmosphere of the gasifier due to thermodynamic limitation [82]. To meet the gas turbine requirement (<20 ppmv) or more stringent requirement of the FT liquid fuel synthesis (<1 ppmv), a downstream H_2S removal to polish the gas further is required.

2.9 Secondary measures or downstream gas removal of NH_3 and H_2S

Although it is desirable to eliminate NH_3 and H_2S at the source or in the gasifier, additional gas cleaning downstream of the gasifier is still required to remove the NH_3 and H_2S almost completely to obtain suitable gas for the FT liquid fuel synthesis. Details of various gas cleaning technologies for the removal of NH_3 and H_2S are discussed as follows:

The secondary measures or downstream gas cleaning for the NH_3 removal include [10, 12, 85]: (1) wet scrubbing or cold gas cleaning; and (2) catalytic decomposition of NH_3 or hot gas cleaning. The water scrubbing is a well-proven gas cleaning method and has been applied in the biomass gasification process, but it is considered to be uneconomically viable due to its high capital cost and energy loss in the process [85-87]. In addition, the wet scrubber system generates waste scrubbing liquid, which requires additional treatment for reuse or disposal [29].

On the other hand, the hot catalytic gas decomposition has attracted much attention recently, in which NH_3 is decomposed into N_2 and H_2 as shown in Equation 2.25 [88, 89]:

$$2NH_3 \leftrightarrow N_2 + 3H_2 \qquad \Delta H^{\circ}_{900°C} = 112 \text{ kJ/mol} \tag{2.25}$$

The decomposition reaction in Equation 2.25 is highly desirable because NH_3 is converted to H_2 and N_2, which can increase the calorific value of the producer gas, and it does not introduce additional contaminants into the producer gas. The hot catalytic method operates at high temperature, thus the sensible heat of the producer gas is not lost and the overall energy efficiency can be increased in the downstream applications such as IGCC [82, 90-92] and IGFC systems [86, 92]. Furthermore, the used catalysts in the hot catalytic reactor can be regenerated by a simple method [37, 79, 93-95]. Therefore, the hot catalytic method for removing NH_3 has been extensively investigated in recent years as one of the most promising technologies [37, 38, 82, 85, 90, 91, 93-97].

Similar to the NH_3 removal, the secondary measures or downstream gas cleaning for the H_2S removal include (1) wet scrubbing or cold gas cleaning; and (2) desulphurisation of H_2S or hot gas cleaning. In the cold gas cleaning, H_2S is scrubbed from the producer gas using a selective amine-based absorption process such as 2-methyldiethanolamine (MDEA) or Sulphinol-M (a mixture of MDEA, water, and tetrahydrothipene dioxide) solvent solutions [82]. The solvent is recovered in a series of flash columns and recycled back to the scrubber. This absorption process is a proven technology in the chemical, petrochemical, and coal conversion industries [82]. However, cooling the hot producer gas represents a potentially significant efficiency penalty, and it requires heat exchangers with high capital cost [82].

For the hot gas cleaning of H_2S, it is based on the adsorption process or gas-solid reaction using metal oxide sorbents in a hot gas desulphurisation unit. The hot gas cleaning offers the potential for energy efficiency improvement in the IGCC system, reduction of capital and operating costs by lowering the duty on the heat exchangers, and elimination of the waste water treatment facilities used in the wet scrubber or absorption process [82]. Metal oxide sorbents such as Fe, Zn, Ca, Mn, and Cu have been intensively tested in various test facility scales including bench-scale, pilot-scale, and commercial-scale [26, 82]. The

regeneration of the used sorbents can be simply performed through oxidation reactions using air, O_2, steam, or SO_2 [26, 82].

Considering all the above advantages, the hot catalytic decomposition for removal of NH_3 and the hot gas desulphurisation of H_2S are discussed and assessed in this research.

2.9.1 Downstream hot gas removal of NH_3

For better understanding of the catalytic decomposition of NH_3, a thermodynamic analysis is first performed for the NH_3 decomposition reaction.

2.9.1.1 Thermodynamic analysis of NH_3 decomposition

Thermodynamic analysis of the NH_3 decomposition reaction (Equation 2.25) can be used to describe the NH_3 conversion at equilibrium state and thus predict the effect of temperature and pressure on the conversion rates. The equilibrium constant (K) of the NH_3 decomposition reaction is calculated from Equation 2.26 [98]:

$$\ln K = \frac{-\Delta G^{o}}{RT} \tag{2.26}$$

where ΔG^{o} is a standard Gibbs free energy change of reaction, R is a universal gas constant, and T is a temperature in kelvins.

The equilibrium constant is plotted as a function of temperature in Figure 2.12. The equilibrium NH_3 conversion is calculated as a function of temperature and pressure for a feed gas containing 2,000 ppm NH_3 in inert gas from the equilibrium constant with an assumption of ideal gas, and the results are shown in Figure 2.13. From Figure 2.12, it can be seen that the equilibrium constant increases with temperature as expected because the NH_3 decomposition reaction is an endothermic reaction and the result is consistent with that published by Alagharu et al. [99]. Correspondingly, the NH_3 conversion at equilibrium also increases with temperature and decreases with pressure, and this trend is the same as reported by Torres et al. [21]. At atmospheric pressure, the NH_3 conversion of 99.99 % at equilibrium can be achieved with the temperatures higher than 300°C, although the equilibrium state will take a long time to reach.

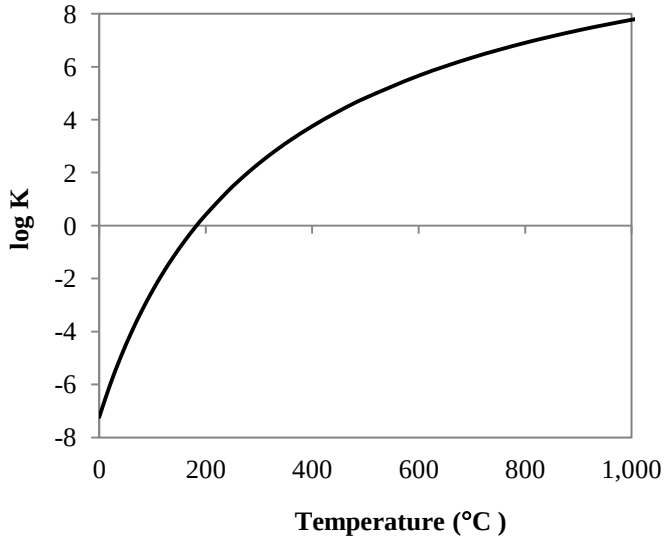

Figure 2.12 Equilibrium constant of NH_3 decomposition reaction as a function of temperature [33]

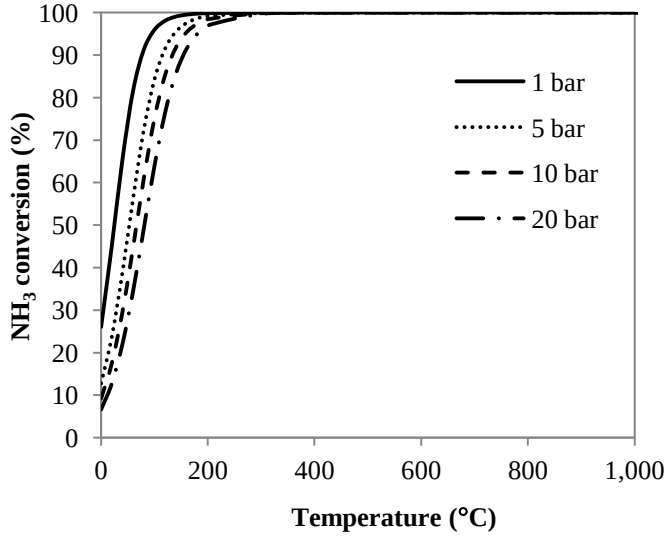

Figure 2.13 NH_3 conversion at equilibrium as a function of temperature and pressure [33]

As expected, with the addition of N_2 or H_2 or the mixture of N_2 and H_2 into the feed gas, the NH_3 conversion at equilibrium is reduced as shown in Figure 2.14. It is observed from the figure that the influence of H_2 in the feed gas is more significant than N_2 on the equilibrium NH_3 conversion. However, the addition of the mixture of N_2 and H_2 has the most

significant influential on the equilibrium NH_3 conversion, which is due to the stoichiometry of the NH_3 decomposition reaction.

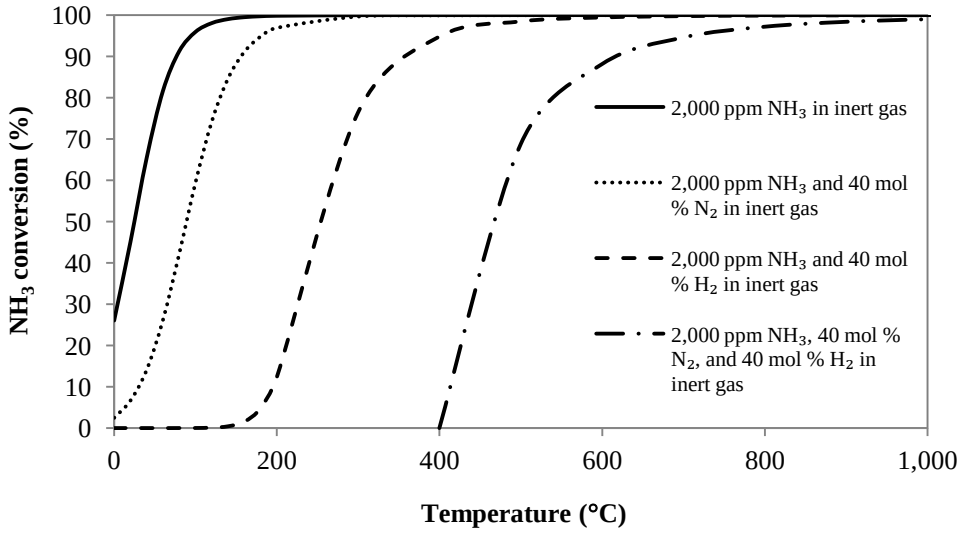

Figure 2.14 NH_3 conversion at equilibrium as a function of temperature at 1 bar when different feed gas concentrations are used [33]

2.9.1.2 Downstream thermal decomposition of NH_3

Thermal decomposition of NH_3 requires a reactor to be operated at a very high temperature because of the high activation energy of the NH_3 decomposition reaction [78, 79]. Wang et al. [39, 40] estimated thermal NH_3 conversion of less than 10% in an empty reactor operated at a temperature of 900°C, pressure of 1.6 MPa, and residence time of 3 s, where the effect of light hydrocarbons was not taken into account. In other studies, inert materials including silicon carbide [24, 32, 88, 100], quartz sand or a quartz surface [39, 88, 101, 102], and alumina [37, 38, 88] were found to reduce NH_3 at high temperatures. It was proposed that the reduction of NH_3 with the inert particles was from (1) thermal decomposition [24, 32, 100]; (2) homogeneous and heterogeneous reactions [24]; and (3) NH_3 adsorption on the surface of the particles [39].

Silicon carbide (SiC), considered as an inert material, was tested at 1,000°C in a downstream reactor following air peat gasification in a pressurised updraft gasifier [32], and the results showed that the NH_3 concentration in the producer gas was reduced from 2,150-2,390 ppmv to 500 ppmv (78% NH_3 conversion). In addition, when the SiC was

tested at 900°C with air peat gasification producer gas from a pressurised fluidised bed gasifier, the NH_3 concentration was reduced by about 44% of the inlet NH_3 [24, 100]. NH_3 decomposition at the high temperatures (>1,000°C for producer gas from updraft gasifier and >900°C for producer gas from a fluidised bed gasifier) may be caused by thermal decomposition [24, 32, 100] or other homogeneous and heterogeneous reactions [24] and, to some extent, due to the effects of reactor wall, made of fireproof steel, at the operation conditions [100]. In addition, Simell et al. [88], who tested the effects of producer gas components on the NH_3 decomposition, found that the NH_3 conversion (50%) with SiC was the highest in the simulated gas mixture with CO_2 present, compared with other simulated gas mixtures without CO_2.

Quartz sand was also found to enhance NH_3 removal, although it is usually regarded as an inert material with no catalytic effects [39]. The study of Wang et al. [39] found that the conversion of NH_3 was 60% at about 650°C in the simulated producer gas with a 15-cm deep bed of sand, which could be due to the adsorption of NH_3 onto the large surface of the sand bed. Cooper and Ljungstrom [101] also found decomposition of NH_3 in inert gas with quartz sand. The catalytic activity of quartz sand was low, ranging from 3 to 16%, when the bed temperature increased from 840 to 960°C [101]. Furthermore, the decomposition of NH_3 (1,000 ppm in Ar) in the quartz sand bed supported on quartz filter in the quartz tube reactor was measured to be about 10% to 45% when temperature increased from 750°C to 940°C, respectively [102]. Simell et al. [88] proposed that the reduction of NH_3 by quartz surface might be from reactions with CO_2. This is because they found NH_3 conversion was much higher in the gas mixtures containing CO_2 than those without CO_2. In contrast to these studies, Shimizu et al. [103] found negligible NH_3 reduction with quartz sand packed in the quartz fixed-bed reactor operated at 850°C.

Inert alumina wash-coat honeycomb monolith also showed the capability for NH_3 removal, which was confirmed in a lab-scale, high-pressure, high-temperature reactor [37]. In this study, NH_3 conversion was increased from about 25% to 60% at 20 bar with the increasing of temperature from 700°C to 900°C for simulated gas mixture with inlet NH_3 concentration of 2,100 ppmv [37]. This inert material also removed NH_3 (23% conversion) at 20 bar and 830°C from the producer gas from air-blown biomass gasification in a pilot-

scale pressurised fluidised bed gasifier [38]. Finally, Simell et al. [88] again observed the NH_3 conversion with alumina was high in the CO_2 containing gas mixtures. However, the mechanism for the catalytic behaviour of the inert material is not fully understood.

2.9.1.3 Downstream catalytic decomposition of NH_3

Catalysts commonly used for tar cracking have also been extensively tested towards the decomposition of NH_3 in a secondary gas cleaning reactor, and these catalysts include:

(1) Alkaline earth metal oxides such as limestone [32, 102, 103], calcined limestone [97, 102-104], dolomite [24, 32, 100, 102], calcined dolomite [79, 88, 102], pure calcium oxide (CaO) [79, 104], pure magnesium oxide (MgO) [79] and modified-Ca catalysts [94];
(2) Coal char [95];
(3) Activated carbon [43, 95, 105];
(4) Iron (Fe)-based catalysts [24, 32, 43, 85, 93, 94, 96, 100, 105, 106];
(5) Nickel (Ni)-based catalysts [24, 32, 37-40, 43, 45, 48, 88, 90, 92, 100, 105].

Noble metal catalysts have also been tested for NH_3 decomposition including ruthenium (Ru) [37, 38, 89, 90, 107-116], rhodium (Rh) [89, 107], iridium (Ir) [89, 111, 112], palladium (Pd) [89, 107], platinum (Pt) [89, 107, 114], manganese (Mn) [106], and tungsten (W) [117-122]. The above catalysts have been investigated at laboratory or pilot scale, but the cost for these catalysts is a major concern for use in commercial scale plants. The noble metal catalysts of Ru, Rh and Ir are very expensive compared with Fe and Ni catalysts [43] and with natural occurring catalysts of dolomite and limestone. In this review paper, only affordable inexpensive catalysts are examined and summarised in Table 2.8 , which include alkaline earth metal oxides, char, activated carbon, Fe-based catalysts, and Ni-based catalysts. It should be noted that some materials reviewed in this paper are reactants as they are consumed in the reactions and needed to be replaced after a certain period of time, but most of the materials reviewed are catalysts, which are not consumed. For some materials, it is uncertain whether they are catalysts or reactants, as the detailed mechanism for enhancement in NH_3 decomposition in the producer gas is not available. However, all the materials used in the enhancement of NH_3 decomposition in the

downstream NH_3 removal will be regarded as catalysts in this review paper, following the statement of the originally published papers.

Most of the research work presented here was conducted in lab-scale facilities with the addition of NH_3 in inert gases, in model compounds, or in simulated producer gases. Only limited studies were conducted with the use of real producer gas from the biomass gasification. The studies for downstream hot gas NH_3 removal have been found in fixed-bed reactors operated either at atmospheric pressure or high pressures.

2.9.1.3.1 Alkaline earth metal oxides

Alkaline earth metal oxides containing Ca and/or Mg such as limestone, dolomite, pure CaO, pure MgO and Ca-based synthetic catalysts have been tested towards NH_3 decomposition. In an inert gas atmosphere, both dolomite and limestone gave a high activity for NH_3 decomposition to form N_2 and H_2 at high temperatures. However, other studies have shown that calcined dolomite and calcined limestone were more effective for NH_3 decomposition in an inert gas environment compared to the original forms of these catalysts [102]. Calcined dolomite and calcined limestone also showed higher activity to remove NH_3 than their main constituents, pure CaO with MgO and pure CaO, respectively [79, 104]. In addition, pure CaO was more effective than pure MgO [79]. As mentioned above, most of the previous studies were conducted in inert gas environments. However, the presence of main gas components in the biomass gasification producer gas such as H_2, N_2, CO, CO_2, CH_4, H_2O or minor contaminants such as N-tar compounds and HCN was found to adversely affect the performance of these alkaline earth metal oxides on the NH_3 decomposition to various extents.

Table 2.8 Summary of published catalysts used for downstream catalytic decomposition of NH_3 and the NH_3 conversion results

Catalysts	**Chemical composition of the catalyst**	**Temperature (°C)**	**Pressure (bar)**	**Space time/ space velocity**	**Feed gas (vol%)**	**NH_3 conversion (%)**	**Reference**
Alkaline earth metal oxides							
Calcined limestone (calcined in Ar, at 900°C for 4 h)	CaO (91.1 wt% $CaCO_3$)	850-875	1	Not available	4,930 ppm NH_3 in Ar	50-63	[104]
Calcined limestone	CaO (96.9 wt% $CaCO_3$)	850	1	Not available	900 ppm NH_3 in He	70	[103]
Calcined limestone (calcined at 900°C for 3 h)	CaO	875	1.3	20,000 h^{-1}	1) 3,000 ppm NH_3 in He 2) 3,000 ppm NH_3, 14 % H_2, 25.4% CO, 7.8% CO_2 in He	1) 73 2) 30	[97]
Calcined limestone	CaO	650-950	1	50-100 ms	1,000 ppm NH_3, 2% O_2 in Ar	100	[102]
Dolomite	$CaCO_3$·$MgCO_3$ (18.9 wt% Ca, 9.8 wt% Mg)	1) 900 2) 1,000	1	0.2-0.3 s	Producer gas from air gasification of peat in a pressurised updraft gasifier (2,150-2,390 ppm NH_3)	1) NH_3 increased 2) 60	[32]
Dolomite	$CaCO_3$·$MgCO_3$ (18.9 wt% Ca, 9.8 wt% Mg)	900-910	1	0.2-0.3 s	Producer gas from air gasification of peat in a pressurised fluidised bed gasifier (4,290-4,990 ppm NH_3)	53	[24, 100]

Table 2.8 (continued)

Catalysts	**Chemical composition of the catalyst**	**Temperature (°C)**	**Pressure (bar)**	**Space time/ space velocity**	**Feed gas (vol%)**	**NH_3 conversion (%)**	**Reference**
Calcined dolomite (calcined in He, at 900°C for 30 min)	CaO·MgO	1) 800 2) 800-950	1	Not available	1) 1,000 ppm NH_3 in He 2) 1,000 ppm NH_3, 4.7% H_2, 16.3% CO, 12.4% CO_2, 3.9% CH_4, 1.6% C_2H_4, 0.4% C_2H_6, 0.4% O_2, 37.9% N_2 in He	1) 100 2) 20-25	[79]
Calcined dolomite (calcined in N_2, at 900°C for 1 h)	CaO·MgO	900	20	0.04 s	1) 910 ppm NH_3, 4 wt% CO_2, 720 ppm C_7H_8 in N_2 2) 1,000 ppm NH_3, 11% H_2, 11% CO, 11% CO_2, 1% CH_4, 790 ppm C_7H_8, 90g H_2O/m^3 in N_2	1) 60 2) 10	[88]
Modified-Ca catalyst	6 wt% Ca on Australian brown coal char	1) 750 2) 850	1	45,000 h^{-1}	2,000 ppm NH_3 in He	1) 33 2) 100	[94]
Coal char							
Coal char (coal from Germany)	2 wt% Fe, 3wt% Ca	750	1	45,000 h^{-1}	1) 2,000 ppm NH_3 in He 2) 2,000 ppm NH_3, 20% H_2, 40% N_2 in He 3) 2,000 ppm NH_3, 13% H_2,13% CO, 7% CO_2, 1% CH_4 in He 4) 2,000 ppm NH_3, 2,000 H_2S in He	1) 80 2) 95 3) 80 4) 40	[95]

Table 2.8 (continued)

Catalysts	**Chemical composition of the catalyst**	**Temperature (°C)**	**Pressure (bar)**	**Space time/ space velocity**	**Feed gas (vol%)**	**NH_3 conversion (%)**	**Reference**
Activated carbon							
Commercial activated carbon	<0.05 wt% Fe, <0.05 wt% Ca	750	1	45,000 h^{-1}	2,000 ppm NH_3 in He	13	[95]
Activated carbon from peat	Not available (0.6 wt% Fe in raw peat)	750	1	45,000 h^{-1}	2,000 ppm NH_3 in He	15	[43, 105]
Iron-based catalysts							
Modified-Fe catalyst	2-6 wt% Fe on Australian brown coal chars	1) 750 2) 850	1	45,000 h^{-1}	2,000 ppm NH_3 in He	1) 57-96 2) 100	[94]
Modified-Fe catalyst	8 wt% Fe on a commercial activated carbon	750	1	45,000 h^{-1}	2,000 ppm NH_3 in He	20-30	[94]
Modified-Fe catalyst	13% Fe on activated carbon from peat	750	1	45,000 h^{-1}	2,000 ppm NH_3 in He	90	[43, 105]
Modified-Fe catalyst	8 wt% Fe_2O_3 (64 wt% TiO_2, 36 wt% Ca-f[a])	780-800	1	500-2,000 h^{-1}	10,000 ppm NH_3 in He	95	[106]
Modified-Fe catalyst	8 wt% Fe_2O_3, 15 wt% MnO_2 (64 wt% TiO_2, 36 wt% Ca-f[a])	750-800	1	500-2,000 h^{-1}	10,000 ppm NH_3 in He	98	[106]

Table 2.8 (continued)

Catalysts	**Chemical composition of the catalyst**	**Temperature (°C)**	**Pressure (bar)**	**Space time/ space velocity**	**Feed gas (vol%)**	**NH_3 conversion (%)**	**Reference**
Hematite	α-Fe_2O_3	750	1	45,000 h^{-1}	2,000 ppm NH_3 in He	< 20%	[93]
Magnetite	Fe_3O_4	750	1	45,000 h^{-1}	2,000 ppm NH_3 in He	< 80%	[93]
Limonite	90 wt% α-FeOOH	1) 500-750 2) 500-750 3) 750 4) 750-950 5) 750 6) 750-950	1	45,000 h^{-1}	1) 2,000 ppm NH_3 in He 2) 2,000 ppm NH_3, 100 ppm H_2S in He 3) 2,000 ppm NH_3, 50-500 ppm H_2S in He 4) 2,000 ppm NH_3, 10% H_2, 20% CO in He 5) 2,000 ppm NH_3, 10% H_2, 20% CO, 10% CO_2 in He 6) 2,000 ppm NH_3, 10% H_2, 20% CO, 3% H_2O in He	1) 100 2) 100 3) 100 4) 45-90 5) 90 6) 90-99	[85, 96] [85] [85] [93] [93] [93]
Iron sinter	59.2 wt% Fe, 5.4 wt% Ca	900	1	0.2-0.3 s	Producer gas from air gasification of peat in a pressurised updraft gasifier (2,150-2,390 ppm NH_3)	87	[32]

Table 2.8 (continued)

Catalysts	**Chemical composition of the catalyst**	**Temperature (°C)**	**Pressure (bar)**	**Space time/ space velocity**	**Feed gas (vol%)**	**NH_3 conversion (%)**	**Reference**
Iron pellet	58.3 wt% Fe, 0.9 wt% Ca	900	1	0.2-0.3 s	Producer gas from air gasification of peat in a pressurised updraft gasifier (2,150-2,390 ppm NH_3)	35	[32]
Ferrous dolomite	4.6 wt% Fe, 19.2 wt% Ca	1) 900 2) 900-910	1	0.2-0.3 s	1) Producer gas from air gasification of peat in a pressurised updraft gasifier (2,150-2,390 ppm NH_3) 2) Producer gas from air gasification of peat in a pressurised fluidised bed gasifier (4,290-4,990 ppm NH_3)	1) 75 2) 53	[32] [24, 100]
Nickel-based catalysts							
Ni-based catalyst	4-11 wt% Ni, 22-23 wt% Al	1) 900 2) 900-910	1	0.2-0.3 s	1) Producer gas from air gasification of peat in a pressurised updraft gasifier (2,150-2,390 ppm NH_3) 2) Producer gas from air gasification of peat in a pressurised fluidised bed gasifier (4,290-4,990 ppm NH_3)	1) 100 2) 100	[32] [24, 100]

Table 2.8 (continued)

Catalysts	**Chemical composition of the catalyst**	**Temperature (°C)**	**Pressure (bar)**	**Space time/ space velocity**	**Feed gas (vol%)**	**NH_3 conversion (%)**	**Reference**
Ni monolith catalyst	Ni/Al_2O_3	910-920	5	0.9-1.2 s	Producer gas from air gasification of peat and wood in a pressurised fluidised bed gasifier (560-2,700 ppm NH_3)	72-94	[100]
Ni-based catalyst	Ni/Al_2O_3 (13.3 wt% Ni, 57 wt% Al	900	20	0.007 s	1) 910 ppm NH_3, 4 wt% CO_2, 720 ppm C_7H_8 in N_2 2) 1,000 ppm NH_3, 11% H_2, 11% CO, 11% CO_2, 1% CH_4, 790 ppm C_7H_8, 90g H_2O/m^3 in N_2	1) 96 2) 67	[88]
Ni honeycomb monolith catalyst	15 wt% Ni/Al_2O_3	1) 850-900 2) 850 3) 800-900	20	0.6 s	1) 2,100 ppm NH_3, 16.7% H_2, 16.5% CO, 10.3% CO_2, 15.1% H_2O, 4.6% CH_4 in N_2 2) 2,100 ppm NH_3, 16.7% H_2, 16.5% CO, 10.3%CO_2, 15.1% H_2O, 4.6% CH_4, 4,000 ppm C_7H_8 in N_2 3) 2,100 ppm NH_3, 16.7% H_2, 16.5% CO, 10.3% CO_2, 15.1% H_2O, 4.6% CH_4, 500-3,000 ppm H_2S in N_2	1) 80-85 2) 80 3) 60-70	[37]

Table 2.8 (continued)

Catalysts	Chemical composition of the catalyst	Temperature (°C)	Pressure (bar)	Space time/ space velocity	Feed gas (vol%)	NH_3 conversion (%)	Reference
Ni honeycomb monolith catalyst	15 wt% Ni/Al_2O_3	830	20	1.1 s	Producer gas from air gasification of wood in a pressurised fluidised bed gasifier (500-800 ppm NH_3)	38	[38]
Ni honeycomb monolith catalyst	Not available	650-720[b] and 820-950[c]	1	1,400-4,300[d] m^3 (nc, wet)/ $h \cdot m^3_{cat}$	Producer gas from air gasification of a mixture of pinewood and orujillo[e] in a BFB gasifier (200-4,780 ppm NH_3)	44-96	[45]
Methanation Ni-based catalyst	Not available	600-800	21	180 h^{-1}	15,000 ppm NH_3 in N_2	85-95	[39]
Methanation Ni-based catalyst	Not available	800-900	12	3,500-4,200 h^{-1}	Producer gas from air gasification of sawdust and sawdust mixed with 20 wt% plastic waste in a pressurised fluidised bed gasifier (350-1,150 ppm NH_3)	35-95	[40]
Ni-based catalyst	Ni (0.026 mol Ni/ 1 mol Al_2O_3)	700-900	1	20,000 h^{-1}	1040 ppm NH_3, 10.5% H_2, 28.4% CO, 3.6% CO_2, 3.1% H_2O in N_2,	90-100	[90]

Table 2.8 (continued)

Catalysts	**Chemical composition of the catalyst**	**Temperature (°C)**	**Pressure (bar)**	**Space time/ space velocity**	**Feed gas (vol%)**	**NH_3 conversion (%)**	**Reference**
Modified-Ni catalyst	4 wt% NiO, 4.3 wt% MoO_3, Al_2O_3	650	1	1,000 h-1	1) 6,000 ppm NH_3, 30% H_2 in N_2 2) 6,000 ppm NH_3, 30% H_2, 6,000 ppm H_2S in N_2	1) 88-93% 2) 80	[92]
Ni-based tar-cracking catalysts	Not available	800-850	1	Not available	Producer gas from steam gasification of wood in a fluidised bed gasifier (2,300-2,700 ppm NH_3)	55-98%	[48]

[a] pillared clay of montmorillonite type in Ca-form

[b] axis monolith face temperature

[c] axis monolith outlet temperature

[d] gas hourly space velocity in the monolith, m^3 (nc, wet)/ $h \cdot m^3_{cat}$, where nc refers to normal conditions at 273 K and 1 atm for the gas

[e] residue from olive oil production

In an inert gas atmosphere, calcined limestone, pure CaO, sulphated limestone and calcium sulphate ($CaSO_4$) were found to catalyse the NH_3 decomposition reaction at high temperatures (725-950°C), where the NH_3 conversion increased with increasing bed temperature [104]. Under the same operation conditions (bed temperature 850- 875°C), the NH_3 conversion decreased in the order of calcined limestone > sulphated limestone > pure CaO > $CaSO_4$. From this finding, it is believed that the inherent trace impurities in the limestone are not the dominant factor, although these impurities might contribute to the NH_3 decomposition to a certain extent [104].

In the study of Shimizu et al. [103], it was found that calcined limestone catalysed the decomposition of NH_3 to N_2 and H_2 in inert gas at a conversion of about 70%. However, addition of either pure CO_2 or a mixture of CO_2 and H_2O reduced the conversion rate of NH_3. Interestingly, in the presence of O_2, the raw and calcined limestone catalysed NH_3 oxidation to NO_x [103, 123-125], whereas in the absence of O_2, both raw and calcined limestone are known to catalyse NH_3 decomposition to N_2 [103].

Although the calcined limestone has high NH_3 conversion (73%) in an inert gas environment at 875°C [97], its activity was significantly reduced in the simulated gas mixture comprising H_2, CO, and CO_2, resulting in the reduction of the NH_3 conversion from 73% to 30%. The reduction of activity of the calcined limestone in the simulated gas was considered to be due to a decrease in the surface area of CaO and the conversion of about 10% (mass basis) of CaO to $CaCO_3$ [97].

The activity of both raw and calcined phase of dolomite and limestone can be affected by the operating temperature. At temperatures below the calcination temperature of about 780°C, raw dolomite and limestone gave similar NH_3 conversion in inert gas, but at temperatures over 780°C, dolomite was more active than limestone [102]. The calcined limestone was more effective than the raw limestone in promoting NH_3 decomposition at operating temperatures below the calcination temperature (780°C) in an oxygen-containing atmosphere (2%) in inert gas. In the gas mixture with the presence of O_2, the decomposition and oxidation reactions removed NH_3 more effectively by using calcined limestone than by raw limestone. When O_2 was present, NH_3 was also removed by oxidation to form N_2 and NO according to Equations 2.27 and 2.28 [102].

$$4NH_3 + 3O_2 \leftrightarrow 2N_2 + 6H_2O \quad (2.27)$$

$$4NH_3 + 5O_2 \leftrightarrow 4NO + 6H_2O \quad (2.28)$$

In the study on the producer gas from a 5MW air-blown pressurised updraft gasifier for gasification of peat, dolomite and limestone contributed to the increase of NH_3 concentration and the decrease of HCN concentration in a downstream fixed-bed catalytic reactor operated at and below 900°C [24, 32]. However, at 1,000°C the conversion of NH_3 in the downstream reactor was found to be 60% with use of the dolomite. The explanation for the increase of NH_3 at lower temperatures was proposed to be the conversion of N-tar compounds to NH_3 [32]. In addition, Equations 2.19 and 2.20 were propounded as the HCN concentration was dropped by the use of dolomite and limestone at 900°C. Although the dolomite operated at 900°C increased the NH_3 concentration in the air peat gasification gas from a pressurised updraft gasifier [32], it gave the NH_3 conversion of about 53% when it was used with the air peat gasification gas from a pressurised fluidised bed gasifier [24, 100]. The reason for this finding is not known.

Another study conducted by Björkman and Sjöström [79] also confirmed that the calcined dolomite, pure CaO, and pure MgO were poor catalysts for NH_3 removal in the presence of simulated producer gas consisting of H_2, N_2, O_2, CO, CO_2, CH_4, C_2H_4, and C_2H_6. The calcined dolomite demonstrated poor catalytic effect in the simulated producer gas at a high temperature of over 900°C, although almost all of NH_3 was decomposed in an inert helium (He) gas environment at 800°C. The inhibition of NH_3 decomposition with calcined dolomite was proposed to be due to carbon formation on the surface of the dolomite from CH_4 and C_2H_6 in the simulated producer gas [79]. It was also found that the decomposition of NH_3 was inhibited by the presence of H_2 or H_2O [79]. The NH_3 decomposition activity in He alone followed the sequence, from high to low, of calcined dolomite > synthetic dolomite > pure CaO > pure MgO. The synthetic dolomite is a mixture of CaO and MgO in a nearly equimolar quantity to natural calcined dolomite. This demonstrated that the activity of calcined dolomite cannot be explained by additive effects from its main constituents (Ca and Mg) or by its larger surface area as compared to other materials. Regeneration of dolomite can be done by burning off the deposited carbon [79].

Simell et al. [88] tested dolomite in both calcined form (CaO·MgO) and in carbonated or half-calcined form ($CaCO_3$·MgO) for NH_3 decomposition in different gas atmospheres at 900°C under a pressuried system. The gas mixtures studied were NH_3 with or without toluene (C_7H_8) in these gas compounds including: (1) N_2; (2) H_2; (3) H_2O; (4) CO; (5) CO_2; (6) CO_2 and H_2O; (7) H_2 and H_2O; (8) CO and CO_2; and (9) simulated producer gas containing H_2, CO, CO_2, CH_4 and H_2O. Note that N_2 was an carrier gas in all cases. The results from this study showed that the rate of NH_3 decomposition by the calcined dolomite and the carbonated dolomite were about the same, which indicated that the MgO might be an active component [88]. It was also found that both dolomites enhanced NH_3 conversion in CO_2 containing gas mixtures, which could be because the dolomite catalysed the reaction of CO_2 with NH_3 [88]. The results of this study showed that the carbonated dolomite gave low NH_3 decomposition in simulated gas due to the deactivation, which was in accordance with the study of Björkman and Sjöström [79]. In addition, dolomite was deactivated in the presence of H_2O possibly by strong adsorption of water on the active sites [88].

Australian brown coal char loaded with Ca (6 wt%) has shown low catalytic activity for NH_3 removal in inert gas of He at 750°C (33% NH_3 conversion), and its activity at 750°C was lower than the same coal char loaded with 6 wt% Fe [94]. In this study, 6 wt% modified-Ca catalyst has been found to have achieved 100% conversion of NH_3 at inlet concentration of 2,000 ppm in the inert gas of He when the reactor was operated at 850°C. The above NH_3 conversion process can be described by the following reactions (Equations 2.29-2.31) with $CaCN_2$ being taken as the intermediate species and Equation 2.29 might occur only at the initial stage of the Ca-catalysed decomposition [94]:

$$CaO + 2NH_3 + 2C \rightarrow CaCN_2 + 3H_2 + CO \quad (2.29)$$

$$CaCN_2 \rightarrow N_2 + Ca\text{-}C \quad (2.30)$$

$$Ca\text{-}C + 2NH_3 \rightarrow CaCN_2 + 3H_2 \quad (2.31)$$

2.9.1.3.2 Coal char

It has been found that coal char loaded with high Fe and Ca contents found naturally in coal could also promote NH_3 decomposition in inert gas, a gas mixture of H_2 and N_2, and simulated producer gas [95]. In this study, five low rank coals from Germany, Russia,

China, and Indonesia, where two coals were from Indonesia, were used to produce chars which were then tested for the removal of NH_3 in a hot gas reactor [95]. High conversion of NH_3 to N_2 of up to 80% in both the inert gas of He and the simulated producer gas (H_2, CO, CO_2 and CH_4) can be achieved with the German coal char. However, the activity of the German coal char decreased with the presence of H_2S at concentration of 2,000 ppm. In a separate study [94], Australian coal chars loaded with 2-6 wt% Fe or 6 wt% Ca were also tested for NH_3 removal. In comparison between the natural German coal char and the modified Australian coal char, it is found that the NH_3 removal efficiency of the German coal char was lower than that of the Australian coal char loaded with 2 wt% Fe, but higher than that of the Australian coal char loaded with 6 wt% Ca in both the simulated producer gas and the inert gas of He with 2,000 ppm H_2S [94, 95]. It was proposed that the natural German coal char with the largest nanoscale metal Fe content of 2 wt% and high Ca content of 3 wt% showed the highest catalytic performance among the five low rank coal chars where the metal Fe played a crucial role in the NH_3 decomposition reaction. The probable mechanisms of NH_3 decomposition in the inert gas were suggested to involve $CaCN_2$ (Equation 2.29) and Fe-nitride (Fe_4N) as described by the following reactions (Equations 2.32 and 2.33) [94, 95]. The Fe-rich low rank coals might be promising as the catalyst precursors for a hot gas cleanup method for NH_3 removal because they are widely available and complex catalyst preparation is not needed [95].

$$8Fe + 2NH_3 \rightarrow 2Fe_4N + 3H_2 \quad (2.32)$$

$$2Fe_4N \rightarrow 8Fe + N_2 \quad (2.33)$$

2.9.1.3.3 Activated carbon

Studies have been performed to test commercially available activated carbon, which has a large surface area, on NH_3 decomposition, however, it was found that the activated carbon has poor performance even in an inert gas environment [43, 95, 105]. In the experiments on a commercial activated carbon with Fe and Ca contents lower than 0.05 wt% [95], the activity for NH_3 conversion to N_2 in inert gas was found to be only 13% at 750°C. This activated carbon gave the lowest performance for NH_3 removal compared with other catalysts including: (1) five low rank coal chars as discussed in 2.9.1.3.2 [95]; (2) 2-6 wt%

Fe loaded on Australian brown coal chars [94]; (3) 6 wt% Ca loaded on Australian brown coal char [94]; and (4) 8 wt% Fe loaded on a commercial activated carbon [94].

In a separate test at the operation temperature of 750°C, the activated carbon derived from raw peat containing 0.6% Fe activated by phosphoric acid (H_3PO_4) gave lower NH_3 conversion (15%) in an inert gas atmosphere than both the peat activated carbon with 13 wt% Fe and the peat activated carbon with 13 wt% Ni [43, 105]. From these observations, it might be concluded that the high contents of Fe, Ca and Ni contribute to the high catalytic NH_3 decomposition.

2.9.1.3.4 Iron-based catalysts

Fe-based catalysts have been widely investigated for NH_3 decomposition, and these catalysts include iron sinter, ferrous dolomite or named ankerite, iron pellet, limonite, magnetite, hematite, and Fe-based metal supported on large surface area materials. The research has shown that the effective conversion of NH_3 in inert gas can be accomplished by applying the Fe-based catalysts at high temperatures. In the presence of CO and/or H_2S in the gas, the catalytic activity of Fe-based catalysts is lowered due to the deposition of carbon resulted from the Boudouard reaction (Equation 2.34) on the catalysts [93, 94], and the catalyst poisoning from H_2S [85, 95]. However, with the addition of CO_2 [93, 94], H_2O [93], and H_2 [95], the catalytic activity of Fe-based catalysts can be regenerated from carbon deposition. For peat gasification producer gas from a pressurised updraft gasifier and a pressurised fluidised bed gasifier, Fe-based catalysts in a fixed-bed downstream reactor achieved high NH_3 conversion at 900°C of up to 53 and 87%, respectively [24, 32, 100].

Boudouard reaction: $2CO \rightarrow C + CO_2$ (2.34)

Various Fe-based catalysts have been investigated for decomposition of NH_3 at concentration of 2,000 ppm to N_2 in the inert gas of He at 750°C and space velocity of 45,000 h^{-1} [43, 85, 93, 94, 96, 105]. These catalysts include: (1) 2-6 wt% Fe loaded on Australian brown coal chars; (2) 8 wt% Fe loaded on a commercial activated carbon; (3) 13 wt% Fe loaded on peat activated carbon (4) limonite; (5) hematite; and (6) magnetite. The

NH_3 conversion results from these catalysts are shown in Table 2.8. Among the tested catalysts, the limonite after reduction with H_2 gas showed the highest performance with respect to NH_3 conversion and catalyst stability [96]. The NH_3 decomposition activity at time on stream of 4 h decreased in the sequence of reduced limonite (100%) > 6 wt% Fe loaded on Australian brown coal char (96%) > 13 wt% Fe loaded on peat activated carbon (90%) > magnetite (60%) > 2 wt% Fe loaded on Australian brown coal char (57%) > 8 wt% Fe loaded on a commercial activated carbon (30%) > hematite (20%).

Fe (2-6 wt%) catalyst supported on Australian brown coal chars could completely decompose NH_3 at concentration of 2,000 ppm in the inert gas of He at 850°C, and these catalysts are more effective than 8 wt% Fe loaded on a commercial activated carbon [94]. From the comparison of catalyst characteristics of Fe on Australian brown coal chars and Fe on an activated carbon, it was suggested that the finer particle sizes (20-50 nm) and highly dispersion of metallic Fe (α-Fe) were more effective for NH_3 decomposition. When the 2 wt% Fe loaded on Australian brown coal char was used in a reactor to decompose 2,000 ppm NH_3 in a gas mixture of H_2, N_2, and He, the addition of H_2 gas helped the catalyst to maintain its high activity for NH_3 conversion at longer time (4 h) compared with only inert gas of He being used. However, when the simulated producer gas of H_2 and CO was treated, the catalyst was deactivated considerably, but the injection of CO_2 into the simulated producer gas restored the catalytic conversion of NH_3 to 95% [94]. Deactivation of Fe-based catalysts might be due to carbon deposition by the Boudouard reaction (Equation 2.34) [94] and formation of iron carbides (Fe_3C) by the reaction with the char substrate that was used as the support [93]. The possible mechanism for NH_3 decomposition with Fe-based catalyst was proposed to involve metallic α-Fe and Fe_4N as proposed for the Fe-rich low rank coals (Equations 2.32 and 2.33).

Catalysts of Fe loaded on activated carbon derived from peat possess high catalytic activity for NH_3 conversion in inert gas [43, 105]. The catalysis of 13 wt% Fe supported on the peat activated carbon showed higher NH_3 conversion (90%) than catalyst with 13 wt% Ni supported on the same activated carbon (75% NH_3 conversion) and pure activated carbon without metal loading (15% NH_3 conversion) in inert gas at 750°C [43, 105]. Different mechanisms have been proposed to explain the catalytic effect of the NH_3 conversion by applying these catalysts, and it is generally agreed that the following factors contribute to

the improvement of NH_3 conversion: (1) the remarkable increase in mesoporous surface area and pore volume of the catalysts; (2) the occurrence of metal phosphides ($Ni_{12}P_5$, Ni_3P, Ni_2P and Fe_2P); and (3) the occurrence of nitrides (Fe_xN) [43]. In comparison with other catalysts, the 13 wt% Fe loaded on the peat activated carbon was initially slightly less active than both the 2-6 wt% Fe on Australian brown coal chars [94] and the 2 wt% Fe naturally existing in German coal char [95]. However, the 13 wt% Fe loaded on the peat activated carbon showed higher performance in long term stability at the same operation conditions. This might be due to its higher Fe loading and large surface area in the 13 wt% Fe-loaded catalyst [105].

At a low temperature of 500°C, 100% conversion of NH_3 with concentration of 2,000 ppm in the inert gas of He can be achieved by using the highly-dispersed nanoscale metallic α-Fe particles (average crystalline size 23 μm) produced from the reduction of α-FeOOH-rich Australian limonite [96]. The conversion mechanisms of NH_3 reactions with nanoscale metallic α-Fe particles formed from the reduced limonite, again, were suggested involving Fe metal and nitrides as the combination of Equations 2.32 and 2.33, or Equations 2.33, 2.35, and 2.36.

$$6Fe + 2NH_3 \rightarrow 2Fe_3N + 3H_2 \quad (2.35)$$

$$8Fe_3N \rightarrow 6Fe_4N + N_2 \quad (2.36)$$

In addition, compared with hematite (α-Fe_2O_3) and magnetite (Fe_3O_4) as Fe-metal catalyst precursors, reduced limonite gave more than 99% NH_3 conversion, which was much higher than the reduced hematite (<20%) and the reduced magnetite (<80%) [93]. Higher catalytic performance of limonite was postulated to be due to the nanoscale particle size of α-Fe formed from limonite, which was much smaller than that derived from hematite and magnetite [93].

Since limonite has shown very high catalytic performance for NH_3 decomposition in inert He gas, it was also tested both in the presence of low concentration of H_2S [85] and in the simulated producer gas from air-blown coal gasification [93]. The reduced limonite decomposed NH_3 almost completely at 500-750°C with the presence of H_2S at concentration of 100 ppm. Moreover, the reduced limonite was not poisoned apparently by

50-500 ppm H_2S at 750°C, but it was dramatically deactivated with 2,000 ppm H_2S [85]. It was speculated that the NH_3 decomposition proceeds via two possible mechanisms as described by: (1) Equations 2.37 and 2.38, which are related to Fe metal and Fe sulphide; and (2) Equations 2.32, 2.33, 2.38 and 2.39, which are related to Fe metal, Fe sulphide and Fe nitride [85].

$$Fe + H_2S \rightarrow FeS + H_2 \quad (2.37)$$

$$FeS + 2NH_3 \rightarrow Fe + N_2 + 2H_2 + H_2S \quad (2.38)$$

$$FeS + H_2 \rightarrow Fe + H_2S \quad (2.39)$$

When the reduced limonite was applied in the simulated producer gas (H_2, CO) at 750°C, the conversion of NH_3 to N_2 decreased gradually from 80% to 45% after 4 h due to the carbon deposition. At the same time, the NH_3 conversion to HCN increased to about 10% [93]. In the same study, the increase of the operating temperature from 750 to 950°C increased the conversion of NH_3 to N_2 to 85-90%, and the conversion of NH_3 to HCN was reduced to below 0.5%. Some of the NH_3 may react with CO in the fed gas to produce HCN and H_2O [93]. The addition of either CO_2 or H_2O into the synthesis gas increased the NH_3 conversion significantly with application of limonite at 750°C from 45% to 90% without the formation of deposited carbon. Also, the presence of H_2O caused no appreciable formation of HCN. The deactivation of the limonite in the simulated producer gas (H_2 and CO) was mainly due to carbon deposition by the disproportionation of CO (Equation 2.34) and the subsequent formation of Fe_3C by the reactions (Equations 2.40 and 2.41) below:

$$3Fe + C \rightarrow Fe_3C \quad (2.40)$$

$$3Fe + 2CO \rightarrow Fe_3C + CO_2 \quad (2.41)$$

Moreover, the limonite catalyst was suggested to be suitable for NH_3 decomposition in N_2-free producer gas because the equilibrium conversion rate of NH_3 to N_2 decreases with increasing N_2 concentration and pressure [93], which is in agreement with thermodynamic equilibrium analysis as discussed in Section 2.9.1.1.

In summary, limonite is a very promising catalyst to be used for removal of NH_3 from the producer gas from biomass gasification due to its very high performance for NH_3 conversion in the simulated producer gas [93, 126]. However, further experiments on the limonite with the real biomass gasification producer gas are needed to confirm its performance before it can be used in commercial scale plants.

Oxides of Fe were employed for the preparation of monolith catalysts based on titania honeycomb support by wet impregnation method [106]. The results showed that the optimal proportions of Fe-oxide component, titania, and the binder as well as the optimal calcination temperature, resulted in high surface area and acceptable mechanical strength of the monolith support. The catalysts with 8 wt% Fe_2O_3 impregnated monolith have shown 95% NH_3 conversion in inert gas at 800°C. The mixed Fe_2O_3/MnO_2 impregnated monolith catalyst seemed to be the most preferable catalyst among all studied catalysts. This is because this catalyst possessed the highest catalytic activity (98% NH_3 conversion) in inert gas at lower temperature (750°C) and was expected to have high potential for H_2S removal as well [106].

Iron sinter and ferrous dolomite were proven to be an ideal catalyst for the decomposition of NH_3 and N-tar compounds in the producer gas from air peat gasification gas in a 5 MW pressurised updraft gasifier [32]. An Fe content as low as 4.6 wt% in the ferrous dolomite was sufficient to create the effective catalytic effect for NH_3 conversion of 75% [32]. This effect was due to the formation of active metallic Fe from the reduction of iron oxides at the high temperature (900°C). However, the ferrous materials enhanced the NH_3 formation by converting some of N-tar compounds to NH_3 when the temperature was below 900°C [32]. Moreover, the ferrous dolomite has also been tested in the producer gas from air peat gasification in a pressurised fluidised bed gasifier [24, 100], and the NH_3 conversion was found to be moderate at 53%. The cause of different performance of the ferrous dolomite in different gas atmospheres might be the higher reduction potential of iron oxide to active metal in the air peat gasification gas from the updraft gasifier than that in the fluidised bed gasifier [100]. Finally, from the comparison of the NH_3 decomposition of iron sinter, ferrous dolomite, and iron pellet with their properties, it was suggested that the combined effect of the higher contents of Fe and Ca might be a factor to improve their activity.

2.9.1.3.5 Nickel-based catalysts

Ni-based catalysts have been extensively investigated with the producer gas from gasification of biomass and peat. The results show that high NH_3 removal can be achieved in most cases, indicating Ni-based catalysts can also be considered as promising catalysts for NH_3 reduction in the biomass gasification producer gas, although the cost for the Ni-based catalysts may be a barrier for commercial applications. In reported studies [24, 32, 100], virtually complete conversion of NH_3 in peat gasification producer gas from both a pressuried updraft gasifier and a pressuried fluidised bed gasifier can be achieved when the downstream hot gas reactor operated at atmospheric pressure and a temperature of 900°C. Ni-based catalysts were also found to have higher catalytic activity for NH_3 decomposition than dolomite, iron sinter, ferrous dolomite, and iron pellet when they were used in the producer gas from peat gasification [24, 32, 100]. In addition, the Ni monolith catalyst tested at 5 bar and 910-920°C achieved high NH_3 conversion of 72-94% in the producer gas from wood gasification and peat gasification in a pressurised fluidised bed gasifier [100]. Also, the long term durability and stability of the Ni-based catalyst at 900°C for 160 h was tested with the producer gas from peat air gasification in a pressured fluidised bed gasifier [24]. During the long term stability test, the NH_3 outlet concentration was measured to be below 30 ppm or over 99% NH_3 conversion was obtained. However, some physical changes in the structure of the Ni catalyst were found after the test [24].

Simell et al. [88] also found higher catalytic activity of Ni-based catalyst than that of dolomite when these catalysts were tested at 900°C and 20 bar under different gas mixtures, either containing C_7H_8 or without C_7H_8, including: (1) N_2; (2) H_2; (3) H_2O; (4) CO; (5) CO_2; (6) CO_2 and H_2O; (7) H_2 and H_2O; (8) CO and CO_2; and (9) simulated producer gas containing H_2, CO, CO_2, CH_4 and H_2O, where N_2 was an carrier gas in all cases.

Another study with simulated producer gas containing H_2, CO, CO_2, CH_4, and H_2O, the NH_3 conversion of more than 80% was attained with 15 wt% Ni honeycomb monolith catalyst at 20 bar and temperature of 850°C or above [37]. The coexistence of toluene and H_2S in the simulated producer gas resulted in the decrease of NH_3 catalytic activity, but the catalysts could be almost fully regenerated by oxygen [37]. The NH_3 removal efficiency was reduced to 38% conversion when the Ni honeycomb monolith catalyst was tested with

the biomass gasification producer gas at 20 bar and 830°C [38]. Overall, much lower NH_3 removal was obtained with the real biomass gasification producer gas than that with the cleaner simulated producer gas. The activity of Ni-based catalysts is increased with Ni content [37, 38]. To enhance the NH_3 decomposition efficiency of the catalysts, the reactor should be operated at higher temperature, lower pressure and longer residence time [37, 38] as discussed in Section 2.9.1.1.

The conversion of NH_3 with Ni honeycomb monolith catalyst in the biomass gasification producer gas obtained from an atmospheric pressure BFB gasifier was found to be in the range from 44 to 96% [45]. The low conversion of NH_3 was due to (1) the inherent of the monolith; (2) the design of the monolithic reactor; (3) the competition between tars and NH_3; (4) the deposition of ash particles on the front monolith Ni catalyst; (5) the coke formation at the exit of the monolith; and (6) catalyst poisoning by H_2S.

The commercial methanation Ni-based catalyst used in a high-pressure fixed-bed reactor gave high NH_3 conversion of 85-95% in N_2 gas environment at the temperature range between 600 and 800°C and under pressure of 21 bar [39]. However, the moderate conversion of NH_3 (35-95%) with the methanation Ni-based catalyst was found when the experiments were conducted in a high-pressure fixed-bed reactor with the producer gas from gasification of two feedstocks: sawdust and sawdust mixed with 20 wt% plastic waste [40]. The degree of the NH_3 conversion is dependent on catalyst bed temperature, space time, and concentrations of NH_3 and light hydrocarbons in the producer gas [40]. Wang et al. [40] proposed that the possible reason of the low NH_3 conversion was due to the competition for active sites between NH_3 decomposition reaction and steam reforming of light hydrocarbons, in addition to the negative effects of tars and H_2S present in the producer gas. However, the performance of the catalyst was found unchanged for both NH_3 and light hydrocarbons with the present of 50 to 150 ppm of H_2S and 10 g/Nm^3 of tars in a six hour operation [40].

The use of Ni catalyst gave high NH_3 conversion of 90-100% in the simulated producer gas with the reactor operating at atmospheric pressure and 700-900°C, but the NH_3 conversion was very low at temperatures below 650°C [90]. The catalytic activity of Ni catalyst at low temperature between 400 and 550°C was increased to 20-50% by introducing small amount

of O_2 (0.004-0.008 mol O_2/mol fuel) into the reactor. These results indicated that Ni catalyst promotes selective catalytic oxidation of NH_3 to N_2 and H_2O below 550°C and promotes catalytic decomposition of NH_3 to N_2 and H_2 above 700°C. Moreover, the carbon deposition on the Ni catalyst can be reduced significantly by adding O_2 and no carbon deposition was observed with 0.008 mol O_2/mol fuel [90]. By increasing the operation pressure from 1 to 9 bar in the simulated producer gas containing 0.008 mol O_2/mol fuel, the NH_3 conversion at 400-550°C was not significantly altered, but it was reduced with increasing pressure at temperature above 600°C. Finally, the addition of different molar ratios of Ru metal on the Ni catalysts reduced the NH_3 conversion from about 30% to nearly zero at 400-550°C and 9 bar, but the NH_3 conversion at above 600°C was similar to that obtained by the pure Ni catalyst [90].

Ni-based catalyst (Ni-Mo) was found to have much higher activity for NH_3 conversion (93%) than that of Fe-based catalyst (Fe-Cr) (35%) in the simulated gas of H_2 and N_2 containing 6,000 ppm NH_3 when the reactor was operated at atmospheric pressure and 650°C [92]. No deactivation of the Ni-based catalyst was observed in the catalyst stability test of 100 h. With the addition of 6,000 ppm H_2S into the simulated gas, the efficiency of the Ni catalyst for NH_3 conversion was decreased to 80% at 650°C. The effect of H_2S on the Ni-based catalyst in NH_3 composition was proposed to be due to (1) the sulphur absorbed on the catalyst, which may occupy some active sites; or (2) the reaction of sulphur with Ni to form Ni_3S_2, resulting in a decrease of the Ni component in catalyst [92].

In a study on commercial Ni-based catalysts [48], two types of catalysts were evaluated for tar and NH_3 removal in the producer gas from biomass steam gasification. By employing the Ni-based catalysts at a temperature range of 800-850°C, NH_3 and NO were decomposed in the tar cracking reactor [48] with the concentration of NH_3 being decreased from 2,300-2,700 ppm to 36-1,100 ppm, while NO was reduced from 8.3 ppm to below 1 ppm [48].

2.9.1.4 Operation conditions of a downstream hot gas reactor

In general, the catalytic activity of applied catalysts for NH_3 decomposition in a pressurised reactor is lower than that in a reactor operated at atmospheric pressure [21, 37, 93, 100] which can be explained by thermodynamic equilibrium analysis in Section 2.9.1.1.

Additionally, at higher pressure the impact of H_2S on NH_3 decomposition is significant [37, 38, 127]. In practice, the catalytic reactor should operate at as high temperature as possible in order to achieve high NH_3 conversion [32, 37, 40, 41, 79, 94, 96, 100], to achieve long stability of catalyst for the NH_3 removal [93, 95], and to prevent sulphur poisoning [37-39, 85, 100, 128]. Finally, the increase of space time or gas residence time also enhances catalytic NH_3 decomposition efficiency [37, 38, 40, 41, 100].

2.9.1.5 Considerations in practical application of hot catalytic NH_3 removal

The practical considerations of integration of the hot catalytic reactor for NH_3 removal in the biomass gasification process include the overall energy efficiency, the impacts on environment, and the recyclability of the catalyst applied. The overall energy efficiency of the implementation of the hot catalytic reactor is related to the downstream gas applications. For the IGCC system, where the producer gas is used in the gas engine or gas turbine operating at high temperature, the temperature of the producer gas after NH_3 removal in the hot catalytic reactor is still high, thus the cleaned producer gas is suitable for the gas engine or gas turbine, and the sensible heat of the producer gas is not lost. The hot catalytic reactor is also suitable for IGFC systems, where molten carbonate fuel cell (MCFC) and solid oxide fuel cell (SOFC) are used because they are operated at about 650°C and 1,000°C, respectively. However, for the IGFC system with proton exchange membrane fuel cell (PEMFC) and phosphoric acid fuel cell (PAFC) being used and for FT liquid fuel synthesis, the hot catalytic reactor may not be the best option because the PEMFC, the PAFC, and the FT synthesis reactor are operated at 50-100°C, 220°C, and 200-250°C, respectively. In these cases, the hot cleaned producer gas has to be cooled down, in which cases some sensible heat is lost, or a series of heat exchangers is needed for the heat recovery.

The impacts on the environment of the application of hot catalytic reactor is related to the disposal of the catalysts, especially the Ni metal, which is considered as a hazardous metal. Therefore, special disposal treatment is needed. However, if the catalysts used in the hot catalytic reactor have high durability and stability and they are able to be regenerated, it would reduce the amount of metal catalyst for disposal.

2.9.1.6 Conclusions

(1) High temperature, low pressure (atmospheric pressure), and long gas space time are required in the downstream hot catalytic reactor to enhance the NH_3 decomposition reaction and to prevent sulphur poisoning of the catalysts applied.

(2) Pure alkaline earth metal oxides such as CaO and MgO and non metal-loaded activated carbon might not be effective for NH_3 removal in the biomass gasification producer gas since these catalysts have shown poor performance even in inert gas.

(3) Fe-based catalysts present in natural minerals, including limonite, coal char, ferrous dolomite and sintered iron ore, are potential catalysts to be used in the hot catalytic reactor for NH_3 decomposition. The highly-dispersed nanoscale metallic α-Fe particle is the key factor to achieve high NH_3 conversion. However, further experimental study of these catalysts with the producer gas is needed to confirm their catalytic activity in the real producer gas from biomass gasification.

(4) Natural minerals with high Fe and Ca contents have high potential to reduce NH_3 in the biomass gasification producer gas.

(5) Ni-based catalysts are also promising for NH_3 removal from the biomass gasification producer gas in a hot catalytic reactor. The higher loading of Ni metal gives better performance for NH_3 removal. However, the costs for the Ni-based catalysts may be a barrier for commercial applications.

(6) For commercial applications, more studies are needed to develop and test more affordable catalysts, which have high catalytic activity without deactivation in a long run and whose activity can easily be regenerated.

2.9.2 Downstream hot gas removal of H_2S

Research is reviewed and discussed on the downstream hot gas desulphurisation of H_2S removal by adsorption or gas-solid reactions. Reduction of H_2S in the producer gas using metal sorbents in the hot gas desulphurisation is well known. The sulphidation reaction and regeneration reaction of metal oxides (MO_x) are generally shown as Equations 2.42 and 2.43 [21, 26, 82].

Sulphidation reaction: $$M_yO_{x(s)} + xH_2S_{(g)} \rightarrow M_yS_{x(s)} + xH_2O_{(g)} \quad (2.42)$$

Sorbent regeneration: $$M_yS_{x(s)} + 1.5xO_{2(g)} \rightarrow M_yO_{x(s)} + xSO_{2(g)} \quad (2.43)$$

The desirable sorbents for desulphurisation to be both economical and operational should be: (1) high equilibrium constant and fast kinetics for the sulphidation reaction; (2) high H_2S adsorption capacity to reduce both the sorbent quantity and process equipment size; (3) high H_2S selectivity to minimise side reactions; (3) high chemical stability in reducing gas atmosphere; (4) high mechanical strength to minimise attrition in turbulent conditions; and (5) regenerable by a suitable pathway and maintaining high H_2S adsorption capacity during repeated sulphidation-regeneration cycles [21, 26].

Oxides of metals including Fe, Zn, Ca, Mn, and Cu are among the most promising and most extensively examined for desulphurisation activities at a temperature window of 350-870°C. Table 2.9 presents the metal oxide sorbents and their sulphidation-regeneration temperatures. Several noble metal oxides such as molybdenum (Mo), tungsten (W), strontium (Sr), and barium (Ba) are also capable of H_2S removal, although they are not suitable [26]. Molybdenum and tungsten oxides form carbides and result in low desulphurisation capacity. Strontium- and barium-based carbonates behave similarly to calcium carbonate, but calcium carbonate is preferable due to its lower cost and wide operation temperatures [26]. Therefore, in the following sections, the findings and details of the studies of Fe, Zn, Ca, Mn, and Cu on H_2S desulphurisation are discussed. The review of the studies of H_2S desulphurisation downstream of the gasification process with metal oxides can be found in Cheah et al. [26], Mitchell [82], and Meng et al. [25].

Table 2.9 Sulphidation-regeneration temperatures of selected metal oxide sorbents [82]

Sorbent material	**Sulphidation temperature (°C)**	**Regeneration temperature (°C)**	**Sorbent utilisation (%)**
Iron oxide	360-500	500-650	25-45
Zinc oxide	480-540	500-700	50-70
Zinc ferrite	450-600	600	20-80
Zinc titanate	450-750	600-750	40-60
Manganese oxide	350-870	900	50
Copper oxide	350-550	650	70
Copper chromite	650-850	750	40-80

2.9.2.1 Iron-based sorbents

Desulphurisation reactivity of Fe_2O_3 is high at the temperatures of 400-450°C, but its reactivity is lower than that of other metal oxides at above 550°C [82]. The principal reactions related to H_2S sulphidation with Fe_2O_3 are described as follows:

Sorbent reduction: $3Fe_2O_{3(s)} + H_{2(g)} \rightarrow 2Fe_3O_{4(s)} + H_2O_{(g)}$ (2.44)

Sulphidation reaction: $Fe_3O_{4(s)} + 3H_2S_{(g)} + H_{2(g)} \rightarrow 3FeS_{(s)} + 4H_2O_{(g)}$ (2.45)

Sorbent regeneration: $2FeS_{(s)} + 3.5O_{2(g)} \rightarrow Fe_2O_{3(s)} + 2SO_{2(g)}$ (2.46)

SO_2 reduction: $xCO_{(g)} + (2\text{-}x)H_{2(g)} + SO_{2(g)} \rightarrow xCO_{2(g)} + (2\text{-}x)H_2O_{(g)} + S_{(g)}$ (2.47)

Fe_2O_3 is reduced to Fe_3O_4 prior to desulphurisation to avoid the use of H_2 in the producer gas for sorbent reduction reaction, and then the sulphidation reaction starts. Iron sulphide (FeS) formed from sulphidation reaction can be simply regenerated by using low O_2 concentration (<1.5 vol%). SO_2 gas produced from sorbent regeneration reaction is recovered to elemental S by the SO_2 reduction reaction using the producer gas at 250°C [82]. Iron oxide materials can be readily reduced in reducing producer gas at high temperature according to Equation 2.48. The two-stage reduction of Fe_2O_3 by H_2 gas was found in which Fe_2O_3 was reduced to Fe_3O_4 and then to metallic Fe [129].

H_2 reduction: $Fe_2O_3 \rightarrow Fe_3O_4 \rightarrow Fe$ (2.48)

Metallic Fe formed from the reduction of Fe_2O_3 was observed to have desulphurisation reactivity with H_2S to form FeS or $FeS_{1.1}$ as shown in Equation 2.49 [85, 130].

Sulphidation reaction: $Fe_{(s)} + H_2S_{(g)} \rightarrow FeS_{(s)} + H_{2(g)}$ (2.49)

Sorbent regeneration: $2FeS_{1.1(s)} + 3.7O_{2(g)} \rightarrow Fe_2O_3(s) + 2.2SO_{2(g)}$ (2.50)

Sorbent regeneration: $3FeS_{1.1(s)} + 2SO_{2(g)} \rightarrow Fe_3O_4(s) + 2.65S_{2(g)}$ (2.51)

The study in the kinetics of regeneration of FeS was conducted using O_2 and SO_2 [130]. It was found that the sorbent regeneration reaction with air was fast and the final product was Fe_2O_3 (Equation 2.50), while with SO_2, the reaction was slow and the major product was Fe_3O_4 (Equation 2.51) [130].

In addition to the desulphurisation performance of iron oxides and metallic Fe, it was found that iron oxides and metallic Fe have a catalytic activity towards the water-gas shift reaction that converts CO and H_2O to H_2 and CO_2 at 350-500°C [26, 131] and 750-950°C [93], respectively. Consequently, consideration of using iron-based sorbents for the H_2S desulphurisation should be also given to their effect on the alteration of producer gas composition due to the water-gas shift reaction. The effect of catalytic activity of iron-based sorbents on the water-gas shift reaction can be positive, as they offer additional production of H_2 in the expense of CO which could be suitable for downstream fuel synthesis.

2.9.2.2 Zinc-based sorbents

Early studies focused on the iron oxide sorbents as they are cheap and abundant. However, due to their limited desulphurisation capacity at high temperatures, more interest changed to zinc oxide sorbents, as their thermodynamic properties are favourable at high temperatures [82]. Common zinc oxide sorbents that have been tested in desulphurisation include zinc oxide (ZnO), zinc ferrite ($ZnFe_2O_4$), and zinc titanate ($ZnTiO_3$, Zn_2TiO_4, and $Zn_2Ti_3O_8$) [21, 26, 82]. Tertiary mixtures of modified zinc oxides have also been investigated, but they are not intensively reviewed in this section.

ZnO filters are considered suitable for removal of H_2S in biomass producer gas for FT liquid fuel synthesis [11, 48, 132]. The reaction of ZnO with H_2S is thermodynamically favourable at temperatures above 600°C [26]. However, reduction of ZnO in the reducing gas stream followed by volatilisation of the zinc metal created a problem [26, 133]. Therefore, the application of ZnO for sulphidation reaction is limited to the temperatures below 550°C [133]. Furthermore, zinc sulphate ($ZnSO_4$) can be formed during regeneration process when excess O_2 was used [26, 82]. Repeated sulphidation and regeneration reactions can cause the mechanical stress and spalling (breaking into small pieces) of the sorbent particles due to a large difference of the molar volume of ZnO (15 cm^3/mol) or ZnS (24 cm^3/mol), and $ZnSO_4$ (46 cm^3/mol) [26, 82, 134]. This leads to increased sorbent losses and to reduction of sorbent reactivity and capacity for H_2S [82]. Consequently, the studies on the stability improvement of ZnO with the addition of Fe_2O_3 or TiO_2 have been intensively conducted.

Zinc ferrite is a double oxide of Zn and Fe with the chemical formula $ZnFe_2O_4$ [82]. The addition of ZnO into Fe_2O_3 improves the sorbent stability, desulphurisation efficiency, and capacity, as well as increases the sulphidation temperature to about 450-600°C [26, 82]. The main reactions related to desulphurisation by zinc ferrite are represented by Equations 2.52 to 2.54 [82]:

Sorbent reduction: $ZnOFe_2O_{3(s)} + 0.33H_{2(g)} \rightarrow ZnO_{(s)} + 0.67Fe_3O_{4(s)} + 0.33H_2O_{(g)}$ (2.52)

Sulphidation reaction: $ZnO_{(s)} + 0.67Fe_3O_{4(s)} + 3H_2S_{(g)} + 0.67H_{2(g)} \rightarrow ZnS_{(s)} + 2FeS_{(s)} + 3.67H_2O_{(g)}$ (2.53)

Sorbent regeneration: $ZnS_{(s)} + 2FeS_{(s)} + 5O_{2(g)} \rightarrow ZnOFe_2O_{3(s)} + 3SO_{2(g)}$ (2.54)

Zinc ferrites showed a high sulphur capacity of more than 30 g S/100 g fresh catalyst and retained their capacity after many sulphidation-regeneration cycles [21]. In a coal gas, they reduced H_2S concentration to about 10 ppmv, and the addition of copper into zinc ferrites can decrease H_2S to below 1 ppmv. However, they tended to accumulate carbon on the surface during the sulphidation-regeneration cycles in which the carbon accumulation increased with steam concentration in the coal gas [21]. When the zinc ferrite was operated above 600°C, excessive sorbent loss and spalling was observed [82]. Disintegration of the zinc ferrite into ZnO and Fe_2O_3 and then reduction of ZnO and Fe_2O_3 to Zn and to Fe_3O_4 or metallic Fe, respectively, was also found at high temperatures [26, 82]. It was thus the applicability of zinc ferrite was limited to below 600°C and to moderately reducing gases.

Zinc titanate is formed by the solid-state reaction of ZnO and TiO_2 at 760-890°C to $ZnTiO_3$ [82]. The zinc titanates present as $ZnTiO_3$, Zn_2TiO_4, or $Zn_2Ti_3O_8$ [82]. Zinc titanates have a sulphur capacity of 20 g S/100 g sorbent and can decrease H_2S concentration in a coal gas to less than 10 ppm [21]. It was found that the TiO_x around the Zn ions protects them against reduction by H_2 and CO and thus zinc titanates can be used at higher temperatures than those of ZnO and zinc ferrites [21]. The main reactions related to desulphurisation by zinc ferrite are represented by Equations 2.55 to 2.57 [82]:

Sulphidation reaction: $ZnTiO_{3(s)} + H_2S_{(g)} \rightarrow ZnS_{(s)} + TiO_{2(s)} + H_2O_{(g)}$ (2.55)

Sulphidation reaction: $Zn_2TiO_{4(s)} + 2H_2S_{(g)} \rightarrow 2ZnS_{(s)} + TiO_{2(s)} + 2H_2O_{(g)}$ (2.56)

Sorbent regeneration: $2ZnS_{(s)} + TiO_{2(s)} + 3O_{2(g)} \rightarrow Zn_2TiO_{4(s)} + 2SO_{2(g)}$ (2.57)

In summary, zinc ferrites and zinc titanates have high S capacity, ability to remove H_2S in the coal-derived fuel gas to a few ppmv, and high feasibility to be regenerated with air. The sulphidation reaction is limited to temperatures below 600°C for zinc ferrite and 700°C for zinc titanate [135].

2.9.2.3 Calcium-based sorbents

As mentioned in Section 2.8.4, Ca-based sorbents, mainly limestone ($CaCO_3$) and dolomite ($CaCO_3{\cdot}MgCO_3$), have been used for in-bed desulphurisation of H_2S in the fluidised bed gasifier. The Ca-based sorbents can also be used downstream of the gasifier in an external reactor as well as injecting into the gas stream [82]. It was found that calcined forms of limestone and dolomite have faster sulphidation kinetics and higher sorbent conversion of CaO or $CaCO_3$ to CaS than those of uncalcined limestone and dolomite [26, 84]. The two sulphidation reactions of CaO and $CaCO_3$ are the same as those shown in Equations 2.21 and 2.23.

The tests of calcined dolomite for hot gas desulphurisation were carried out by Álvarez-Rodríguez and Clemente-Jul [136]. They studied the effects of main operating parameters (i.e. gas velocity, bed length, grain size, gas temperature, and gas composition) on the performance of dolomite adsorption. They concluded that the main factors for the decrease in H_2S content during the initial stages of the bed use were gas velocity, bed length, and inlet H_2S concentration [136]. Lower gas velocity, lower inlet H_2S concentration, and higher bed length contributed to reduction of H_2S content in the gas. The two temperatures studied at 850 and 950°C had very small effects on the conversion of H_2S and COS. The H_2S reduction from 20,000 ppmv to about 200-500 ppmv in the initial stages could be achieved with calcined dolomite [136].

2.9.2.4 Manganese-based sorbents

Due to the reduction and volatilisation problem of using zinc-based sorbents at high temperatures above 700°C for H_2S desulphurisation in reducing producer gas, interest was paid on the development of other metal oxides for the high temperature desulphurisation [135]. Manganese oxides were found to be promising sorbents for a high temperature desulphurisation process [135].

Four stable manganese oxides include MnO, Mn_3O_4, Mn_2O_3, and MnO_2. Manganese oxides are resistant to reduction to elemental Mn by H_2 and CO due to the presence of CO_2 and H_2O in the producer gas [135]. In a reducing atmosphere, manganese oxides of higher oxidation state tend to be reduced to MnO [135]. MnO showed high desulphurisation in the temperatures of 600-700°C and did not decompose to elemental Mn [135]. However, the thermodynamics of MnO sulphidation was not as high as that of some other metal oxides such as zinc and copper oxides, but MnO offered high stability at higher temperatures [26, 135]. Another disadvantage of manganese oxides is that they are likely to form sulphate and require very high temperature for regeneration process [26]. It was discovered that oxidative regeneration at 900°C is necessary to avoid the sulphate formation [26].

In the study conducted by Bakker et al. [137], monolith and particle-shaped Mn sorbents, containing mainly Mn_3O_4, superimposed on the pattern of γ-Al_2O_3, had high desulphurisation capacity. These Mn sorbents could be used between 400 and 1,000°C, and the optimum capacity was obtained when the temperature was between 827 and 927°C. The sorbents removed H_2S from 6,400 ppmv down to 5-50 ppmv and the sulphur capacity was as high as 20 wt% S [137]. After the sulphidation reaction, the XRD detected MnS and γ-Al_2O_3. The sorbents can be regenerated with SO_2 to produce elemental S and the regeneration temperature should be above 600°C to avoid sulphate formation. The sorbent performance appeared to be stable during at least 110 sulphidation and regeneration cycles at 850°C [137].

2.9.2.5 Copper-based sorbents

Copper-based sorbents are the other promising sorbents that have been widely investigated due to their favourable sulphidation reaction equilibrium [26]. Copper oxides such as CuO

and Cu_2O have shown high performance to remove H_2S to very low level provided that the reduction of copper oxides to elemental Cu did not occur. Similar to iron oxides, copper oxides are readily reduced to elemental Cu in a reducing gas at high temperature which lower the reactivity for desulphurisation [26]. Thus, more studies of copper-based sorbents have been emphasized on the stabilisation of them with other metal oxides and successful results have been obtained [26].

The studies have shown that iron oxide (Fe_2O_3) and aluminium oxide (Al_2O_3) play an important role in stabilisation of CuO against complete reduction to elemental Cu in the temperature between 538 and 600°C [138, 139]. The sulphided sorbents can be regenerated using a mixture of N_2-air or N_2-air-steam without deterioration of subsequent sulphidation performance [138, 139]. However, sulphate formation of $CuO{\cdot}Al_2O_3$ sorbents during desulphurisation and regeneration reactions was found, and it resulted in copper sulphate or aluminum sulphate [138, 140]. Chromium oxide (Cr_2O_3) also enhanced the stabilisation of Cu_2O against complete reduction to Cu in the temperature range of 550-650 °C [141]. Copper chromite ($Cu_2O{\cdot}Cr_2O_3$) was able to remove H_2S from 2 vol% down to less than 5 ppmv at 600°C. The optimum desulphurisation temperature was determined to be about 600°C in terms of sorbent efficiency (H_2S levels in the cleaned fuel gas) and utilisation (sulphur capacity at breakthrough or effective capacity) for the copper chromite sorbent [141]. A dilute mixture of O_2-N_2 was used for sorbent regeneration at 750°C and complete conversion of the copper sulphide to oxide without sulphate formation or reactivity deterioration in over 15 cycles was achieved [141].

2.9.2.6 Regeneration process

Regeneration is required to reactivate the sulphided metal sorbents back to their original states (metal oxides) via oxidation reaction [26, 82]. The oxidants commonly used include steam, air, O_2, and SO_2. The types of products such as H_2S, SO_2, elemental S, or a combination of these gases generated from the regeneration reactions depend on the oxidant and operation conditions employed. Therefore, in this section, three regeneration processes based on the oxidant type are described.

2.9.2.6.1 Regeneration with steam

Regeneration of sulphided metal sorbents by using steam is the reverse reaction of sulphidation reaction (Equation 2.42) as shown in Equation 2.58. With the use of steam, H_2S is produced.

Reverse sulphidation reaction: $M_yS_{x(s)} + xH_2O_{(g)} \rightarrow M_yO_{x(s)} + xH_2S_{(g)}$ (2.58)

A simplified schematic diagram of the regeneration process with steam is shown in Figure 2.15. In the schematic diagram, a system consisting of two stationary packed bed reactors is used: one reactor is used for sulphidation reaction while the other reactor is used for regeneration of the spent sorbents [26]. H_2S is produced in the regeneration reaction and it is a precursor of SO_2, therefore, a scrubber is used to remove H_2S in the tail gas [26].

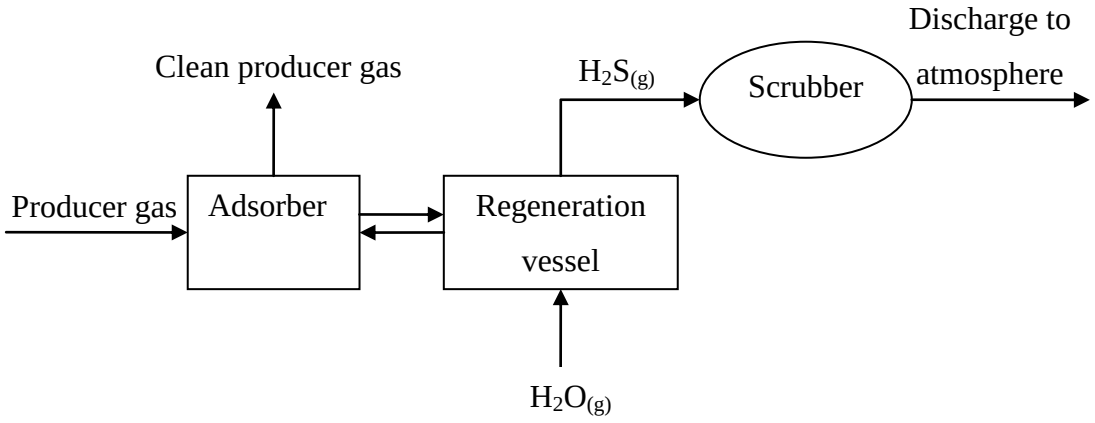

Figure 2.15 Schematic diagram of the regeneration process with steam [26]

2.9.2.6.2 Regeneration with O_2 or air

Regeneration of sulphided metal sorbents with O_2 or air is commonly used for regenerable metal oxides [82]. The O_2 or air oxidation regeneration is highly exothermic, and thus low O_2 concentration or a large amount of diluents such as N_2 or steam is required to control the temperature and prevent sorbent sintering, spalling, and sulphate formation [26, 82]. The O_2 regeneration reactions of iron sulphide (FeS) to form iron oxide (Fe_2O_3) are presented in Equations 2.46 and 2.50. For the regeneration of zinc sulphide (ZnS) with low concentration of O_2, SO_2 is produced as shown in Equation 2.59. With too high O_2

concentration, zinc sulphate ($ZnSO_4$) is formed as shown in Equations 2.60 and 2.61. Prevention of $ZnSO_4$ formation can be carried out by using sufficiently high temperature and controlling an O_2 concentration as well as operation pressure [26].

Sorbent regeneration: $2ZnS_{(s)} + 3O_{2(g)} \rightarrow 2ZnO(s) + 2SO_{2(g)}$ (2.59)

Sulphation reaction: $ZnS_{(s)} + 2O_{2(g)} \rightarrow ZnSO_4(s)$ (2.60)

Sulphation reaction: $2ZnO_{(s)} + 2SO_{2(g)} + O_{2(g)} \rightarrow 2ZnSO_4(s)$ (2.61)

A schematic diagram of the regeneration process with O_2 is given in Figure 2.16. SO_2 produced from the regeneration can be recovered to elemental S through the conventional Claus process or the direct sulphur recovery process (DSRP) [26]. In the DSRP, a slipstream of the producer gas containing H_2 and CO is injected into the vessel.

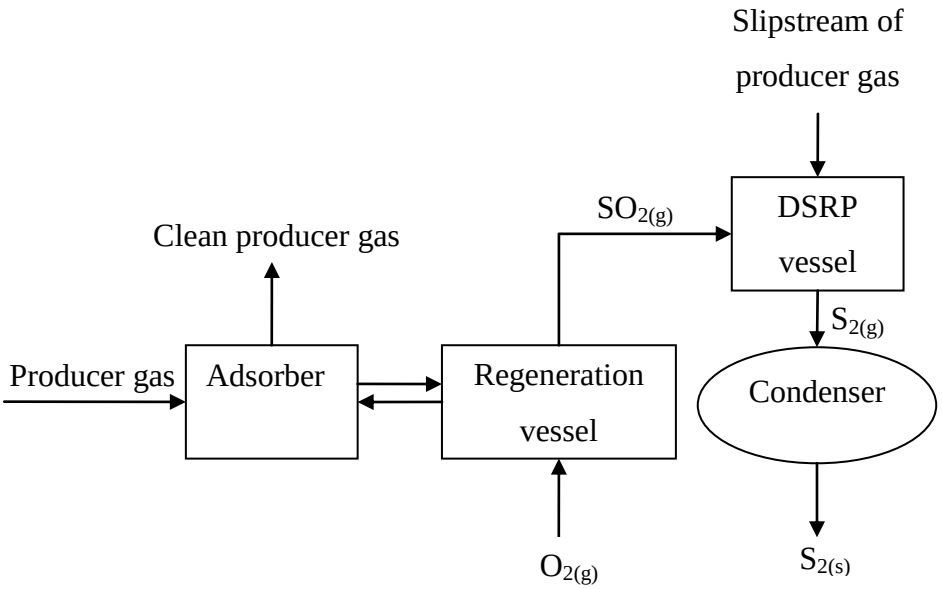

Figure 2.16 Schematic diagram of the regeneration process with O_2 [26]

2.9.2.6.3 Regeneration with SO_2

A direct production of elemental S can be achieved by using SO_2 as an oxidant. Sorbents of Fe, Ma, and cerium (Ce) can be regenerated with SO_2 to produce elemental S [82]. A schematic diagram of the regeneration process with SO_2 to directly produce elemental S is shown in Figure 2.17. MnS is regenerated with SO_2 to produce elemental S based on

Equations 2.62 and 2.63 [137]. MnO, $MnAl_2O_4$, and elemental S are the product of regeneration reactions [137]. The regeneration temperature should be above 600°C to avoid sulphate formation [137].

Sorbent regeneration: $4MnS_{(s)} + 2SO_{2(g)} \rightarrow 4MnO(s) + 3S_{2(g)}$ (2.62)

Sorbent regeneration: $4MnS_{(s)} + 4Al_2O_{3(s)} + 2SO_{2(g)} \rightarrow 4MnAl_2O_4(s) + S_{2(g)}$ (2.63)

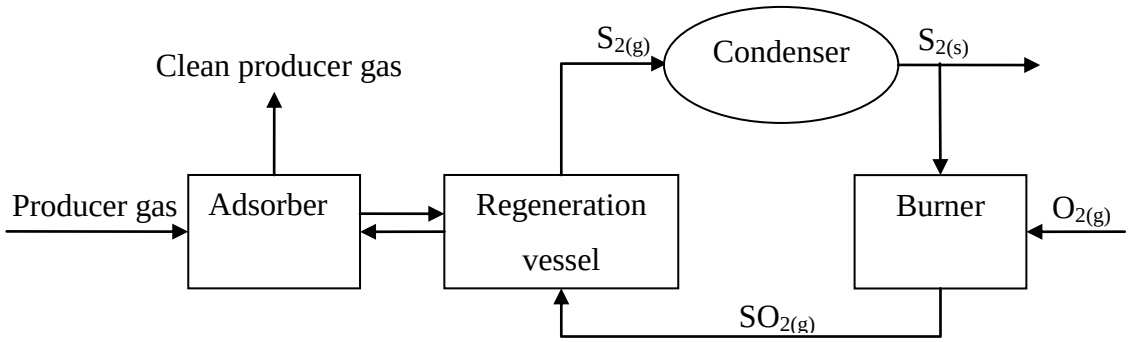

Figure 2.17 Schematic diagram of the regeneration process with SO_2 to directly produce elemental S [26]

2.9.2.7 Conclusions

(1) Metal oxides including Fe, Zn, Ca, Mn, and Cu are the potential sorbents to be effectively used to remove H_2S in the coal and biomass producer gas at the temperature between 350 and 870°C. Fe, Zn, and Cu are prone to reduction to metallic elements at high temperature in a reducing gas stream and thus they are suitable to be used at mid-temperature ranges. Zinc titanate, copper chromite, and Mn-based sorbents have high stability against reduction reaction at higher temperatures, therefore, they are potentially used above 600°C.

(2) Ca-based sorbents, mainly limestone ($CaCO_3$) and dolomite ($CaCO_3 \cdot MgCO_3$), can be applied for H_2S desulphurisation in the bed of the fluidised bed gasifier, in downstream of the gasifier in an external reactor, and by injecting into the gas stream. They are commonly used as a once-through mode because they are cheap and soft to form sulphate during regeneration process.

(3) Fe-based materials are promising for the simultaneous removal of H_2S and NH_3 as they are found to be effective sorbents for H_2S desulphurisation and effective catalysts for NH_3 decomposition reaction. Further studies with the Fe-based materials are necessary to determine their performance and efficiency on the simultaneous removal of H_2S and NH_3.

2.10 Sampling and analysis of NH_3 and H_2S in producer gas

Sampling and analysis of NH_3 and H_2S in producer gas from biomass gasification process has been reviewed in this section. A reliable sampling method is a prerequisite for the determination of NH_3 and H_2S concentrations. The analysis of NH_3 and H_2S can be divided into two methods: (1) wet chemical methods by impinger system and (2) direct analytical methods, for example gas chromatography (GC) and chemical vial tube.

2.10.1 Sampling of NH_3 and H_2S

There are some aspects to be considered in the sampling system for NH_3 and H_2S: (1) material used for the sampling line; (2) removal of particulates (char and fine bed material) and tars; and (3) avoidance of water vapour condensation. The material aspect is of primary concern because NH_3 can be catalytically or non-catalytically reacted with some reactive materials [142], and H_2S is a reactive gas that can be selectively adsorbed on glass or metal surfaces [143, 144]. In laboratory tests, it was found that 60 ppmv NH_3 in N_2 and 25 ppm H_2S in N_2 can be successfully transported through the stainless steel (type 316) tubing at temperature lower than 200°C [52, 144]. At a higher temperature of 400°C, NH_3 can still be passed through the stainless steel without any detectable losses, however, major H_2S losses were observed [52, 144]. The use of stainless steel tubing coated with an inert amorphous silicon material (Silcosteel or SilcoNert 1000 coating), developed by the SilcoTek Company, proved successful for H_2S sampling at 400°C [144]. Moreover, desirable results were obtained with 60 ppmv NH_3 in N_2 when using the polytetrafluoroethylene (PTFE) tubing at 25 and 200 °C [52]. As PTFE melts at 400 °C, a test at that temperature was not performed [52]. Thus, the metal surface of the sampling line that is in contact with NH_3 and H_2S gases at high temperatures above 200°C should be coated with inert materials such as amorphous silicon material (Silcosteel or SilcoNert 1000 coating) and carboxysilicon material (Dursan) from SilcoTek Company [145]. Below 200°C, PTFE and

Perfluoroalkoxy (PFA) should be used to ensure effective sample transport over a wide range of H_2S concentration [143, 144].

Producer gas from the gasification process contains mainly gas components (H_2, CO, CO_2, CH_4, and H_2O) and a small amount of particulates (char and fine bed material) and tars. The particulates and tars can cause damage or interference to the analytical instruments [143]. Thus, they must be removed from producer gas before it can be analysed for NH_3 and H_2S. A small quartz thimble filter is a good option for particulate removal as it is made from inert quartz material, and its low surface area minimises the potential for NH_3 and H_2S losses on the wall surface [52]. A ceramic filter (SiC) can also be used for particulate removal at the process temperature and pressure in which the filter can be back-flushed with N_2 to clean up the sampling line [143]. An additional quartz filter operated at a gas temperature of 150-200°C is used as a safeguard in case of failure of the SiC high temperature filter [143]. After particulates are removed from producer gas, the tars are condensed in the coil, which consists of 3-6 m of 9.5 mm OD tubing [52]. The condensation coil is heated to about 100°C, which is above the moisture dew point of the producer gas. This allows the tars to condense in the coil while avoiding moisture condensation [52]. In addition, since NH_3 and H_2S are soluble in water, condensation of water vapour in the sampling line has to be avoided [52]. Thus, the sampling line should be heated to above the water dew point of the producer gas.

2.10.2 Analysis of NH_3 and H_2S

2.10.2.1 Wet chemical methods

With consideration of the sampling aspects in mind, an off-line, wet chemical technique for the determination of NH_3 and H_2S in the producer gas has been widely employed [30, 32, 48, 49, 52, 56, 58, 60, 72, 146]. In the wet chemical method, the producer gas is sampled through the impinger bottles containing acidic solution for NH_3 absorption and alkaline or cadmium solution for H_2S absorption. The NH_3 in the solution is then analysed by ion chromatography (IC) [56, 58, 146], ion selective electrode (ISE) [30, 48, 60, 72], titration [32, 49, 52], and colourimetry [52]. For H_2S in the solution, it can be analysed by potentiometric titration method [146] and iodometry [60].

2.10.2.2 Direct analytical methods

Direct gas stream analytical methods have also been used for NH_3 and H_2S analysis. NH_3 gas can be determined by Fourier transform infrared (FTIR) gas analyser [18, 40, 41], whereas H_2S gas is analysed by gas chromatography (GC) [19, 48, 75, 144], chemical vial tube [52], and mass spectrometer (MS) [40, 41]. H_2S in producer gas is typically determined by a GC equipped with a sulphur chemiluminescence detector (SCD) [48] or a flame photometric detector (FPD) [19, 75, 144]. The significant cost of the GC, FTIR, and MS instruments creates a barrier for their use in NH_3 and H_2S analysis [144].

The chemical vial tube, such as Dräger tube from Dräger Company [147], is a glass vial filled with a chemical reagent that reacts to a specific chemical and changes its colour. A calibrated sample gas volume is drawn through the tube with a Dräger accuro bellows pump. The targeted chemical present in the gas changes the colour of the reagent in the tube, and the length of the colour change indicates the measured concentration. The Dräger tubes are available for measurement of various H_2S concentrations from 0.2 ppmv to 40 vol%. The standard deviations of the H_2S tubes are within ±5-20% [147]. There do not appear to be significant interferences for the gas of interest. However, the Dräger tubes are calibrated to be used at a temperature between 0 and 60°C and at a maximum absolute humidity of no more than 40 mg H_2O/L [147]. Thus, the producer gas must be cooled down to below 60°C and the gas moisture should be lower than 40 mg H_2O/L. These specifications could limit the use of the Dräger tube for H_2S measurement in the producer gas.

2.11 Conclusions

Biomass as a clean renewable energy source has gained increased attention worldwide due to a rapid growth in energy consumption and environmental concern. Gasification is a promising and versatile technology for the conversion of various biomass feedstocks into combustible gas or producer gas that can be utilised for the production of heat, power, Fischer-Tropsch (FT) liquid fuel, and other chemical products. In New Zealand, woody biomass is widely available from log harvesting and wood processing for use in biomass gasification for energy production.

At the University of Canterbury in New Zealand, a dual fluidised bed (DFB) steam gasifier has been developed, and extensive experiments have been conducted [17, 148-150]. One of the main objectives of application of the DFB steam gasifier is to produce producer gas containing high H_2 and CO contents with an optimum H_2/CO molar ratio of 2 for FT liquid fuel synthesis, and this has been achieved [17, 150]. However, it has become apparent that ammonia (NH_3) and hydrogen sulphide (H_2S) generated in the producer gas are major obstacles for FT liquid fuel synthesis. The NH_3 and H_2S gases are poisonous to employed catalysts including cobalt (Co) and iron (Fe)-based catalysts [11], and thus they must be removed from the biomass producer gas to an acceptable level for the FT liquid fuel synthesis.

Removal of NH_3 and H_2S from the producer gas in gasification process can be effectively conducted by the primary and secondary measures. The primary measures have been extensively studied in various gasifier configurations mainly in the BFB and CFB gasifiers. However, very limited studies of the primary measures in the DFB steam gasifier have been found [146]. Therefore, this research examined the effect of the DFB gasifier operation conditions and various bed materials used in the DFB steam gasifier on the NH_3 and H_2S concentrations and conversions. In addition, the influence of lignite to fuel ratio on the NH_3 and H_2S concentrations and conversions in co-gasification of blended lignite and wood pellets was also investigated.

For the secondary measures, cold and hot gas cleaning processes have been extensively studied for the removal of NH_3 and H_2S from the biomass producer gas. In the integrated biomass gasification to FT liquid fuel synthesis experiments [11, 132], cold gas cleaning was used for NH_3 removal, whereas hot gas cleaning was used for H_2S removal. This research, therefore, aimed to study the simultaneous hot gas removal of NH_3 and H_2S in one reactor with a perspective to reduce the capital and operating costs involving in the gas cleaning process.

In the hot gas cleaning process, many studies have been conducted on the downstream catalytic decomposition of NH_3 and desulphurisation of H_2S, and review papers on these studies have recently been published [25, 33]. However, very few studies on the simultaneous removal of NH_3 and H_2S in the hot gas cleaning process have been found

[151, 152]. Fe-based materials are found to be promising for the simultaneous removal of NH_3 by decomposition reaction and H_2S by desulphurisation reaction. The Fe-based materials will be studied in this research towards their performance and efficiency on the simultaneous removal of H_2S and NH_3.

2.12 References

[1] Biomass Energy Centre, What is biomass, 2011, from: http://www.biomassenergycentre.org.uk/portal/page?_pageid=76,15049&_dad=portal&_schema=PORTAL.

[2] U.S. Energy Information Administration, International Energy Outlook 2013, 2013, from: http://www.eia.gov/forecasts/ieo/index.cfm.

[3] United Nations Framework Convention on Climate Change, Kyoto Protocol, 2013, from: http://unfccc.int/kyoto_protocol/items/2830.php.

[4] Ministry for Primary Industries of New Zealand, Forestry and the New Zealand Economy, 2012, from: http://www.mpi.govt.nz/forestry.

[5] New Zealand Forest Owners Association and Ministry for Primary Industries of New Zealand, New Zealand Plantation Forest Industry Facts & Figures 2012/2013, 2014, from: http://www.nzfoa.org.nz/publications-5/facts-and-figures.

[6] Energy Efficiency and Conservation Authority, Energy from woody biomass in New Zealand, Wellington, New Zealand, 2001.

[7] P. McKendry, Energy production from biomass (part 2): conversion technologies, Bioresource Technology, 83 (2002) 47-54.

[8] C. Higman, M. van der Burgt, Gasification, in: Gulf Professional Publishing, 2008.

[9] H. Boerrigter, R. Rauch, Review of applications of gases from biomass gasification, in: the Energy research Centre of the Netherlands (ECN), the Netherlands, report no: ECN-RX--06-066, 2006.

[10] D.J. Stevens, Hot gas conditioning: Recent progress with larger-scale biomass gasification systems, in: National Renewable Energy Laboratory, the U.S. Department of Energy Laboratory, report no: NREL/SR-510-29952, 2001.

[11] H. Boerrigter, H.P. Calis, D.J. Slort, H. Bodenstaff, A.J. Kaandorp, H. den Uil, L.P.L.M. Rabou, Gas cleaning for integrated biomass gasification (BG) and Fischer-Tropsch (FT) systems: Experimental demonstration of two BG-FT systems ("Proof-of-Principle"), in: the Energy research Centre of the Netherlands (ECN), the Netherlands, report no: ECN-C--04-056, 2004.

[12] R.W.R. Zwart, Gas cleaning downstream biomass gasification: Status report 2009, in: the Energy research Centre of the Netherlands (ECN), the Netherlands, report no: ECN-E--08-078, 2009.

[13] R.C. Brown, C. Stevens, Thermochemical processing of biomass: conversion into fuels, chemicals and power, Wiley, 2011.

[14] R.C. Brown, T.R. Brown, Biorenewable resources: Engineering new products from agriculture, Wiley, 2013.

[15] H. Knoef, J. Ahrenfeldt, Handbook biomass gasification, BTG Biomass Technology Group, 2005.

[16] C. Franco, F. Pinto, I. Gulyurtlu, I. Cabrita, The study of reactions influencing the biomass steam gasification process, Fuel, 82 (2003) 835-842.

[17] W.L. Saw, S. Pang, Co-gasification of blended lignite and wood pellets in a 100 kW dual fluidised bed steam gasifier: The influence of lignite ratio on producer gas composition and tar content, Fuel, 112 (2013) 117-124.

[18] X. Meng, W. de Jong, N. Fu, A.H.M. Verkooijen, Biomass gasification in a 100 kWth steam-oxygen blown circulating fluidized bed gasifier: Effects of operational conditions on product gas distribution and tar formation, Biomass and Bioenergy, 35 (2011) 2910-2924.

[19] C. Gai, Y. Dong, T. Zhang, Distribution of sulfur species in gaseous and condensed phase during downdraft gasification of corn straw, Energy, 64 (2014) 248-258.

[20] C.V. Huynh, S.-C. Kong, Performance characteristics of a pilot-scale biomass gasifier using oxygen-enriched air and steam, Fuel, 103 (2013) 987-996.

[21] W. Torres, S.S. Pansare, J.G. Goodwin Jr., Hot gas removal of tars, ammonia, and hydrogen sulfide from biomass gasification gas, Catalysis Reviews, 49 (2007) 407-456.

[22] P. Pérez, P.M. Aznar, M.A. Caballero, J. Gil, J.A. Martin, J. Corella, Hot gas cleaning and upgrading with a calcined dolomite located downstream a biomass fluidized bed gasifier operating with steam-oxygen mixtures, Energy & Fuels, 11 (1997) 1194-1203.

[23] F. Pinto, H. Lopes, R.N. André, I. Gulyurtlu, I. Cabrita, Effect of catalysts in the quality of syngas and by-products obtained by co-gasification of coal and wastes. 1. Tars and nitrogen compounds abatement, Fuel, 86 (2007) 2052-2063.

[24] J. Leppälahti, E. Kurkela, P. Simell, P. Ståhlberg, Formation and removal of nitrogen compounds in gasification processes, in: Advances in thermochemical biomass conversion, Blackie Academic and Professional, 1994.

[25] X. Meng, W. De Jong, R. Pal, A.H.M. Verkooijen, In bed and downstream hot gas desulphurization during solid fuel gasification: A review, Fuel Processing Technology, 91 (2010) 964-981.

[26] S. Cheah, D.L. Carpenter, K.A. Magrini-Bair, Review of mid-to high-temperature sulfur sorbents for desulfurization of biomass- and coal-derived syngas, Energy & Fuels, 23 (2009) 5291-5307.

[27] P. Basu, Combustion and gasification in fluidized beds, CRC Press, 2006.

[28] P.C.A. Bergman, S.V.B. van Paasen, H. Boerrigter, The novel "OLGA" technology for complete tar removal from biomass producer gas, in: Pyrolysis and Gasification of Biomass and Waste, Expert Meeting, Strasbourg, France, 2002.

[29] J. Leppälahti, T. Koljonen, Nitrogen evolution from coal, peat and wood during gasification: literature review, Fuel Processing Technology, 43 (1995) 1-45.

[30] J. Zhou, S.M. Masutani, D.M. Ishimura, S.Q. Turn, C.M. Kinoshita, Release of fuel-bound nitrogen during biomass gasification, Industrial & Engineering Chemistry Research, 39 (2000) 626-634.

[31] M. Berg, P. Vriesman, E. Heginuz, K. Sjöström, B.-G. Espenäs, Fuel-bound nitrogen conversion: Results from gasification of biomass in two different small scale fluidized beds, in: Progress in Thermochemical Biomass Conversion, Blackwell Science, 2008.

[32] J. Leppälahti, P. Simell, E. Kurkela, Catalytic conversion of nitrogen compounds in gasification gas, Fuel Processing Technology 29 (1991) 43-56.

[33] J. Hongrapipat, W.-L. Saw, S. Pang, Removal of ammonia from producer gas in biomass gasification: integration of gasification optimisation and hot catalytic gas cleaning, Biomass Conversion and Biorefinery, 2 (2012) 327-348.

[34] E. Kurkela, P. Ståhlberg, Air gasification of peat, wood and brown coal in a pressurized fluidized-bed reactor. II. formation of nitrogen compounds, Fuel Processing Technology, 31 (1992) 23-32.

[35] J. Leppälahti, Formation and behaviour of nitrogen compounds in an IGCC process, Bioresource Technology, 46 (1993) 65-70.

[36] J. Leppälahti, Formation of NH_3 and HCN in slow-heating-rate inert pyrolysis of peat, coal and bark, Fuel, 74 (1995) 1363-1368.

[37] W. Mojtahedi, J. Abbasian, Catalytic decomposition of ammonia in a fuel gas at high temperature and pressure, Fuel, 74 (1995) 1698-1703.

[38] W. Mojtahedi, M. Ylitalo, T. Maunula, J. Abbasian, Catalytic decomposition of ammonia in fuel gas produced in pilot-scale pressurized fluidized-bed gasifier, Fuel Processing Technol, 45 (1995) 221-236.

[39] W. Wang, N. Padban, Z. Ye, A. Andersson, I. Bjerle, Kinetics of ammonia decomposition in hot gas cleaning, Industrial & Engineering Chemistry Research, 38 (1999) 4175-4182.

[40] W. Wang, N. Padban, Z. Ye, G. Olofsson, A. Andersson, I. Bjerle, Catalytic hot gas cleaning of fuel gas from an air-blown pressurized fluidized-bed gasifier, Industrial & Engineering Chemistry Research, 39 (2000) 4075-4081.

[41] W. Wang, G. Olofsson, Reduction of ammonia and tar in pressurized biomass gasification, in: 5th International symposium on gas cleaning at high temperature, Morgantown, USA, 2002.

[42] K.M. Hansson, J. Samuelsson, C. Tullin, L.E. Amand, Formation of HNCO, HCN, and NH_3 from the pyrolysis of bark and nitrogen-containing model compounds, Combustion and Flame, 137 (2004) 265-277.

[43] J. Donald, C.C. Xu, H. Hashimoto, E. Byambajav, Y. Ohtsuka, Novel carbon-based Ni/Fe catalysts derived from peat for hot gas ammonia decomposition in an inert helium atmosphere, Applied Catalysis A: General, 375 (2010) 124-133.

[44] S.Q. Turn, C.M. Kinoshita, D.M. Ishimura, J. Zhou, The fate of inorganic constituents of biomass in fluidized bed gasification, Fuel, 77 (1998) 135-146.

[45] J. Corella, J.M. Toledo, R. Padilla, Catalytic hot gas cleaning with monoliths in biomass gasification in fluidized beds. 3. their effectiveness for ammonia elimination, Industrial & Engineering Chemistry Research, 44 (2005) 2036-2045.

[46] P. Mehrling, H. Vierrath, Gasification of lignite and wood in the Lurgi circulating fluidized-bed gasifier: Final report, in: Electric Power Research Institute, Palo Alto, CA (USA); Lurgi GmbH, Frankfurt am Main (Germany, FR), report no: GS-6436, 1989.

[47] H. Boerrigter, S.V.B. van Paasen, P.C.A. Bergman, J.W. Könemann, R. Emmen, A. Wijnands, "OLGA" tar removal technology: Proof-of-Concept (PoC) for application in integrated biomass gasificaion combined heat and power (CHP) systems, in: the Energy research Centre of the Netherlands (ECN), report no: ECN-C--05-009, 2005.

[48] H. Cui, S.Q. Turn, V. Keffer, D. Evans, T. Tran, M. Foley, Contaminant estimates and removal in product gas from biomass steam gasification, Energy & Fuels, 24 (2010) 1222-1233.

[49] J. Leppälahti, E. Kurkela, Behaviour of nitrogen compounds and tars in fluidized bed air gasification of peat, Fuel, 70 (1991) 491-497.

[50] I. De Bari, D. Barisano, M. Cardinale, D. Matera, F. Nanna, D. Viggiano, Air gasification of biomass in a downdraft fixed bed: A comparative study of the inorganic and organic products distribution, Energy & Fuels, 14 (2000) 889-898.

[51] J. Corella, J.M. Toledo, R. Padilla, Olivine or dolomite as in-bed additive in biomass gasification with air in a fluidized bed: which is better?, Energy & Fuels, 18 (2004) 713-720.

[52] G.A. Norton, R.C. Brown, Wet chemical method for determining levels of ammonia in syngas from a biomass gasifier, Energy & Fuels, 19 (2005) 618-624.

[53] S. Turn, C. Kinoshita, Z. Zhang, D. Ishimura, J. Zhou, An experimental investigation of hydrogen production from biomass gasification, International Journal of Hydrogen Energy, 23 (1998) 641-648.

[54] E. Kurkela, P. Ståhlberg, Air gasification of peat, wood and brown coal in a pressurized fluidized-bed reactor. I. carbon conversion, gas yields and tar formation, Fuel Processing Technology, 31 (1992) 1-21.

[55] A. van der Drift, J. van Doorn, J.W. Vermeulen, Ten residual biomass fuels for circulating fluidized-bed gasification, Biomass and Bioenergy, 20 (2001) 45-56.

[56] C. Pfeifer, B. Puchner, H. Hofbauer, Comparison of dual fluidized bed steam gasification of biomass with and without selective transport of CO_2, Chemical Engineering Science, 64 (2009) 5073-5083.

[57] H. Hofbauer, G. Veronik, T. Fleck, R. Rauch, H. Mackinger, E. Fercher, The FICFB gasification process, in: Developments in thermochemical biomass conversion, Blackie Academic and Professional, London, 1997.

[58] T. Pröll, I.G. Siefert, A. Friedl, H. Hofbauer, Removal of NH_3 from biomass gasification producer gas by water condensing in an organic solvent scrubber, Industrial & Engineering Chemistry Research, 44 (2005) 1576-1584.

[59] B.A. van der Drift, H. Boerrigter, C.M. van der Meijden, Milena: lab-scale facility to produce a low-N_2 gas from biomass, in: 2nd World Conference and Technology Exhibition on Biomass for Energy, Industry and Climate Protection, Rome, Italy, 2004.

[60] F. Pinto, R.N. André, C. Franco, H. Lopes, C. Carolino, R. Costa, I. Gulyurtlu, Co-gasification of coal and wastes in a pilot-scale installation. 2: Effect of catalysts in syngas treatment to achieve sulphur and nitrogen compounds abatement, Fuel, 89 (2010) 3340-3351.

[61] F. Pinto, H. Lopes, R.N. André, I. Gulyurtlu, I. Cabrita, Effect of catalysts in the quality of syngas and by-products obtained by co-gasification of coal and wastes. 2: Heavy metals, sulphur and halogen compounds abatement, Fuel, 87 (2008) 1050-1062.

[62] P. Basu, Biomass gasification and pyrolysis: practical design and theory, Academic press, 2010.

[63] E. Fercher, H. Hofbauer, T. Fleck, R. Rauch, G. Veronik, Two years experience with the FICFB-gasification process, in: Proceedings of the Tenth European Conference and Technology Exhibition on Biomass for Energy and Industry, Wurzburg, Germany, 1998.

[64] H. Hofbauer, R. Rauch, G. Löeffler, S. Kaiser, E. Fercher, H. Tremmel, Six years experience with the FICFB-gasification process, in: 12th European Conference and Technology Exhibition on Biomass for Energy, Industry and Climate Protection, Amsterdam, The Netherlands, 2002.

[65] D. Bull, Performance improvements to a fast internally circulating fluidized bed (FICFB) biomass gasifier for combined heat and power plants, in: the Department of Chemical and Process Engineering, University of Canterbury, 2008.

[66] H. McKinnon, Improved hydrogen production from biomass gasification in a dual fluidised bed reactor, in: the Department of Chemical and Process Engineering, University of Canterbury, 2009.

[67] W. Vielstich, A. Lamm, H. Gasteiger, Handbook of Fuel Cells: Fundamentals, Technology and Applications, Wiley, 2003.

[68] A. Steynberg, M. Dry, Fischer-Tropsch Technology, Elsevier, 2004.

[69] L. Devi, K.J. Ptasinski, F.J.J.G. Janssen, A review of the primary measures for tar elimination in biomass gasification processes, Biomass and Bioenergy, 24 (2003) 125-140.

[70] J.H.A. Kiel, S.V.B. van Paasen, J.P.A. Neeft, L. Devi, K.J. Ptasinski, F.J.J.G. Janssen, R. Meijer, R.H. Berends, H.M.G. Temmink, G. Brem, N. Padban, E.A. Bramer, Primary measures to reduce tar formation in fluidised-bed biomass gasifiers, in: the Energy research Centre of the Netherlands (ECN), the Netherlands, report no: ECN-C--04-014, 2004.

[71] A.Z. Farzam, R.M. Felder, J.K. Ferrell, Analysis of nitrogenous compounds in the effluent streams from a fluidized bed coal gasification reactor, Fuel process technol, 10 (1985) 249-259.

[72] P. Vriesman, E. Heginuz, K. Sjöström, Biomass gasification in a laboratory-scale AFBG: influence of the location of the feeding point on the fuel-N conversion, Fuel, 79 (2000) 1371-1378.

[73] M. Pell, J.B. Dunson, T.M. Knowlton, Gas-Solid Operations and Equipment, in: Perry's chemical engineers' handbook McGraw-Hill, New York, 2008.

[74] J. Zhou, S.M. Masutani, D.M. Ishimura, S.Q. Turn, C.M. Kinoshita, Release of fuel-bound nitrogen in biomass during high temperature pyrolysis and gasification, in: Proceedings of the 32nd Intersociety Energy Conversion Engineering Conference, IECEC-97, Hawaii, USA, 1997.

[75] S.H. Aljbour, K. Kawamoto, Bench-scale gasification of cedar wood – Part II: Effect of operational conditions on contaminant release, Chemosphere, 90 (2013) 1501-1507.

[76] M. Dias, I. Gulyurtlu, H_2S and HCl formation during RDF and coal co-gasification: a comparison between the predictions and experimental results, in: Proceedings of the biomass gasification technologies workshop MRC Gebze Campus-Türkiye, 2008.

[77] H. Kuramochi, W. Wu, K. Kawamoto, Prediction of the behaviors of H_2S and HCl during gasification of selected residual biomass fuels by equilibrium calculation, Fuel, 84 (2005) 377-387.

[78] M. Yumura, T. Asaba, Rate constants of chemical reactions in the high temperature pyrolysis of ammonia, in: Symposium (International) on Combustion, Baltimore, 1981.

[79] E. Björkman, K. Sjöström, Decomposition of ammonia over dolomite and related compounds, Energy & Fuels, 5 (1991) 753-760.

[80] A. Orio, J. Corella, I. Narvaez, Performance of different dolomites on hot raw gas cleaning from biomass gasification with air, Industrial & Engineering Chemistry Research, 36 (1997) 3800-3808.

[81] S. Rapagna, N. Jand, A. Kiennemann, P. Foscolo, Steam-gasification of biomass in a fluidised-bed of olivine particles, Biomass and Bioenergy, 19 (2000) 187-197.

[82] S.C. Mitchell, Hot gas cleanup of sulphur, nitrogen, minor and trace elements, in: IEA Coal Research, 1998.

[83] A.B.M. Heesink, W.P.M. Van Swaaij, The sulphidation of calcined limestone with hydrogen sulphide and carbonyl sulphide, Chemical Engineering Science, 50 (1995) 2983-2996.

[84] K.P. Yrjas, C.A.P. Zevenhoven, M.M. Hupa, Hydrogen sulfide capture by limestone and dolomite at elevated pressure. 1. Sorbent performance, Industrial & Engineering Chemistry Research, 35 (1996) 176-183.

[85] N. Tsubouchi, H. Hashimoto, Y. Ohtsuka, Sulfur tolerance of an inexpensive limonite catalyst for high temperature decomposition of ammonia, Powder Technology, 180 (2008) 184-189.

[86] C.C. Xu, J. Donald, E. Byambajav, Y. Ohtsuka, Recent advances in catalysts for hot-gas removal of tar and NH_3 from biomass gasification, Fuel, 89 (2010) 1784-1795.

[87] J.S. Norman, M. Pourkashanian, A. Williams, The formation of ammonia in IGCC gasifiers and its control, in: Proceedings of the 2nd International Conference on Combustion and Emissions Control, London, England, 1995.

[88] P.A. Simell, J.O. Hepola, A.O.I. Krause, Effects of gasification gas components on tar and ammonia decomposition over hot gas cleanup catalysts, Fuel, 76 (1997) 1117-1127.

[89] H. Rönkkönen, P. Simell, M. Reinikainen, O. Krause, M.V. Niemelä, Catalytic clean-up of gasification gas with precious metal catalysts – a novel catalytic reformer development, Fuel, 89 (2010) 3272-3277.

[90] Y. Ozawa, Y. Tochihara, Catalytic decomposition of ammonia in simulated coal-derived gas, Chemical Engineering Science., 62 (2007) 5364-5367.

[91] Y. Ozawa, Y. Tochihara, Catalytic decomposition of ammonia in simulated coal-derived gas over supported nickel catalysts, Catalysis Today, 164 (2011) 528-532.

[92] B. Dou, M. Zhang, J. Gao, W. Shen, X. Sha, High-temperature removal of NH_3, organic sulfur, HCl, and tar component from coal-derived gas, Industrial & Engineering Chemistry Research, 41 (2002) 4195-4200.

[93] N. Tsubouchi, H. Hashimoto, Y. Ohtsuka, Catalytic performance of limonite in the decomposition of ammonia in the coexistence of typical fuel gas components produced in an air-blown coal gasification process, Energy & Fuels, 21 (2007) 3063-3069.

[94] Y. Ohtsuka, C. Xu, D. Kong, N. Tsubouchi, Decomposition of ammonia with iron and calcium catalysts supported on coal chars, Fuel, 83 (2004) 685-692.

[95] C.C. Xu, N. Tsubouchi, H. Hashimoto, Y. Ohtsuka, Catalytic decomposition of ammonia gas with metal cations present naturally in low rank coals, Fuel, 84 (2005) 1957-1967.

[96] N. Tsubouchi, H. Hashimoto, Y. Ohtsuka, High catalytic performance of fine particles of metallic iron formed from limonite in the decomposition of a low concentration of ammonia, Catalysis Letters, 105 (2005) 203-208.

[97] A. Chambers, Y. Yoshii, T. Inada, T. Miyamoto, Ammonia decomposition in coal gasification atmospheres, The Canadian Journal of Chemical Engineering, 74 (1996) 929-934.

[98] J.M. Smith, H.C. Van Ness, M.M. Abbott, Introduction to chemical engineering thermodynamics, McGraw-Hill, 2005.

[99] V. Alagharu, S. Palanki, K.N. West, Analysis of ammonia decomposition reactor to generate hydrogen for fuel cell applications, Journal of Power Sources, 195 (2010) 829-833.

[100] P. Simell, E. Kurkela, P. Ståhlberg, J. Hepola, Catalytic hot gas cleaning of gasification gas, Catalysis Today, 27 (1996) 55-62.

[101] D.A. Cooper, E.B. Ljungström, Decomposition of NH_3 over quartz sand at 840-960°C, Energy & Fuels, 2 (1988) 716-719.

[102] M. Abul-Milh, B.M. Steenari, The effect of calcination on the reactions of ammonia over different carbonates and limestones in fluidized bed combustion conditions, Energy & Fuels, 15 (2001) 874-880.

[103] T. Shimizu, E. Karahashi, T. Yamaguchi, M. Inagaki, Decomposition of NH_3 over calcined and uncalcined limestone under fluidized bed combustion conditions, Energy & Fuels, 9 (1995) 962-965.

[104] D.A. Cooper, S. Ghardashkani, E.B. Ljungström, Decomposition of NH_3 over calcined and sulfated limestone at 725-950°C, Energy & Fuels, 3 (1989) 278-283.

[105] C. Xu, J. Donald, H. Hashimoto, E. Byambajav, Y. Ohtsuka, Ammonia decomposition with metal catalysts supported on Canadian peat-derived carbons, in: 8th World Congress on Chemical Engineering, Montreal, Canada, 2009.

[106] Z.R. Ismagilov, R.A. Shkrabina, S.A. Yashnik, N.V. Shikina, I.P. Andrievskaya, S.R. Khairulin, V.A. Ushakov, J.A. Moulijn, I.V. Babich, Supported honeycomb monolith catalysts for high-temperature ammonia decomposition and H_2S removal, Catalysis Today, 69 (2001) 351-356.

[107] S.F. Yin, Q.H. Zhang, B.Q. Xu, W.X. Zhu, C.F. Ng, C.T. Au, Investigation on the catalysis of CO_x-free hydrogen generation from ammonia, Journal of Catalysis., 224 (2004) 384-396.

[108] X.K. Li, W.J. Ji, J. Zhao, S.J. Wang, C.T. Au, Ammonia decomposition over Ru and Ni catalysts supported on fumed SiO_2, MCM-41, and SBA-15, Journal of Catalysis, 236 (2005) 181-189.

[109] M.C.J. Bradford, P.E. Fanning, M.A. Vannice, Kinetics of NH_3 decomposition over well dispersed Ru, Journal of Catalysis, 172 (1997) 479-484.

[110] K. Hashimoto, N. Toukai, Decomposition of ammonia over a catalyst consisting of ruthenium metal and cerium oxides supported on Y-form zeolite, Journal of Molecular Catalysis A: Chemical, 161 (2000) 171-178.

[111] T.V. Choudhary, C. Sivadinarayana, D.W. Goodman, Production of CO_x-free hydrogen for fuel cells via step-wise hydrocarbon reforming and catalytic dehydrogenation of ammonia, Chemical Engineering Journal, 93 (2003) 69-80.

[112] T.V. Choudhary, C. Sivadinarayana, D.W. Goodman, Catalytic ammonia decomposition: CO_x-free hydrogen production for fuel cell applications, Catalysis Letters, 72 (2001) 197-201.

[113] J. Zhang, H. Xu, Q. Ge, W. Li, Highly efficient Ru/MgO catalysts for NH_3 decomposition: synthesis, characterization and promoter effect, Catalysis Communications, 7 (2006) 148-152.

[114] A.S. Chellappa, C.M. Fischer, W.J. Thomson, Ammonia decomposition kinetics over Ni-Pt/Al_2O_3 for PEM fuel cell applications, Applied Catalysis A: General, 227 (2002) 231-240.

[115] S.F. Yin, B.Q. Xu, C.F. Ng, C.T. Au, Nano Ru/CNTs: a highly active and stable catalyst for the generation of CO_x-free hydrogen in ammonia decomposition, Applied Catalysis B: Environmental, 48 (2004) 237-241.

[116] L. Li, Z.H. Zhu, Z.F. Yan, G.Q. Lu, L. Rintoul, Catalytic ammonia decomposition over Ru/carbon catalysts: the importance of the structure of carbon support, Applied Catalysis A: General, 320 (2007) 166-172.

[117] S.S. Pansare, W. Torres, J.J.G. Goodwin, Ammonia decomposition on tungsten carbide, Catalysis Communications, 8 (2007) 649-654.

[118] S.S. Pansare, J.J.G. Goodwin, S. Gangwal, Simultaneous ammonia and toluene decomposition on tungsten-based catalysts for hot gas cleanup, Industrial & Engineering Chemistry Research, 47 (2008) 8602-8611.

[119] S.S. Pansare, J.J.G. Goodwin, Ammonia decomposition on tungsten-based catalysts in the absence and presence of syngas, Industrial & Engineering Chemistry Research, 47 (2008) 4063-4070.

[120] H. Shindo, C. Egawa, T. Onishi, K. Tamaru, Reaction mechanism of ammonia decomposition on tungsten, Journal of Chemical Society, Faraday Transactions 1: Physical Chemistry in Condensed Phases 76 (1980) 280-290.

[121] A.P.C. Reed, R.M. Lambert, Mechanism of ammonia decomposition on (100) oriented polycrystalline tungsten and single-crystal W (100), The Journal of Physical Chemistry, 88 (1984) 1954-1959.

[122] P. Alnot, A. Cassuto, D.A. King, Decomposition (and synthesis) of ammonia on W{100}. A thermal molecular beam study, Faraday Discussions of the Chemical Society, 87 (1989) 291-302.

[123] T. Shimizu, Y. Tachiyama, D. Fujita, K. Kumazawa, O. Wakayama, K. Ishizu, S. Kobayashi, S. Shikada, M. Inagaki, Effect of SO_2 removal by limestone on NO_x and N_2O emissions from a circulating fluidized bed combustor, Energy & Fuels, 6 (1992) 753-757.

[124] T. Shimizu, T. Fujikawa, M. Tonsho, M. Inagaki, Effect of batch feeding of limestone on NO_x and SO_2 emissions during petroleum coke combustion in a bubbling fluidized bed combustor, Energy & Fuels, 15 (2001) 1220-1224.

[125] T. Shimizu, M. Satoh, K. Sato, M. Tonsho, M. Inagaki, Reduction of SO_2 and N_2O emissions without increasing NO_x emission from a fluidized bed combustor by using fine limestone particles, Energy & Fuels, 16 (2002) 161-165.

[126] Y. Ohtsuka, N. Tsubouchi, T. Kikuchi, H. Hashimoto, Recent progress in Japan on hot gas cleanup of hydrogen chloride, hydrogen sulfide and ammonia in coal-derived fuel gas, Powder Technology, 190 (2009) 340-347.

[127] J. Hepola, P. Simell, Sulphur poisoning of nickel-based hot gas cleaning catalysts in synthetic gasification gas: II. Chemisorption of hydrogen sulphide, Applied Catalysis B: Environmental, 14 (1997) 305-321.

[128] J. Hepola, P. Simell, Sulphur poisoning of nickel-based hot gas cleaning catalysts in synthetic gasification gas: I. effect of different process parameters, Applied Catalysis B: Environmental, 14 (1997) 287-303.

[129] H.-Y. Lin, Y.-W. Chen, C. Li, The mechanism of reduction of iron oxide by hydrogen, Thermochimica Acta, 400 (2003) 61-67.

[130] S.C. Tseng, S.S. Tamhankar, C.Y. Wen, Kinetic studies on the reactions involved in the hot gas desulfurization using a regenerable iron oxide sorbent—II: Reactions of iron sulfide with oxygen and sulfur dioxide, Chemical Engineering Science, 36 (1981) 1287-1294.

[131] J. Yu, F.J. Tian, L.J. McKenzie, C.Z. Li, Char-supported nano iron catalyst for water-gas-shift reaction: Hydrogen production from coal/biomass gasification, Process Safety and Environmental Protection, 84 (2006) 125-130.

[132] H. Hofbauer, Fischer-Tropsch-Fuels and Bio-SNG, in: Central European Biomass Conference, Graz, Austria, 2008.

[133] W. Mojtahedi, J. Abbasian, H_2S removal from coal gas at elevated temperature and pressure in fluidized bed with zinc titanate sorbents. 1. cyclic tests, Energy & Fuels, 9 (1995) 429-434.

[134] T.R. Armstrong, R.D. Carneim, D.A. Berry, A review of current state-of-the-art materials for hot gas desulfurization, in: 9th Annual International Pittsburgh Coal Conference, Pittsburgh, USA, 2002.

[135] R. Ben-Slimane, M.T. Hepworth, Desulfurization of hot coal-derived fuel gases with manganese-based regenerable sorbents. 1. Loading (sulfidation) tests, Energy & Fuels, 8 (1994) 1175-1183.

[136] R. Álvarez-Rodríguez, C. Clemente-Jul, Hot gas desulphurisation with dolomite sorbent in coal gasification, Fuel, 87 (2008) 3513-3521.

[137] W.J.W. Bakker, F. Kapteijn, J.A. Moulijn, A high capacity manganese-based sorbent for regenerative high temperature desulfurization with direct sulfur production: Conceptual process application to coal gas cleaning, Chemical Engineering Journal, 96 (2003) 223-235.

[138] V. Patrick, G.R. Gavalas, M. Flytzani-Stephanopoulos, K. Jothimurugesan, High-temperature sulfidation-regeneration of copper (II) oxide-alumina sorbents, Industrial & Engineering Chemistry Research, 28 (1989) 931-940.

[139] S.S. Tamhankar, M. Bagajewicz, G.R. Gavalas, P.K. Sharma, M. Flytzani-Stephanopoulos, Mixed-oxide sorbents for high-temperature removal of hydrogen sulfide, Industrial & Engineering Chemistry Process Design and Development, 25 (1986) 429-437.

[140] K.S. Yoo, S.D. Kim, S.B. Park, Sulfation of Al_2O_3 in flue gas desulfurization by CuO/γ-Al_2O_3 sorbent, Industrial & Engineering Chemistry Research, 33 (1994) 1786-1791.

[141] J. Abbasian, R.B. Slimane, A Regenerable Copper-Based Sorbent for H_2S Removal from Coal Gases, Industrial & Engineering Chemistry Research, 37 (1998) 2775-2782.

[142] C. Li, P. Nelson, Interactions of quartz, zircon sand and stainless steel with ammonia: implications for the measurement of ammonia at high temperatures, Fuel, 75 (1996) 525-526.

[143] P. Ståhlberg, M. Lappi, E. Kurkela, P. Simell, P. Oesch, M. Nieminen, Sampling of contaminants from product gases of biomass gasifiers, in: VTT Technical Research Centre of Finland, report no: VTT Research Notes 1903, 1998.

[144] R.C. Brown, J. Smeenk, G. Norton, Development of analytical techniques and scrubbing options for contaminants in gasifier streams intended for use in fuel cells, in: Center for Sustainable Environmental Technologies at Iowa State University, 2001.

[145] SilcoTek, Dursan, 2014, from: www.silcotek.com/dursan.

[146] I. Aigner, C. Pfeifer, H. Hofbauer, Co-gasification of coal and wood in a dual fluidized bed gasifier, Fuel, 90 (2011) 2404-2412.

[147] Dräger Safety AG & Co. KGaA, Dräger-Tubes & CMS-Handbook, 16th edition, 2011.

[148] W. Saw, H. McKinnon, I. Gilmour, S. Pang, Production of hydrogen-rich syngas from steam gasification of blend of biosolids and wood using a dual fluidised bed gasifier, Fuel, 93 (2012) 473-478.

[149] W.L. Saw, S.S. Pang, Influence of mean gas residence time in the bubbling fluidised bed on the performance of a 100-kW dual fluidised bed steam gasifier, Biomass Conversion and Biorefinery, 2 (2012) 197-205.

[150] W.L. Saw, S. Pang, The influence of calcite loading on producer gas composition and tar concentration of radiata pine pellets in a dual fluidised bed steam gasifier, Fuel, 102 (2012) 445-452.

[151] H.K. Jun, S.Y. Jung, T.J. Lee, C.K. Ryu, J.C. Kim, Decomposition of NH_3 over Zn–Ti-based desulfurization sorbent promoted with cobalt and nickel, Catalysis Today, 87 (2003) 3-10.

[152] S.Y. Jung, S.J. Lee, J.J. Park, S.C. Lee, H.K. Jun, T.J. Lee, C.K. Ryu, J.C. Kim, The simultaneous removal of hydrogen sulfide and ammonia over zinc-based dry sorbent supported on alumina, Separation and Purification Technology, 63 (2008) 297-302.

3. Development of a combined hot catalytic reactor and adsorber for NH_3 and H_2S removal

3.1 Introduction

Secondary measures or downstream gas cleaning of NH_3 and H_2S conducted after the gasifier can be classified into cold gas cleaning and hot gas cleaning processes. In the cold gas cleaning, a wet scrubber with water or acid solution operated at room temperature is used to remove NH_3 [1, 2], whereas a wet scrubber with basic solution is used to scrub H_2S [3]. In the hot gas cleaning, NH_3 is removed by the catalytic decomposition reaction with catalysts and H_2S is adsorbed onto the adsorbent [4, 5]. The hot gas cleaning process operates at high temperatures and has the potential to simultaneously remove NH_3 and H_2S with proper materials that can catalyse the NH_3 decomposition reaction and adsorb H_2S.

A combined hot catalytic reactor and adsorber for simultaneous removal of NH_3 and H_2S has low investment and operating cost, and its design and operation is simple. This novel technology has a potential to remove NH_3 and H_2S in only one reactor instead of two or more as current technologies. In the present study, a lab-scale hot gas reactor has been designed, constructed, and tested, and it can be operated either in fixed-bed or bubbling fluidised bed regimes. The reaction temperature was investigated as an operating parameter affecting the efficiency of the NH_3 and H_2S removal.

This chapter presents the fundamentals of fluidisation, calculations of main parameters in fluidisation, basic design and construction of the lab-scale reactor, and experimental procedures. Additionally, preliminary experiments and results on the NH_3 decomposition in inert Ar gas are also given.

From a literature review in Chapter 2, Section 2.9, Fe-based metals present in natural minerals were identified as potential catalysts and adsorbents for removal of NH_3 and H_2S. Therefore, Fe-based sand was the main focus to be studied. Titanomagnetite sand is titanium-bearing iron sand which is abundant in New Zealand. Titanomagnetite has a high Fe content of about 58-60 wt% after it has been concentrated. Titanomagnetite with high Fe content was expected to be a high potential catalyst for NH_3 decomposition, and it was tested in the preliminary experiments. Concentration of 2,000 ppmv of NH_3 was used in the

experiments as it was the maximum concentration from wood gasification published in the literature.

Based on the reactor development and preliminary results achieved in this chapter, a set of experiments of the NH_3 and H_2S removal in the combined ht catalytic reactor and adsorber was conducted. Various natural sands abundantly available in New Zealand including titanomagnetite, iron sand containing ilmenite, and silica sand were tested in a bubbling fluidised bed regime. Details of the experiments, experimental results, and discussion on the NH_3 and H_2S removal are presented in Chapter 5.

3.2 Fundamentals of fluidisation

The understanding of fluidisation fundamentals and the determination of fluidisation velocities through the bed are important for the design and operation of a lab-scale reactor for removal of NH_3 and H_2S. This section provides comprehensive information on the phenomenon and regimes of fluidisation, advantages and disadvantages of fluidised bed, and important parameters for fluidisation operation such as minimum fluidisation velocity and particle terminal velocity.

3.2.1 Phenomenon and regimes of fluidisation

Fluidisation is the operation by which solid particles are transformed into fluidlike state through suspension in gas or liquid [6]. Introduction of gas or liquid from the bottom of a column containing solid particles via a gas distributor can cause the particles to be fluidised. The contacting modes or regimes of gas and solid particles are presented in Figure 3.1. By increasing the gas velocity or flow rate, the bed transitions from a fixed-bed to minimum fluidisation, bubbling fluidisation, slugging fluidisation, turbulent fluidisation, and lean-phase fluidisation with pneumatic transport.

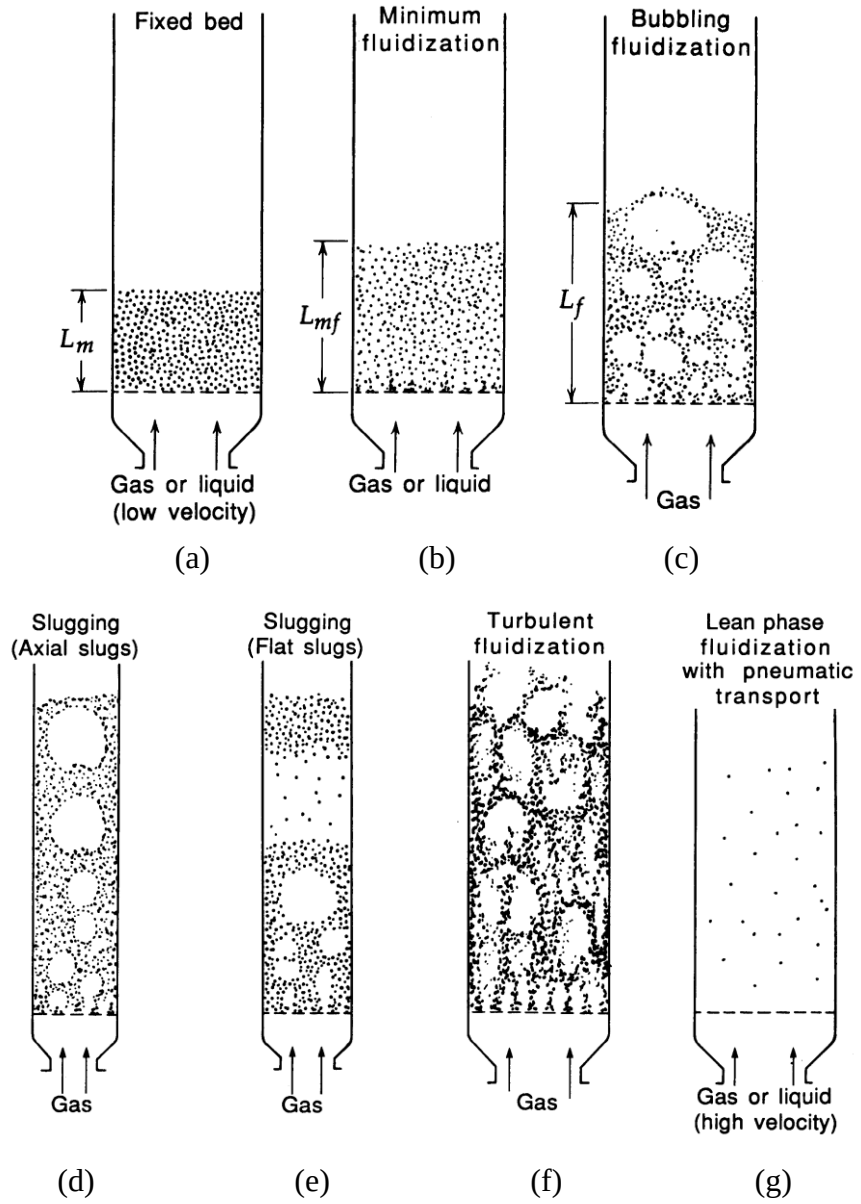

Figure 3.1 Contacting modes or regimes of gas and solid particles [6]

The fixed-bed regime occurs when gas at low velocities moves upward through a bed of solid particles, and the gas merely percolates through the void spaces between stationary particles as shown in Figure 3.1 (a) [6]. With the gas velocity increases to a point (minimum fluidisation velocity, u_{mf}), where all the particles are just suspended by the upward-flowing gas, the frictional (drag) force between particle and gas counterbalances the weight of the particles. This bed characteristic is considered to be just fluidised, and it is called an incipiently fluidised bed or a bed at minimum fluidisation (Figure 3.1 (b)) [6].

With the gas velocity increases further beyond minimum fluidisation velocity, the bed becomes unstable with gas bubbling and channelling and the bed does not expand much beyond its volume at minimum fluidisation as shown in Figure 3.1 (c). This particular bed is called an aggregative fluidised bed, a heterogeneous fluidised bed, or a bubbling fluidised bed [6]. The onset of bubbling is indicated by the minimum bubbling velocity (u_{mb}) [7].

With a continuing increase of the gas velocity, gas bubbles coalesce and become larger when they rise. When these bubbles are large enough to spread across the column, especially in a deep bed of a small diameter column, the bed is called slugging, which is classified as axial slugging or flat slugging as shown in Figure 3.1 (d) and Figure 3.1 (e), respectively. The axial slugging normally occurs with fine particles, where the particles flow smoothly down along the wall around the rising void of gas. For flat slugging with coarse particles, the portion of the bed above the bubbles is pushed upwards as by a piston and the particles fall down from the slug [6].

At a very high gas velocity which exceeds the terminal velocity (u_t) of the solid particles, the turbulent motion of solid clusters occurs, the particles are entrained, and the upper surface of the bed disappears. This type of bed is called a turbulent fluidised bed (Figure 3.1 (f)). Further increase of the gas velocity results in a disperse-, dilute-, or lean-phase fluidised bed with pneumatic transport (Figure 3.1 (g)), in which essentially large amount of solid particles are carried out of the bed by the flowing gas [6].

The classification of gas-solid contacting regimes for the fixed-bed, minimum fluidisation, bubbling fluidisation, slugging fluidisation, and turbulent fluidisation are identified by the minimum fluidisation velocity (u_{mf}), minimum bubbling velocity (u_{mb}), minimum slugging velocity (u_{ms}), particle terminal velocity (u_t), and turbulent transition velocity (u_c), and their calculations are discussed in details in Sections 3.2.3 to 3.2.7. Table 3.1 summarises the major characteristics of gas-solid contacting regimes.

Table 3.1 Major characteristics of gas-solid contacting regimes [7]

Gas velocity range	Regime	Appearance and principle features
$0 < u < u_{mf}$	Fixed-bed	- Particles are stationary - Gas flows through interstices
$u_{mf} < u < u_{mb}$	Bubble-free fluidisation	- Bed expands smoothly and uniformly - Top surface is well defined - Some small scale particle motion - Little tendency for particles to aggregate - Very little pressure fluctuation
$u_{mb} < u < u_{ms}$	Bubbling fluidisation	- Voids form near the distributor, grow mostly by coalescence, and rise to the surface - Top surface is well defined with bubbles breaking through periodically - Irregular pressure fluctuations of appreciable amplitude - Bubble size increases as u_o increases
$u_{ms} < u < u_c$	Sluggish fluidisation	- Voids fill most of the column cross section - Top surface rises and collapses periodically with a reasonably regular frequency - Large and regular pressure fluctuations
$u_c < u < u_{se}$	Turbulent fluidisation	- Small voids and particle clusters dart to and fro - Top surface difficult to distinguish - Small amplitude pressure fluctuations only

3.2.2 Advantages and disadvantages of fluidised bed

Table 3.2 compares the advantages and disadvantages of the fluidised bed reactor (bubbling and turbulent fluidised beds) with fixed-bed reactor for gas-solid systems.

Table 3.2 Advantages and disadvantages of fluidised bed and fixed-bed reactors for gas-solid systems [6]

Characteristic	**Fluidised bed (bubbling and turbulent)**	**Fixed-bed**
1. Solid-catalysed gas-phase reaction	- For small granular or powdery non-friable catalyst - Can handle rapid deactivation of solids - Excellent temperature control allows large scale operations	- Only for very slow or non-deactivating catalyst - Serious temperature control problems limiting the size of units
2. Gas-solid reaction	- Can use wide range of solids with much fines - Large scale operations at uniform temperature possible - Excellent for continuous operation, yielding a uniform product	- Unsuited for continuous operations while batch operations yield non-uniform product
3. Temperature distribution in the bed	- Temperature is almost constant throughout, controlled by heat exchange or proper continuous feed and removal of solids	- Where much heat is involved, large temperature gradients occur
4. Particles	- Wide size distribution and much fines possible - Erosion of vessel and attrition or entrainment of particles may be serious	- Must be fairly large and uniform - With poor temperature control, these may sinter and clog the reactor
5. Pressure drop	- High pressure drop for deep bed, resulting in large power supply	- Pressure drop is not a serious problem due to large particle size
6. Heat exchange and heat transport	- Efficient heat exchange and large heat transport by circulating solids	- Inefficient heat exchange, hence large exchanger surface needed
7. Conversion	- Close to 100% theoretical conversion is possible with plug flow of gas and proper temperature control	- For continuous operations, mixing of solids and gas bypassing result in poor performance

Overall, the advantages of fluidised beds include: (1) the rapid mixing of solids leading to isothermal conditions throughout the reactor; (2) high heat and mass transfer rates between gas and solids; and (3) the well-mixed solids in a reactor representing a large thermal flywheel that can achieve uniform temperature profile and thus avoiding hot spot and overheating in highly exothermic reactions [6]. However, the fluidised bed has some disadvantages such as: (1) friable particles are pulverised and entrained in the gas; (2) erosion of vessel and pipes from abrasion can be serious; and (3) high pressure drop in a deep bed leads to large power consumption and supply [6].

3.2.3 Minimum fluidisation velocity

The transition from fixed-bed to fluidisation is denoted by the minimum fluidisation velocity (u_{mf}), which is the lowest gas velocity at which all bed particles are suspended in the gas [7]. As stated in Section 3.2.1, the beginning of minimum fluidisation occurs when the frictional (drag) force between particle and fluid counterbalances the weight of the particles. The principles and equations for determination of u_{mf} are given as follows [6]. The variables in the equations can be found from Glossary section.

$$\begin{pmatrix}\text{drag force by}\\ \text{upward moving gas}\end{pmatrix} = \begin{pmatrix}\text{weight of}\\ \text{particles}\end{pmatrix} \tag{3.1}$$

or

$$\begin{pmatrix}\text{pressure drop}\\ \text{across bed}\end{pmatrix}\begin{pmatrix}\text{cross sectional}\\ \text{area of tube}\end{pmatrix} = \begin{pmatrix}\text{volume}\\ \text{of bed}\end{pmatrix}\begin{pmatrix}\text{fraction consisting}\\ \text{of solids}\end{pmatrix}\begin{pmatrix}\text{specific weight}\\ \text{of solid}\end{pmatrix} \tag{3.2}$$

The above principles can be mathematically expressed by:

$$\Delta p_b A_t = W = A_t L_{mf}(1-\varepsilon_{mf})\left[(\rho_s - \rho_g)\frac{g}{g_c}\right] \tag{3.3}$$

By rearranging Equation 3.3, the minimum fluidisation happens when

$$\frac{\Delta p_b}{L_{mf}} = (1-\varepsilon_{mf})\left[(\rho_s - \rho_g)\frac{g}{g_c}\right] \tag{3.4}$$

At the beginning of the minimum fluidisation, the voidage is slightly larger than that in a fixed-bed, which corresponds to the loosest state of a fixe bed. Thus, the voidage at the

minimum fluidisation (ε_{mf}) can be estimated as 5% higher than that of the fixed-bed (ε_m) [6]. The ε_{mf} can also be measured experimentally and Table 3.3 presents the experimental values of ε_{mf}.

Note that the voidage of the fixed-bed (ε_m) can be calculated from Equation 3.5.

$$\varepsilon_m = 1 - \frac{\rho_{bu}}{\rho_s} \tag{3.5}$$

Table 3.3 Voidage at minimum fluidisation conditions (ε_{mf}) [6]

Particle	**Size, d_p (mm)**						
	0.02	**0.05**	**0.07**	**0.10**	**0.20**	**0.30**	**0.40**
Sharp sand, ϕ_s = 0.67	-	0.60	0.59	0.58	0.54	0.50	0.49
Round sand, ϕ_s = 0.86	-	0.56	0.52	0.48	0.44	0.42	-
Mixed round sand	-	-	0.42	0.42	0.41	-	-
Coal and glass powder	0.72	0.67	0.64	0.62	0.57	0.56	-
Anthracite coal, ϕ_s = 0.63	-	0.62	0.61	0.60	0.56	0.53	0.51
Absorption carbon	0.74	0.72	0.71	0.69	-	-	-
FT catalyst, ϕ_s = 0.58	-	-	-	0.58	0.56	0.55	-
Carborundum	-	0.61	0.59	0.56	0.48	-	-

Superficial velocity at the minimum fluidisation or minimum fluidisation velocity (u_{mf}) can be calculated from combining Equation 3.4 with Ergun equation for fixed-bed as shown in Equation 3.6 (a reasonable extrapolation for the fixed-bed expression). Thus, u_{mf} is calculated from Equation 3.7.

$$\frac{\Delta p_{fr}}{L_m} g_c = 150 \frac{(1-\varepsilon_m)^2}{\varepsilon_m^3} \frac{\mu u_o}{(\emptyset_s d_p)^2} + 1.75 \left(\frac{1-\varepsilon_m}{\varepsilon_m^3}\right)\left(\frac{\rho_g u_o^2}{\emptyset_s d_p}\right) \tag{3.6}$$

$$\frac{1.75}{\varepsilon_{mf}^3 \emptyset_s}\left(\frac{d_p u_{mf} \rho_g}{\mu}\right)^2 + \frac{150(1-\varepsilon_{mf})}{\varepsilon_{mf}^3 \emptyset_s^2}\left(\frac{d_p u_{mf} \rho_g}{\mu}\right) = \frac{d_p^3 \rho_g \left(\rho_s - \rho_g\right) g}{\mu^2} \tag{3.7}$$

Equation 3.7 can be simplified to Equation 3.8

$$\frac{1.75}{\varepsilon_{mf}^3 \emptyset_s} Re_{p,mf}^2 + \frac{150(1-\varepsilon_{mf})}{\varepsilon_{mf}^3 \emptyset_s^2} Re_{p,mf} = Ar \tag{3.8}$$

where the particle Reynolds number ($Re_{p,mf}$) at minimum fluidisation is

$$Re_{p,mf} = \left(\frac{d_p u_{mf} \rho_g}{\mu}\right) \tag{3.9}$$

and the Archimedes number (Ar) is defined as

$$Ar = \frac{d_p^3 \rho_g (\rho_s - \rho_g) g}{\mu^2} \tag{3.10}$$

In the special case of very small particles, Equation 3.7 can be simplified to

$$u_{mf} = \left(\frac{d_p^2 (\rho_s - \rho_g) g}{150\mu}\right)\left(\frac{\varepsilon_{mf}^3 \emptyset_s^2}{1-\varepsilon_{mf}}\right), \qquad Re_{p,mf} < 20 \tag{3.11}$$

In the case of very large particles, Equation 3.7 becomes

$$u_{mf}^2 = \left(\frac{d_p (\rho_s - \rho_g) g}{1.75 \rho_g}\right)(\varepsilon_{mf}^3 \emptyset_s), \qquad Re_{p,mf} > 1{,}000 \tag{3.12}$$

When ε_{mf} and/or $\emptyset_s$ are unknown, u_{mf} can be estimated for a bed of irregular particles with no seemingly longer or shorter dimension as follows:

First, rewrite Equation 3.8 as

$$K_1 Re_{p,mf}^2 + K_2 Re_{p,mf} = Ar \tag{3.13}$$

where

$$K_1 = \frac{1.75}{\varepsilon_{mf}^3 \emptyset_s} \quad \text{and} \quad K_2 = \frac{150(1-\varepsilon_{mf})}{\varepsilon_{mf}^3 \emptyset_s^2} \tag{3.14}$$

Note that K_1 and K_2 were found to be nearly constant for different types of particles over a wide range of conditions (Re = 0.001 to 4,000), thus giving predictions of u_{mf} with a

standard deviation of ±34%. Constants of K_1 and K_2 reported by researchers are given in Table 3.4.

By using the values for K_1 and K_2 listed in Table 3.4, Equation 3.13 can be solved for the value of $Re_{p,mf}$ as in Equation 3.15.

$$Re_{p,mf} = \left[\left(\frac{K_2}{2K_1}\right)^2 + \frac{1}{K_1}\,Ar\right]^{1/2} - \frac{K_2}{2K_1} \tag{3.15}$$

The values for K_1 and K_2 recommended by Wen and Yu [8] are used for fine particles and Chitester et al. [9] are for coarse particles. By using the values for K_1 and K_2 from Wen and Yu [8], $Re_{p,mf}$ is calculated from Equation 3.16.

$$Re_{p,mf} = [(33.7)^2 + 0.0408\,Ar]^{1/2} - 33.7 \tag{3.16}$$

For bubbling fluidised bed regime, it occurs at moderate gas velocities slightly above u_{mf} ($u_o > u_{mf}$), or less than about $10u_{mf}$ ($u_o < 10u_{mf}$) [6].

Table 3.4 Values of the two constants K_1 and K_2 [6]

Researchers	**First, $K_2/2K_1$**	**Second, $1/K_1$**
Wen and Yu [8] 284 data points from the literature	33.7	0.0408
Grace [10]	27.2	0.0408
Chitester et al. [9] coal, char, Ballotini; up to 64 bar	28.7	0.0494

3.2.4 Minimum bubbling velocity

The onset of bubbling is indicated by the minimum bubbling velocity (u_{mb}), which is the gas velocity at which the bubbles first appear in the bed [7]. u_{mb} strongly depends on particle properties. For fine particles in group A of the Geldart particle classification (see Section 3.2.8), u_{mb} is higher than u_{mf} [7]. For group B and group D particles, bubbles

appear as soon as the gas velocity exceeds u_{mf} and thus u_{mb} is equal to u_{mf} [6, 7]. A bubble-free fluidisation regime between u_{mf} and u_{mb} thus exists only for group A particles [7]. u_{mb} can be estimated by Equation 3.17 [7].

$$u_{mb} = 33 d_p \left(\frac{\rho_g}{\mu_g}\right)^{0.1} \tag{3.17}$$

3.2.5 Minimum slugging velocity

Slugging fluidisation occurs when the bubbles grow to sizes comparable with the column diameter and the gas velocity exceeds the minimum slugging velocity (u_{ms}). u_{ms} can be estimated by Equation 3.18 [6, 7].

$$u_{ms} = u_{mf} + 0.07(g d_t)^{1/2} \tag{3.18}$$

where d_t is bed or column diameter (m)

However, slugging is not encountered for the beds shallower than the height at which slugging sets in (z_s) [6].

$$z_s = 60 d_t^{0.175}, \quad \text{(cm)} \tag{3.19}$$

Slugging should be a mode of contacting in tall beds when gas velocity is in excess of u_{ms} ($u_o > u_{ms}$). The slugging fluidisation sets in at a height z_s above the distributor and the beds shallower than z_s should show no slugging [6].

3.2.6 Particle terminal velocity

Individual particles are carried out of the bed when the gas velocity exceeds the terminal particle velocity (u_t) [6]. When a particle of size d_p falls through a fluid, its terminal free-fall velocity can be estimated from Equation 3.20 [6].

$$u_t = \left[\frac{4 d_p (\rho_s - \rho_g) g}{3 \rho_g C_D}\right]^{1/2} \tag{3.20}$$

C_D is an experimentally determined drag coefficient. From Haider and Levenspiel [11], C_D can be calculated from.

$$C_D = \frac{24}{Re_p}\left[1 + (8.1716e^{-4.0655\emptyset_s})Re_p^{0.0964+0.5565\emptyset_s}\right] + \frac{73.69(e^{-5.0748\emptyset_s})Re_p}{Re_p + 5.378e^{6.2122\emptyset_s}} \quad (3.21)$$

For spherical particles ($\emptyset_s = 1$), the equation for C_D is simplified to Equation 3.22.

$$C_D = \frac{24}{Re_p} + 3.3643\,Re_p^{0.3471} + \frac{0.4607Re_p}{Re_p + 2682.5}, \quad \text{for } \emptyset_s = 1 \quad (3.22)$$

Another set of equations for the direct determination of u_t can also be used by introducing a dimensionless particle size (d_p^*) and a dimensionless gas velocity (u^*) as follows [11]:

$$d_p^* = d_p\left[\frac{\rho_g(\rho_s - \rho_g)g}{\mu^2}\right]^{1/3} = Ar^{1/3} \quad (3.23)$$

$$u^* = u\left[\frac{\rho_g^2}{\mu(\rho_s - \rho_g)g}\right]^{1/3} = \frac{Re_p}{Ar^{1/3}} \quad (3.24)$$

u_t can then be calculated by Equation 3.25.

$$u_t^* = \left[\frac{18}{(d_p^*)^2} + \frac{2.335 - 1.744\emptyset_s}{(d_p^*)^{0.5}}\right]^{-1}, \quad 0.5 < \emptyset_s < 1 \quad (3.25)$$

For spherical particles ($\emptyset_s = 1$), the equation for u_t^* is simplified to Equation 3.26.

$$u_t^* = \left[\frac{18}{(d_p^*)^2} + \frac{0.591}{(d_p^*)^{0.5}}\right]^{-1}, \quad \emptyset_s = 1 \quad (3.26)$$

Knowing gas properties (ρ_g and μ) and particle properties (d_p, ρ_s and $\emptyset_s$), d_p^* is calculated from Equation 3.23 and then by using d_p^* value, u_t^* can be calculated from Equation 3.25 or 3.26. Finally, u_t can be found from Equation 3.27 which is formulated based on Equation 3.24.

$$u_t^* = u_t\left[\frac{\rho_g^2}{\mu(\rho_s - \rho_g)g}\right]^{1/3} \quad \text{or} \quad u_t = u_t^*\left[\frac{\mu(\rho_s - \rho_g)g}{\rho_g^2}\right]^{1/3} \quad (3.27)$$

In summary, the gas velocity used in the fluidised bed should be between u_{mf} and u_t to avoid or reduce the particle entrainment from the fluidised bed. For the calculation of u_{mf}, the mean particle diameter for the size distribution that presents in the bed is used. However, for u_t, the smallest particle size that is present in large quantities should be used in the calculation [6].

3.2.7 Turbulent transition velocity

Turbulent transition velocity (u_c) is used to describe the transition from bubbling fluidisation to turbulent fluidisation. u_c is the superficial gas velocity at which the standard deviation of the pressure fluctuations reaches a maximum, as the onset of the turbulent regime [7]. Based on differential pressure fluctuation measurements reported by Bi and Grace [12], u_c is predicted from Equations 3.28 and 3.29.

$$Re_{p,c} = 1.24Ar^{0.45}, \quad 2 < Ar < 1 \times 10^8 \tag{3.28}$$

$$u_c = \left(\frac{Re_{p,c}\mu}{d_p\rho_g}\right) \tag{3.29}$$

For fine particles, typically, u_c/u_t = 8-13 and this ratio decreases with an increase in pressure [6].

3.2.8 The Geldart classification of Particles

Geldart [13] classified the particles into four specific particle groups based on fluidisation behaviour. From smallest to largest particle size, they are group C, A, B, and D as follows [6, 13]:

Group C: cohesive, or very fine powders. Normal fluidisation is extremely difficult for these solids because inter-particle cohesive forces are greater than the dragging forces by the flowing gas. Face powder, flour, and starch are typical of these solids.

Group A: aeratable, or materials having a small mean particle size and/or low particle density (< 1,400 kg/m^3). These solids fluidise easily, with smooth fluidisation at low gas

velocities and controlled bubbling with small bubbles at higher gas velocities. Fluid catalytic cracking (FCC) catalyst is representative of these solids.

Group B: sandlike, or most particles of sizes between 40 and 500 μm and density between 1,400 and 4,000 kg/m^3. These solids fluidise well with vigorous bubbling action and bubbles that grow large.

Group D: spoutable, or large and/or dense particles. Deep beds of these solids are difficult to fluidise. They behave erratically, giving large exploding bubbles or severe channelling, or spouting behaviour if the gas distributor is very uneven. Grains and peas in drying, coals in gasification, and some roasting metals are examples of solids in this group. Group D particles are normally processed in shallow beds or in the spouting mode.

3.2.9 Mapping of fluidisation regimes

The identification of the fluidisation regime is very important for prediction of the behaviour of gas-solid operation. To simply identify the fluidisation regime of a particular gas-solid system, a flow regime map as shown in Figure 3.2 can be used. The dimensionless variables d_p^* and u^* are defined in Equations 3.23 and 3.24, respectively. The flow regime map represents the experimental data from many researchers at various conditions as follows [6]:

Gases:	air, N_2, CO_2, He, H_2, Freon-12, and CCl_4
Temperature:	20-300°C
Pressure:	1-85 bar

From Figure 3.2, it can be pointed out that bubbling fluidised beds are operated stably over a wide range of conditions and particle sizes for Geldart group A and B particles. Moreover, the modified boundaries for the Geldart classification of solids are located. To account for conditions other than ambient and for other gases, the AB boundary is given by Equation 3.30 [6].

$$(d_p^*)_{AB} = 101\left(\frac{\rho_g}{\rho_s - \rho_g}\right)^{0.425} \tag{3.30}$$

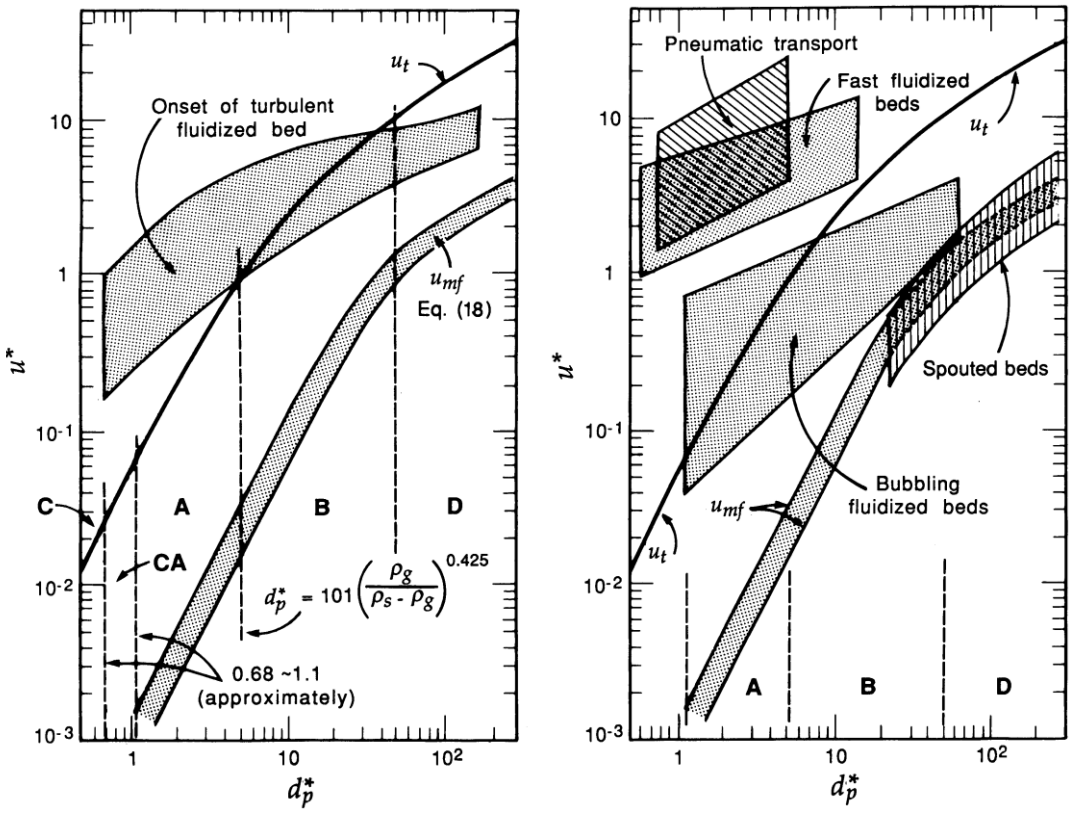

Figure 3.2 General flow regime map for gas-solids fluidisation [6]
(C, A, B, and D refer to the Geldart classification of solids)

3.3 Calculation of main parameters in fluidisation

A lab-scale hot gas reactor for NH_3 and H_2S removal was planned to be operated in the BFB regime due to its advantages over the fixed-bed as discussed in Section 3.2.2. The design calculations of the BFB conditions were based on the superficial velocity (u_o), the minimum fluidisation velocity (u_{mf}), the minimum bubbling velocity (u_{mb}), the minimum slugging velocity (u_{ms}), the terminal particle velocity (u_t), and the turbulent transition velocity (u_c). The equations and calculations of these parameters are described in Sections 3.2.3 to 3.2.7.

To identify the operation conditions in the BFB regime, the calculation of main parameters in fluidisation for titanomagnetite sand, which has been identified to be the most promising natural occurring catalyst available in New Zealand, with Ar gas flow at 800°C are given as an example. The details and results of the calculation are shown in this section. For the test

with other types of sands in Ar gas or in simulated producer gas at different temperatures, the calculation was performed in the same procedures as those for titanomagnetite sand with Ar gas at 800°C shown below.

3.3.1 Parameters used for flow regime calculations

Properties of gas:

Type of gas:	Ar
Gas flow rate ($Q_{20°C}$):	3.65 L/min at room temperature (20°C)
Gas density (ρ_g):	0.453 kg/m^3 (data was from [14])
Gas viscosity (μ):	6.226×10^{-5} kg/m·s (data was from [14])

Properties of particle:

Type of particle:	titanomagnetite sand
Particle density (ρ_s):	4,540 kg/m^3 (data was from [15])
Sphericity of particle ($\emptyset_s$):	0.86
Particle diameter (d_p):	106-125 μm, 180-250 μm, and 300-355 μm based on screen analysis from which the corresponding mean particle diameters were calculated to be 115, 215 and 327 μm
Voidage (ε_{mf}):	data was found in Table 3.3 voidage at minimum fluidisation conditions which varies with d_p

Other parameters and constants:

Bed or column diameter (d_t): 0.04 m

Bed cross-sectional area (A_t): 0.00126 m^2

Acceleration of gravity (g): 9.8 m/s^2

3.3.2 Details of the calculations

First, superficial gas velocity (u_o) at 800°C was calculated from the gas flow rate at 800°C ($Q_{800°C}$) and bed cross-sectional area (A_t) as shown in Equation 3.31.

$$u_o = \frac{Q_{800°C}}{A_t} \tag{3.31}$$

where $Q_{800°C}$ was calculated from $Q_{20°C}$ based on an ideal gas law

Next, the minimum fluidisation velocity (u_{mf}) was calculated from Equations 3.8 - 3.10 when ε_{mf} and/or $\emptyset_s$ were known. However, ε_{mf} and $\emptyset_s$ for titanomagnetite were not measured and they were estimated from Table 3.3. Therefore, u_{mf} calculated from two constants (K_1 and K_2 in Table 3.4) as recommended by Wen and Yu [8], Grace [10], and Chitester et al. [9] were also provided for comparison.

As described in Section 3.2.4, the minimum bubbling velocity (u_{mb}) of titanomagnetite was equal to u_{mf} because titanomagnetite sand was classified as group B particle based on the Geldart particle classification.

The minimum slugging velocity (u_{ms}) was estimated by Equation 3.18. To identify whether slugging occurred in the bed, the height at which slugging sets in (z_s) was also calculated from Equation 3.19.

Finally, the terminal particle velocity (u_t) was determined by using Equations 3.20 and 3.21 as well as using the direct evaluation method by Equation 3.23, 3.25, and 3.27. As long as u_o is lower than u_t, it is unnecessary to calculate the turbulent transition velocity (u_c) because u_c is typically much larger than u_t.

In addition to the calculations presented, the flow regime map for gas-solids fluidisation in Figure 3.2 was also used to find out the regime of the interested sand and conditions. Therefore, the dimensionless particle size (d_p^*) and dimensionless gas velocity (u^*) were computed by Equations 3.23 and 3.24.

3.3.3 Results and discussion

Results of u_o, u_{mf}, u_{ms}, u_t, d_p^*, and u^* of Ar gas through the titanomagnetite bed at 800°C are given in Table 3.5. From the results, it can be seen that over the particle size ranges of interest of 106-355 μm, u_o was found to be higher than u_{mf} and lower than u_t ($u_{mf} < u_o < u_t$) which indicates that the operation conditions were in the BFB regime. Due to the fact that u_o was lower than u_t, the entrainment of the titanomagnetite particles was avoidable or reduced. However, it was also observed that u_o was higher than u_{ms} which suggests slugging fluidisation might have occurred in the bed. Thus, by using Equation

3.19, the height at which slugging sets in (z_s) was calculated to be 76 cm. The height of the bed above the distributor of the quartz reactor was shallower than z_s, and thus there was no slugging in the bed (see Figure 3.4). Additionally, by using the values of d_p^*, and u^* in the flow regime map for gas-solids fluidisation in Figure 3.2, it is found that all the results were in between the u_{mf} and u_t curves.

3.3.4 Experimental verification of the calculated results

The verification of the above calculations was conducted by testing the titanomagnetite sand at room temperature (approximately 20°C) in a transparent quartz reactor and observing the fluidisation behaviour of the sand in the bed. The particle diameters (d_p) of the titanomagnetite used in the experiment were 106-125 μm and the Ar gas flow rate used at 20°C ($Q_{20°C}$) was 3.65 L/min.

The calculation of the main parameters in fluidisation was done by using the equations as previously described in Section 3.3.2. The results of u_o, u_{mf}, u_{ms}, u_t, d_p^*, and u^* of Ar gas through the titanomagnetite bed at 20°C are given in Table 3.6. Again, from the results in Table 3.6, the value of u_o was in between u_{mf} and u_t and thus the BFB regime should be obtained. The behaviour of the titanomagnetite sand fluidised by Ar gas flow rate (3.65 L/min) was shown in Figure 3.3 which confirmed the occurrence of the BFB regime.

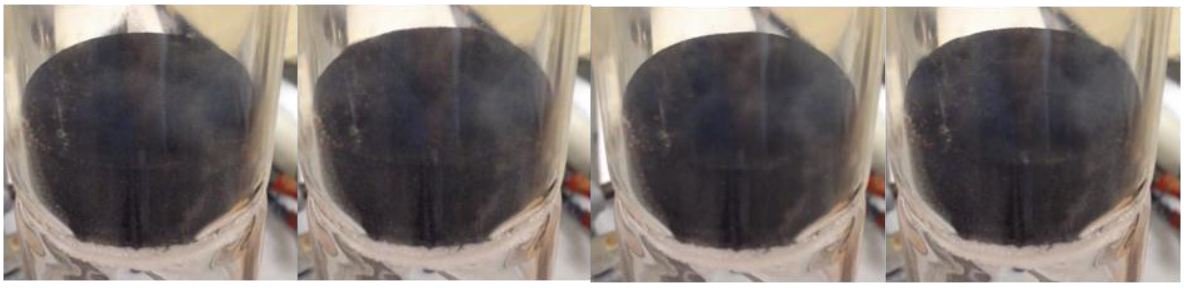

Figure 3.3 Behaviour of the titanomagnetite sand fluidised by Ar gas flow rate (3.65 L/min) at 20°C

Table 3.5 Results of main parameters for titanomagnetite with Ar gas flow at 800°C

d_p (m)	u_o (m/s)	u_{mf} (m/s)				u_{ms} (m/s)				u_t (m/s)		d_p^*	u^*
		Equations 3.8-3.9	Wen and Yu [8]	Grace [10]	Chitester et al. [9]	Equations 3.8-3.9	Wen and Yu [8]	Grace [10]	Chitester et al. [9]	Equations 3.20-3.21	Direct evaluation Method		
0.000106	0.177	0.009	0.005	0.006	0.007	0.053	0.049	0.050	0.051	0.271	0.400	1.837	0.074
0.000125	0.177	0.011	0.007	0.008	0.010	0.055	0.051	0.052	0.053	0.318	0.541	2.166	0.074
0.000180	0.177	0.019	0.014	0.017	0.020	0.063	0.058	0.061	0.064	0.454	1.025	3.119	0.074
0.000250	0.177	0.030	0.027	0.033	0.038	0.074	0.071	0.077	0.082	0.624	1.751	4.332	0.074
0.000300	0.177	0.039	0.039	0.048	0.055	0.083	0.083	0.092	0.099	0.745	2.307	5.199	0.074
0.000355	0.177	0.049	0.054	0.067	0.077	0.093	0.098	0.111	0.121	0.876	2.932	6.152	0.074

Table 3.6 Results of main parameters for titanomagnetite with Ar gas flow at 20°C

d_p (m)	u_o (m/s)	u_{mf} (m/s)				u_{ms} (m/s)				u_t (m/s)		d_p^*	u^*
		Equations 3.8-3.9	Wen and Yu [8]	Grace [10]	Chitester et al. [9]	Equations 3.8-3.9	Wen and Yu [8]	Grace [10]	Chitester et al. [9]	Equations 3.20-3.21	Direct evaluation Method		
0.000106	0.048	0.025	0.014	0.017	0.019	0.069	0.057	0.061	0.063	0.230	0.770	5.625	0.068
0.000125	0.048	0.032	0.019	0.023	0.027	0.076	0.063	0.067	0.071	0.269	0.967	6.633	0.068

3.4 Lab-scale reactor design and construction

3.4.1 Material selection

Material selection is of primary importance for construction of the reactor because NH_3 can be catalytically or non-catalytically reacted with certain reactive materials [16] and H_2S is selectively adsorbed on glass or metal surfaces [17, 18]. Therefore, inner surfaces of the reactor and components that contacted with NH_3 and H_2S gases were made of inert material including Perfluoroalkoxy (PFA) and fused quartz. PFA was used with the gas at temperature less than 200°C as its maximum operating temperature and melting temperature are 200 and 305°C, respectively. Fused quartz was used with hot gas of the temperature over 200°C, thus it was used both for the reactor and for the gas outlet pipe. However, a few parts that were used at room temperature including a flame arrester and gas flow meters were made of stainless steel and glass due to unavailability of inert material for use on this purpose. This would not be a concern because it was found in the laboratory tests that low concentration of NH_3 or H_2S in N_2 gas could be easily transported through the stainless steel tubing at low temperatures without any detectable losses [18, 19].

3.4.2 Design of the lab-scale reactor and operation system

The design of the reactor and all components needed careful consideration because the reactor was tested at high temperatures (400-800°C). A schematic diagram of a lab-scale reactor system is shown in Figure 3.4 and a diagram for electrical heating and control system is also given in Figure 3.5. From Figure 3.4, the system mainly comprises: (1) three-zone heating tube furnace that can be operated continuously up to 1,150°C; (2) quartz reactor, (3) gas cylinders of various types and concentrations including pure Ar, pure H_2, H_2S in Ar, NH_3 in Ar, and simulated producer gas (H_2, CO, CO_2, and CH_4); (4) gas feeding pipes, gas controlling valves, gas flow controllers, and gas exhaustion hood. Figure 3.5 shows the electrical heating and control system which measured and recorded temperatures in the reactor and at gas outlet as well as pressure drop across the reactor. Besides, Figure 3.5 displays the emergency system via the use of solenoid valve, air operated valves, and main control panel.

Before these two diagrams could be drawn, the design, calculation, and safety and risk assessment were performed and are described and discussed as follows:

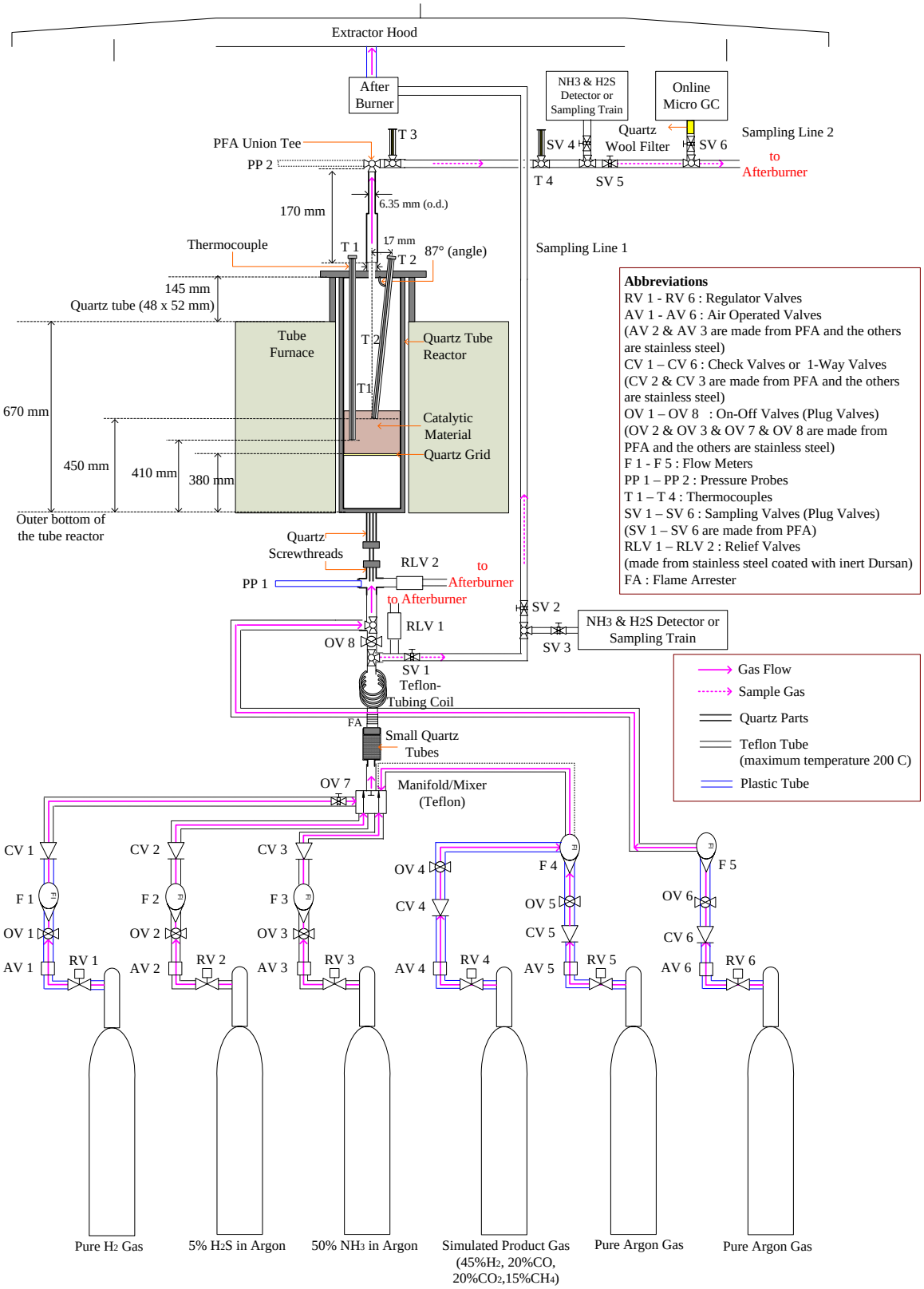

Figure 3.4 Schematic diagram of a lab-scale reactor

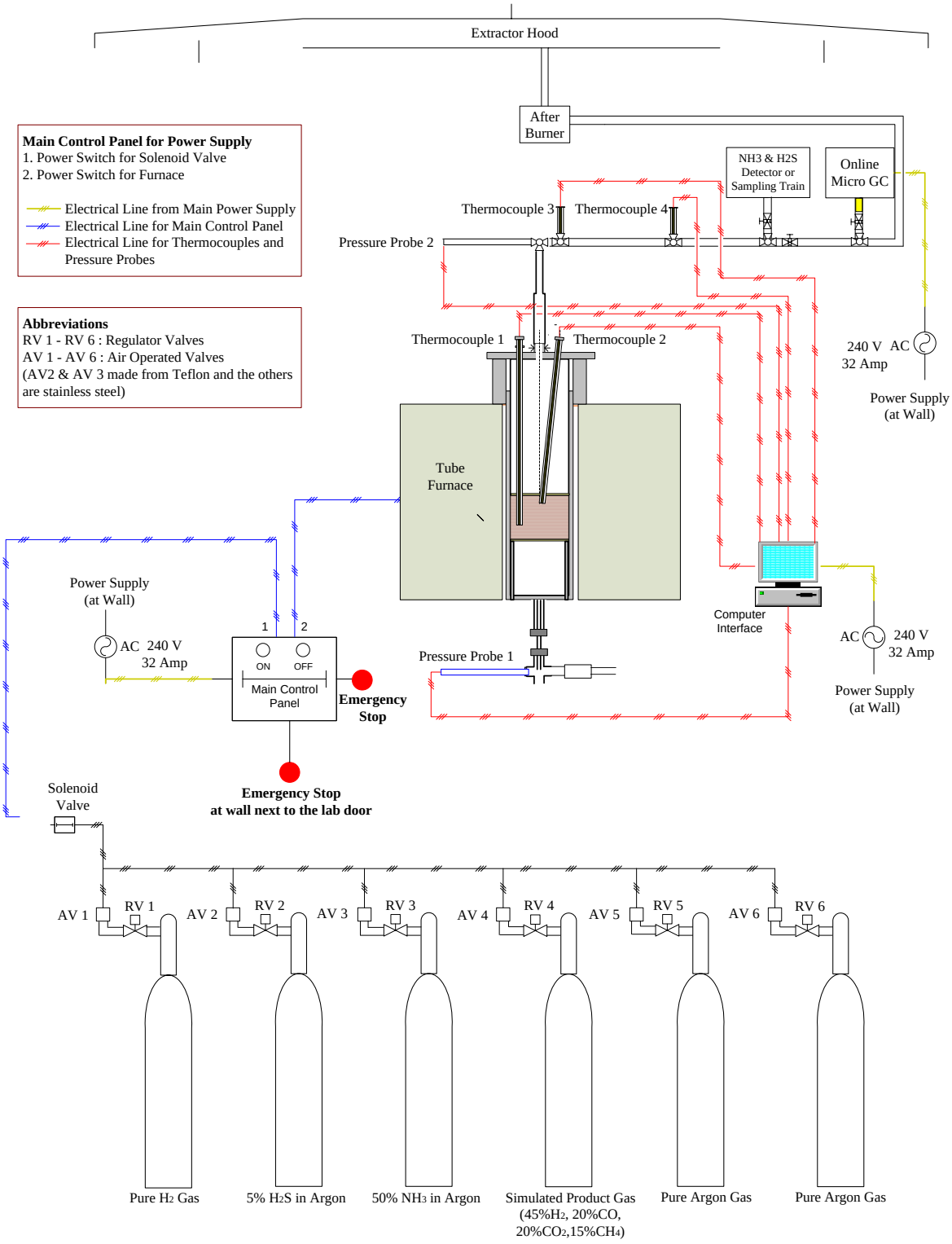

Figure 3.5 Electrical line diagram of a lab-scale reactor

3.4.3 Design of a quartz reactor

The design of a vertical cylindrical fused quartz reactor was simple, and it was based on the dimensions of the three-zone tube furnace which was purchased for this study. The tube furnace has an internal diameter (i.d.) of 50 mm and a length of 670 mm. The quartz reactor dimensions were selected as an internal diameter (i.d.) of 40 mm, an outer diameter (o.d.) of 46 mm, and a length of 1,020 mm as shown in Figure 3.6.

The external diameter of the reactor was chosen to be closely fitted in the tube furnace with a very small gap of 2 mm between the reactor outer wall and the furnace inner wall in order to minimise the heat loss from convection. A fused quartz screw thread at the bottom end of the reactor was used with a cap to connect the reactor with the quartz fittings.

The total length of the reactor was designed to be longer than the furnace to avoid high temperature at: (1) the screw thread cap; and (2) the reactor flange, which was connected with the quartz reactor lid by the use of viton O-rings and stainless steel clips. The maximum operating temperature of the screw thread cap and viton O-rings is about 200°C. The pictures of the connection between the screw thread of the reactor and caps as well as between the reactor flange and lid are shown in Figure 3.7.

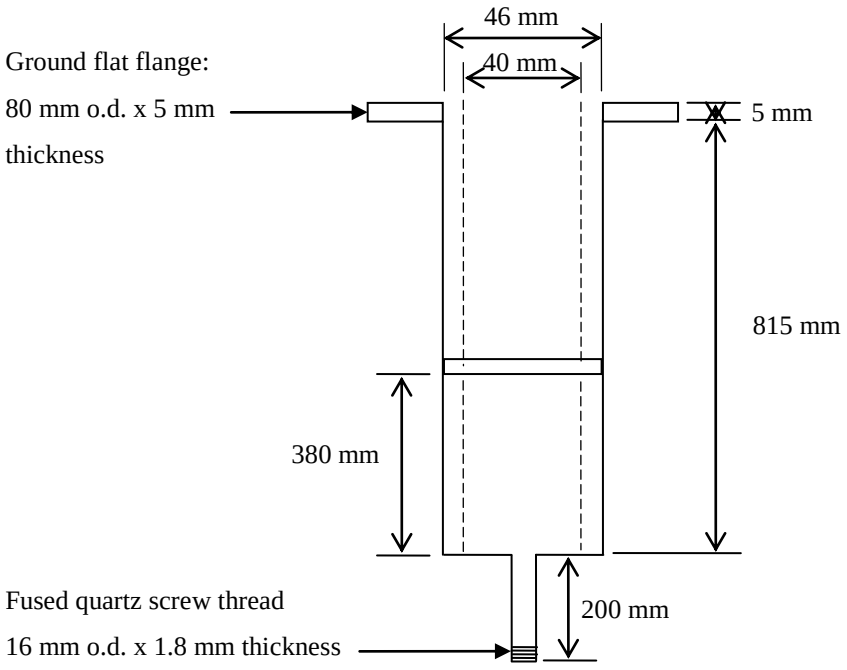

Figure 3.6 Sketch of a vertical cylindrical fused quartz reactor

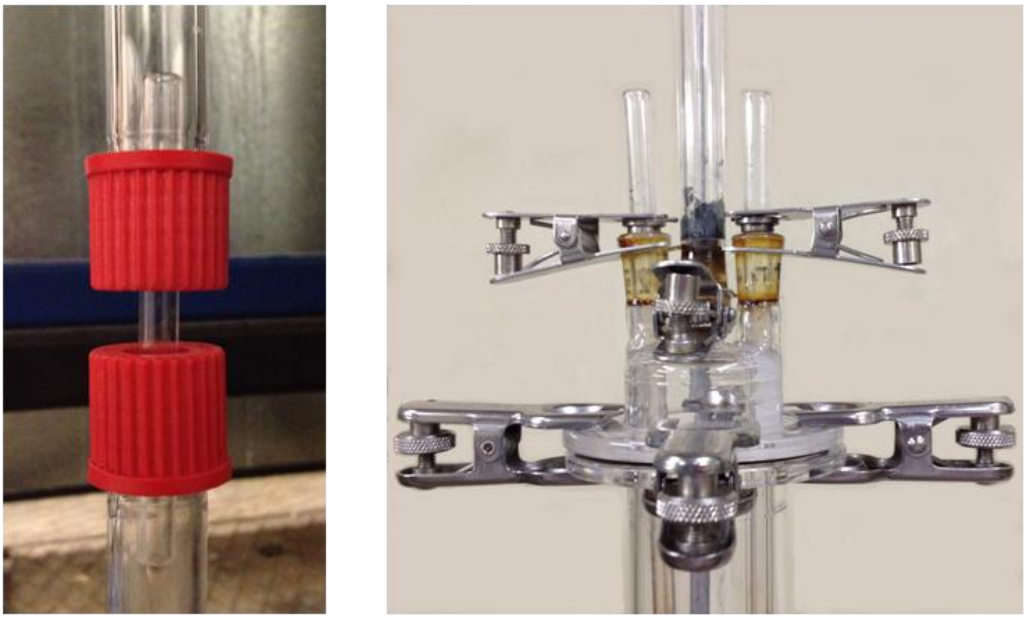

(a) (b)

Figure 3.7 Pictures of connection (a) between the screw thread of the reactor and caps and (b) between the reactor flange and lid

To find out the length of the screw thread and the extended length of the reactor at the flange in which they were not inside the furnace (see Figure 3.4), preliminary tests were conducted. In the test, an empty reactor made from stainless steel (SS) was placed inside the furnace. N_2 gas at a flow rate of 5 L/min was fed from the bottom of the reactor. The furnace was set at various temperatures of 600, 800, and 1,000°C. The outer surface temperatures of pipes at the top and bottom of the reactor were then measured using thermocouples type K. The experimental set up is shown in Figure 3.8.

The results of temperature measurements are given in Figure 3.9. The x-axis represents the length of the pipe measured either from the furnace top surface or the furnace bottom surface. The y-axis represents the outer surface temperature of the inlet or outlet of the pipe. It can be seen that the minimum length of the reactor should be at least 100 mm away from the furnace top surface or the furnace bottom surface to avoid high temperatures of above 150°C. Therefore, the length of quartz screw thread of 200 mm and the extended length of the reactor at the flange of 145 mm were selected. Once the quartz reactor was built, it was tested with Ar gas at a flow rate of 3.65 L/min and furnace temperature of 800°C. The outer surface temperature of the quartz reactor away from the furnace was measured and plotted

in Figure 3.9. As can be seen, the results received from the quartz reactor with Ar gas were consistent with those from the SS reactor and N_2 gas.

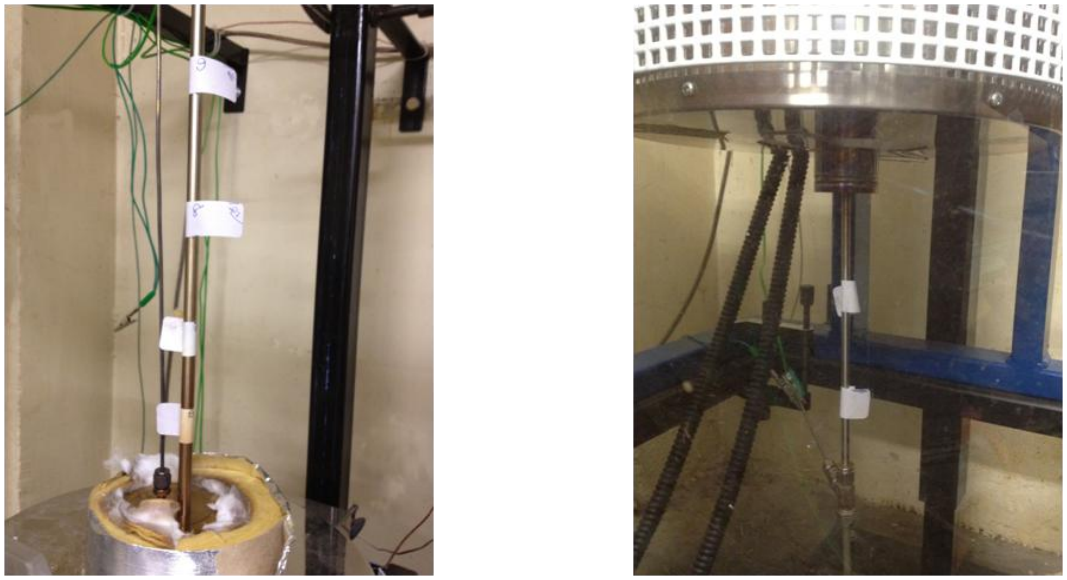

(a) (b)

Figure 3.8 Experimental set up for temperature measurement of (a) pipe at the top and (b) pipe at the bottom of the reactor

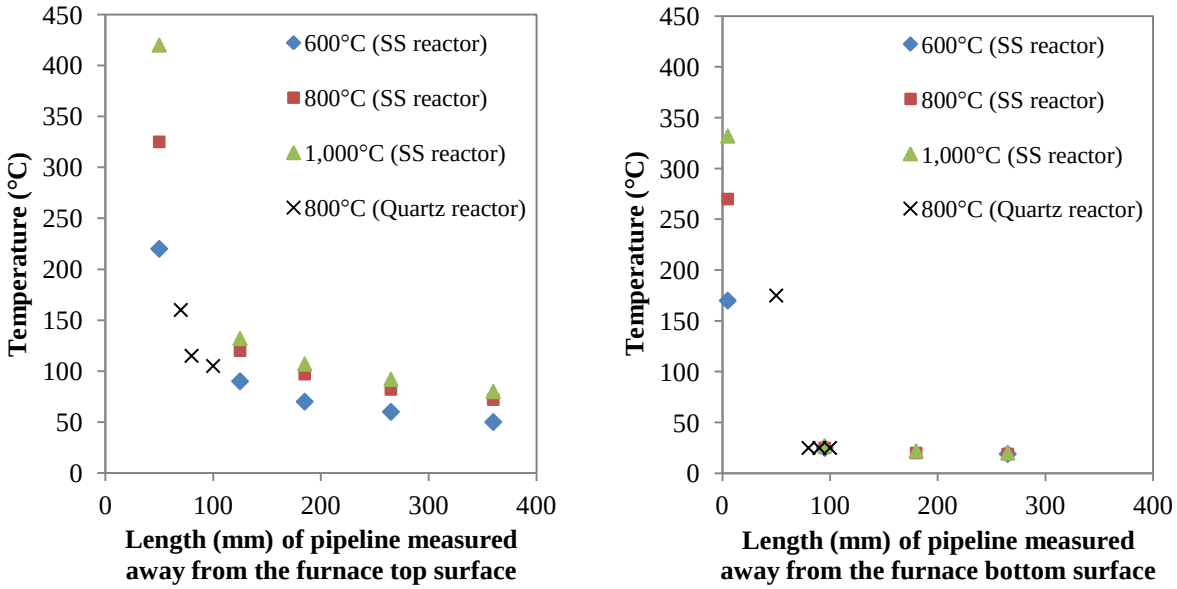

(a) (b)

Figure 3.9 Temperature profile of (a) pipe at the top and (b) pipe at the bottom of the reactor with various furnace temperature set points

The last important part of the reactor design was the quartz porous distributor. It was necessary to find the position for placing the distributor to ensure that the uniform temperature gradients along the vertical axis of the bed could be achieved. Thus, experiments were conducted with both an empty SS reactor and a SS reactor with 190 g silica sand particle sizes of 300-425 µm, corresponded to 10 cm long fixed-bed. N_2 gas at a flow rate of 5 L/min was fed from the bottom of the reactor. The temperature profile of the gas inside the reactor was measured by using thermocouple type K that was movable along the vertical axis of the reactor. The results of the gas temperature profile along the vertical axis of the reactor are given in Figure 3.10. From the results, constant gas temperature profile was obtained along the vertical axis between 360 and 540 mm above the bottom of the reactor. The quartz distributor, therefore, was placed at 380 mm from the reactor bottom. The quartz porous distributor used has dimensions of 40 mm diameter, 4 mm thickness, and pore size of 90-150 µm.

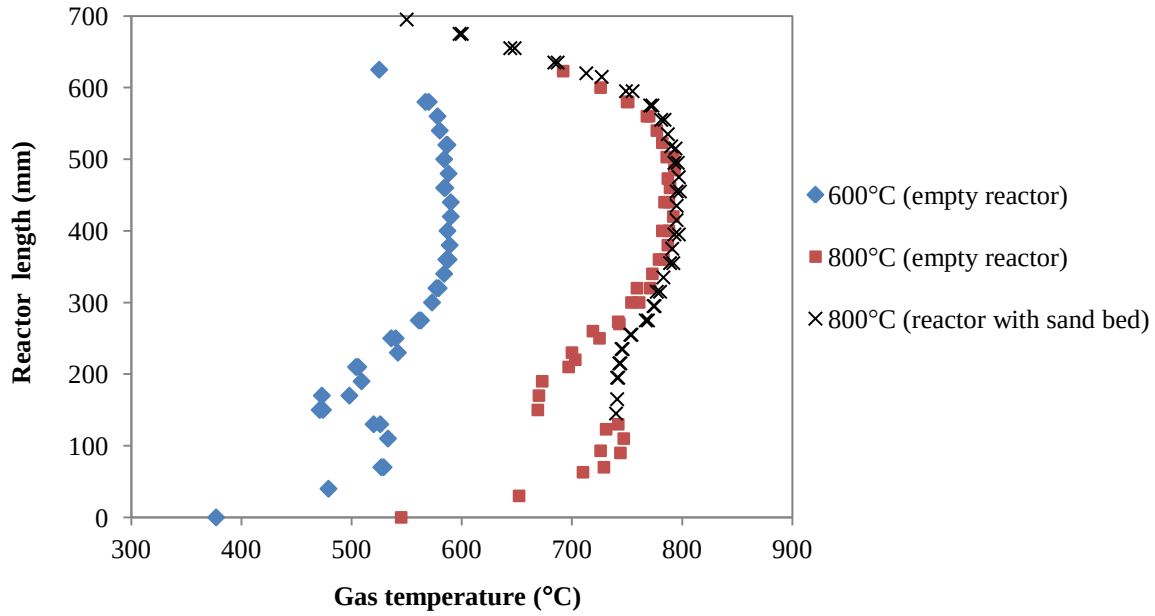

Figure 3.10 Gas temperature profile along the vertical axis of the reactor with furnace temperatures of 600 and 800°C

3.4.4 Calculation of NH_3 and H_2S concentrations in the feed gas

The concentrations of NH_3 and H_2S found in the producer gas from gasification of woody biomass were 100-2,000 ppmv and 20-230 ppmv, respectively. It was thus planned to use

the feed gas containing about 2,000 ppmv NH_3 and 230 ppmv H_2S in the present study. However, certified NH_3 and H_2S gases cannot be supplied by a BOC Company in New Zealand due to unavailability of equipment and certificate to manufacture gas mixtures containing highly toxic or reactive gases for an assurance towards safety and stability. Therefore, the certified gas cylinders of 50 vol% NH_3 in Ar and 5 vol% H_2S in Ar were purchased from the BOC Company in Australia. The high concentrations of NH_3 and H_2S gases were then diluted with pure Ar gas to reduce their concentrations to 2,000 ppmv and 230 ppmv, respectively. The dilution of the NH_3 and H_2S concentrations was carried out by the use of variable area flow meters from ABB Company. Flow rates of pure Ar gas, 50 vol% NH_3 in Ar, and 5 vol% H_2S can be adjusted through the flow meter floats.

For each flow rate measurement, the accuracy or error of the gas flow rate can be calculated from an equation given in the flow meter manual as in Equation 3.32.

$$\Delta f\% = \left(\frac{3}{4}M + \frac{1}{4}E\right)\left(\frac{C}{M}\right) \tag{3.32}$$

where

M is a measured value in a flow rate unit (L/min)
E is a scale end (full scale) value in a flow rate unit (L/min)
C is an accuracy class value
Δf % is an error in % of a flow rate

For a mixture of gases from two gas flows, a total error of NH_3 or H_2S in a flow rate unit (L/min) or a concentration unit (ppmv) can be estimated from Equation 3.33 with a very good approximation.

$$\Delta q\% = \sqrt{(\Delta x\%)^2 + (\Delta y\%)^2} \tag{3.33}$$

where

$\Delta x\%$ is an error in % of pure Ar gas flow rate
$\Delta y\%$ is an error in % of a flow rate of either 50 vol% NH_3 in Ar or 5 vol% H_2S in Ar gas
$\Delta q\%$ is a total in % error of NH_3 or H_2S concentration (ppmv) in a gas mixture from two gas flows

The results of Δx%, Δy%, and Δq% of the gas mixture of NH_3 and H_2S are given in Table 3.7 and Table 3.8, respectively.

Table 3.7 NH_3 gas concentration and accuracy

Ar gas low rate (L/min)	**50 vol% NH_3 in Ar gas flow rate (L/min)**	**Diluted NH_3 concentration (ppmv)**	**% error of Ar gas flow rate (Δx%)**	**% error of flow rate of 50 vol% NH_3 in Ar gas (Δy%)**	**% total error of NH_3 concentration (Δq%)**
1.2	0.0012	500	4.9	114.5	114.6
1.2	0.0028	1,164	4.9	51.6	51.9
1.2	0.0052	2,157	4.9	29.9	30.3
2.35	0.0012	255	3.4	114.5	114.6
2.35	0.0028	595	3.4	51.6	51.8
2.35	0.0052	1,104	3.4	29.9	30.1
2.35	0.0092	1,950	3.4	18.8	19.2
2.35	0.0145	3,066	3.4	13.6	14.0
3.2	0.0012	187	3.0	114.5	114.5
3.2	0.0028	437	3.0	51.6	51.7
3.2	0.0052	811	3.0	29.9	30.0
3.2	0.0092	1,433	3.0	18.8	19.1
3.2	0.0145	2,255	3.0	13.6	13.9
3.65	0.0012	164	2.9	114.5	114.5
3.65	0.0028	383	2.9	51.6	51.7
3.65	0.0052	711	2.9	29.9	30.0
3.65	0.0092	1,257	2.9	18.8	19.1
3.65	**0.0145**	**1,978**	**2.9**	**13.6**	**13.9**
3.65	0.0230	3,131	2.9	10.2	10.6
4.9	0.0012	122	2.6	114.5	114.5
4.9	0.0028	286	2.6	51.6	51.7
4.9	0.0052	530	2.6	29.9	30.0
4.9	0.0092	937	2.6	18.8	19.0
4.9	0.0145	1,475	2.6	13.6	13.9
4.9	0.0230	2,336	2.6	10.2	10.6

Table 3.8 H_2S gas concentration and accuracy

Ar gas low rate (L/min)	**5 vol% H_2S in Ar gas flow rate (L/min)**	**Diluted H_2S concentration (ppmv)**	**% error of Ar gas flow rate (Δx%)**	**% error of flow rate of 5 vol% H_2S in Ar gas (Δy%)**	**% total error of H_2S concentration (Δq%)**
1.2	0.0021	87	4.9	54.3	54.5
1.2	0.0035	145	4.9	33.6	34.0
1.2	0.0066	273	4.9	20.0	20.5
2.35	0.0021	45	3.4	54.3	54.4
2.35	0.0035	74	3.4	33.6	33.8
2.35	0.0066	140	3.4	20.0	20.2
2.35	0.0108	229	3.4	13.9	14.4
2.35	0.017	359	3.4	10.5	11.0
3.2	0.0021	33	3.0	54.3	54.3
3.2	0.0035	55	3.0	33.6	33.8
3.2	0.0066	103	3.0	20.0	20.2
3.2	0.0108	168	3.0	13.9	14.3
3.2	0.017	264	3.0	10.5	10.9
3.65	0.0021	29	2.9	54.3	54.3
3.65	0.0035	48	2.9	33.6	33.8
3.65	0.0066	90	2.9	20.0	20.2
3.65	0.0108	148	2.9	13.9	14.2
3.65	**0.017**	**232**	**2.9**	**10.5**	**10.9**
3.65	0.024	327	2.9	8.8	9.3
4.9	0.0021	21	2.6	54.3	54.3
4.9	0.0035	36	2.6	33.6	33.7
4.9	0.0066	67	2.6	20.0	20.1
4.9	0.0108	110	2.6	13.9	14.2
4.9	0.017	173	2.6	10.5	10.8
4.9	0.024	244	2.6	8.8	9.2

From the analysis of data in Table 3.7 and Table 3.8, it was decided to use pure Ar gas flow rate of 3.65 L/min to mix with 50 vol% NH_3 in Ar gas of 0.0145 L/min or with 5 vol% H_2S in Ar gas of 0.017 L/min, which corresponded to 2,000±14% ppmv NH_3 and 230±11% ppmv H_2S in Ar gas, respectively. To ensure the uniform gas mixing in the feed gas, a mixing quartz chamber filled with quartz tubes of 4 mm (i.d.), 8 mm (o.d.), and 10 mm long and a 4 m PFA tube were installed after the ABB flow meters and before the quartz reactor (see Figure 3.4). Also, the verification of the NH_3 and H_2S inlet concentrations was performed by sampling the feed gas in a sampling train and analysis the concentration by an Ion Selective Electrode (ISE) method, which is described in details in Chapter 4.

3.4.5 Safety and risk assessment

Safety is one of the most important aspects for the experimentation on the lab-scale hot gas reactor for NH_3 and H_2S removal. In the experiment, not only have the NH_3 and H_2S gases been used, but the simulated producer gas containing 45 vol% H_2, 20 vol% CO, 20 vol% CO_2, and 15 vol% CH_4 has also been tested. NH_3, H_2S, and CO gases are known as hazardous and toxic substances even at low concentrations. High concentrations of H_2, CO, and CH_4 in the producer gas can cause explosion as they are in the explosive range as shown in Table 3.9. All the properties and standards related to safety of the above-mentioned gases are shown in Table 3.9.

Table 3.9 Gas properties and standards related to safety

Gas properties	**NH_3**	**H_2S**	**H_2**	**CO**	**CO_2**	**CH_4**
Workplace Exposure Standards (ppm[a])	TWA = 25 STEL = 35	TWA = 10 STEL = 15	Simple asphyxiant	TWA = 25 STEL = 200	TWA = 5,000 STEL = 30,000	Simple asphyxiant
Explosive range (vol% in air)	LEL = 15 UEL = 28	LEL = 4 UEL = 46	LEL = 4 UEL = 75	LEL = 12 UEL = 75	-	LEL = 5 UEL = 15
Auto-ignition temperature (°C)	651	260	500	609	-	580

[a] Parts of vapour or gas per million of contaminated air by volume at 25˚C and 760 torr

Explanation of the gas properties and standards listed in Table 3.9 are given as follows:

- Workplace Exposure Standards (WES) are set by the Department of Labour, New Zealand Government [20]. WES can be used as an important tool for monitoring the health and safety hazardous levels in a workplace environment. Note that WES is a guide only because compliance with WES does not guarantee protection from ill-health outcomes for all workers, due to the wide range of individual tolerance.
- Time-Weighted Average (WES-TWA): most WESs in New Zealand have an eight-hour TWA, representing a work shift of 8 h over one day. This means that the value assigned for a WES-TWA should not be exceeded over the period of 8 h during a working shift.
- Short-Term Exposure Limit (WES-STEL) is the limit over any 15-minute period in the working day. WES-STEL is designed to protect the worker against adverse effects of irritation, chronic or irreversible tissue change, or narcosis that may increase the likelihood of accidents. The WES-STEL is not an alternative to the WES-TWA and both of them should apply for applicable situations.
- The explosive range (or flammable range) is the range of concentration of gas or vapour that will burn (or explode) if an ignition source is introduced. Below the explosive or flammable range, the mixture is too lean to burn and above the upper explosive or flammable limit the mixture is too rich to burn. The limits are commonly called the "Lower Explosive or Flammable Limit" (LEL/LFL) and the "Upper Explosive or Flammable Limit" (UEL/UFL) [21].
- The auto-ignition temperature is the minimum temperature required to ignite gas or vapour in air without a spark or flame being present [22].

In this study, safety and risk assessment was conducted prior to the construction of the lab-scale reactor system using the Hazard and Operability Study (HAZOP) tool. The HAZOP is an examination of the process and engineering intentions of new or existing facilities to identify and assess potential hazards, consequential effects, and protective and corrective actions.

The HAZOP analysis was a time consuming process, and it required extensive data and knowledge on impacts of each operation unit as well as all materials involved. The HAZOP report had to be approved by the safety committee before the rig construction and

experiments could be performed. Details of HAZOP analysis are described in Appendix A. In this section, risk control measures and additional protective measures that were implemented to minimise risk and hazard are summarised as follows:

- Adequate ventilation system was set up in the lab.
- Fume hoods as well as close plastic curtains were installed, where the gas cylinders and furnace located.
- Air operated valves were fitted with the gas cylinders to allow or stop the gas flowing into a reactor or a lab.
- A main control panel was installed to switch on and off power supply to a furnace and a solenoid valve.
- Two emergency stop switches were connected with a main control panel. In case of an emergency, pressing an emergency stop will shut off the power to the furnace and the solenoid valve, which in turn stops the air operated valves to prevent the gas flow from the cylinders.
- The fume hoods were equipped with interlocking system which automatically disables the power supply to the main control panel when the fume hoods stop working. Besides, interlock also keeps the fume hoods working by an emergency power supply in case of the power cut or general power loss.
- One way valves or check valves were used to avoid the gas reverse flow and then contaminate the gas in the cylinders.
- A flame arrester was fitted between the reactor and gas cylinders to prevent flame from the reactor passing into the gas cylinders which will cause explosions.
- Two pressure relief valves were fitted to prevent pressure build up in the gas inlet pipe and in the reactor.
- Portable gas detectors were used to monitor the level of all explosive and hazardous gases in the lab including H_2, CO, CH_4, NH_3, and H_2S.
- A webcam was installed to show a picture of the rig and the gas level on the portable gas detectors every 5 minutes. The pictures can be accessed via an internet connection.
- To operate the lab-scale reactor system safely and successfully, an experimental checklist was prepared for each experiment as shown in Appendix B as an example.

After the HAZOP analysis was completed, the lab-scale reactor system was then constructed based on a schematic diagram and an electrical line diagram of a lab-scale rector shown in Figure 3.4 and Figure 3.5, respectively. Pictures of the lab-scale reactor system are given in Figure 3.11.

Figure 3.11 A lab-scale reactor system

3.5 Experimental procedure and gas analysis

3.5.1 Experimental procedure

The experimental procedure for a lab-scale reactor can be divided into 4 phases: (1) preparation of the test materials and reactor setup; (2) heating and/or H_2 reduction process; (3) operational/removal process, and (4) shutdown. Brief description of the procedure is given below.

In the preparation process, the sand was sieved by a sieve shaker to particle size ranges required, and the sand was then dried in an oven at 105°C for 2 h. The dried sand of specified weight was filled in the quartz reactor which was then placed in the furnace. The quartz and PFA fittings were then connected to the reactor as shown in Figure 3.12.

Figure 3.12 Reactor setup

In the heating process, pure Ar gas was used to purge air out of the system, and it was monitored by N_2 concentration in the outlet gas analysed by the micro GC (see Figure 3.4 for location of the micro GC). Once the N_2 concentration in the outlet gas was found to be lower than the detection limit of N_2 by the micro GC (280 ppmv), the reactor heating began. If the H_2 reduction process of the sand was required, pure H_2 gas of 1.35 L/min was

mixed with pure Ar gas of 2.35 L/min to obtain 36.5 vol% H_2 in Ar gas. While 36.5 vol% H_2 in Ar gas flowed into the reactor, the reactor was heated by the furnace. The sand bed temperature in the reactor was detected by two thermocouples. The furnace heating rate was set at 10°C/min. The time spent for heating the sand bed temperature from room temperature to 800°C was about 3 h. The reduction process was kept at 800°C until it was completed, which was identified when no change was found between inlet and outlet H_2 concentrations of the reactor by the micro GC.

After the heating and/or H_2 reduction process, the removal process started. Pure Ar gas was first restored and the sand bed was cooled down to the temperature set point for the test. At constant bed temperature, the flow of a gas mixture of 1,978 ppmv NH_3 and/or 232 ppmv H_2S in Ar or in simulated producer gas was passed through the sand bed. Next, gas samples were collected at the outlet of the reactor and the operation conditions (bed temperature and pressure) were monitored and automatically recorded. The outlet simulated producer gas was measured online via the micro GC. Details of gas analysis by the micro GC is provided in Section 3.5.2. The sampling and analysis for NH_3 and H_2S is described in Chapter 4.

Once the experiment was completed, the furnace was shut off. All the gas flow meters, gas controlling valves, and gas cylinders were closed. Next, all the electric instruments and devices were shut off. Finally, a main control panel and power supply was switched off. Details of experimental procedures can also be found from the experimental checklist in Appendix B.

3.5.2 Gas analysis by the micro GC

An Agilent 3000 micro GC was used for analysis of major components in a gas mixture which utilises two TCD detectors. A 10 m × 0.32 mm Molecular Sieve 5A Plot column was used and operated at 110°C for analysis of H_2, N_2, CH_4 and CO while a 8 m × 0.32 mm Plot Q column was used and operated at 60°C for analysis of CO_2, C_2H_4, and C_2H_6. The micro GC utilises two TCD detectors. Calibration of the micro GC was performed by dilution of interested gases by the mass flow controllers to varied concentrations expected in the feed and outlet gas. This gives confidence in the accuracy of the data. Calibration curves of low concentrations of H_2 and N_2 are given in Figure 3.13, whereas calibration curves of

simulated producer gas are shown in Figure 3.14. Area count on the y-axis of Figure 3.13 and Figure 3.14 is the area of the peak of each gas components obtained from GC analysis. All of the calibration curves shown in this section were also used in Chapter 5.

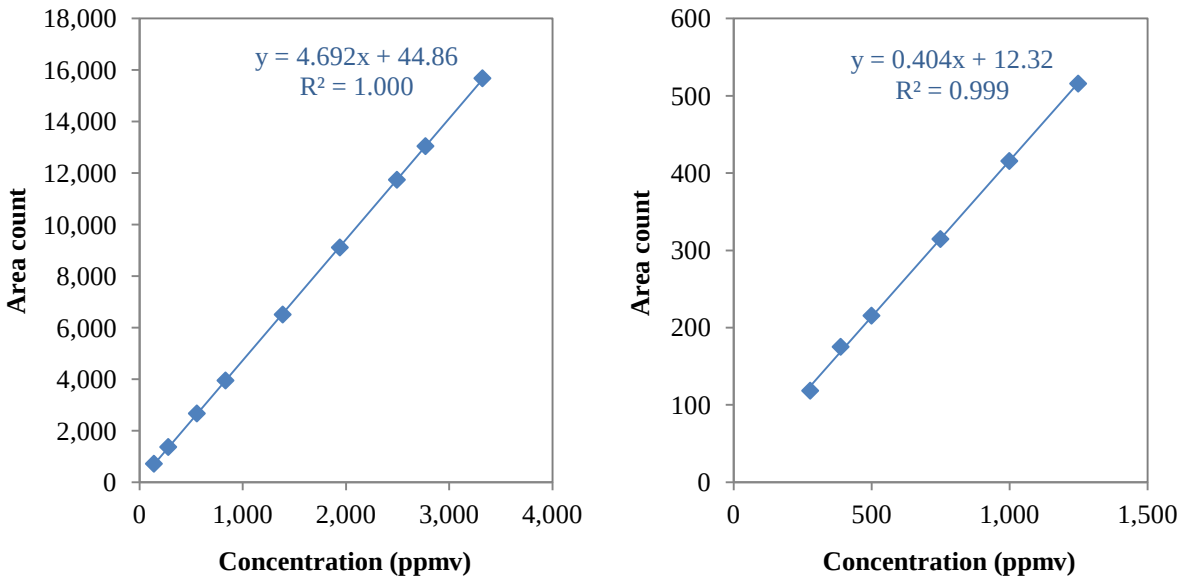

(a) (b)

Figure 3.13 Calibration curves of low concentrations of (a) H_2 and (b) N_2

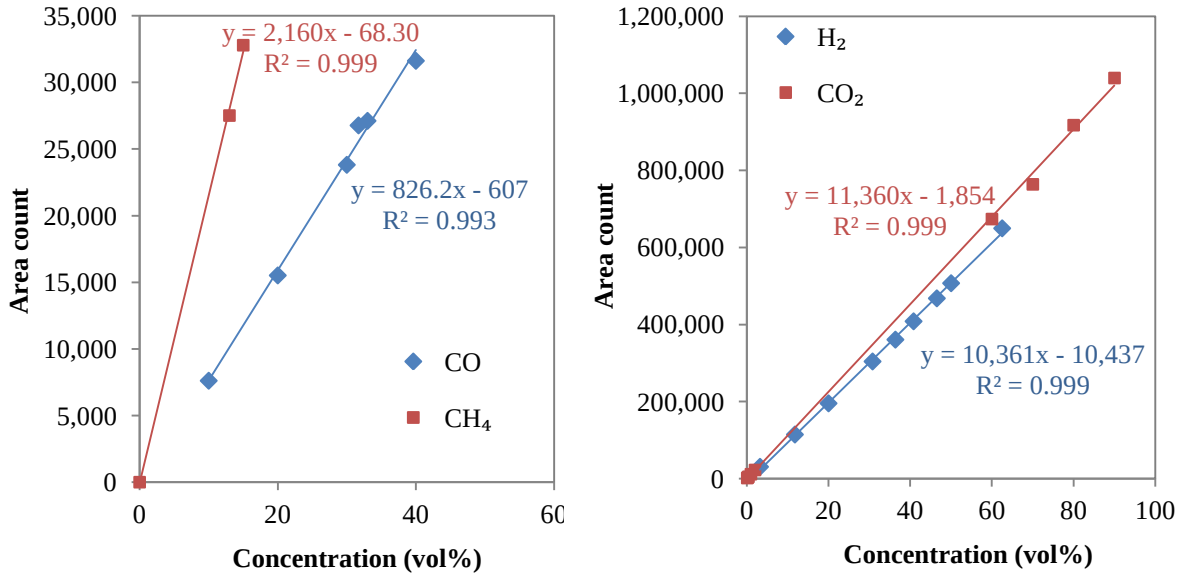

(a) (b)

Figure 3.14 Calibration curves of high concentrations of simulated producer gas (a) CO and CH_4 and (b) H_2 and CO_2

3.6 Preliminary experiments on the NH_3 decomposition

Preliminary experiments on catalytic NH_3 decomposition reaction were performed with 2,000±14% ppmv NH_3 in Ar gas at temperatures between 400 and 800°C. Titanomagnetite sand was used in the experiments as an as-received form, and with simple pre-treatment methods including calcination and H_2 reduction. This was to identify the effect of the reaction temperature and the pre-treatment method on the NH_3 decomposition reaction by titanomagnetite. Preliminary experiments presented in this section include: (1) blank test; (2) experiment on the NH_3 decomposition by titanomagnetite sand in the as-received form (or original form), in the calcined form, in the reduced-calcined form, and in the reduced form; and (3) reactor cleaning. The results from these preliminary experiments could lead to a proper experimental methodology and a pre-treatment method of titanomagnetite sand and other iron sands that were used in the set of experiments presented in Chapter 5.

3.6.1 Blank test

Before the experiments on the NH_3 removal by decomposition reaction, blank tests were performed in the empty fused quartz reactor and porous fused quartz distributor using 2,000 ppmv NH_3 in Ar gas at 500-800°C. This was to check if the reactor wall and thermal decomposition have any effects on the NH_3 removal. The test was simply conducted by heating the empty reactor with the furnace while a gas mixture of 2,000 ppmv NH_3 in Ar gas at a flow rate of 3.7 L/min flew through the reactor from the bottom to the top. At the gas outlet pipe, the micro GC was used to detect and measure H_2 and N_2 gases which were the products of NH_3 decomposition reaction. Based on the calibration curves of H_2 and N_2 given in Figure 3.13 in Section 3.5.2, the micro-GC detection limit for H_2 concentration was about 20 ppmv or equivalent to 0.7% NH_3 decomposition, whereas the detection limit for N_2 concentration was about 280 ppmv or 28% NH_3 decomposition.

From the results of the blank tests at 500-800°C, the H_2 and N_2 gases were formed below the detection limits and thus are regarded as non-detectable by the micro GC. Therefore, it can be concluded that the NH_3 decomposition was almost zero with empty reactor, and the thermal decomposition and the effect of the reactor wall on NH_3 removal was negligible.

3.6.2 Experiment on the NH_3 decomposition by titanomagnetite sand

In this part of the preliminary experiment, NH_3 inlet concentration was set at 2,000 ppmv and the total flow rate of the gas mixture of NH_3 and Ar was controlled at 3.7 L/min. In most of the experiments, the titanomagnetite sand of 250 g with particle size 180-250 μm was used, unless stated otherwise. The NH_3 decomposition was calculated from the inlet concentration of NH_3 and the outlet concentrations of H_2 and/or N_2 measured by the micro GC based on the stoichiometric NH_3 decomposition reaction.

Before the GC method in Section 3.5.2 (new GC method) can be developed for detection of very low concentrations of H_2 and N_2, another GC method (old GC method) was first used. Calibration curves for H_2 and N_2 with the old GC method are shown in Figure 3.15. The detection limit of H_2 was 120 ppmv and N_2 was 400 ppmv which corresponded to 4% and 40% NH_3 decomposition, respectively.

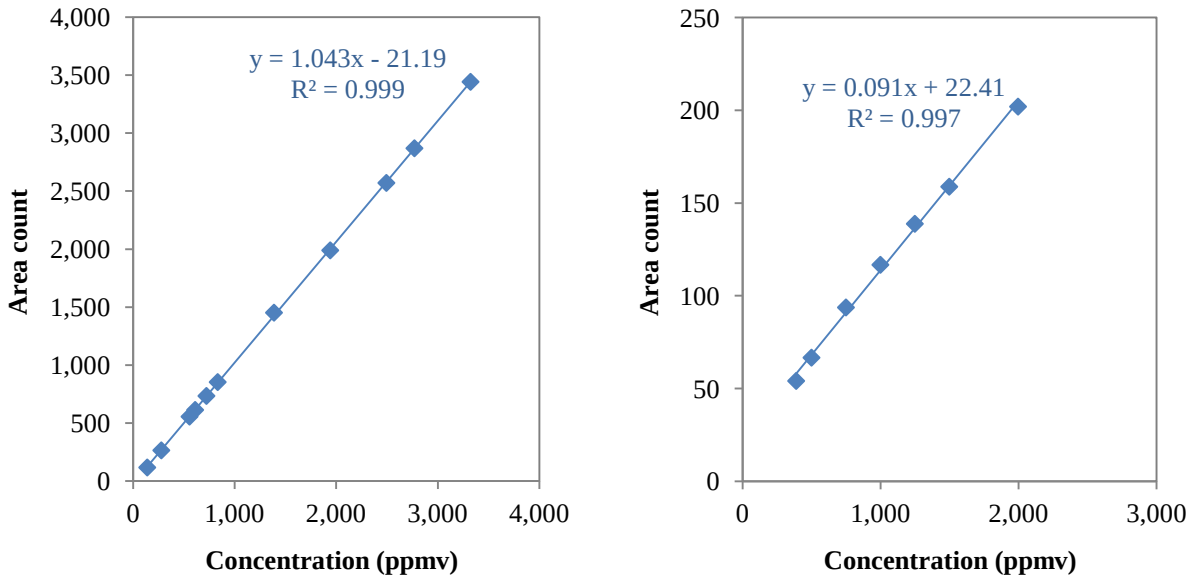

(a) (b)

Figure 3.15 Calibration curves of (a) H_2 and (b) N_2 with the old GC method

3.6.2.1 Experiment on as-received titanomagnetite

In this experiment, the as-received titanomagnetite ($Fe_{2.9}Ti_{0.1}O_4$) of 250 g with particle size 180-250 μm was used. The titanomagnetite was first sieved to particle size 180-250 μm and

then dried in an oven at 105°C for 2 h. Next, the dried titanomagnetite was put in the reactor for NH_3 decomposition test in sequence at 400, 600, and 800°C, respectively.

Results of NH_3 decomposition with as-received titanomagnetite at 400-800°C are shown in Figure 3.16, which was calculated from the NH_3 inlet concentration and the H_2 outlet concentration. At temperatures of 400 and 600°C, it was found that no H_2 was detected within 0.7 h. It could be either NH_3 decomposition was almost zero or below 4% according to H_2 detection limit of 120 ppmv (or 4% NH_3 decomposition). At 800°C, H_2 was detected and NH_3 decomposition increased gradually over 5 h. N_2 in the outlet gas was not detected at 400-800°C due to its detection limit of 400 ppmv (or 40% NH_3 decomposition). From the results, it was assumed that the catalytic activity of titanomagnetite sand was increased by heat pre-treatment at 800°C over time in the reactor.

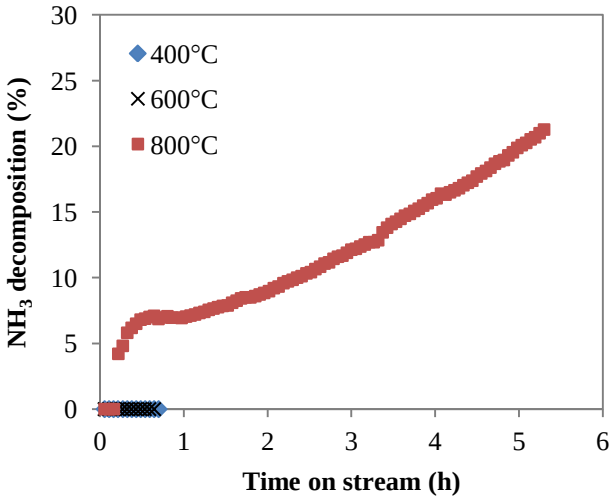

Figure 3.16 Decomposition of NH_3 in Ar gas with as-received titanomagnetite at 400-800°C

(Accuracy of NH_3 decomposition calculated from H_2 was ±14%)

3.6.2.2 Experiment on calcined titanomagnetite

As from the assumption presented in Section 3.6.2.1, the heat pre-treatment increased the titanomagnetite catalytic activity towards NH_3 decomposition. In this experiment, 1 kg of titanomagnetite (180-250 μm) was first calcined in a muffle furnace at 800°C for 24 h. After calcination, it was found that the colour of the sand changed from black to reddish-

brown and the sand was agglomerated. The calcined titanomagnetite was then sieved to required particle size of 180-250 μm. The calcined titanomagnetite of 250 g was used for NH_3 decomposition in Ar test at 600°C and the results are shown in Figure 3.17. The NH_3 decomposition was calculated from the NH_3 inlet concentration and the H_2 outlet concentration. N_2 in the outlet gas was not detected. Comparing the results of the calcined titanomagnetite and the as-received titanomagnetite at 600°C, the calcined titanomagnetite showed higher catalytic activity for NH_3 decomposition. Because the NH_3 decomposition reaction is endothermic, it was expected that the catalytic activity of the calcined titanomagnetite at 800°C would be higher than that at 600°C.

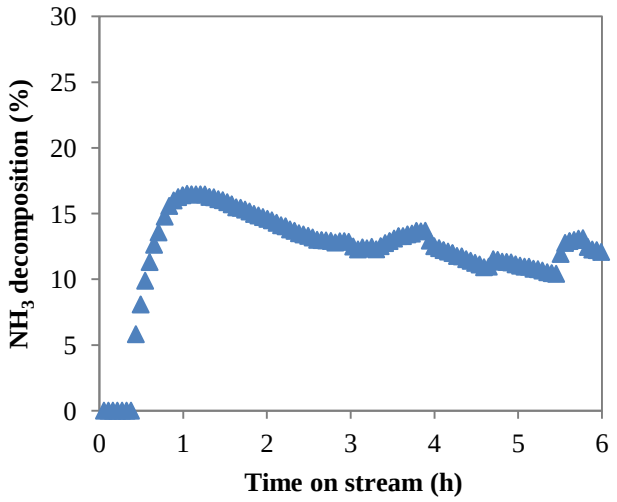

Figure 3.17 Decomposition of NH_3 in Ar gas with calcined titanomagnetite at 600°C (Accuracy of NH_3 decomposition calculated from H_2 was ±14%)

Based on the above observations, the experiment on the decomposition of NH_3 in Ar gas with calcined titanomagnetite at 800°C was conducted for 5 h. Unexpectedly, the results shown in Figure 3.18 demonstrated that NH_3 decomposition at 800°C (< 10% NH_3 decomposition) was less than that of 600°C (10-15% NH_3 decomposition) as shown in Figure 3.17. From these results, it was thus decided to continue the experiment at various temperatures which followed time sequence as: (1) 800°C; (2) 600°C, (3) 400°C; and (4) 500°C.

Results of NH_3 decomposition with calcined titanomagnetite at various temperatures are shown in Figure 3.18. The NH_3 decomposition was calculated from the NH_3 inlet concentration and the H_2 outlet concentration. N_2 in the outlet gas was not detected. The catalytic activity of calcined titanomagnetite at 600°C (30-40% NH_3 decomposition) as shown in Figure 3.18 was higher than that at 600°C (10-15% NH_3 decomposition) as shown in Figure 3.17 which could be due to the treatment of calcined titanomagnetite with Ar, NH_3, and/or H_2 produced from NH_3 decomposition at 800°C for 5 h.

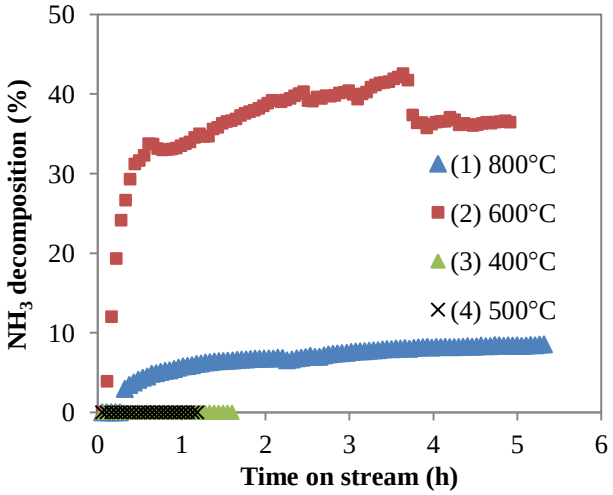

Figure 3.18 Decomposition of NH_3 in Ar gas with calcined titanomagnetite at various temperatures followed time sequence as: (1) 800°C; (2) 600°C, (3) 400°C; and (4) 500°C (Accuracy of NH_3 decomposition calculated from H_2 was ±14%)

Another experiment was therefore conducted in order to verify the effect of the reaction temperature and the pre-treatment process of the calcined titanomagnetite with Ar, NH_3, and/or H_2 produced from NH_3 decomposition. The reaction temperature was varied between 400 and 800°C over 25 h. Normal furnace heating/cooling rate was set at 10°C/min except during 7-22 h the furnace heating/cooling rate of 1°C/min was used. The results of NH_3 decomposition calculated from the NH_3 inlet concentration with both H_2 and N_2 outlet concentrations are shown in Figure 3.19.

From the results, the explanation of the effect of reaction temperature and the pre-treatment process on the NH_3 decomposition could be:

(1) at low temperatures (below 500°C), both H_2 and N_2 outlet concentrations were low and thus low NH_3 decomposition was obtained due to a slow kinetic reaction rate;

(2) when the temperature increases from 500 to 600°C, the kinetic reaction rate increased and thus the NH_3 decomposition increased;

(3) at high temperatures from 600 to 800°C, N_2 outlet concentration stayed high, but H_2 outlet concentration dropped, which indicated that NH_3 was decomposed and the H_2 produced was being consumed in another reaction probably reduction reaction of iron oxides.

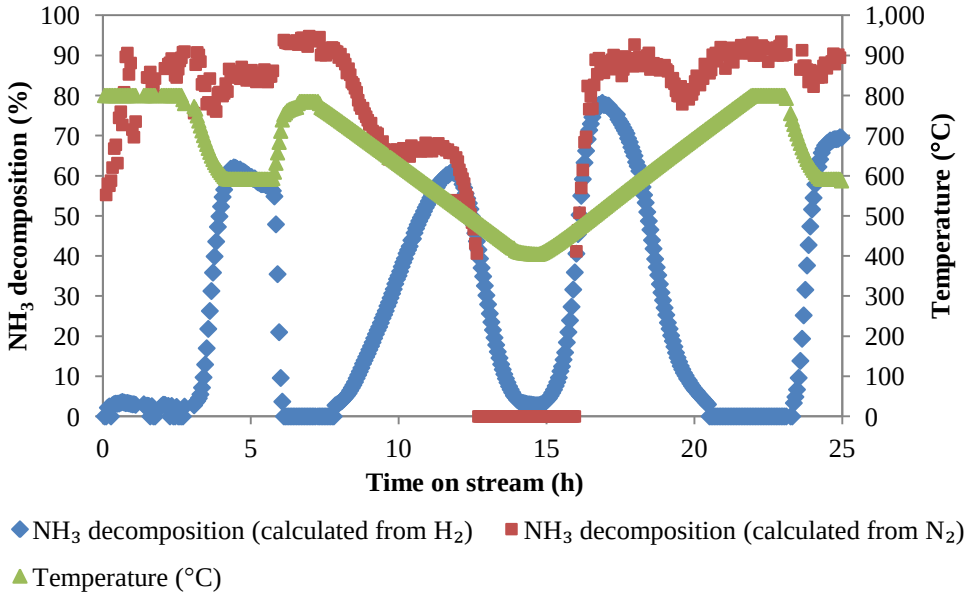

Figure 3.19 Decomposition of NH_3 in Ar gas with calcined titanomagnetite at various temperatures between 400 and 800°C
(Accuracy of NH_3 decomposition calculated from H_2 and N_2 was ±14%)

3.6.2.3 Experiment on reduced-calcined titanomagnetite

To identify the effect of reaction temperature and the pre-treatment process on the NH_3 decomposition and to obtain accurate and reliable NH_3 decomposition values calculated from the outlet concentrations of H_2 and/or N_2, more experiments have been conducted. Based on the results and discussion in Section 3.6.2.2, it was planned to pre-treat the calcined titanomagnetite by H_2 reduction process at high temperatures. The calcined titanomagnetite was reduced in the reactor with 3.2 vol% H_2 in Ar gas at 800°C until the H_2

reduction process was completed, which was determined when no detectable change was observed between the inlet and outlet H_2 concentrations of the reactor. In the reduction process, the total flow rate of 3.2 vol% H_2 in Ar gas was controlled at 3.7 L/min. Since it was the first time using H_2 gas for the reduction process, it was decided to set the H_2 concentration below lower explosive limit (4 vol%) for safety purpose. The maximum reduction temperature of 800°C was chosen to be the same as the calcination temperature to avoid the influence of excessively high temperatures on the sand properties.

Results of the temperature-programmed reduction (TPR) are presented in Figure 3.20. As can be seen, the H_2 reduction started at about 500°C and the peak was found at the maximum temperature of 800°C. Thus, H_2 produced from NH_3 decomposition would not be consumed by calcined titanomagnetite at temperatures below 500°C. Due to the H_2 concentration used was low (3.2 vol%), the process was conducted for 30 h. However, from Figure 3.20 (a), it seemed the H_2 reduction was not totally completed.

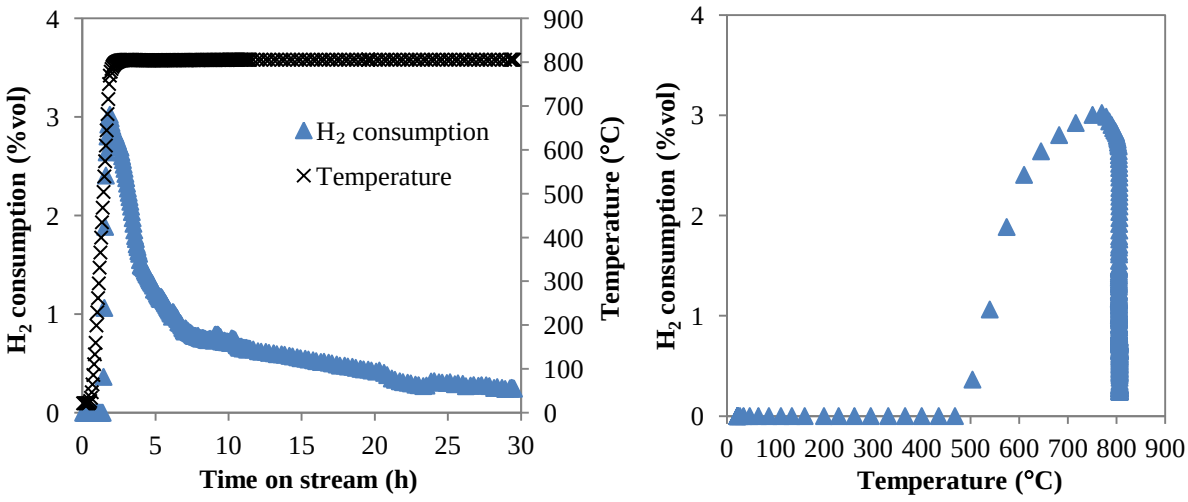

(a) (b)

Figure 3.20 Temperature-programmed reduction (TPR) for calcined titanomagnetite with 3.2 vol% H_2 in Ar gas as a function of (a) time on stream and (b) temperature

After the H_2 reduction of the calcined titanomagnetite, NH_3 in Ar gas flowed into the reactor at 800°C. After the steady state condition was observed, the reaction temperature was reduced to 700°C. This process was repeated at lower temperatures in the sequence of

600, 550, 500, and 400°C, respectively. The normal furnace heating/cooling rate used was 10°C/min. Results of NH_3 decomposition with reduced-calcined titanomagnetite are given in Figure 3.21. It was found that over the first 4 h, NH_3 decomposition calculated from H_2 outlet concentration was lower than that of calculation from N_2, which could be because the H_2 produced from NH_3 decomposition was consumed for the H_2 reduction reaction. Thus, to ensure the H_2 reduction process was completed as well as to shorten the time for this process, a modification must be made by increasing the H_2 vol%.

From Figure 3.21, NH_3 decomposition of about 90% could be achieved with reduced-calcined titanomagnetite over a wide temperature range of 500-800°C. Below 500°C, NH_3 decomposition calculated from H_2 concentration was decreased and N_2 concentration was not detected. Comparing the results of this test with those of calcined titanomagnetite, shown in Figure 3.19, H_2 in the outlet gas was found in this test at 800°C as expected due to the H_2 reduction process before NH_3 decomposition reaction. Therefore, it was necessary to reduce the calcined titanomagnetite with H_2 in order to increase the activity for NH_3 decomposition and to be able to use either H_2 or N_2 outlet concentration for calculation of NH_3 decomposition.

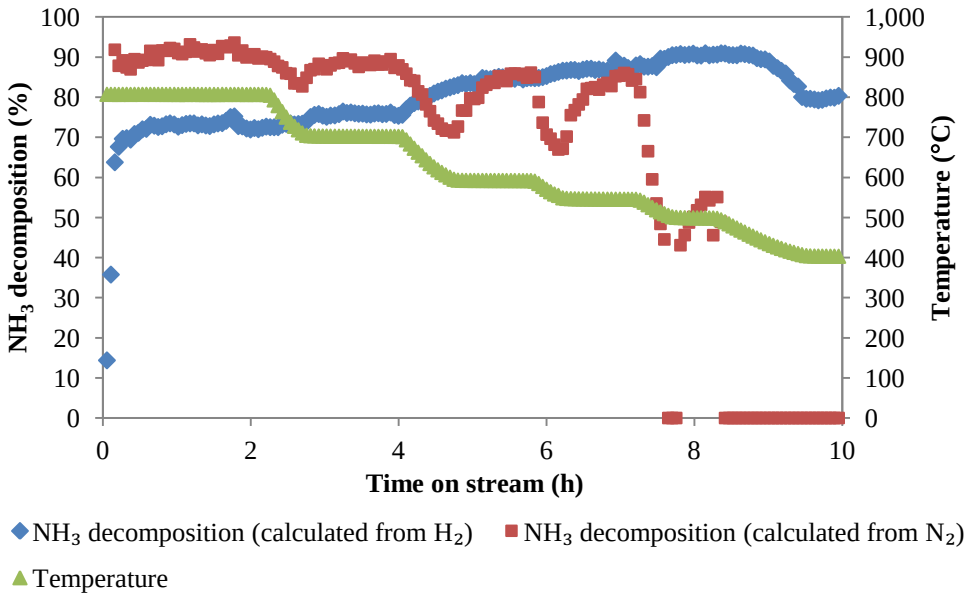

Figure 3.21 Decomposition of NH_3 in Ar gas with reduced-calcined titanomagnetite at various temperatures between 400 and 800°C
(Accuracy of NH_3 decomposition calculated from H_2 and N_2 was ±14%)

The area count of N_2 in the outlet gas measured by the old GC method was found to vary within a very small range between 60 and 110 in which they were corresponded to 45 and 95% NH_3 decomposition, respectively. For the H_2 area count, a little wider range from 425 to 2,800, (equivalent to 15 and 95% NH_3 decomposition, respectively) could be obtained. Then, the improvement of detection limit of H_2 and N_2 by the micro GC was performed and the calibration curves with the new GC method can be found in Figure 3.13.

Finally, during the temperature decrease, NH_3 decomposition calculated from H_2 was quite steady, whereas NH_3 decomposition calculated from N_2 was reduced which was clearly seen when temperature was below 700°C. This phenomenon was interesting and it required more experiments for the explanation, which is discussed in the last experiment of this section.

In the next experiment, 36.5 vol% H_2 in Ar gas for H_2 reduction process as well as the new GC method for detection of very low concentrations of H_2 and N_2 (Figure 3.13) was used. Moreover, the total weight of calcined titanomagnetite of 125 g was tested instead of 250 g. As it was found that 90% NH_3 decomposition was obtained at a wide temperature range of 500-800°C, it was believed that the NH_3 decomposition reaction was not kinetic limited with the reduced-calcined titanomagnetite. To confirm whether the reaction is not a kinetic limit, the test was performed by reducing the weight of the sand by half which in turn lowering the gas residence time in the BFB bed almost in half. If the NH_3 decomposition is found unchanged when reducing the residence time of the gas, it might be concluded that the reaction is not kinetics limited.

The TPR results are presented in Figure 3.22. These results are similar to those shown in Figure 3.20, except that much less time was required (6 h) for the completion of H_2 reduction. Results of NH_3 decomposition with reduced-calcined titanomagnetite (125 g) are given in Figure 3.23. High NH_3 decomposition of about 90-100% was again obtained with reduced-calcined titanomagnetite at 500-800°C, although the amount of the sand was reduced by half. Therefore, it can possibly be concluded that the reaction is not kinetics limited with reduced-calcined titanomagnetite.

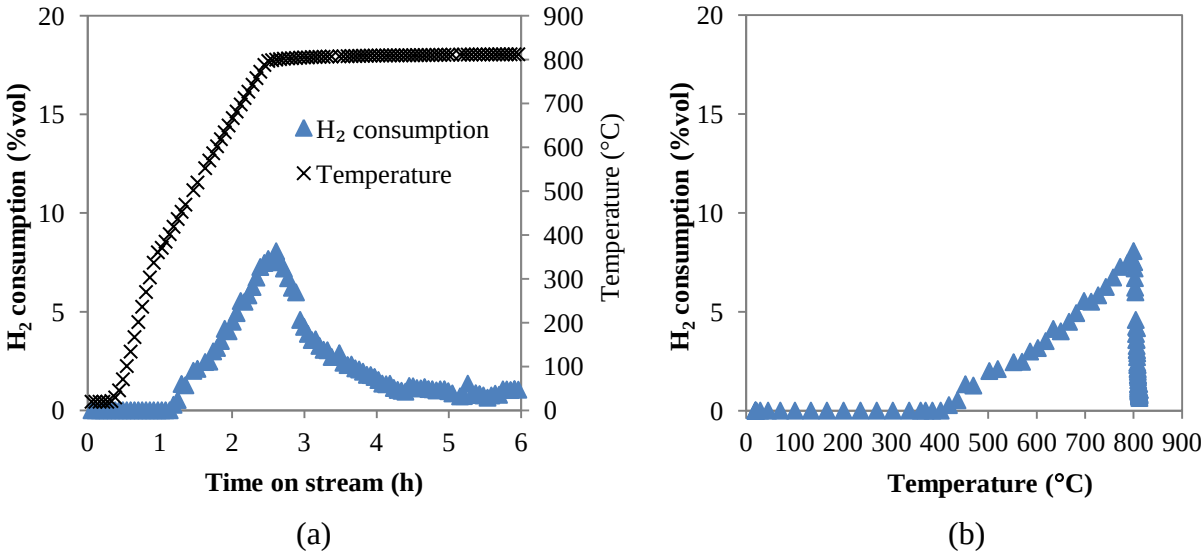

Figure 3.22 Temperature-programmed reduction (TPR) for calcined titanomagnetite (125 g) with 36.5 vol% H_2 in Ar gas as a function of (a) time on stream and (b) temperature

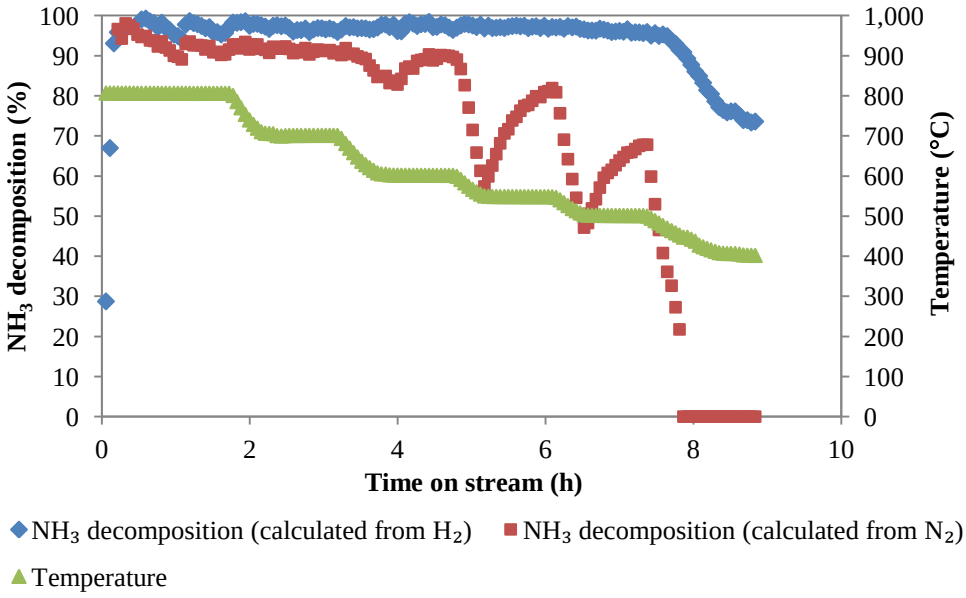

Figure 3.23 Decomposition of NH_3 in Ar gas with reduced-calcined titanomagnetite (125 g) at various temperatures between 400 and 800°C
(Accuracy of NH_3 decomposition calculated from H_2 and N_2 was ±14%)

As mentioned previously, an experiment must be conducted to describe the phenomenon of N_2 outlet concentration reduction when temperature decreased. From a literature review

[23], a mechanism of the catalytic synthesis of NH_3 on Fe-based catalysts was proposed. It was also found that dissociative adsorption was a rate limiting step of NH_3 synthesis reaction [23].

Based on the mechanism of NH_3 synthesis, the mechanism of NH_3 decomposition which is a reverse of NH_3 synthesis could be formulated as the following steps:

$NH_3 + S \leftrightarrow NH_3{\cdot}S$

$NH_3{\cdot}S + S \leftrightarrow NH_2{\cdot}S + H{\cdot}S$

$NH_2{\cdot}S + S \leftrightarrow NH{\cdot}S + H{\cdot}S$

$NH{\cdot}S + S \leftrightarrow N{\cdot}S + H{\cdot}S$

$2N{\cdot}S \leftrightarrow N_2{\cdot}S + S$ (dissociative desorption)

$N_2{\cdot}S \leftrightarrow N_2 + S$ (molecular desorption)

$2H{\cdot}S \leftrightarrow H_2 + 2S$

where S denotes a vacant site on the catalyst surface

From the mechanism, either dissociative or molecular desorption would be the slowest step that resulted in a slow desorption of N_2 from the surface, given less N_2 concentration in the outlet gas. Thus, it was planned to study the effect of temperature on the N_2 outlet concentration reduction in two parts as follows:

(1) When reducing temperature from 600 to 550°C, set a cooling rate of the furnace at 0.5°C/min instead of a normal cooling rate at 10°C/min. With this method, the effect of the temperature cooling rate on the rate of desorption of nitrogen molecule and/or N atom can be studied;

(2) When reducing temperature from 550 to 500°C, stop the inlet NH_3 flow and at the same time feed 1,000 ppmv N_2 gas in Ar, which was a product of 100% decomposition of 2,000 ppmv NH_3. With this method, it can be determined that either dissociative or molecular desorption is the rate limiting step in NH_3 decomposition when temperature decreased.

The results of this test are provided in Figure 3.24. For the first part when temperature was reduced from 600 to 550°C, it was found that the rate of desorption of nitrogen molecule and/or atom was not significantly affected by a slow change of temperature. For the second part during 15-21 h, 1,000 ppmv N_2 was fed while the temperature was reduced from 550 to 500°C, it was found that about 1,000 ppmv N_2 was measured in the outlet gas, which identified that the molecular adsorption and desorption reactions were rapid on the catalyst surface. Moreover, when N_2 gas flow was stopped and the 2,000 ppmv NH_3 gas was resumed at 21 h, reduction of N_2 concentration in the outlet gas was observed during 21-25 h. It was, therefore, believed that the dissociative desorption reaction is the rate limiting step in NH_3 decomposition with reduced-calcined titanomagnetite when temperature decreased.

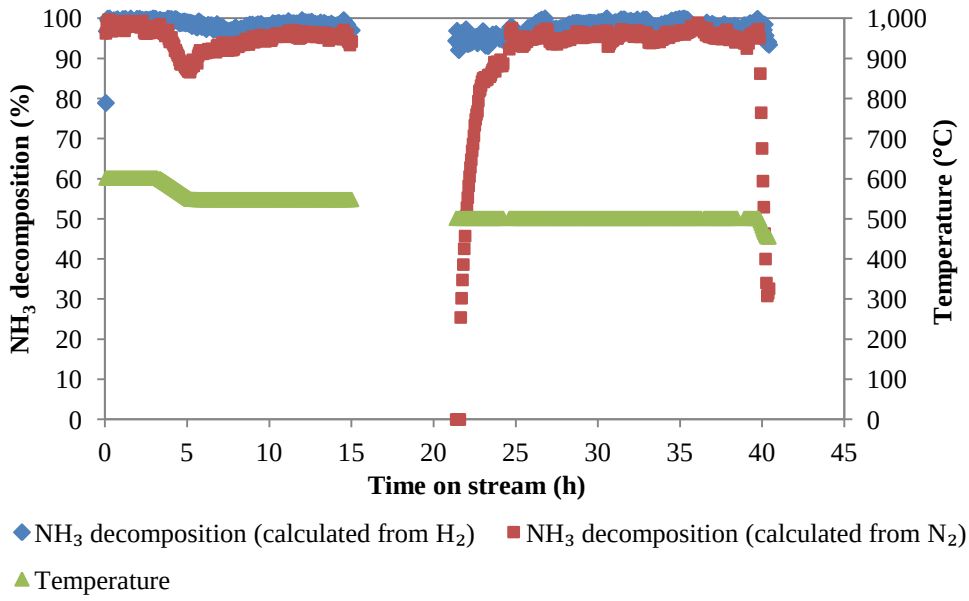

Figure 3.24 Results of the study of the N_2 adsorption onto the surface of reduced-calcined titanomagnetite (125 g) when temperature decreased (Accuracy of NH_3 decomposition calculated from H_2 and N_2 was ±14%)

3.6.2.4 Experiment on reduced titanomagnetite

From the results obtained in Section 3.6.2.3, it was expected that the titanomagnetite with reduction only may also show a very high NH_3 decomposition as much as those with reduced-calcined titanomagnetite. Thus, the as-received titanomagnetite and calcined titanomagnetite were analysed for their surface area, cumulative pore volume, and average

pore diameter. The surface area was measured using the Brunauer-Emmett-Teller (BET) method, and the adsorption cumulative pore volume and the adsorption average pore diameter were determined by the Barrett-Joyner-Halenda (BJH) method. The results of these analyses are given in Table 3.10. Titanomagnetite after calcination at 800°C for 24 h led to the decrease of surface area and pore volume, which could be due to the agglomeration of the sand heated at high temperature.

Table 3.10 BET surface area, and BJH adsorption cumulative pore volume and average pore diameter of as-received titanomagnetite and calcined titanomagnetite

Sample	**BET surface area (m^2/g)**	**BJH adsorption cumulative pore volume (cm^3/g)**	**BJH adsorption average pore diameter (nm)**
Titanomagnetite	1.1	0.002	10.6
Calcined titanomagnetite	0.2	0.001	22.6

An experiment with 125 g reduced titanomagnetite was conducted with the same operation conditions as those of reduced-calcined titanomagnetite, shown in Figure 3.23. These TPR results of titanomagnetite are given in Figure 3.25 and they are similar to those of calcined titanomagnetite (Figure 3.22). The H_2 reduction started at about 500°C, and the peak was found at maximum temperature operated at 800°C.

Figure 3.26 shows the NH_3 decomposition with reduced titanomagnetite. As predicted, 90% NH_3 decomposition could be achieved with reduced titanomagnetite over a temperature range of 500-800°C. The phenomenon of N_2 outlet concentration reduction when temperature decreased was again observed with reduced titanomagnetite. Therefore, an experiment to verify and confirm that the dissociative desorption reaction is the rate limiting step in NH_3 decomposition was repeatedly performed with reduced titanomagnetite.

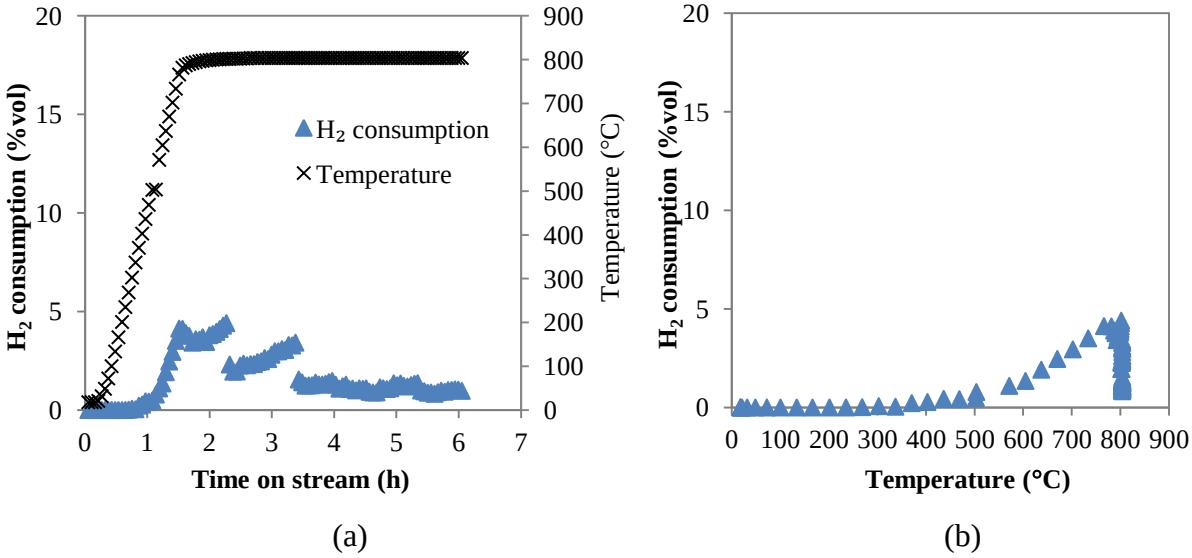

(a) (b)

Figure 3.25 Temperature-programmed reduction (TPR) for titanomagnetite with 36.5 vol% H_2 in Ar gas as a function of (a) time on stream and (b) temperature

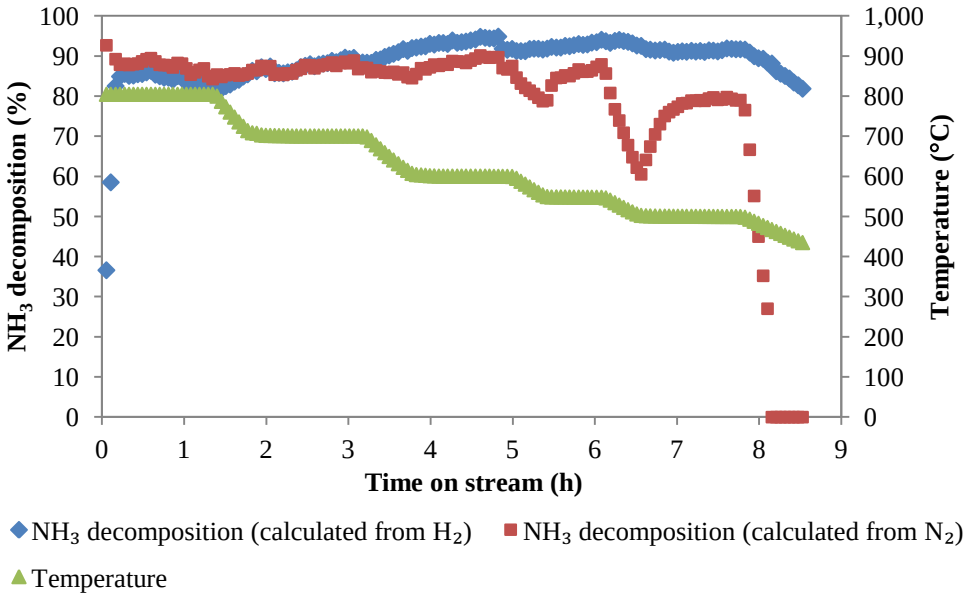

Figure 3.26 Decomposition of NH_3 in Ar gas with reduced titanomagnetite (125 g) at various temperatures between 400 and 800°C

(Accuracy of NH_3 decomposition calculated from H_2 and N_2 was ±14%)

The results are shown in Figure 3.27. In the initial 6-11 h while the temperature was reduced from 550 to 500°C, the feed gas of 2,000 ppmv NH_3 in Ar was switched to 1,000 ppmv N_2 gas in Ar. It was found that 1,000 ppmv N_2 was measured in the outlet gas over 6-11 h. At 11 h, the N_2 gas flow was stopped and the 2,000 ppmv NH_3 gas was resumed, and the reduction of N_2 concentration in the outlet gas was observed in the following period, during 11-15 h from the start. These results are similar to those obtained with reduced-calcined titanomagnetite shown in Figure 3.24. Therefore, the dissociative desorption reaction is the rate limiting step in NH_3 decomposition with reduced titanomagnetite when temperature decreased.

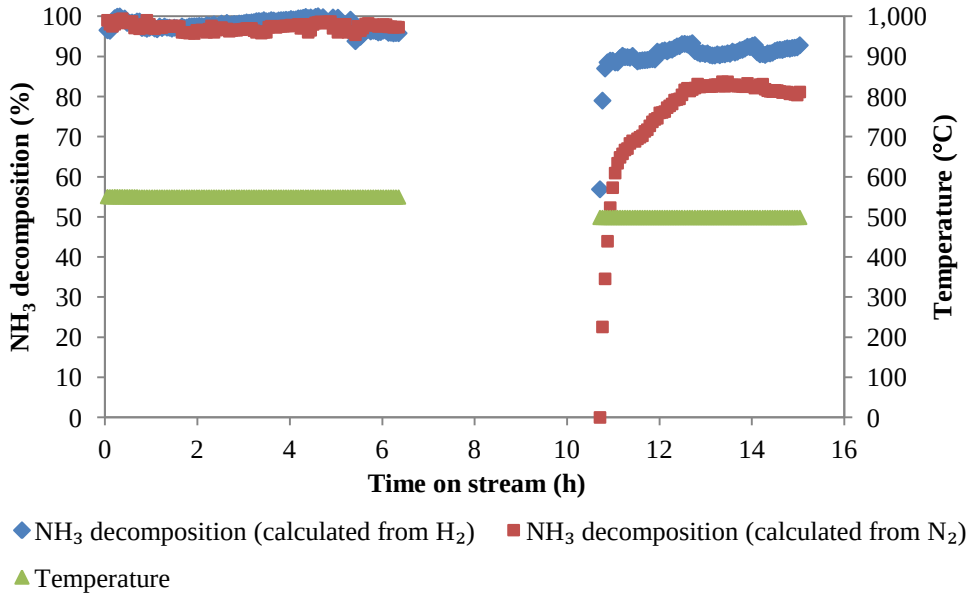

Figure 3.27 Results of the study of the N_2 adsorption onto the surface of reduced titanomagnetite (125 g) when temperature decreased (Accuracy of NH_3 decomposition calculated from H_2 and N_2 was ±14%)

3.6.2.5 Conclusions

A methodology to study the NH_3 decomposition reaction with Fe-based catalyst has been developed. Titanomagnetite in its original form as-received ($Fe_{2.9}Ti_{0.1}O_4$) did not show high NH_3 decomposition unless it was pre-treated with a H_2 reduction process. As-received titanomagnetite and calcined titanomagnetite after processing with H_2 reduction have shown a very high NH_3 decomposition of 90-100% over a wide range of temperatures from

500 to 800°C, and the NH_3 decomposition decreases with a decrease in temperature below 500°C. When temperature is decreased, the dissociative desorption reaction is the rate limiting step in NH_3 decomposition with reduced titanomagnetite and reduced-calcined titanomagnetite.

The Fe-based catalyst, therefore, should be reduced with H_2 to improve the catalytic activity towards NH_3 decomposition. Once the Fe-based catalyst is reduced, H_2 and/or N_2 concentrations in the outlet gas detected by the micro GC can be used to calculate the NH_3 decomposition, otherwise NH_3 outlet concentration needs to be measured. The reduced-calcined titanomagnetite would not be further tested because it shows similar catalytic activity as the reduced titanomagnetite, while consuming more energy for the calcination process. The temperature between 500 and 800°C will be used for the further tests.

3.6.3 Reactor cleaning

Reactor cleaning is required after each experiment to ensure that there is no effect of the small amount of fine catalyst left inside the quartz distributor and on the reactor wall. The reactor cleaning process is described in Appendix C. After the reactor cleaning process, the cleaned-empty reactor was tested with the 2,000 ppmv NH_3 in Ar gas at temperature between 500 and 800°C as the same process as the blank test (Section 3.6.1).

3.7 References

[1] H. Boerrigter, H.P. Calis, D.J. Slort, H. Bodenstaff, A.J. Kaandorp, H. den Uil, L.P.L.M. Rabou, Gas cleaning for integrated biomass gasification (BG) and Fischer-Tropsch (FT) systems: Experimental demonstration of two BG-FT systems ("Proof-of-Principle"), in: the Energy research Centre of the Netherlands (ECN), the Netherlands, report no: ECN-C--04-056, 2004.

[2] P. McKendry, Energy production from biomass (part 3): gasification technologies, Bioresource Technology, 83 (2002) 55-63.

[3] D. Mamrosh, C. Beitler, K. Fisher, S. Stem, Consider improved scrubbing designs for acid gases, Hydrocarbon Processing, (2008) 69-74.

[4] D.J. Stevens, Hot gas conditioning: Recent progress with larger-scale biomass gasification systems, in: National Renewable Energy Laboratory, the U.S. Department of Energy Laboratory, report no: NREL/SR-510-29952, 2001.

[5] W. Torres, S.S. Pansare, J.G. Goodwin Jr., Hot gas removal of tars, ammonia, and hydrogen sulfide from biomass gasification gas, Catalysis Reviews, 49 (2007) 407-456.

[6] D. Kunii, O. Levenspiel, Fluidization engineering, Butterworth-Heinemann, 1991.

[7] J.R. Grace, A.A. Avidan, T.M. Knowlton, Circulating fluidized beds, Blackie Academic & Professional, 1997.

[8] C.Y. Wen, Y.H. Yu, A generalized method for predicting the minimum fluidization velocity, AIChE Journal, 12 (1966) 610-612.

[9] D.C. Chitester, R.M. Kornosky, L.-S. Fan, J.P. Danko, Characteristics of fluidization at high pressure, Chemical Engineering Science, 39 (1984) 253-261.

[10] J. Grace, G. Hetsroni, Handbook of multiphase systems, Hemisphere, 1982.

[11] A. Haider, O. Levenspiel, Drag coefficient and terminal velocity of spherical and nonspherical particles, Powder Technology, 58 (1989) 63-70.

[12] H. Bi, J. Grace, Effect of measurement method on the velocities used to demarcate the onset of turbulent fluidization, The Chemical Engineering Journal and the Biochemical Engineering Journal, 57 (1995) 261-271.

[13] D. Geldart, Types of gas fluidization, Powder Technology, 7 (1973) 285-292.

[14] A.F. Mills, Basic heat and mass transfer, Prentice Hall, 1999.

[15] Industrial Sands Ltd., Iron sand concentrate, 2006, from: http://www.industrialsands.co.nz/iron_sand.html.

[16] C. Li, P. Nelson, Interactions of quartz, zircon sand and stainless steel with ammonia: implications for the measurement of ammonia at high temperatures, Fuel, 75 (1996) 525-526.

[17] P. Ståhlberg, M. Lappi, E. Kurkela, P. Simell, P. Oesch, M. Nieminen, Sampling of contaminants from product gases of biomass gasifiers, in: VTT Technical Research Centre of Finland, report no: VTT Research Notes 1903, 1998.

[18] R.C. Brown, J. Smeenk, G. Norton, Development of analytical techniques and scrubbing options for contaminants in gasifier streams intended for use in fuel cells, in: Center for Sustainable Environmental Technologies at Iowa State University, 2001.

[19] G.A. Norton, R.C. Brown, Wet chemical method for determining levels of ammonia in syngas from a biomass gasifier, Energy & Fuels, 19 (2005) 618-624.

[20] the Department of Labour, Innovation & Employment, Workplace exposure standards, 2013, from: http://www.dol.govt.nz/workplace/knowledgebase/item/1444.

[21] The Engineering Toolbox, Gases - Explosive and Flammability Concentration Limits, 2012, from:http://www.engineeringtoolbox.com/explosive-concentration-limits-d_423.html

[22] The Engineering Toolbox, Fuels and Chemicals - Autoignition Temperatures, 2012, from: http://www.engineeringtoolbox.com/fuels-ignition-temperatures-d_171.html.

[23] G.A. Somorjai, Y. Li, Introduction to surface chemistry and catalysis, John Wiley & Sons, 2010.

4. Development of sampling and analysis of NH_3 and H_2S in producer gas

4.1 Introduction

Determination of NH_3 and H_2S concentrations in producer gas from the DFB steam gasifier is required in this research. Various gas components and other species in the producer gas including H_2, CO, CO_2, CH_4, water vapour, char, and tars can lead to significant interferences and/or unreliability of the measurement methods for NH_3 and H_2S. Therefore, reliable and accurate sampling and analysis of NH_3 and H_2S concentrations has to be developed. The cost and size of the analytical instruments are also considered in the development.

This chapter describes the development of sampling and analysis of NH_3 and H_2S in the producer gas from the DFB steam gasifier. The sampling of the NH_3 and H_2S gases is performed via a wet chemical method by using an impinger system. Sulphuric acid solution (H_2SO_4) is used to absorb NH_3 in the gas into the solution, whereas sodium hydroxide solution (NaOH) is used to absorb H_2S. The Ion Selective Electrode (ISE) analytical method is selected for the analysis of NH_3 and H_2S in the absorbing solution because it is highly specific, very sensitive, and cheap.

In addition, experiments to investigate the effect of concentration of H_2SO_4 or NaOH solution on the NH_3 or H_2S measurement were conducted by the employment of a lab-scale reactor, which is presented in Chapter 3. The verification tests of the sampling and analysis of NH_3 and H_2S by the wet chemical and ISE methods were also performed to find out the accuracy, reliability, and repeatability of the NH_3 and H_2S measurement.

4.2 Sampling of NH_3 and H_2S in the producer gas

In the DFB steam gasifier experiments, the producer gas samples were collected from the top of the BFB cyclone (see Figure 4.1). The main gas composition (H_2, CO, CO_2, CH_4, C_2H_6, and C_2H_4) in the gas sample was analysed using a micro GC. A dedicated sampling line for NH_3 and H_2S analysis was designed in the present study as shown in Figure 4.2 and Figure 4.3. In the newly designed sampling line, the gas sample was first drawn through

two filters and then through impinger bottles in a water bath, where NH_3 or H_2S was absorbed into the absorbing solution. The water in the bath was controlled at 4°C to cool down the gas stream to room temperature. The stainless steel 316 tube of the sampling line was made as short as possible and coated with Dursan inert and corrosion resistant coating by SilcoTek Company [1]. The Dursan coating prevented reactions and adsorption of NH_3 or H_2S onto the stainless steel inner surface.

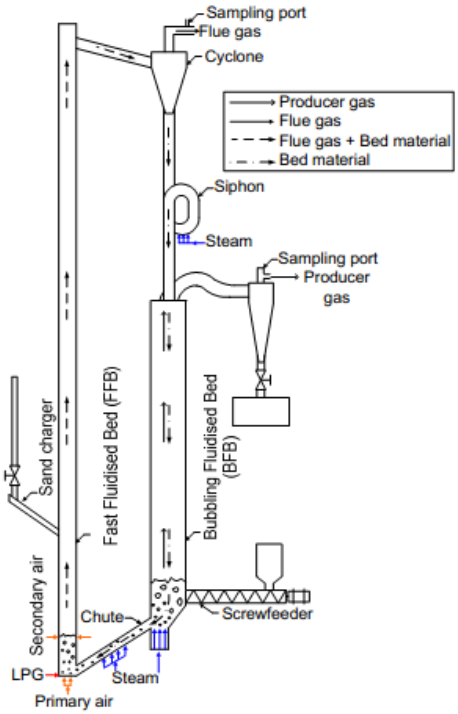

Figure 4.1 Schematic diagram of the DFB steam gasifier used in this study [2]

During the NH_3 and H_2S sampling, particulates and tars in the producer gas were removed by two filters (see Figure 4.1). The first filter was filled with coarse quartz wool (5-15 μm), and the second filter was equipped with a quartz microfiber thimble and coarse quartz wool as a safeguard if the quartz microfiber thimble was damaged during the experiment. The two filters were temperature-controlled with trace heating and insulation (ceramic fibers, K-wool) so that the tars in the gas were condensed and trapped in the filters, but condensation of moisture in the gas in the sampling line was prevented due to the solubility of NH_3 and H_2S in water. Therefore, the controlled temperatures (T1 and T2) were set below the tar dew point but higher than the water dew point of the producer gas. The sampling line was occasionally back-flushed by N_2 gas with the flow rate of 15 L/min for about 30 min to prevent sampling line blockage.

In the water bath, each of the first three impinger bottles was filled with 100 ml of absorbing solution, either 0.05 molar sulphuric acid solution (H_2SO_4) to absorb NH_3 or 0.05 molar sodium hydroxide solution (NaOH) to absorb H_2S, respectively. The last bottle was empty to collect the solution in case of an overflow. The NH_3 or H_2S in the solution was measured by the Ion Selective Electrode (ISE) method through direct calibration technique. The moisture in the producer gas was also condensed in the absorbing solution during sampling, but this did not affect the measurement of NH_3 or H_2S because the total volume of the solution after each sampling was measured. The sampling gas flow rate was maintained at approximately 3 L/min for all the wood gasification tests in Chapters 6 and a total of 18 L dry producer gas flowed into the impinger bottles. In Chapter 7, the sampling gas flow rate was used at 3 L/min for all tests, and a total of 9 L dry producer gas flowed into the impinger bottles except for the 100% wood feedstock run in which 18 L dry producer gas was drawn. In the wood gasification runs in Chapters 6 and 7, the NH_3 and H_2S concentrations in the producer gas were expected to be lower than those for feedstocks with addition of lignite. Therefore, to ensure that the concentrations of NH_3 and H_2S in the absorbing solution were in the range of standard solutions prepared for the calibration, more producer gas was drawn into the impinger bottles in the wood runs than those of the blended lignite and wood runs. The experimental checklist for sampling of NH_3 and H_2S in the producer gas from the DFB steam gasifier is shown in Appendix D.

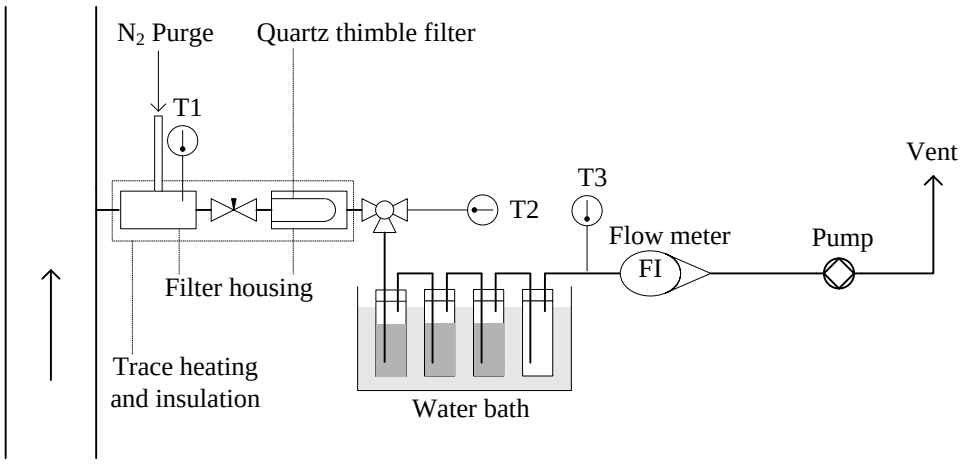

Figure 4.2 Schematic diagram of a sampling line for NH_3 and H_2S measurement

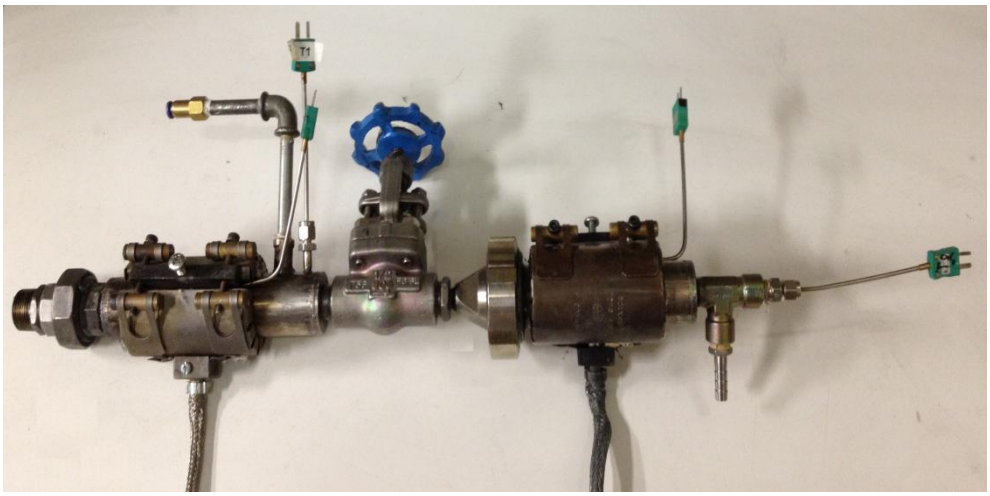

(a)

(b)

Figure 4.3 Pictures of a sampling line for NH_3 and H_2S measurement (a) all assembled parts and (2) after being insulated and installed in the DFB steam gasifier

4.3 NH_3 analysis

The absorbing solution used for absorption of NH_3 was 0.05 molar H_2SO_4 solution. In the acid solution, where hydrogen ion was readily available, the NH_3 could be converted to ammonium ion (NH_4^+). Due to the polarity of NH_3 molecules and their ability to form hydrogen bonds, NH_3 dissolved in water and reacted with water and H_2SO_4 to form NH_4^+ and ammonium sulphate ($(NH_4)_2SO_4$), respectively, as shown in the following reactions (Equations 4.1 and 4.2):

$$NH_3 + H_2O \leftrightarrow NH_4^+ + OH^- \quad (4.1)$$

$$2NH_3 + H_2SO_4 \leftrightarrow (NH_4)_2SO_4 \quad (4.2)$$

NH_3 in water exists both as molecular form (NH_3) and as ionized from (NH_4^+). The relative concentrations of NH_3 and NH_4^+ in the solution were determined by the pH at a given temperature of the solution as shown in Figure 4.4, where the data was obtained from U.S. EPA. [3].

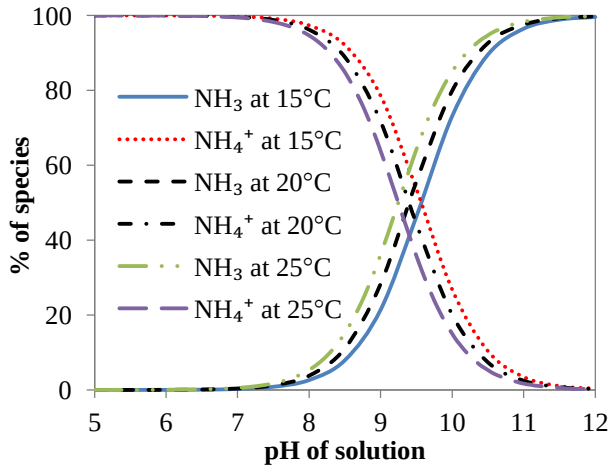

Figure 4.4 Percentage of NH_3 and NH_4^+ concentrations present in the solution as a function of the pH value at 15-25°C

After each sampling, the $(NH_4)_2SO_4$ or NH_4^+ was preserved in the solution by controlling the pH of the solution to 2 or lower to ensure that all the NH_3 was converted to NH_4^+ considering that the stability of NH_4^+ in the solution is higher than that of NH_3. Then, the solution was stored at 4°C according to the standard of ASTM D 1426 (standard test methods for ammonia nitrogen in water).

The analysis of the NH_3 in the sample solutions was conducted within 24 h after sampling by ISE method according to the ASTM D 1426. In the analysis of NH_3, the standard solutions and the sample solutions were made to be alkaline with 10 M NaOH for the pH to be greater than 11 so that all of the NH_4^+ was converted to NH_3 (Figure 4.4). This is because the NH_3 ISE allows only NH_3 gas to diffuse through the gas-permeable membrane [4]. With the specific NH_3 ISE, only volatile amines can interfere with the electrode

measurement. However, amines have not been reported to be found in the gasification producer gas, therefore, it is assumed that there is no interference in the NH_3 measurements. In addition, most gases do not interfere as they are converted to ionic form in alkaline solution with pH above 11. These ionic species are not allowed to cross the gas permeable membrane and thus they do not inference with the measurements [4].

The electrode potential of the solution read in millivolt scale (mV) was measured by the pH meter or direct-reading concentration could be determined by the ISE meter. Having obtained the calibration curve between concentration (mg/L) and mV reading of the standard solutions by the pH meter based on the direct calibration technique, the NH_3 concentration in the sample solutions can be calculated. The actual NH_3 concentration in the producer gas, therefore, was calculated from the known NH_3 concentration in the solution, the total volume of absorbing solution after sampling, and the total producer gas volume drawn into the absorbing solution.

4.4 H_2S analysis

0.05 molar NaOH solution was used as an absorbing solution for H_2S. H_2S dissolved in the solution which reacted with NaOH to form sodium hydrosulphide (NaHS) and then sodium sulphide (Na_2S) as given in Equations 4.3 and 4.4 below:

$$H_2S + NaOH \rightarrow NaHS + H_2O \quad (4.3)$$

$$NaHS + NaOH \rightarrow Na_2S + H_2O \quad (4.4)$$

The dissolved sulphide can be in the form of H_2S or HS^- or S^{2-} depending primarily on the pH of the solution in which their proportions can be calculated from the dissociation constant (K_a) presented in Equations 4.5 and 4.6.

$$K_{a1} = \frac{[HS^-][H^+]}{[H_2S]} \qquad \text{where} \quad pK_{a1} = -logK_{a1} \quad (4.5)$$

$$K_{a2} = \frac{[S^{2-}][H^+]}{[HS^-]} \qquad \text{where} \quad pK_{a2} = -logK_{a2} \quad (4.6)$$

Figure 4.5 shows the fractions of dissolved sulphide in water as a function of pH, where pK_{a1} and pK_{a2} used for calculation at 25°C were 7.0 [5] and 12.97 [6], respectively. As shown in Figure 4.5, sulphide is mainly in the form of H_2S in acid solution. In an intermediate pH range of up to about pH 12, almost all the sulphide is in the form of HS^- [7]. Only in very high alkaline solution does the sulphide exist primarily as free ion (S^{-2}).

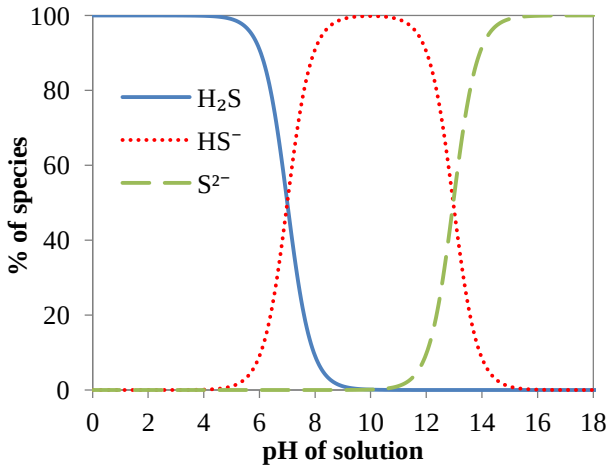

Figure 4.5 Percentage of H_2S, HS^-, and S^{2-} concentrations present in the solution as a function of the pH value at 25°C

After the sampling of H_2S gas, the sulphide sample solution was preserved with zinc acetate and sodium hydroxide following the standard of ASTM D 4658 (standard test method for sulphide ion in water). The zinc acetate in the solution precipitated and preserved sulphide in the form of zinc sulphide. This was to avoid the loss of sulphide ion which could readily react with oxygen in the solution of high pH value.

In the analysis of sulphide free ion (S^{2-}) by the ISE method based on the ASTM D 4658, the sulphide samples were mixed with sulphide anti-oxidant buffer. The sulphide anti-oxidant contained NaOH to adjust the pH to a highly alkaline level, ascorbic acid to retard air oxidation of sulphide ion, and Ethylenediaminetetraacetic acid disodium salt to redissolve the zinc and free the sulphide. Since the sulphide samples were buffered to a very high pH, all the sulphide existed as S^{2-} ion, thus the sulphide ISE was used to measure S^{2-} because it only detected sulphide in free ion (S^{2-}) form [7]. All the samples were analysed by the

sulphide ISE method based on the ASTM D 4658, given the electrode potential in mV scale by the pH meter or concentration reading directly by the ISE meter.

Similar to the NH_3 measurement, based on the calibration curve, the S^{2-} concentration in the solutions was determined. The actual H_2S concentration in the producer was calculated from the known S^{2-} concentration in the solution, the total volume of absorbing solution after sampling, and the total producer gas volume drawn into the absorbing solution.

4.5 Reliability experiments on the sampling and analysis of NH_3 and H_2S

Reliability experiments performed are presented into two parts in this section: (1) the investigation of the effect of concentration of H_2SO_4 or NaOH solution on the NH_3 or H_2S measurement, respectively; and (2) the verification of the sampling and analysis of NH_3 and H_2S by the wet chemical and ISE methods. The lab-scale reactor developed and presented in Chapter 3 was used in these tests. The NH_3 or H_2S in Ar gas with known concentration was fed into the reactor system and the inlet NH_3 or H_2S gas was drawn into the impinger bottles at the inlet sampling valve (SV3) as shown in Figure 3.4 in Chapter 3. The impinger bottles were assembled as those shown in Figure 4.2. The NH_3 or H_2S in Ar gas was tested at room temperature and atmospheric pressure. The temperature of the water in the bath was set at 4°C. The experimental results of NH_3 or H_2S concentration were then compared with those specified feed gas concentrations.

4.5.1 Investigation of the effect of concentrations of H_2SO_4 and NaOH solutions

Based on the literature [8-11], the concentrations of H_2SO_4 absorption solution used for NH_3 sampling were within 0.05-0.9 M. Thus, two concentrations of H_2SO_4 and NaOH solutions of 0.05 M and 0.5 M were chosen for these experiments. The feed gas tested has concentration of NH_3 in Ar of 2,000±14% ppmv or H_2S in Ar of 230±11% ppmv, respectively. The total gas flow rate was controlled at 3.7 L/min and the sampling time was within 3-5 min.

In the tests of 2,000 ppmv NH_3 in Ar gas sampled in 0.5 M H_2SO_4, a technical problem was found during the analysis. The addition of 10 ml of 10 M NaOH into the sample solution to adjust the pH from less than 2 to be higher than 11, as described earlier in Section 4.3,

generated heat and thus increased the temperature of the solution to over 35°C. Due to the high solution temperature, NH_3 gas could be rapidly lost to the air which resulted in the unsteady mV readings. Furthermore, according to the ASTM D 1426, the temperature of the sample solutions and standard solutions during analysis must be about the same. In fact, the temperature of the standard solutions was measured to be 25±2°C, whereas the temperature of the sample solutions was 35±3°C. The high temperature of the sample solutions reduced the accuracy of the NH_3 measurement. Thus, it can be concluded that H_2SO_4 of 0.5 M was unsuitable for the NH_3 absorption and analysis by the ISE method.

In contrast, satisfactory results were obtained with the use of 0.05 M H_2SO_4 for absorption of 2,000 NH_3 gas and analysis via the ISE method. The results from the experiments are given in Figure 4.6. The x-axis represents the number of samples and the y-axis represents the measured NH_3 concentration in the gas. The two dash lines represent the upper and lower limit values of NH_3 concentration in the gas based on the accuracy of the NH_3 gas (2,000±14% ppmv). As it can be seen in Figure 4.6, the measured values of the NH_3 concentration were within the accuracy of the specified feed gas. Therefore, the H_2SO_4 absorbing solution of 0.05 M H_2SO_4 was considered as suitable for the further experiments conducted in Section 4.5.2 of this chapter as well as in Chapters 5, 6, and 7.

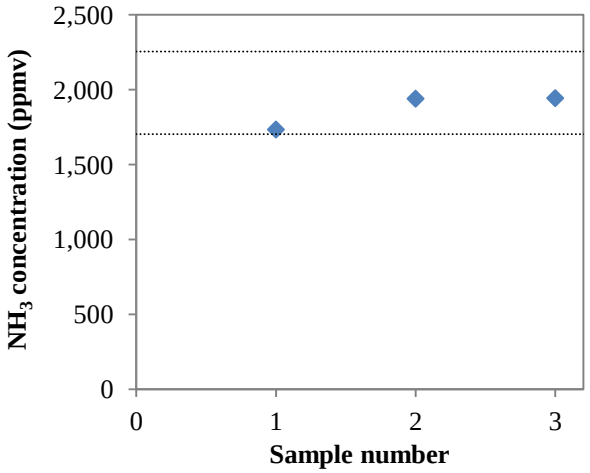

Figure 4.6 Measured NH_3 concentration in the gas by wet chemical and ISE methods

In the tests of 230 ppmv H_2S in Ar gas sampled in 0.05 M and 0.5 M solutions, the measured values of the H_2S concentration in the gas are given in Figure 4.7. The two dash

lines represent the upper and lower limit values of H_2S concentration in the gas based on the accuracy of the H_2S gas (230±11% ppmv). From Figure 4.7, the measured values of H_2S concentration were about the same with the use of both 0.05 M and 0.5 M NaOH absorbing solutions. Furthermore, it is found that the measured H_2S concentration was outside the marginal errors which could be due to the error (20%) from sampling and analysis performed by the operator. It is therefore decided to use the lower concentration of 0.05 M NaOH, which is more practical as it is less hazardous to handle and dispose while wastage of chemical can be reduced. The NaOH absorbing solution of 0.05 M was, again, used in the further experiments performed in Section 4.5.2 for the verification of the sampling and analysis of H_2S.

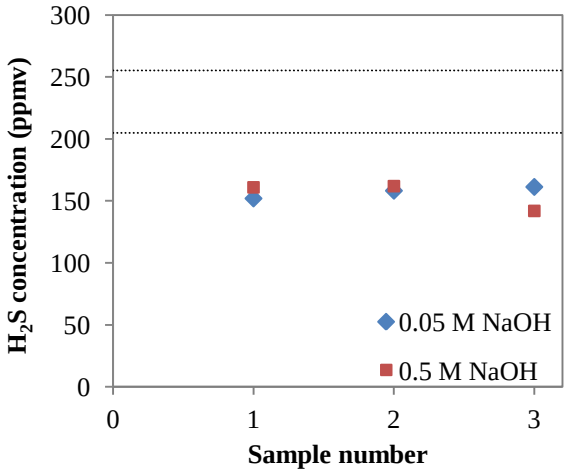

Figure 4.7 Measured H_2S concentration in the gas by wet chemical and ISE methods

4.5.2 Verification of the sampling and analysis of NH_3 and H_2S

Verification tests of the sampling and analysis of NH_3 and H_2S by the wet chemical and ISE methods were conducted. The tests were to find out the accuracy, reliability, and repeatability of the sampling and analysis method for the NH_3 and H_2S measurement. In the tests, it was planned to conduct the measurement of NH_3 in Ar gas with concentrations of 2,000±14% ppmv and 5,550±8% ppmv as well as of H_2S in Ar gas with 230±11% ppmv and 2,680±8% ppmv. The total gas flow rate was set at 3.7 L/min and the sampling time used was 3-5 min for almost all the tests except the tests with H_2S in Ar gas of 2,680±8% ppmv, where the total gas flow rate was 1.2 L/min and the sampling time was 3 min.

The NH_3 and H_2S concentrations of 2,000 ppmv and 230 ppmv, respectively, were tested as they were the inlet concentrations set for the experiments in Chapter 3 and 5. For the NH_3 and H_2S concentrations of 5,550 ppmv and 2,680 ppmv, respectively, they were set based on the maximum NH_3 concentration (5,590 ppmv) and H_2S concentration (2,473 ppmv) produced in the co-gasification of blended lignite and wood pellets in the DFB steam gasifier presented in Chapter 7. Additionally, NH_3 concentration of 1,000-5,000 ppmv was typically found in high temperature coal gasification [12].

The experiments for both NH_3 and H_2S measurement were conducted repeatedly on different days and the results are shown in Figure 4.8 and Fgure 4.9, respectively. Overall, the results of lower concentrations of NH_3 (2,000 ppmv) and H_2S (230 ppmv) are satisfactory as almost all the data points were within the accuracy of the specified feed gas. Besides, more accurate values of H_2S concentration were obtained in Figure 4.9 (a) than those of Figure 4.7. For the higher concentrations of NH_3 and H_2S, half of the data points were located inside the marginal errors, where the other half was outside. The errors of the concentrations of both NH_3 and H_2S gases were found to be 10%, and it could occur from the timing during the gas sampling as well as the analysis performed by the operator.

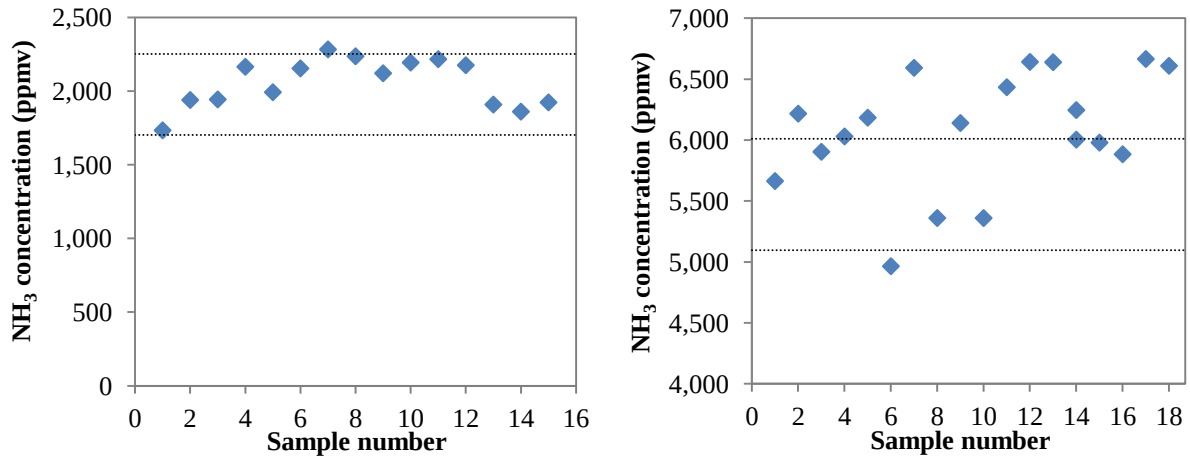

Figure 4.8 Measured NH_3 concentration in the gas when the NH_3 feed gas concentration is (a) 2,000±14% ppmv and (b) 5,550±8% ppmv

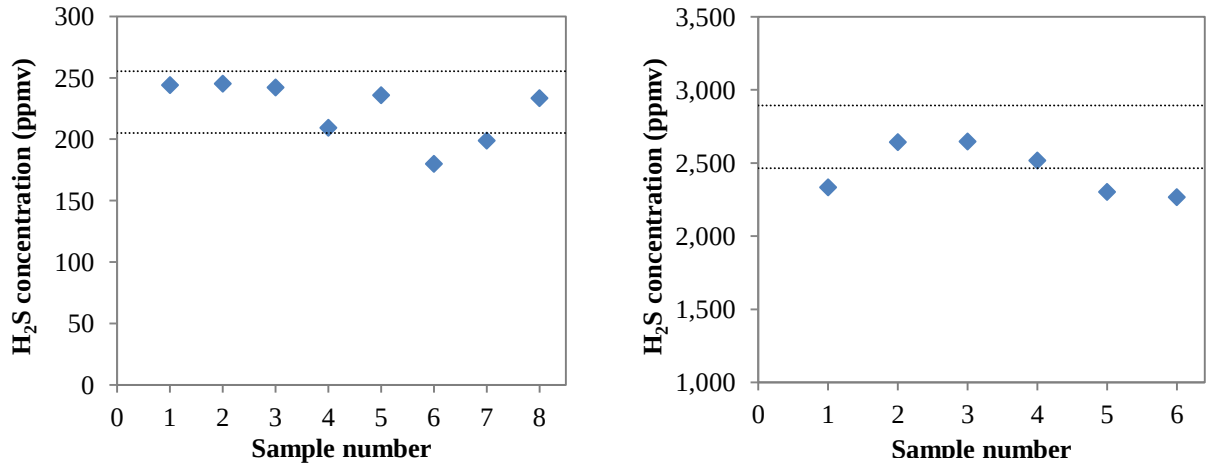

Figure 4.9 Measured H_2S concentration in the gas when the H_2S feed gas concentration is (a) 230±11% ppmv and (b) 2,680±8% ppmv

In summary, the sampling of the NH_3 and H_2S in the producer gas via a wet chemical method by using an impinger system and the analysis of the sample solution by the ISE method has been developed in this research project. The absorbing solutions of 0.05 M H_2SO_4 and 0.05 NaOH were found to be suitable for the studied concentration ranges of the NH_3 and H_2S gases, respectively. The sampling and analysis method are found to be accurate, reliable, and repeatable. Therefore, these methods have been used in the subsequent experiments which will be presented in Chapters 5, 6, and 7.

4.6 References

[1] SilcoTek, Dursan, 2014, from: www.silcotek.com/dursan.

[2] W.L. Saw, S. Pang, Co-gasification of blended lignite and wood pellets in a 100 kW dual fluidised bed steam gasifier: The influence of lignite ratio on producer gas composition and tar content, Fuel, 112 (2013) 117–124.

[3] R.V. Thurston, R.C. Russo, K. Emerson, Aqueous ammonia equilibrium - tabulation of percent un-ionized ammonia, in: U.S. Environmental Protection Agency, Duluth, Minnesota, report no: EPA-600/3-79-091, 1979.

[4] Thermo Fisher Scientific Inc., User guide of high performance ammonia ion selective electrode, in: Thermo Fisher Scientific Inc., 2007.

[5] R.D. Pomeroy, Process design manual for sulfide control in sanitary sewerage systems, in: U.S. Environmental Protection Agency, Cincinnati, Ohio, 1974.

[6] D. Mamrosh, C. Beitler, K. Fisher, S. Stem, Consider improved scrubbing designs for acid gases, Hydrocarbon Processing, (2008) 69-74.

[7] Thermo Fisher Scientific Inc., User guide of silver/sulfide ion selective electrode, in: Thermo Fisher Scientific Inc., 2009.

[8] J. Leppälahti, P. Simell, E. Kurkela, Catalytic conversion of nitrogen compounds in gasification gas, Fuel Processing Technology 29 (1991) 43-56.

[9] G.A. Norton, R.C. Brown, Wet chemical method for determining levels of ammonia in syngas from a biomass gasifier, Energy & Fuels, 19 (2005) 618-624.

[10] H. Cui, S.Q. Turn, V. Keffer, D. Evans, T. Tran, M. Foley, Contaminant estimates and removal in product gas from biomass steam gasification, Energy & Fuels, 24 (2010) 1222-1233.

[11] I. Aigner, C. Pfeifer, H. Hofbauer, Co-gasification of coal and wood in a dual fluidized bed gasifier, Fuel, 90 (2011) 2404-2412.

[12] N. Tsubouchi, H. Hashimoto, Y. Ohtsuka, Catalytic performance of limonite in the decomposition of ammonia in the coexistence of typical fuel gas components produced in an air-blown coal gasification process, Energy & Fuels, 21 (2007) 3063-3069.

5. Experiment on simultaneous removal of ammonia and hydrogen sulphide from producer gas in biomass gasification by titanomagnetite

5.1 Introduction

In FT liquid fuel synthesis, NH_3 and H_2S are poisonous to employed catalysts including cobalt (Co) and iron (Fe)-based catalysts [1], thus, they must be removed from the biomass producer gas to an acceptable level for FT liquid fuel synthesis. In the biomass gasification process, NH_3 and H_2S gases are formed from nitrogen (N) and sulphur (S) in biomass feedstock under reducing gasification conditions at high temperatures [1-3]. In the producer gas from gasification of woody biomass, which commonly has the N content below 0.5 wt%, the NH_3 concentration ranges from 100 to 2,000 ppmv [4], whereas the H_2S concentration in the biomass producer gas varies from 20 to 230 ppmv [5].

The removal of NH_3 and H_2S from the biomass producer gas can be performed by a cold or hot gas cleaning processes. In cold gas cleaning, a wet scrubber with water or acid solutions is used to remove NH_3 [1, 6], whereas a wet scrubber with basic solutions is used to scrub H_2S [7]. In hot gas cleaning, NH_3 is removed by decomposition reaction with catalysts and H_2S is adsorbed into the adsorbents [2, 8]. However, in the experiments on integrated biomass gasification to FT liquid fuel synthesis, cold gas cleaning was used for NH_3 removal, whereas hot gas cleaning was used for H_2S removal [1]. If the simultaneous removal of NH_3 and H_2S in one reactor can be achieved, both the capital and operating costs involved in the cleaning process could be reduced.

For the hot gas cleaning process, many studies have been conducted on the downstream catalytic decomposition of NH_3 and a review on these studies has recently been published [4]. However, a few reported studies focusing on the simultaneous removal of NH_3 and H_2S in the hot gas cleaning process have been found [9, 10]. From the review paper by Hongrapipat et al. [4], the iron (Fe)-based catalysts have shown complete NH_3 decomposition (100%) in inert gas and very high NH_3 decomposition (>80%) in real producer gas from air gasification of peat produced in a pressurised updraft gasifier. Moreover, the use of limonite iron ore (α-FeOOH) following reduction with H_2 achieved

almost complete decomposition of 2,000 ppm NH_3 in He gas at 500, 750, 850, and 950°C [11-13]. Although the reduced limonite (α-Fe) was reported to have a high tolerance to H_2S with respect to NH_3 decomposition in He gas [11], the specific removal of H_2S was not reported. Furthermore, in the presence of simulated producer gas, the activity of the reduced limonite for NH_3 decomposition was drastically reduced to 45% at 750°C [13].

In this study, the simultaneous removal of NH_3 and H_2S in inert gas using a naturally available Fe-based material, namely titanomagnetite, in a hot gas cleaning reactor is investigated. The impact of producer gas species (H_2, CO, CO_2 and CH_4) on this removal is subsequently established. The titanomagnetite was tested for its activity in regard to the NH_3 decomposition reaction and the H_2S adsorption reaction as described in Equations 5.1 and 5.2, respectively [11].

$$2NH_3 \rightarrow N_2 + 3H_2 \qquad \Delta H^{\circ}_{800°C} = 112 \text{ kJ/mol} \qquad (5.1)$$

$$Fe + H_2S \rightarrow FeS + H_2 \qquad \Delta H^{\circ}_{800°C} = -43 \text{ kJ/mol} \qquad (5.2)$$

Based on Equations 5.1 and 5.2, titanomagnetite with a high Fe content was expected to be a promising catalytic and adsorbing precursor for the simultaneous removal of NH_3 and H_2S from the producer gas in the biomass gasification process.

5.2 Materials and methods

5.2.1 Sand materials and preparation

Titanomagnetite ($Fe_{2.9}Ti_{0.1}O_4$) deposits in the western coast of the North Island of New Zealand are some of the largest deposits in the world, containing a total identified reserve of concentrate titanomagnetite of over 850 Mt [14]. There is a limited extent of similar magnetite-bearing sand deposits that have been mined for iron ore in Japan, Philippines, and Indonesia [14]. In this research, this Fe-based material was used as a catalytic and adsorbing precursor for the removal of NH_3 and H_2S. The hot gas reactor was operated in a bubbling fluidised bed (BFB) regime. Titanomagnetite was chosen due to its high Fe content (60.3 wt% Fe) and its abundance locally in New Zealand. In addition, another type of natural iron sand containing ilmenite ($FeTiO_3$) and natural silica sand was tested in the first stage with 2,000 ppmv NH_3 in Ar gas for comparison. Iron sand containing ilmenite is

denoted as ilmenite sand in this study. These three natural sands are readily available in New Zealand. All of the sands were first sieved to specified particle sizes and pre-dried in an oven at 105°C for 2 h before filling into the reactor. The iron sands containing titanomagnetite and ilmenite were reduced in the reactor with 36.5 vol% H_2 in Ar gas at 800°C until the H_2 reduction process was completed, which was identified when no change was observed between the inlet and outlet H_2 concentrations of the reactor by an Agilent 3000 micro-gas chromatography (micro-GC). In the reduction process, a total flow rate of 36.5 vol% H_2 in Ar gas was controlled to be 3.7 L/min. The time required for the complete reduction of the titanomagnetite and ilmenite was approximately 6 h and 3 h, respectively.

5.2.2 Sand material characterisation

An X-ray fluorescence (XRF) analysis of all three sands was conducted using a Phillips PW2400 sequential wavelength dispersive X-ray fluorescence spectrometer to determine their composition. For titanomagnetite, N_2 physisorption isotherms were determined at a liquid nitrogen temperature (-195°C) using a Micromeritics Tristar 3000 instrument. The samples were degassed at 100°C under N_2 for 1 h prior to the N_2 adsorption measurement. The specific surface area was calculated based on the Brunauer-Emmett-Teller (BET) method from the N_2 adsorption data. The cumulative pore volume and average pore diameter were calculated from the adsorption isotherms by the Barrett-Joyner-Halenda (BJH) method. Finally, the X-ray powder diffraction (XRD) analysis of the titanomagnetite samples was conducted with a Philips PW1700 series diffractometer using Co $K\alpha_1$ radiation at an X-ray wavelength of 1.78896 Å.

5.2.3 Equipment setup

The hot gas cleaning reactor was a vertical cylindrical fused quartz reactor with an internal diameter of 40 mm, an outer diameter of 46 mm, and a length of 1,020 mm. The reactor was operated in the BFB regime due to its uniform temperature gradients along the radius and axis of the bed and the uniform mixing of gas and fluidised material, which provided a high contact surface area between the gas and the fluidised material. The BFB reactor was operated isothermally between 500 and 800°C at atmospheric pressure. The sand was supported on a porous fused quartz distributor 380 mm from the bottom of the reactor. The inlet gas was fed from the bottom of the reactor to fluidise the sand. The heat to the reactor

was supplied by a three heating-zone ceramic tube furnace and the operation temperature was controlled by the electric current to the furnace. Two sets of K-type thermocouples were installed at two different radial and height positions of the BFB bed. The gas temperature profiles between the two thermocouples in the fluidised bed at temperatures of 500-800°C were approximately ±2°C, indicating a relatively uniform temperature within the fluidised bed. All parts of the reactor system that were in contact with the NH_3 and H_2S gases were made of inert materials such as fused quartz and perfluoroalkoxy (PFA) to avoid NH_3 decomposition and H_2S adsorption at the inner surface of the equipment and parts.

5.2.4 Experimental operation conditions and procedures

The experiments were conducted in three parts: for part (1), catalyst screening tests were conducted at operation temperatures of 500-800°C for three natural sands, namely titanomagnetite, ilmenite, and silica sand. The gas used in this part of the study was 2,000 ppmv NH_3 in Ar gas. For parts (2) and (3), the titanomagnetite tests were conducted using: 2,000 ppmv NH_3 and 230 ppmv H_2S in Ar gas at operation temperatures of 500-800°C; and 2,000 ppmv NH_3 and 230 ppmv H_2S in simulated biomass producer gas at 500 and 800°C, respectively. The simulated biomass producer gas was obtained in a gas cylinder comprising 45 vol% H_2, 20 vol% CO, 20 vol% CO_2, and 15 vol% CH_4, which has a similar composition to the gas produced from the DFB steam gasifier (100 kW) at the University of Canterbury. Steam was not added to the simulated producer gas because our overall process incorporated a low temperature tar stripping process (similar to [15]), such that steam from the gasification process is condensed and removed prior to entering the hot gas cleaning process investigated in this study. The accuracy of the NH_3 and H_2S concentrations was 2,000±14% ppmv and 230±11% ppmv, respectively.

Before part (1) of the experiment, blank tests were performed at 500-800°C with the empty fused quartz reactor and porous fused quartz distributor using 2,000 ppmv NH_3 in Ar gas to determine if the reactor wall and the thermal decomposition have any effects on the NH_3 decomposition.

In part (1) of the experiment, the screening test was designed to identify the most effective catalyst among the three proposed sands for the NH_3 decomposition reaction in inert Ar

gas. In the screening tests, 125 g of sand was used in each test and the particle sizes were in the range of 180-250 μm. The particle densities of the titanomagnetite, ilmenite, and silica sands are 4,540, 3,040, and 2,560 kg/m^3, respectively. The total flow rate of the gas mixture of NH_3 and Ar was controlled to be 3.7 L/min which corresponded to a mean gas residence time of 0.3-0.4 s through the BFB for all three sands over 500-800°C. The calculation of the mean gas residence time in the BFB was based on the equations reported in Saw and Pang [16] .

Further tests were performed in part (1) of this experiment to examine if the mass transfer resistance plays an important role in the NH_3 decomposition. This was investigated by using titanomagnetite of 125 g at various particle sizes, 106-125 μm, 180-250 μm, and 300-355 μm, with the corresponding average particle sizes being 116, 215, and 328 μm. The operation temperature was 800°C and the concentration of NH_3 in the inert Ar gas was 2,000 ppmv. In these tests, the mean gas residence time in the BFB was 0.2-0.3 s.

In parts (2) and (3) of the experiments, 125 g of titanomagnetite with a particle size range of 106-125 μm was used and the total flow rate of the gas remained the same as in part (1) at 3.7 L/min. The mean gas residence time in the BFB was 0.2 s for part (2) and part (3) of the experiment over temperatures of 500-800°C.

5.2.5 Gas analysis

5.2.5.1 Gas analysis for NH_3 decomposition

The inlet and outlet NH_3 concentrations were sampled by the impinger method, where a 0.05 M sulphuric acid solution (H_2SO_4) of 200 ml was used as an absorbing solution. The NH_3 concentration in the sampled solutions was measured by an ion selective electrode (ISE) according to ASTM D 1426-08 (standard test methods for ammonia nitrogen in water). Moreover, the outlet concentrations of H_2 and N_2, which are the products of the NH_3 decomposition reaction, were measured by an Agilent 3000 micro-GC with a thermal conductivity detector (TCD). In analysing H_2 and N_2, a 10 m × 0.32 mm molecular sieve 5A plot column operated at 110°C was used in the micro-GC. The decomposition of NH_3 (%) was calculated using either of the two methods:

(1) the inlet and outlet concentrations of NH_3 measured by the ISE method; and/or

(2) the inlet concentration of NH_3 measured by the ISE method and the outlet concentration of H_2 or N_2 measured by the micro-GC based on the stoichiometric NH_3 decomposition reaction (Equation 5.1). The micro-GC detection limit for the H_2 concentration is approximately 20 ppmv, which is equivalent to 0.7% NH_3 decomposition.

5.2.5.2 Gas analysis for H_2S adsorption

The inlet and outlet H_2S concentrations were sampled by the impinger method, where a 0.05 M sodium hydroxide solution (NaOH) of 200 ml was used as an absorbing solution. The H_2S concentration in the sampled solutions was measured by the ISE method according to ASTM D 4658-09 (standard test method for sulphide ion in water). The adsorption of H_2S (%) was calculated from the inlet and outlet concentrations of H_2S measured using the ISE method.

5.2.5.3 Gas analysis for producer gas composition

The simulated biomass producer gas comprising 45 vol% H_2, 20 vol% CO, 20 vol% CO_2, and 15 vol% CH_4 was certified and supplied by the BOC Company, Australia. The composition of the inlet and outlet producer gases was measured by the micro-GC in which a 10 m × 0.32 mm molecular sieve 5A plot column operated at 110°C was used to measure H_2, N_2, CH_4 and CO, while an 8 m × 0.32 mm plot Q column operated at 60°C was used to measure the CO_2, C_2H_4, and C_2H_6.

5.3 Results and discussion

5.3.1 Sand material properties

The XRF analysis of the titanomagnetite, ilmenite, and silica sand is presented in Table 5.1. From Table 5.1, it was determined that titanomagnetite contains the highest Fe content (60.3 wt%), followed by ilmenite (8.2 wt%) and silica (0.03 wt%). Based on the NH_3 decomposition reaction presented in Equation 5.1, the NH_3 decomposition rate depends on the content of active catalytic form (Fe). Therefore, it was expected that the % NH_3 decomposition in Ar alone would follow the sequence: titanomagnetite > ilmenite > silica.

The XRD patterns of the as-received titanomagnetite and reduced titanomagnetite are shown in Figure 5.1. It is clear that the as-received titanomagnetite contains mainly

$Fe_{2.9}Ti_{0.1}O_4$ (titanomagnetite). After the titanomagnetite was reduced with H_2 at 800°C, the diffraction peaks of $Fe_{2.9}Ti_{0.1}O_4$ disappeared and α-Fe (ferrite) was the predominant crystalline phase. It indicated that H_2 gas reduced the $Fe_{2.9}Ti_{0.1}O_4$ phase in the titanomagnetite sand to α-Fe.

Table 5.1 XRF analysis of the natural sands used in the present study

Analysis (wt%)	**Titanomagnetite**	**Ilmenite**	**Silica**
SiO_2	1.7	56.6	99.3
Al_2O_3	3.5	9.5	<0.2
Fe_2O_3	86.2	11.8	0.05
CaO	0.5	9.1	0.03
MgO	2.7	6.9	<0.05
Na_2O	0.1	1.9	<0.1
K_2O	0.04	0.9	0.01
TiO_2	7.4	1.8	0.07
MnO	0.5	0.3	<0.1
P_2O_5	0.08	0.1	<0.01

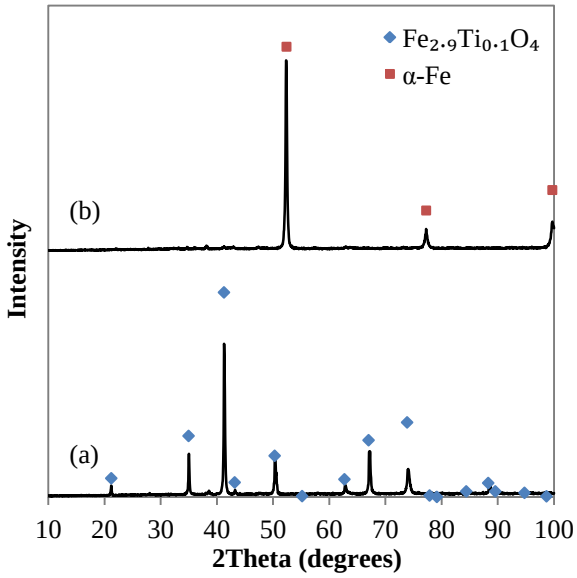

Figure 5.1 XRD patterns of titanomagnetite samples (a) as-received and (b) after H_2 reduction at 800°C

5.3.2 Decomposition of NH_3 in Ar gas in the screening test

From the blank tests, both H_2 and N_2 gases in the outlet gas from the empty reactor were not detected by the micro-GC over a temperature range of 500-800°C. Thus, the NH_3 decomposition was almost zero with the empty reactor, and the thermal decomposition and the reactor wall effect on NH_3 removal was negligible.

Figure 5.2 shows the NH_3 decomposition in inert Ar gas averaged over 1 h for the three natural sands tested: titanomagnetite, ilmenite, and silica. The NH_3 decomposition was calculated from the NH_3 inlet concentration and from the H_2 or N_2 concentration in the outlet gas. As expected, titanomagnetite with the highest Fe content presented the highest NH_3 decomposition of 85-90% over the operated reaction temperatures of 500-800°C. Under the same operation conditions, the NH_3 decomposition decreased for ilmenite and silica showed the lowest decomposition. The low NH_3 decomposition of 7 and 20% at temperatures of 600 and 800°C, respectively, was obtained with the silica sand, which could be attributed to the presence of a very small amount of Fe in the silica sand. From the screening test, it was shown that Fe-based catalysts with high Fe contents have high catalytic activities toward NH_3 decomposition in inert gases over a wide range of reaction temperatures [12, 13, 17, 18].

From the XRD analysis in Figure 5.1, it is suggested that α-Fe is the active phase for high NH_3 decomposition. The results from the present study are consistent with the study of Tsubouchi et al. [12, 13] on the catalytic performance of limonite ore in NH_3 decomposition in inert He gas. At 500, 750, 850, and 950°C, Tsubouchi et al. [12, 13] determined that α-Fe formed by the H_2 reduction of goethite (α-FeOOH) in the limonite achieved almost complete decomposition of 2,000 ppm NH_3 in He gas.

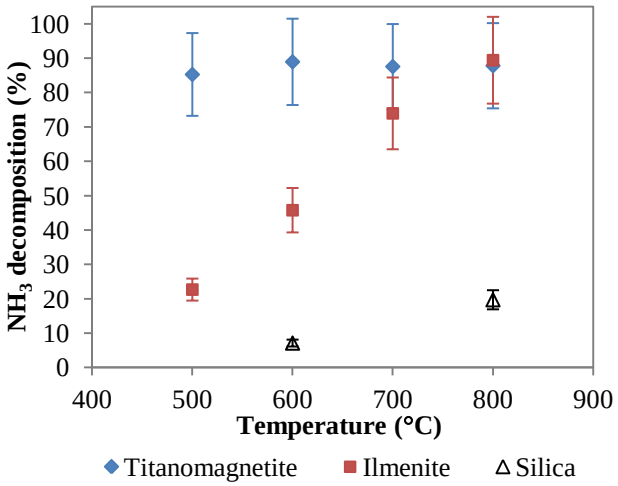

Figure 5.2 Decomposition of NH_3 in Ar gas in the screening test for titanomagnetite, ilmenite, and silica at 500-800°C

Further study of the influence of mass transfer resistance was conducted with only titanomagnetite for the three particle size ranges of 106-125 μm, 180-250 μm, and 300-355 μm, from which the corresponding average particle sizes were calculated to be 116, 215 and 328 μm, respectively. The results from the examination of the mass transfer resistance of the H_2-reduced titanomagnetite on the NH_3 decomposition averaged over 1 h are presented in Figure 5.3. From Figure 5.3, it can be observed that the particle size has no effect on the NH_3 decomposition within the level of uncertainty in the measurements, suggesting that the reaction rate is not limited by mass transfer effects. This is most likely due to the non-porous structure of the titanomagnetite and the BFB fluid dynamics, which minimise the internal and external mass transfer resistance, respectively.

The specific surface area, cumulative pore volume, and average pore diameter of the titanomagnetite are shown in Table 5.2. These results further confirm that titanomagnetite is a non-porous material, such that it can be assumed that the NH_3 decomposition reaction and H_2S adsorption reaction would occur only on the external surface of the titanomagnetite sand.

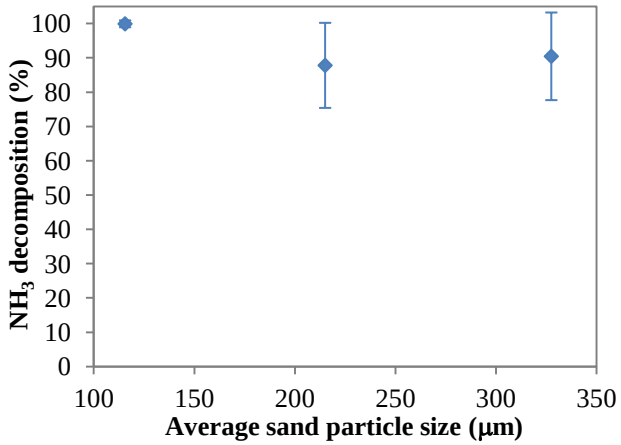

Figure 5.3 Decomposition of NH_3 in Ar gas with titanomagnetite of various particle sizes at 800°C

Table 5.2 BET surface area, BJH adsorption cumulative pore volume and average pore diameter of titanomagnetite

Sample	**BET surface area (m^2/g)**	**BJH adsorption cumulative pore volume (cm^3/g)**	**BJH adsorption average pore diameter (nm)**
Titanomagnetite	1.1	0.002	10.6

5.3.3 Decomposition of NH_3 and adsorption of H_2S in Ar gas

In part (2) and part (3) of the experiments, titanomagnetite with particle sizes of 106-125 μm was used because the mass transfer resistance for all studied particle sizes is negligible; smaller particle sizes have more surface area per unit weight/volume; and its quantity on an as-received basis contributed to 30 wt% compared to less than 5 wt% for the other two particle size ranges. In part (2) of the experiments, the H_2-reduced titanomagnetite was first exposed to 2,000 ppmv NH_3 in Ar gas for 3 h and subsequently 2,000 ppmv NH_3 and 230 ppmv H_2S in Ar gas for 6 h which was followed by exposure to 2,000 ppmv NH_3 in Ar gas for 2 h. This procedure was designed to determine whether the catalytic activity for NH_3 decomposition would be recovered after a period of exposure to the H_2S gas. The experiments were conducted for three temperatures of 500, 700, and 800°C. The NH_3

decomposition and H_2S adsorption were calculated using the methods described in Sections 5.2.5.1 and 5.2.5.2, respectively.

Figure 5.4 shows the removal of NH_3 and H_2S in Ar gas by titanomagnetite at 800°C. In a gas atmosphere containing only 2,000 ppmv NH_3 in Ar, the stable NH_3 outlet concentration below 1 ppmv or approximately the 100% NH_3 decomposition was achieved for the initial 3 h. The results of the NH_3 decomposition calculated from the H_2 outlet concentration measured by the micro-GC are consistent with those calculated from the NH_3 outlet concentration measured using the ISE method.

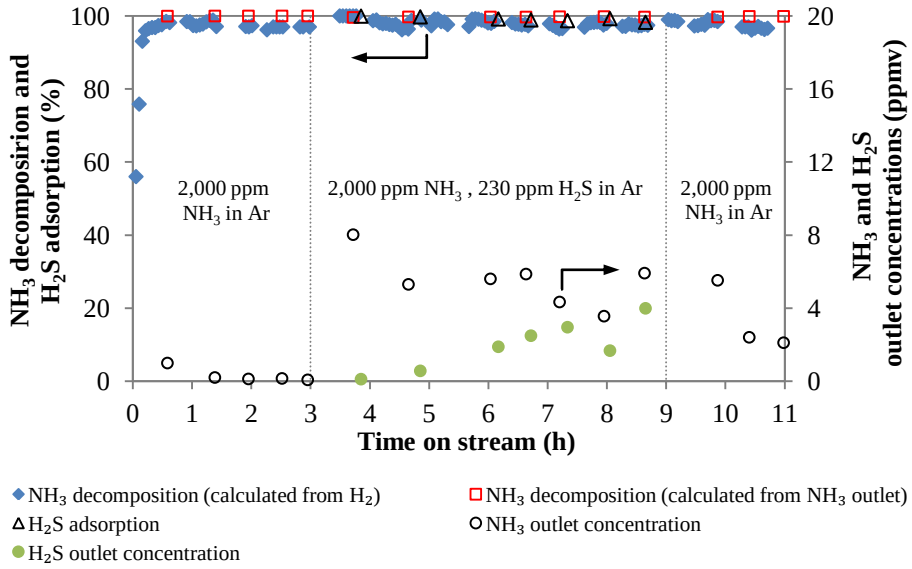

Figure 5.4 Decomposition of NH_3 and adsorption of H_2S in Ar gas using titanomagnetite at 800°C

(The accuracy of NH_3 decomposition calculated from H_2 was ±14%, the accuracy of NH_3 decomposition calculated from NH_3 outlet concentration and of H_2S adsorption was ±1%, and the accuracy of NH_3 and H_2S outlet concentrations was ±5%)

When H_2S was added to the feed gas in the subsequent 6 h test, the catalytic activity of titanomagnetite for NH_3 decomposition was still greater than 99% and the adsorption capacity for H_2S was greater than 98%, with the H_2S outlet concentration below 5 ppmv. Once the H_2S feed was stopped after 9 h, the NH_3 decomposition was maintained at high decomposition of greater than 99% during the next 2 h in which the NH_3 outlet

concentration was less than 10 ppmv. The results of the NH_3 decomposition in the presence of H_2S in the present study are in agreement with those of the study of Tsubouchi et al. [11]. They determined that reduced limonite (α-Fe) showed complete decomposition of 2,000 ppm NH_3 at 750°C in the presence of 100 ppm H_2S in He gas for 50 h and of 50-500 ppm H_2S in He gas for 4 h [11]. However, they did not report the H_2S outlet concentration, and therefore they did not present the removal of H_2S by the reduced limonite.

Following the experiment, the titanomagnetite was analysed by the XRD and α-Fe was determined to be the major Fe phase (Figure 5.5). This suggests that titanomagnetite still maintains the active α-Fe state after it had been exposed to the gas mixture for 11 h. Although an evidence of FeS phase was not found in the titanomagnetite sample, there is a possibility that the FeS is present after exposure to H_2S. Given that the FeS content will be less than 1% from the adsorption of 230 ppmv H_2S over 6 h using 125 g of titanomagnetite, it is highly likely that this level of FeS would not be detected by the XRD, especially if the FeS is a thin layer on the active α-Fe or is poorly crystalline. To verify the adsorption of H_2S, the XRF analysis of the tested titanomagnetite was conducted, and it was determined that sulphur was detected and that its content in the sand was below 1%. Moreover, in a separate study, the formation of FeS was found by the XRD analysis in 0.4 g H_2-reduced limonite (α-Fe) used at 750°C for 50 h for the coexistence of 2,000 ppm NH_3 and 100 ppm H_2S in He gas [11].

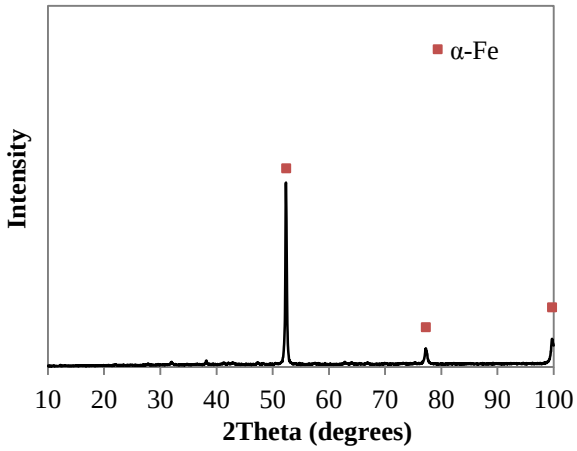

Figure 5.5 XRD pattern of titanomagnetite samples after NH_3 decomposition and H_2S adsorption in Ar at 800°C

To investigate the effect of the operation temperature, further tests were conducted at lower temperatures of 700 and 500°C for the removal of NH_3 and H_2S, and the results are shown in Figure 5.6 and Figure 5.7 for the 700 and 500°C tests, respectively. From Figure 5.6, it is observed that the NH_3 decomposition in the initial 3 h at 700°C was similar to that at 800°C in which almost complete NH_3 decomposition was achieved with the NH_3 outlet concentration being below 1 ppmv. However, with the presence of H_2S gas during the following 6 h, the NH_3 decomposition was slightly reduced to 96-97% and the NH_3 outlet concentration was determined to be from 63 to 76 ppmv. In this period, the H_2S removal by adsorption was 98% and the H_2S outlet concentration was determined to be less than 5 ppmv. After the H_2S gas was removed in the feed gas from 9-11 h, the NH_3 decomposition remained steady at 96-97%.

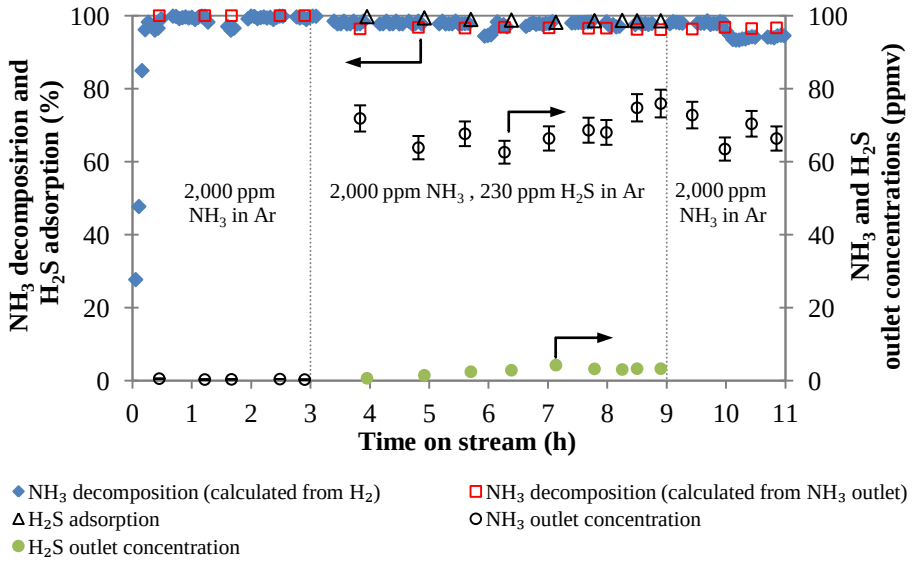

Figure 5.6 Decomposition of NH_3 and adsorption of H_2S in Ar gas using titanomagnetite at 700°C

(The accuracy of NH_3 decomposition calculated from H_2 was ±14%, the accuracy of NH_3 decomposition calculated from NH_3 outlet concentration and of H_2S adsorption was ±1%, and the accuracy of NH_3 and H_2S outlet concentrations was ±5%)

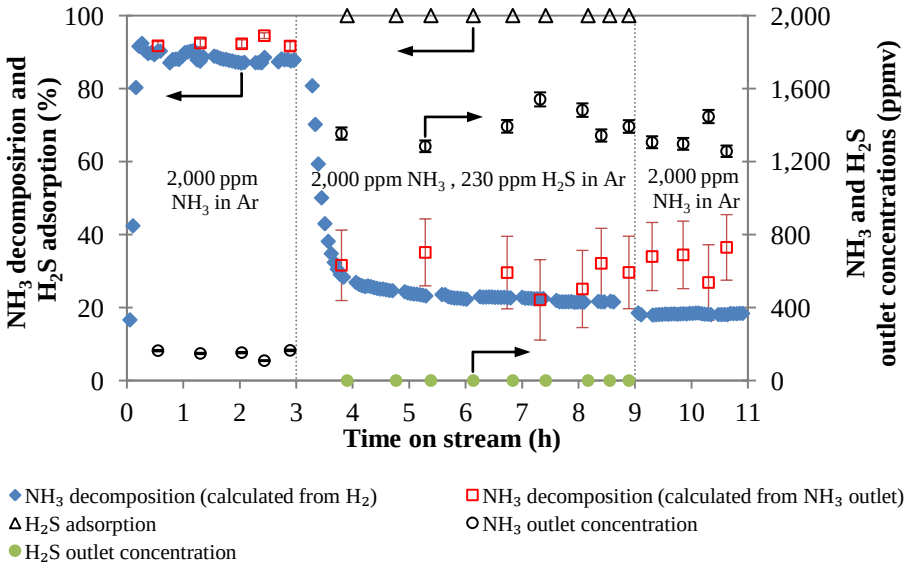

Figure 5.7 Decomposition of NH_3 and adsorption of H_2S in Ar gas using titanomagnetite at 500°C

(The accuracy of NH_3 decomposition calculated from H_2 was ±14%, the accuracy of H_2S adsorption was ±1%, and the accuracy of H_2S outlet concentration was ±5%)

From Figure 5.7, it is clear that the NH_3 decomposition was significantly reduced at an operation temperature of 500°C. The NH_3 decomposition was only 92% in the first 3 h when only NH_3 and Ar gas was fed and this was reduced to 30% once the H_2S gas was added to the feed gas at 3 h from the beginning of the experiment. The NH_3 decomposition remained at a low level of 30%, even when the H_2S gas was stopped in the feed gas at 9 h. However, almost complete H_2S adsorption (100%) was achieved at the low operation temperature (500°C) with the H_2S outlet concentration being below 1 ppmv. The above observation clearly shows that the titanomagnetite was significantly deactivated towards NH_3 decomposition with the addition of H_2S at a low temperature of 500°C. It is likely that the FeS phase formed during H_2S removal is much less active for NH_3 removal at 500°C than the α-Fe phase. At the higher temperatures of 700 and 800°C the kinetics of NH_3 decomposition over this FeS phase would be greatly enhanced enabling almost complete removal.

The increase of the NH_3 decomposition rate with higher temperatures for the coexistence of H_2S in the present study is consistent with that of the study of Tsubouchi et al. [11], but with a different explanation. The complete decomposition of 2,000 ppm NH_3 in the

presence of 100 ppm H_2S in He gas at 650°C can be obtained with reduced limonite (α-Fe) within 10 h, but the NH_3 decomposition gradually decreased from 10-30 h. Comparing the results obtained at 650°C for 30 h with those at 750°C which showed complete NH_3 decomposition for a longer reaction time of 50 h, it was determined that the FeS content in the limonite sample tested at 650°C for 30 h was higher than that in the limonite sample tested at 750°C for 50 h, indicating higher amounts of α-Fe on the limonite surface tested at 750°C [11].

A summary of the decomposition of NH_3 and adsorption of H_2S for temperatures of 500-800°C is shown in Table 5.3. The results clearly demonstrated that very high decomposition of NH_3 of above 99% and adsorption of H_2S of 98% can be obtained with titanomagnetite as a catalytic and adsorbing precursor at 800°C.

Table 5.3 Summary of decomposition of NH_3 and adsorption of H_2S for temperatures of 500-800°C

Exposed gas atmospheres	**Time on stream (h)**	**% NH_3 decomposition**[†]			**% H_2S adsorption**[‡]		
		800°C	**700°C**	**500°C**	**800°C**	**700°C**	**500°C**
NH_3 in Ar	0-3	≈100	≈100	92%			
NH_3 and H_2S in Ar	3-9	>99	96-97	30%	>98	>98	≈100
NH_3 in Ar	9-11	>99	96-97	30%			

[†] The accuracy of the NH_3 decomposition calculated from the NH_3 outlet at 700 and 800°C was ±1%

[‡] The accuracy of the H_2S adsorption was ±1%

5.3.4 Decomposition of NH_3 and adsorption of H_2S in simulated biomass producer gas

In part (3) of the experiments, the titanomagnetite after H_2 reduction was tested with 2,000 ppmv NH_3 and 230 ppmv H_2S in simulated biomass producer gas composed of 45 vol% H_2, 20 vol% CO, 20 vol% CO_2, and 15 vol% CH_4. The experiment was first performed at a reaction temperature of 800°C for 4 h with the goal of removing NH_3 and H_2S based on the findings as discussed in Section 5.3.3. The results of the NH_3 decomposition and H_2S

adsorption were calculated from the inlet and outlet concentrations of NH_3 and H_2S, respectively, as measured by the ISE method and their averaged values over 4 h are presented in Table 5.4. It is clear that the presence of a mixture of gas species had an adverse effect on the NH_3 decomposition and H_2S adsorption at 800°C. The NH_3 decomposition was approximately 60%, whereas the H_2S adsorption was only 9%. The corresponding NH_3 and H_2S outlet concentrations were determined to be 800 and 210 ppmv, respectively. The reduction of the NH_3 decomposition and H_2S adsorption can be due to the addition of H_2 at high concentration of 45 vol%, which increases the driving force behind the reverse reactions of both Equation 5.1 and Equation 5.2, the increased surface coverage of the active α-Fe phase by adsorbed hydrogen, and the competition of α-Fe for the reverse water-gas shift reaction, which is presented in the latter part. Moreover, from thermodynamic calculations, NH_3 decomposition at equilibrium is reduced with increasing H_2 concentration or N_2 concentration or the concentration of the mixture of H_2 and N_2 in the feed gas [4].

Table 5.4 Decomposition of NH_3 and adsorption of H_2S in simulated biomass producer gas with titanomagnetite at 500 and 800°C

Temperature (°C)	**% NH_3 decomposition**[†]	**% H_2S adsorption**[‡]
500	40	80
800	60	9

[†]Accuracy of NH_3 decomposition was ±5%. [‡]Accuracy of H_2S adsorption was ±5%

From the XRD analysis of the titanomagnetite samples after being tested at 800° (Figure 5.8), two major Fe phases were found: α-Fe and titanomagnetite ($Fe_{2.9}Ti_{0.1}O_4$), where the α-Fe content was much higher than the titanomagnetite. The titanomagnetite is likely to be residual traces from the as-received sand that were not completely reduced during the pre-treatment and gas cleaning experiments. The deactivation of titanomagnetite for NH_3 and H_2S removal could also be due to the loss of α-Fe in the sand. In the study of Tsubouchi et al. [13], the activity of reduced limonite (α-Fe) for NH_3 decomposition at 750°C was drastically reduced in the coexistence of 10% H_2 and 20% CO in the feed gas, which was due to the deactivation by Fe_3C formed in the sand. Moreover, they also found carbon

deposited on the limonite surface and reactor wall from the disproportionation of CO to C and CO_2 or from the Boudouard reaction (Equation 5.3).

$$2CO \rightarrow C + CO_2 \qquad \Delta H^{\circ}_{800°C} = -170 \text{ kJ/mol} \qquad (5.3)$$

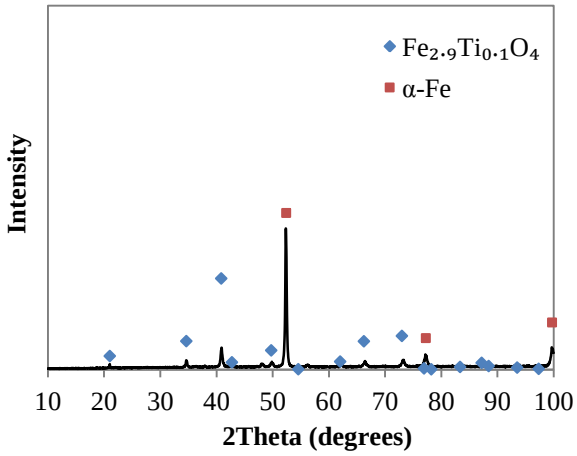

Figure 5.8 XRD pattern of the titanomagnetite sample after NH_3 decomposition and H_2S adsorption in the simulated biomass producer gas at 800°C

To clarify the effect of producer gas on the titanomagnetite for NH_3 and H_2S removal, additional studies should be conducted as future work by testing the titanomagnetite with individual gases, and binary or ternary mixtures of gas components in the producer gas.

Due to a very low H_2S adsorption rate at 800°C, an additional experiment was conducted at an operation temperature of 500°C in which it was expected to improve the H_2S adsorption because the adsorption process is favourable at lower temperatures. The results for this test are shown in Table 5.4. As expected, the H_2S adsorption was significantly increased to approximately 80%, with the corresponding H_2S outlet concentration being approximately 40 ppmv. The NH_3 decomposition of approximately 40% was also achieved at 500°C, which was lower than that operated at 800°C due to endothermic NH_3 decomposition reaction.

For the inlet and outlet producer gas, its dry basis composition was measured by the micro-GC in the experiments at 500 and 800°C. By using a mole balance and a reverse water-gas

shift reaction stoichiometry (Equation 5.4) for the experiment at 800°C, the measured outlet producer gas composition in a dry basis can be converted to a wet basis as shown in Table 5.5. It should be noted that the reverse water-gas shift reaction may occur at 800°C, which is favoured at high temperatures and enhanced by the α-Fe catalysts (see Table 5.5). Consequently, the CO concentration was increased and H_2O was formed at the expense of the H_2 and CO_2 concentrations in the gas. However, the reverse water-gas shift reaction (Equation 5.4) was insignificant at a low operation temperature of 500°C because the measured inlet and outlet dry producer gas composition was the same. Moreover, C_2H_4, and C_2H_6 were not found in the outlet gas from the reactor operated at 500 and 800°C.

$$H_2 + CO_2 \rightarrow CO + H_2O \qquad \Delta H^{\circ}_{800°C} = 34 \text{ kJ/mol} \tag{5.4}$$

Table 5.5 Summary of inlet and outlet producer gas composition for the experiment at 800°C

Producer gas component	**Measured inlet producer gas composition (mol%)**	**Inlet molar flow rate (mol/s)**	**Measured outlet dry producer gas composition (mol%)**	**Calculated outlet molar flow rate (mol/s)**	**Calculated outlet wet producer gas composition (mol%)**	**Calculated outlet dry producer gas composition (mol%)**
H_2	45	0.0011	39	0.0009	35.5	39.2
CO	20	0.0005	33	0.0007	29.5	32.6
CO_2	20	0.0005	12	0.0003	10.5	11.6
CH_4	15	0.0004	16	0.0004	15.0	16.6
H_2O	0	0.0000	0	0.0002	9.5	0.0

Figure 5.9 shows the gas composition at equilibrium as a function of temperature at 1 bar when the simulated biomass producer gas is used as a feed gas. Based on the results in Table 5.5 and Figure 5.9, it was determined that the reverse water-gas shift reaction almost reached equilibrium at 800°C due to the larger thermodynamic driving force and the faster kinetics expected at 800°C compared to 500°C. No carbon was found by the XRF analysis

in the titanomagnetite following the test at 800°C, indicating that the Boudouard reaction (Equation 5.3) did not occur.

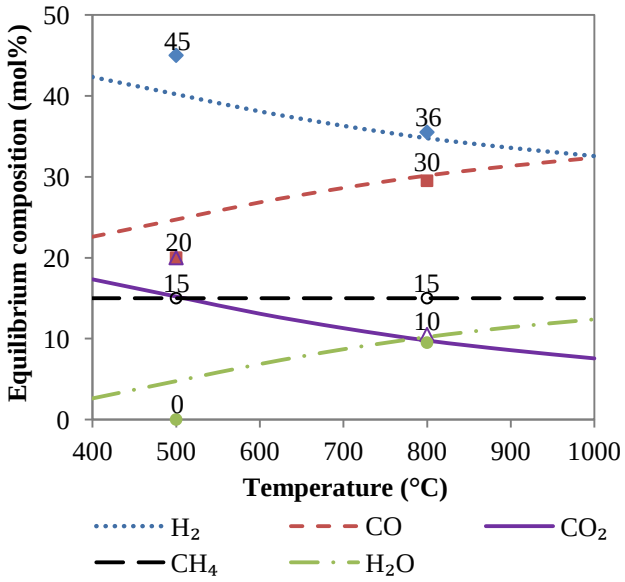

Figure 5.9 Gas composition at equilibrium as a function of temperature at 1 bar when simulated biomass producer gas is used as a feed gas
(the data points at 500°C represent the measured outlet composition, whereas the data points at 800°C represent the outlet composition from the hot gas cleaning reactor as calculated from the measured outlet composition (on a dry basis) and a mole balance to account for the reverse water-gas shift reaction)

5.4 Conclusions

The simultaneous removal of NH_3 and H_2S from producer gas in biomass gasification by the hot gas cleaning process was performed in the present study. The experiments with titanomagnetite were conducted in three parts based on the feed gas composition. A pre-treatment of titanomagnetite by a H_2 reduction process generates α-Fe, which is an active phase for catalytic NH_3 decomposition and H_2S adsorption. The H_2-reduced titanomagnetite achieves 100% NH_3 decomposition of 2,000 ppmv NH_3 in Ar gas at 700 and 800°C. Moreover, for the coexistence of 230 ppmv H_2S in 2,000 ppmv NH_3 in Ar gas, the H_2-reduced titanomagnetite has shown greater than 96% NH_3 decomposition and greater than 98% H_2S adsorption at 700 and 800°C. However, it is determined that the presence of the simulated biomass adversely affected the NH_3 decomposition and H_2S

adsorption rates. At 800°C, 60% NH_3 decomposition and 9% H_2S adsorption were obtained, whereas at 500°C, 40% NH_3 decomposition and 80% H_2S adsorption were obtained. The H_2-reduced titanomagnetite also catalysed the reverse water-gas shift reaction at 800°C, where H_2 and CO_2 are reacted to produce CO and H_2O.

5.5 References

[1] H. Boerrigter, H.P. Calis, D.J. Slort, H. Bodenstaff, A.J. Kaandorp, H. den Uil, L.P.L.M. Rabou, Gas cleaning for integrated biomass gasification (BG) and Fischer-Tropsch (FT) systems: Experimental demonstration of two BG-FT systems ("Proof-of-Principle"), in: the Energy research Centre of the Netherlands (ECN), the Netherlands, report no: ECN-C--04-056, 2004.

[2] D.J. Stevens, Hot gas conditioning: Recent progress with larger-scale biomass gasification systems, in: National Renewable Energy Laboratory, the U.S. Department of Energy Laboratory, report no: NREL/SR-510-29952, 2001.

[3] F. Pinto, R.N. André, C. Franco, H. Lopes, C. Carolino, R. Costa, I. Gulyurtlu, Co-gasification of coal and wastes in a pilot-scale installation. 2: Effect of catalysts in syngas treatment to achieve sulphur and nitrogen compounds abatement, Fuel, 89 (2010) 3340-3351.

[4] J. Hongrapipat, W.-L. Saw, S. Pang, Removal of ammonia from producer gas in biomass gasification: integration of gasification optimisation and hot catalytic gas cleaning, Biomass Conversion and Biorefinery, 2 (2012) 327-348.

[5] S. Cheah, D.L. Carpenter, K.A. Magrini-Bair, Review of mid-to high-temperature sulfur sorbents for desulfurization of biomass- and coal-derived syngas, Energy & Fuels, 23 (2009) 5291-5307.

[6] P. McKendry, Energy production from biomass (part 3): gasification technologies, Bioresource Technology, 83 (2002) 55-63.

[7] D. Mamrosh, C. Beitler, K. Fisher, S. Stem, Consider improved scrubbing designs for acid gases, Hydrocarbon Processing, (2008) 69-74.
[8] W. Torres, S.S. Pansare, J.G. Goodwin Jr., Hot gas removal of tars, ammonia, and hydrogen sulfide from biomass gasification gas, Catalysis Reviews, 49 (2007) 407-456.

[9] H.K. Jun, S.Y. Jung, T.J. Lee, C.K. Ryu, J.C. Kim, Decomposition of NH_3 over Zn–Ti-based desulfurization sorbent promoted with cobalt and nickel, Catalysis Today, 87 (2003) 3-10.

[10] S.Y. Jung, S.J. Lee, J.J. Park, S.C. Lee, H.K. Jun, T.J. Lee, C.K. Ryu, J.C. Kim, The simultaneous removal of hydrogen sulfide and ammonia over zinc-based dry sorbent supported on alumina, Separation and Purification Technology, 63 (2008) 297-302.

[11] N. Tsubouchi, H. Hashimoto, Y. Ohtsuka, Sulfur tolerance of an inexpensive limonite catalyst for high temperature decomposition of ammonia, Powder Technology, 180 (2008) 184-189.

[12] N. Tsubouchi, H. Hashimoto, Y. Ohtsuka, High catalytic performance of fine particles of metallic iron formed from limonite in the decomposition of a low concentration of ammonia, Catalysis Letters, 105 (2005) 203-208.

[13] N. Tsubouchi, H. Hashimoto, Y. Ohtsuka, Catalytic performance of limonite in the decomposition of ammonia in the coexistence of typical fuel gas components produced in an air-blown coal gasification process, Energy & Fuels, 21 (2007) 3063-3069.

[14] T. Christie, B. Brathwaite, Mineral commodity report 15 - iron, in: New Zealand Ministry of Business, Innovation & Employment, 1997.

[15] H. Hofbauer, Fischer-Tropsch-Fuels and Bio-SNG, in: Central European Biomass Conference, Graz, Austria, 2008.

[16] W.L. Saw, S.S. Pang, Influence of mean gas residence time in the bubbling fluidised bed on the performance of a 100-kW dual fluidised bed steam gasifier, Biomass Conversion and Biorefinery, 2 (2012) 197-205.

[17] C. Xu, J. Donald, H. Hashimoto, E. Byambajav, Y. Ohtsuka, Ammonia decomposition with metal catalysts supported on Canadian peat-derived carbons, in: 8th World Congress on Chemical Engineering, Montreal, Canada, 2009.

[18] J. Donald, C.C. Xu, H. Hashimoto, E. Byambajav, Y. Ohtsuka, Novel carbon-based Ni/Fe catalysts derived from peat for hot gas ammonia decomposition in an inert helium atmosphere, Applied Catalysis A: General, 375 (2010) 124-133.

6. Experiment on NH_3 and H_2S removal in the DFB steam gasifier by optimisation of operation conditions and application of catalytic bed material

6.1 Introduction

Biomass gasification has been worldwide accepted as a promising technology for conversion of various biomass feedstocks to fuels and chemicals. Gasification is a thermo-chemical conversion process of biomass to producer gas primarily contains H_2, CO, CO_2, and CH_4. The producer gas can then be used in various applications such as electricity generation, Fischer-Tropsch (FT) liquid fuel synthesis, synthetic natural gas production, methanol, mixed alcohols, and pure hydrogen [1-4]. The trace contaminants, however, are also produced in the producer gas including mainly tars, and nitrogen (N) and sulphur (S) gas compounds. The research on tar removal has been intensively conducted in an in situ gasifier [5] and in a conventional downstream process after the gasifier using a wet scrubber [3, 4, 6, 7]. However, the study on the removal of N- and S-gas compounds from the biomass gasification process is inadequate.

Ammonia (NH_3) and hydrogen sulphide (H_2S) gases are the dominant species of the N- and S-gas compounds, respectively, found in the producer gas [8-10]. Formation of NH_3 and H_2S is inevitable as they are mainly generated from N and S in the biomass feedstock [11, 12]. The N- and S-binding structures of the woody biomass are mainly in proteins [13] and in organic-S forms [14], respectively. NH_3 can be formed via three major routes [15, 16]: (1) reactions of N-containing structure in the solid phase during initial pyrolysis; (2) thermal cracking and steam reforming of volatile-N; and (3) thermal cracking and hydrogenation/steam reactions of N in the char. It might be possible to identify the main routes of H_2S formation as above-mentioned for NH_3. Attar [14] suggested that H_2S was produced from organic-S via: (1) thermal cracking; (2) hydrogenation of organic-S; and (3) reactions of organic molecules with S. The concentrations of NH_3 and H_2S produced from the gasification process depend on several factors, including N and S contents in the fuel feedstock, gasifier operation conditions, gasifier types, types of gasifying agent, N- and S-binding structures of the fuel feedstock, and mineral matter present in the fuel feedstock [13, 14, 17-19]. NH_3 and H_2S gases are undesirable in the downstream applications of the

producer gas. NH_3 and H_2S are the main precursors of NO_x and SO_x when combusted in a gas turbine in the integrated gasification combined cycle (IGCC) system [9, 10, 20], as well as they are poisonous to the catalysts used in the FT liquid fuel synthesis [3] and methanol synthesis [21]. Therefore, NH_3 and H_2S must be removed to meet the requirements for end-user applications.

Similar to the tar removal, NH_3 and H_2S can be eliminated both in the in situ gasifier and in the downstream gas cleaning system [10, 15]. The removal of NH_3 and H_2S inside the gasifier can be applied through optimisation of the gasification operation conditions and an application of catalytic or desulphurisation bed materials in the fluidised bed gasifiers [10, 15]. This measure is advantageous as it may eliminate any downstream gas cleaning systems used for the removal of NH_3 and H_2S. In recent reviews [10, 15], the experimental results are summarised for the effect of gasification operation parameters and application of catalytic bed materials on the NH_3 concentration [15] and application of in-bed desulphurisation of H_2S [10]. Majority of the published studies have reported the in situ removal of NH_3 and H_2S in the bubbling fluidised bed (BFB) gasifiers and in the fixed-bed gasifiers with various gasifying agents (steam, O_2, air, or a combination of them). However, information on the removal of NH_3 and H_2S inside a dual fluidised bed (DFB) steam gasifier is scarce. Due to the inconsistency of the effect of gasification conditions and bed materials on the NH_3 and H_2S concentrations in different gasifiers, the results obtained in the other gasifier types may not be applicable to the DFB steam gasifier used in the present study.

Therefore, this study investigated the effect of main operation conditions and various bed materials used in the DFB steam biomass gasifier on the NH_3 and H_2S concentrations and the conversions of fuel-N and fuel-S in the feed to NH_3 and H_2S (also called NH_3 and H_2S conversions). The main operation conditions studied include temperature of the BFB reactor, steam to fuel (S/F) ratio, and mean gas residence time (τ_f), whereas the bed materials include silica, iron-based or ilmenite, and calcined olivine sands. Silica sand, which was typically considered as inert material, was found to have a low catalytic activity for NH_3 decomposition as shown in Figure 5.2 of Chapter 5. The iron-based sands and calcined olivine were found to have high catalytic activity for NH_3 decomposition reaction and high adsorption capacity for H_2S desulphurisation in either the in situ gasifier and/or

the downstream reactor [10, 15, 22]. Based on the experimental results obtained in this study, it was expected that NH_3 and H_2S can be reduced to a minimal level by the optimisation of temperature, S/F ratio, and τ_f, as well as by the use of appropriate bed materials.

6.2 Experiments and materials

6.2.1 Equipment setup

Figure 6.1 shows a schematic diagram of the DFB steam gasifier that was used in this study. The DFB steam gasifier's main components are a bubbling fluidised bed (BFB) reactor for gasification of biomass and a fast fluidised bed (FFB) reactor for combustion of derived char transported from the BFB reactor. With the internal circulation of bed materials between the two reactors, the exothermic combustion reactions of solid char as well as supplementary liquefied petroleum gas (LPG) in the FFB reactor provides heat for the endothermic gasification reactions in the BFB reactor.

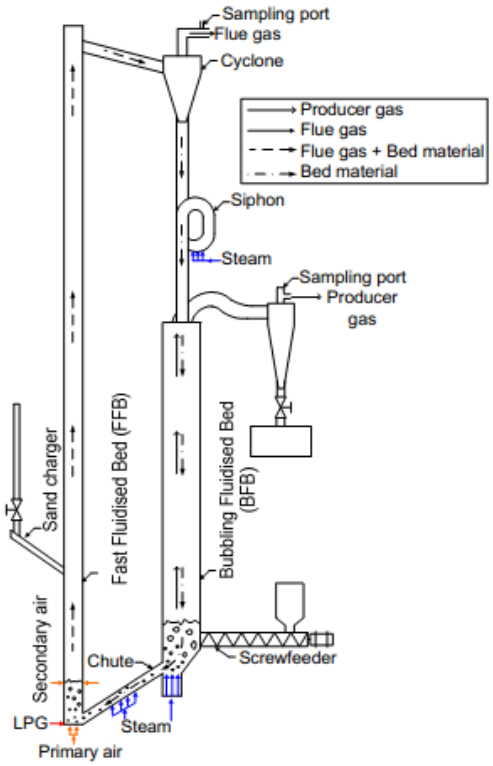

Figure 6.1 Schematic diagram of the DFB steam gasifier used in this study [23]

In the experiment, the fuel feedstock was fed into the BFB bed via a screw auger connected to the hopper. N_2 gas of 5 L/min was also fed with the fuel to prevent the back flow of the producer gas to the hopper. Steam at 200°C and 6 bar (gauge) was supplied by an in house boiler and used as the gasifying agent. The steam was supplied at the BFB base, chute, and siphon for fluidisation of the bed material. The steam flow rate at each location can be adjusted using the flow meters. The temperature of the BFB reactor was controlled by the circulation of hot bed material from the FFB reactor. In addition, LPG can be added at the FFB reactor base, if required, to increase the BFB temperature. More information on the configurations and operations of the DFB steam gasifier can be found in Saw and Pang [23, 24].

6.2.2 Materials and operation conditions

Considering that Pinus radiata (radiata pine) is a major renewable biomass resource harvested from New Zealand's plantation forests, its processed residues from wood industry in the form of wood pellets were chosen as a raw material to be tested in the DFB steam gasifier. The wood pellets have dimensions of 6 mm (diameter) by 15 mm (length) and were supplied by a wood pellet plant near Christchurch, New Zealand. The proximate and ultimate analysis of the wood pellets was conducted and the results are given in Table 6.1. The XRF analysis results of major elements present in the ash of the wood pellets are also provided in Table 6.2.

Table 6.1 Proximate and ultimate analysis results of radiata pine wood pellets

	Analysis (wt%)	**Method**	**Wood pellets**
Proximate analysis (as-received basis)	Moisture	ASTM E871	7.0
	Ash	ASTM D1102	0.6
	Volatile matter	ISO 562	78.4
	Fixed carbon	By difference	14.0
Ultimate analysis (dry and ash free, daf)	C	ISO 12902	51.2
	H	ISO 12902	6.1
	N	ISO 12902	0.05
	S	ASTM D4239	0.01
	O	By difference	42.6

Table 6.2 XRF analysis based on ASTM D4326 method of major elements presented in the ash of radiata pine wood pellets

Analysis (wt%)	**Wood pellet**
SiO_2	40.7
Al_2O_3	9.1
Fe_2O_3	3.1
CaO	14.4
MgO	5.6
Na_2O	3.7
K_2O	14.0
TiO_2	0.4
Mn_3O_4	0.8
SO_3	1.6
P_2O_5	2.1

The three natural sands that were used as bed materials are silica (SiO_2), ilmenite ($FeTiO_3$), and calcined olivine ($(Mg, Fe)_2SiO_4$). The silica and ilmenite sands were supplied by Industrial Sand Company in New Zealand, whereas the calcined olivine sand was sourced from Vienna University of Technology, Austria. The XRF analysis results of the three sands are shown in Table 6.3.

The gasifier operation conditions used in this study are summarized in Table 6.4. For all the experiments, temperature in the BFB reactor was maintained at the set point, and the temperatures at four different height locations of both the BFB reactor and in the FFB reactor were recorded. The average value of the four temperature measurements in the BFB and FFB reactors is shown in Table 6.4. The S/F ratio (kg/kg_{dry}) is defined as the mass flow rate of feeding steam and the mass flow rate of moisture in the wood pellets to the mass flow rate of dry wood pellets. As shown in Table 6.4, steam feed rate (kg/h) includes the steam used for fluidisation of the bed material at the BFB base, chute (1 kg/h), and siphon (1 kg/h). In order to adjust the S/F ratio, either the fuel feed rate (kg_{dry}/h) or the steam feed rate fed at the BFB bed was varied. The τ_f in the BFB reactor was calculated based on the

equations reported in Saw and Pang [24]. The τ_f was altered from 0.19 to 0.25 s by increasing total bed material inventory in the DFB steam gasifier from 20 to 30 kg.

In the experiments using silica sand, the levels of the three operation conditions studied were in the range of 750-850°C, 0.6-1.4 kg/kg_{dry}, and 0.19-0.25 s for temperature, S/F ratio, and τ_f, respectively. In the study of the effect of temperature, which was varied within 750-850°C, S/F ratio was fixed at 0.6. When the S/F ratio was studied in a range of 0.6-1.4, temperature was set at 800°C. Finally, temperature was set at 800°C and S/F was 0.6 for the study of the effect of τ_f (0.19-0.25 s). Furthermore, in the experiments with ilmenite and calcined olivine, temperature was fixed at 800°C while the S/F ratio was varied within 0.6-1.2.

Table 6.3 XRF analysis of the natural sands used in the present study

Analysis (wt%)	**Silica**	**Ilmenite**	**Calcined olivine**
SiO_2	99.3	56.6	39.2
Al_2O_3	<0.2	9.5	0.3
Fe_2O_3	0.05	11.8	9.2
CaO	0.03	9.1	0.7
MgO	<0.05	6.9	50.4
Na_2O	<0.1	1.9	0.1
K_2O	0.01	0.9	<0.01
TiO_2	0.07	1.8	0.01
MnO	<0.1	0.3	0.2
P_2O_5	<0.01	0.1	0.01

Table 6.4 Gasifier operation conditions

Bed material type	Silica	Ilmenite	Calcined Olivine
Bed material particle size (μm)	180-300	180-300	180-300
Bed material particle density (kg/m^3)	2,600	3,000	2,900
Total amount of bed material in the DFB steam gasifier (kg)	20-30	30	30
Fuel feed rate (kg_{dry}/h)	7.4-14.9	7.4-11.2	7.4-14.9
Average FFB temperature (°C)	770-900	850	860
Average BFB temperature (°C)	750-850	800	800
Steam feed rate (kg/h)	6-10	6-7	8
Steam to fuel (S/F) ratio (kg/kg_{dry})	0.6-1.4	0.6-1.0	0.6-1.2

6.2.3 Sampling and analysis of NH_3 and H_2S in the producer gas

Details of the sampling and analysis method of NH_3 and H_2S in the producer gas can be found in Chapter 4 (Sections 4.2-4.4).

6.3 Results and discussion

The present study investigated the influence of main operation conditions in the DFB steam gasifier on the concentrations and conversions of NH_3 and H_2S in the biomass producer gas. The operation conditions studied included temperature, S/F ratio, and τ_f with the use of silica sand as a bed material. The other bed materials including ilmenite and calcined olivine sands were also investigated on the removal of NH_3 and H_2S. NH_3 and H_2S concentrations in the producer gas were measured two or three times during the steady state of the gasification process. NH_3 or H_2S conversion (wt%) was calculated from N or S content in the feed wood pellets and N or S content as NH_3 and H_2S in the producer gas as presented in Equations 6.1 and 6.2. Therefore, the results of NH_3 and H_2S concentrations and conversions were averaged from two or three repeated measurements, and the error bars represent the standard deviations.

NH_3 conversion (wt%) = [N in NH_3 (g/h) × 100] / N in fuel (g/h) (6.1)

H_2S conversion (wt%) = [S in H_2S (g/h) × 100] / S in fuel (g/h) (6.2)

6.3.1 Influence of temperature on the NH_3 and H_2S concentrations and conversions

Figure 6.2 shows the influence of temperature on the NH_3 and H_2S concentrations and conversions when silica sand was used and the S/F ratio was set at 0.6. It can be seen from Figure 6.2 that the NH_3 and H_2S concentrations and conversions increased with an increase of temperature. With temperature increased from 750 to 850°C, the NH_3 concentration increased sharply from 130 to 330 ppmv and the NH_3 conversion increased from 9 to 37 wt%. Similarly, H_2S concentration increased gradually, whereas H_2S conversion increased significantly with the temperature.

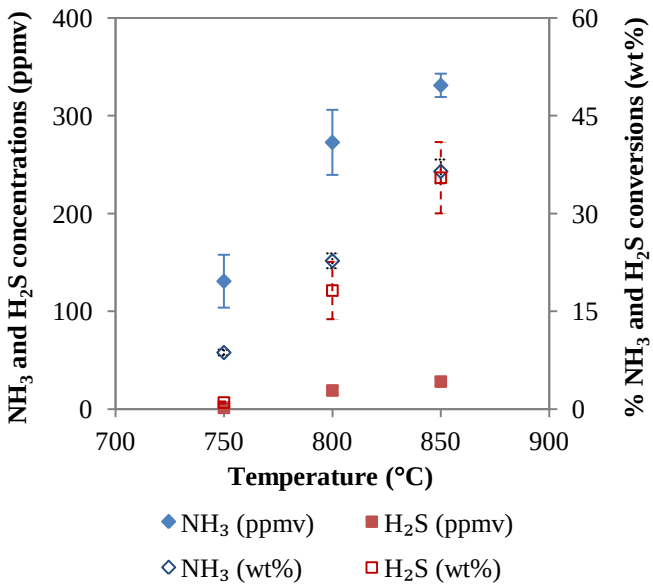

Figure 6.2 Influence of temperature on the NH_3 and H_2S concentrations and conversions using silica sand (S/F = 0.6)

The higher NH_3 and H_2S concentrations and conversions with increasing temperature are believed to be due to the enhancement of kinetic and equilibrium of steam gasification reactions, favouring the production of volatile gases [25, 26]. The experimental results from the present study showed the producer gas yield ($Nm^3_{dry,\ nitrogen\ free\ gas}/kg_{fuel,\ daf}$) increased from 0.57 to 0.94 with temperature (Figure 6.3). Thus, more volatile-N and -S compounds are released from the solid fuel and react with accessible H radicals from H_2O present in the system to form more NH_3 and H_2S in the producer gas [11, 26, 27]. Another factor influencing the NH_3 formation could be an increase of the heating rate with higher

temperature, which led to the more rapid generation of the H radicals, produced originally from H in solid fuel and in steam, for the hydrogenation and steam reactions of N in the char to form NH_3 [16, 27, 28]. In addition, increasing themperature possibly led to the enhancement of thermal cracking of volatile-N and -S compounds. Finally, higher H_2S concentration and conversion with temperature could be due to the reduction of metal sulphides formed in the solid phase, mainly FeS [26]. The formation of metal sulphides from the reactions of H_2S and metallic compounds in the fuel ash are favoured at low temperatures [26].

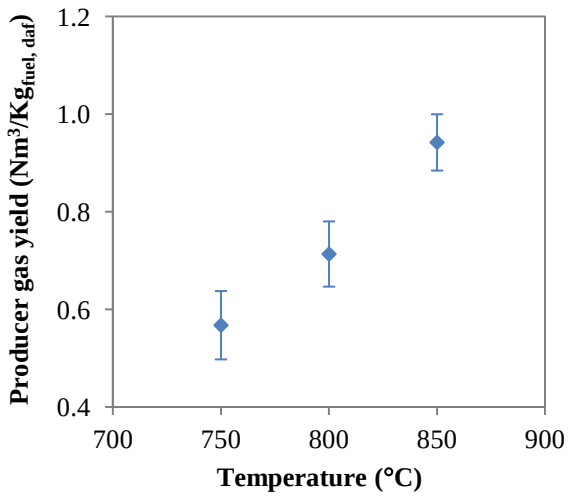

Figure 6.3 Influence of temperature on the producer gas yield (S/F = 0.6)

The results of NH_3 conversion in the present study are in the agreement with those obtained in the study of Tian et al. [27]. Higher NH_3 conversion with steam gasification of cane trash was observed when the temperature was raised from 600 to 800°C [27]. It was believed that the higher NH_3 conversion with the increase of temperature was mainly from the higher volatile yield that participated in thermal cracking and/or steam reforming to produce more NH_3 [27].

The effect of temperature on the H_2S concentration and conversion in the present study is consistent with that was found in co-gasification of 30% coal and 70% refuse derived fuel (RDF) [11] and of 75% coal, 10% pine, 10% polyethylene, and 5% petcoke [29] in a BFB gasifier with steam and oxygen as the gasifying agent. Increasing the temperature from 720

to 850°C in co-gasification of coal and RDF resulted in an increase of H_2S concentration from 808 to 1,081 ppmv [11]. The experimental results from Dias and Gulyurtlu [11] also showed that higher S content in the solid char was obtained at lower temperatures. Therefore, it was believed that the increased release of volatile gases with the rise in temperature led to more S leaving the solid matrix to form more H_2S [11].

Furthermore, the results of concentration in the present study are in agreement with thermodynamic equilibrium calculation performed by Kuramochi et al. [26]. From the calculation, H_2S concentration at equilibrium was found to increase with temperature from 400 to 850°C. In addition, they also reported that metal sulphides such as FeS, ZnS, MnS, PbS, Ni_3S_2, and Cu_2S were significantly formed at low temperatures, and thus it led to higher H_2S concentration with increasing temperature from 400 to 850°C [26].

6.3.2 Influence of S/F ratio on the NH_3 and H_2S concentrations and conversions

Figure 6.4 presents the influence of S/F ratio on the NH_3 and H_2S concentrations and conversions when temperature was controlled at 800°C. It is clear from Figure 6.4 that the NH_3 and H_2S concentrations and conversions increased with the S/F ratio. When the S/F ratio was increased from 0.6 to 1.4, NH_3 and H_2S concentrations increased from 273 to 582 ppmv and from 19 to 122 ppmv, respectively.

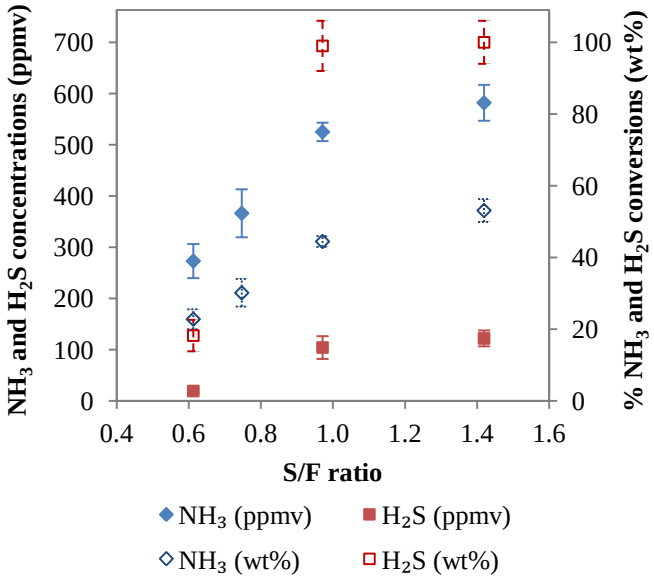

Figure 6.4 Influence of S/F ratio on the NH_3 and H_2S concentrations and conversions

An explanation for the increase of the NH_3 and H_2S concentrations and conversions with higher S/F ratio could be due to the increased availability of H radicals for both steam reforming of volatile-N- and -S compounds and hydrogenation/steam reactions of N and S in the char [11, 18, 19, 27]. Generally, increasing the S/F ratio resulted in an increase of gas yield and H_2 concentration [30-34], and this is consistent with the results in the present study as shown in Figure 6.5. Therefore, it could be expected that more volatile-N and -S compounds released from the solid fuel and reacted with a larger amount of H radicals, from increasing steam content or the S/F ratio in the system, to form more NH_3 and H_2S.

In the studies of steam gasification, a large amount of H radicals generated from feeding steam acted as an intermediate between the reactions of steam and char, resulting to the significant enhancement of NH_3 formation [18, 19]. It is also believed that the higher H radicals generated from the higher steam feed rate could also enhance the formation of H_2S from reactions of steam and S in the char. In addition, due to higher H_2 concentration was produced with an increase in the S/F ratio (Figure 6.5), it is believed that more H_2 would enhance the hydrogenation of organic-S, such as thiophenes, to produce more H_2S in the producer gas [14]. Overall, the H radicals generated from steam present in the system play an important role in the formation of NH_3 and H_2S, and thus the operation conditions that affect the availability of H radicals will influence the NH_3 and H_2S conversions [19].

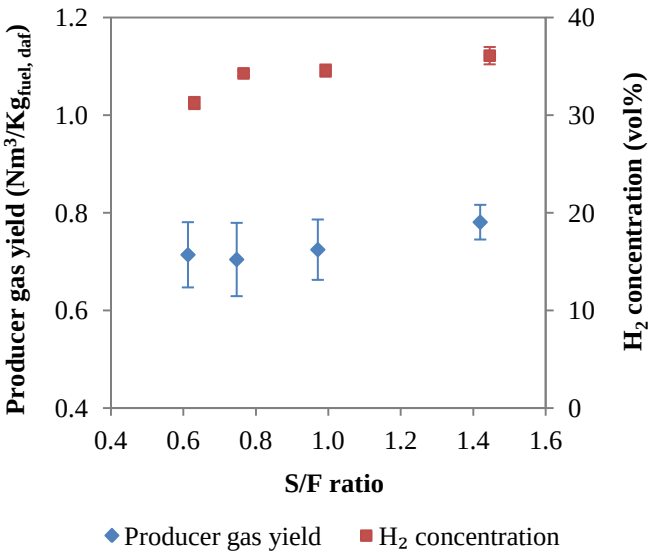

Figure 6.5 Influence of S/F ratio on the producer gas yield and H_2 concentration at 800°C

6.3.3 Influence of mean gas residence time (τ_f) on the NH_3 and H_2S concentrations and conversions

Figure 6.6 presents the influence of mean gas residence time (τ_f) on the NH_3 and H_2S concentrations and conversions when temperature was controlled at 800°C and S/F ratio was fixed at 0.6. From Figure 6.6, the NH_3 concentration and conversion increased with the τ_f, whereas the H_2S concentration and conversion slightly decreased with the τ_f. The NH_3 concentration and conversion increased from 195 to 277 ppmv and from 16 to 24%, respectively, when the τ_f was raised from 0.19 to 0.25 s. The effect of τ_f on the NH_3 concentration and conversion could be due to the longer gas-char contact time which enhanced the reactions between N in char and H radicals, leading to higher NH_3 formation and lower N in the char [13]. It was found that the N content retained in char decreased as the residence time was increased [13]. Available gasifier data supported that the longer gas residence time or gas-char contact time in fixed-bed and fluidised bed reactors than in entrained-bed reactor led to higher NH_3 formation [13]. All of this information support the observation found in the present study.

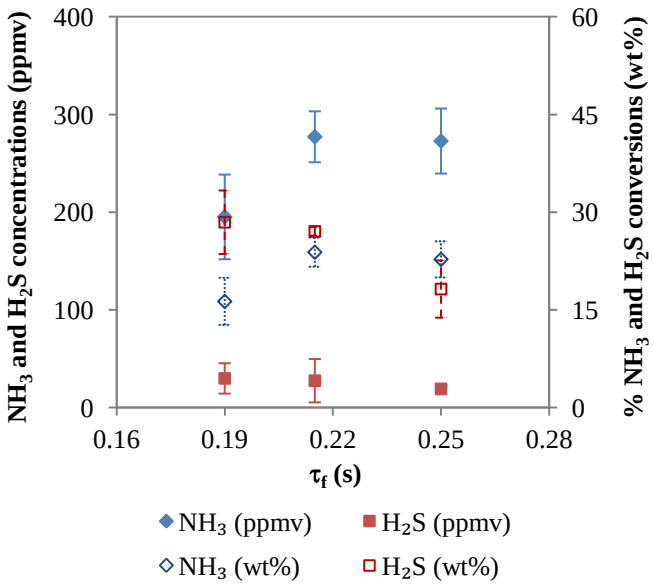

Figure 6.6 Influence of mean gas residence time (τ_f) on the NH_3 and H_2S concentrations and conversions (temperature = 800°C and S/F ratio = 0.6)

In contrast, the H_2S concentration and conversion slightly decreased with the τ_f from 30 to 19 ppmv and from 28 to 18%, respectively. Although longer gas-char contact time would

enhance the reactions between S in char and H radicals, the extent to which it effected might be lower than the effect of longer contact time between metal in ash and H_2S to form metal sulphides. It is well known that metal compounds in the ash such as Fe, Ca, Mn (see Table 6.2) can adsorb and react with sulphide in the producer gas to form metal sulphides [8, 10, 26, 35, 36].

6.3.4 Influence of various bed materials on the NH_3 and H_2S concentrations and conversions

Figure 6.7 shows the influence of different types of bed materials on the NH_3 and H_2S concentrations and conversions when temperature was controlled at 800°C, S/F ratio was varied within 0.6-1.4. It is clearly observed that the use of ilmenite and calcined olivine sands in the DFB steam gasifier led to lower NH_3 and H_2S concentrations and conversions compared with those obtained with silica sand. The effect of ilmenite and calcined olivine on the reduction of the NH_3 and H_2S concentrations and conversions is very competitive. In addition, the NH_3 and H_2S concentrations and conversions increased with the S/F ratio irrespective of the bed material types and they were discussed previously in Section 6.3.2.

The lower NH_3 and H_2S concentrations and conversions obtained with calcined olivine than that of silica sand in the present study is consistent to the studied of Pinto et al. [29, 37] in co-gasification of coal and wastes in a BFB gasifier using steam and oxygen as a gasifying agent at 850°C. The high activity of ilmenite and calcined olivine for NH_3 reduction is believed to be due to their much higher Fe, Ca, and Mg contents than that of silica sand (see Table 6.3). These metals have shown high catalytic activity for NH_3 decomposition reaction at high temperature to produce N_2 and H_2 [15, 38]. Similarly, the ilmenite and calcined olivine can remove H_2S in the gasifier due to the high Fe, Ca, and Mn contents which react with H_2S to form corresponding metal sulphides [8, 10, 26, 35, 36].

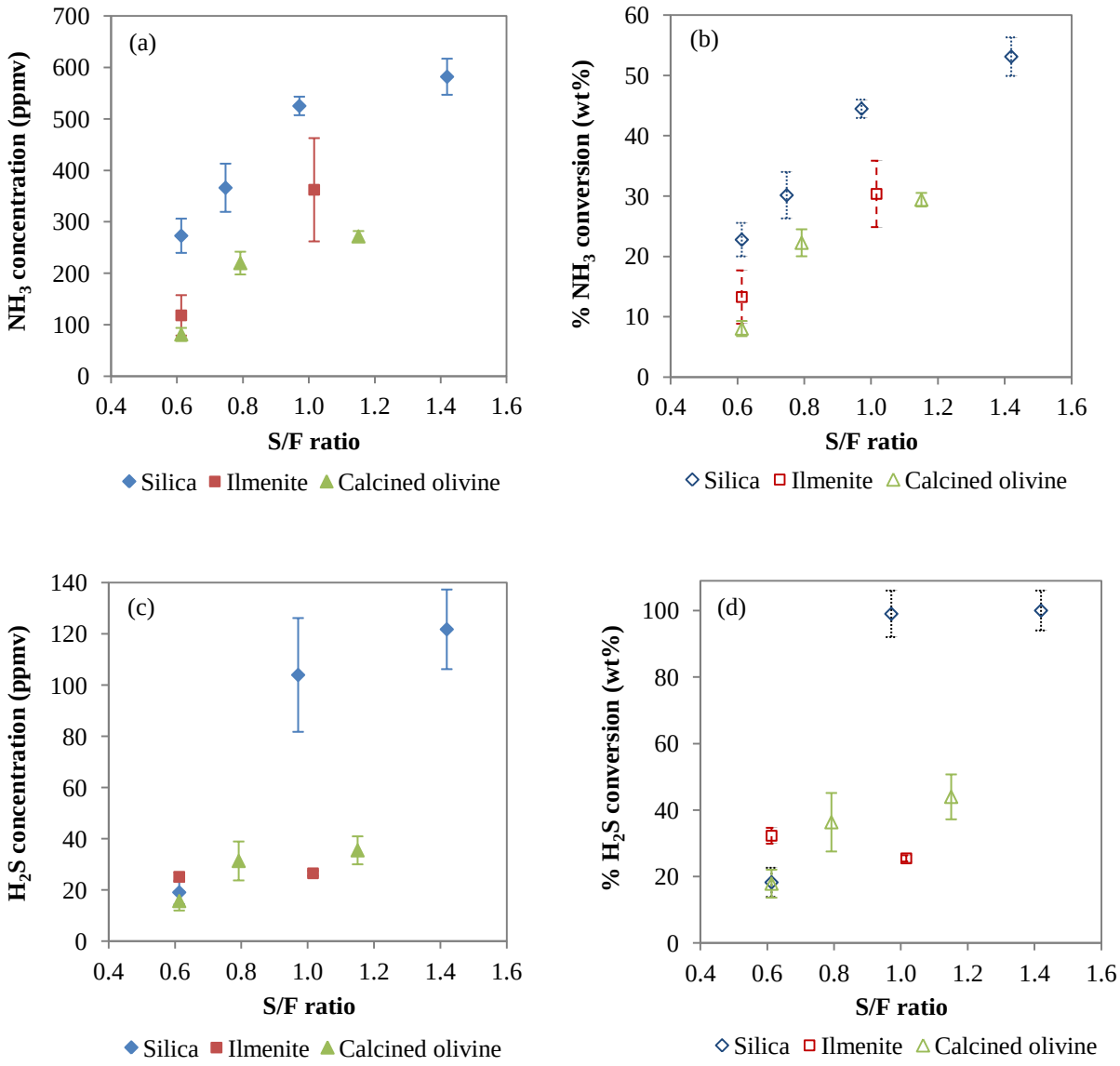

Figure 6.7 Influence of various bed materials on the NH_3 and H_2S concentrations and conversions at 800°C (a) NH_3 concentration, (b) NH_3 conversion, (c) H_2S concentration, and (d) H_2S conversion

6.4 Conclusions

The measures for NH_3 and H_2S removal/reduction in the in situ DFB steam gasifier were studied in the present work. It was found that the temperature of the BFB reactor, S/F ratio, and τ_f, as well as the use of various bed materials, influenced the NH_3 and H_2S concentrations and conversions. By increasing the temperature from 750 to 850°C and S/F ratio from 0.6-1.4, the NH_3 and H_2S concentrations and conversions were increased. However, the increase of τ_f from 0.19 to 0.25 s led to the increase in NH_3 concentration and

conversion, whereas the H_2S concentration and conversion slightly decreased. Ilmenite and calcined olivine were found to reduce the NH_3 and H_2S concentrations and conversions when compared with silica sand which could be due to their much higher Fe, Ca, Mg, and Mn contents than that of silica sand. Overall, minimisation of NH_3 and H_2S formation in the producer gas can be performed by operating the DFB steam gasifier at low temperature and low S/F ratio when silica sand is used an as bed material or at low S/F ratio and 800°C with the use of ilmenite and calcined olivine sands.

6.5 References

[1] A. Van der Drift, H. Boerrigter, Synthesis gas from biomass for fuels and chemicals, in: the Energy research Centre of the Netherlands (ECN), the Netherlands, report no: ECN-C--06-001, 2006.

[2] H. Boerrigter, Economy of Biomass-to-Liquids (BTL) plants, in: the Energy research Centre of the Netherlands (ECN), the Netherlands, report no: ECN-C--06-019, 2006.

[3] H. Boerrigter, H.P. Calis, D.J. Slort, H. Bodenstaff, A.J. Kaandorp, H. den Uil, L.P.L.M. Rabou, Gas cleaning for integrated biomass gasification (BG) and Fischer-Tropsch (FT) systems: Experimental demonstration of two BG-FT systems ("Proof-of-Principle"), in: the Energy research Centre of the Netherlands (ECN), the Netherlands, report no: ECN-C--04-056, 2004.

[4] H. Hofbauer, Fischer-Tropsch-Fuels and Bio-SNG, in: Central European Biomass Conference, Graz, Austria, 2008.

[5] L. Devi, K.J. Ptasinski, F.J.J.G. Janssen, A review of the primary measures for tar elimination in biomass gasification processes, Biomass and Bioenergy, 24 (2003) 125-140.

[6] R. Rauch, H. Hofbauer, K. Bosch, I. Siefert, C. Aichernig, H. Tremmel, K. Voigtlaender, R. Koch, R. Lehner, Steam gasification of biomass at CHP plant Guessing–status of the demonstration plant, in: 2nd World Conference and Technology Exhibition on Biomass for Energy, Industry and Climate Protection, Rome, Italy, 2004.

[7] H. Boerrigter, S.V.B. van Paasen, P.C.A. Bergman, J.W. Könemann, R. Emmen, A. Wijnands, "OLGA" tar removal technology: Proof-of-Concept (PoC) for application in integrated biomass gasificaion combined heat and power (CHP) systems, in: the Energy research Centre of the Netherlands (ECN), report no: ECN-C--05-009, 2005.

[8] W. Torres, S.S. Pansare, J.G. Goodwin Jr., Hot gas removal of tars, ammonia, and hydrogen sulfide from biomass gasification gas, Catalysis Reviews, 49 (2007) 407-456.

[9] J. Leppälahti, Formation and behaviour of nitrogen compounds in an IGCC process, Bioresource Technology, 46 (1993) 65-70.

[10] X. Meng, W. De Jong, R. Pal, A.H.M. Verkooijen, In bed and downstream hot gas desulphurization during solid fuel gasification: A review, Fuel Processing Technology, 91 (2010) 964-981.

[11] M. Dias, I. Gulyurtlu, H_2S and HCl formation during RDF and coal co-gasification: a comparison between the predictions and experimental results, in: Proceedings of the biomass gasification technologies workshop MRC Gebze Campus-Türkiye, 2008.

[12] S.H. Aljbour, K. Kawamoto, Bench-scale gasification of cedar wood – Part II: Effect of operational conditions on contaminant release, Chemosphere, 90 (2013) 1501-1507.

[13] J. Leppälahti, T. Koljonen, Nitrogen evolution from coal, peat and wood during gasification: literature review, Fuel Processing Technology, 43 (1995) 1-45.

[14] A. Attar, Chemistry, thermodynamics and kinetics of reactions of sulphur in coal-gas reactions: A review, Fuel, 57 (1978) 201-212.

[15] J. Hongrapipat, W.-L. Saw, S. Pang, Removal of ammonia from producer gas in biomass gasification: integration of gasification optimisation and hot catalytic gas cleaning, Biomass Conversion and Biorefinery, 2 (2012) 327-348.

[16] F.-J. Tian, J.-l. Yu, L.J. McKenzie, J.-i. Hayashi, T. Chiba, C.-Z. Li, Formation of NOx precursors during the pyrolysis of coal and biomass. Part VII. Pyrolysis and gasification of cane trash with steam, Fuel, 84 (2005) 371-376.

[17] F. Pinto, R.N. André, C. Franco, H. Lopes, C. Carolino, R. Costa, I. Gulyurtlu, Co-gasification of coal and wastes in a pilot-scale installation. 2: Effect of catalysts in syngas treatment to achieve sulphur and nitrogen compounds abatement, Fuel, 89 (2010) 3340-3351.

[18] M. Jeremiáš, M. Pohořelý, P. Bode, S. Skoblia, Z. Beňo, K. Svoboda, Ammonia yield from gasification of biomass and coal in fluidized bed reactor, Fuel, 117 (2014) 917-925.

[19] L. Chang, Z. Xie, K.-C. Xie, K.C. Pratt, J.-i. Hayashi, T. Chiba, C.-Z. Li, Formation of NO_x precursors during the pyrolysis of coal and biomass. Part VI. Effects of gas atmosphere on the formation of NH_3 and HCN, Fuel, 82 (2003) 1159-1166.

[20] W. Mojtahedi, M. Ylitalo, T. Maunula, J. Abbasian, Catalytic decomposition of ammonia in fuel gas produced in pilot-scale pressurized fluidized-bed gasifier, Fuel Processing Technol, 45 (1995) 221-236.

[21] G.W. Roberts, D.M. Brown, T.H. Hsiung, J.J. Lewnard, Deactivation of methanol synthesis catalysts, Industrial & Engineering Chemistry Research, 32 (1993) 1610-1621.

[22] J. Corella, J.M. Toledo, R. Padilla, Olivine or dolomite as in-bed additive in biomass gasification with air in a fluidized bed: which is better?, Energy & Fuels, 18 (2004) 713-720.

[23] W.L. Saw, S. Pang, Co-gasification of blended lignite and wood pellets in a 100 kW dual fluidised bed steam gasifier: The influence of lignite ratio on producer gas composition and tar content, Fuel, 112 (2013) 117–124.

[24] W.L. Saw, S.S. Pang, Influence of mean gas residence time in the bubbling fluidised bed on the performance of a 100-kW dual fluidised bed steam gasifier, Biomass Conversion and Biorefinery, 2 (2012) 197-205.

[25] C. Franco, F. Pinto, I. Gulyurtlu, I. Cabrita, The study of reactions influencing the biomass steam gasification process, Fuel, 82 (2003) 835-842.

[26] H. Kuramochi, W. Wu, K. Kawamoto, Prediction of the behaviors of H_2S and HCl during gasification of selected residual biomass fuels by equilibrium calculation, Fuel, 84 (2005) 377-387.

[27] F.-J. Tian, J. Yu, L.J. McKenzie, J.-i. Hayashi, C.-Z. Li, Conversion of fuel-N into HCN and NH_3 during the pyrolysis and gasification in steam: A comparative study of coal and biomass, Energy & Fuels, 21 (2007) 517-521.

[28] C.-Z. Li, L.L. Tan, Formation of NO_x and SO_x precursors during the pyrolysis of coal and biomass. Part III. Further discussion on the formation of HCN and NH_3 during pyrolysis, Fuel, 79 (2000) 1899-1906.

[29] F. Pinto, H. Lopes, R.N. André, I. Gulyurtlu, I. Cabrita, Effect of catalysts in the quality of syngas and by-products obtained by co-gasification of coal and wastes. 2: Heavy metals, sulphur and halogen compounds abatement, Fuel, 87 (2008) 1050-1062.

[30] J. Herguido, J. Corella, J. Gonzalez-Sáiz, Steam gasification of lignocellulosic residues in a fluidized bed at a small pilot scale. Effect of the type of feedstock, Industrial & Engineering Chemistry Research, 31 (1992) 1274-1282.

[31] C. Pfeifer, R. Rauch, H. Hofbauer, In-bed catalytic tar reduction in a dual fluidized bed biomass steam gasifier, Industrial & Engineering Chemistry Research, 43 (2004) 1634-1640.

[32] C. Pfeifer, R. Rauch, H. Hofbauer, Hydrogen-rich gas production with a catalytic dual fluidized bed biomass gasifier, in: 2nd World Conference on Biomass for Energy, Industry and Climate Protection, Florence, Italy, 2004.

[33] L. Wei, S. Xu, J. Liu, C. Lu, S. Liu, C. Liu, A novel process of biomass gasification for hydrogen-rich gas with solid heat carrier: Preliminary experimental results, Energy & Fuels, 20 (2006) 2266-2273.

[34] L. Wei, S. Xu, L. Zhang, C. Liu, H. Zhu, S. Liu, Steam gasification of biomass for hydrogen-rich gas in a free-fall reactor, International Journal of Hydrogen Energy, 32 (2007) 24-31.

[35] S.C. Mitchell, Hot gas cleanup of sulphur, nitrogen, minor and trace elements, in: IEA Coal Research, 1998.

[36] S. Cheah, D.L. Carpenter, K.A. Magrini-Bair, Review of mid-to high-temperature sulfur sorbents for desulfurization of biomass- and coal-derived syngas, Energy & Fuels, 23 (2009) 5291-5307.

[37] F. Pinto, H. Lopes, R.N. André, I. Gulyurtlu, I. Cabrita, Effect of catalysts in the quality of syngas and by-products obtained by co-gasification of coal and wastes. 1. Tars and nitrogen compounds abatement, Fuel, 86 (2007) 2052-2063.

[38] J. Hongrapipat, A.C.K. Yip, A.T. Marshall, W.L. Saw, S. Pang, Investigation of simultaneous removal of ammonia and hydrogen sulphide from producer gas in biomass gasification by titanomagnetite, Fuel, 135 (2014) 235-242.

7. Experiment on co-gasification of blended lignite and wood pellets in a DFB steam gasifier: the influence of lignite to fuel ratio on NH_3 and H_2S concentrations and conversions

7.1 Introduction

Coal gasification technology has been well established globally and a number of commercial coal gasification plants have been in operation for heat and power generation [1]. However, the adverse impact of using coal as a feedstock has caused environmental concerns such as the emission of greenhouse gas (GHG), mainly carbon dioxide (CO_2), and nitrogen (N) and sulphur (S)-based gases.

As an alternative energy resource to substitute fossil fuels, biomass has attracted increasing interest and biomass gasification has been recognized as one of the most promising technologies for biomass processing. In biomass gasification, the emission of N- and S-based compounds and the ash particulates is lower than from coal gasification. Furthermore, the reactivity of biomass is higher than coal in a gasification environment. However, due to its nature of low energy density, heterogeneous properties, scattered distribution, and seasonal harvesting, costs for biomass collection, transportation, and storage are high which result in unfavourable economic returns for commercial production of biomass energy [2]. Therefore, commercialisation of the biomass gasification is still in the early stage compared with coal gasification [1], and the biomass gasification plants are mainly at pilot and demonstration scale.

Co-gasification of coal and biomass has the potential to offer combined benefits of coal and biomass for gasification. The addition of biomass to coal reduces the GHG emissions compared to coal gasification. On the other hand, adding coal to biomass ensures reliable supply of feedstocks and reduces operation costs for a commercial operation. In addition, co-gasification provides the adjustment of H_2/CO ratio in the producer gas to meet the requirement of downstream applications [2-5]. In practical operations, the biomass can be employed in the existing coal operated gasifiers [2, 6], and thus only feeding systems need to be modified.

However, the coal, in general, contains higher contents of N and S than the biomass. Therefore, the producer gas from co-gasification of coal and biomass contains varying concentrations of N- and S-based gases, mainly NH_3 and H_2S. The formation of NH_3 and H_2S in the producer gas depends on several factors including N and S contents in the fuel feedstock, gasifier operation conditions, N- and S-binding structures of the fuel, and mineral matter present in the fuel [7, 8]. The presence of N- and S-based gases in the producer gas is one of the main technical challenges in downstream applications of the producer gas. Therefore, it is important to understand the formation of NH_3 and H_2S during the co-gasification and to develop technologies to remove these gas contaminants.

During the gasification process, fuel-bound N and S in coal and biomass are released as: (1) N- and S-based gases; (2) N- and S-containing aromatic hydrocarbons (N-tar and S-tar compounds); and (3) N and S in solid char (N-char and S-char) [7, 9]. NH_3 and H_2S are the major N- and S-based gases, respectively, in the producer gas due to strongly reducing atmosphere in the gasification process [8, 10]. When the producer gas is used in integrated gasification combined cycle (IGCC), NH_3 and H_2S are the main precursors of nitrogen oxides (NO_x) and sulphur oxides (SO_x) [10]. In Fischer-Tropsch (FT) liquid fuel synthesis and in the fuel cell application, these gas contaminants are poisonous to catalysts used [11, 12]. For the FT liquid fuel synthesis, the acceptable levels of both the NH_3 and H_2S are below 1 ppmv [11] while the NH_3 and H_2S concentrations in the producer gas from the co-gasification may be varied from 10 to 6,000 ppmv [3, 8, 13, 14], therefore, gas cleaning is needed before this downstream application.

Co-gasification has been studied in different types of gasifiers including fixed-bed gasifiers [15], bubbling fluidised bed gasifiers [8, 13-19], dual fluidised bed (DFB) gasifiers [3, 5, 20-22], and entrained flow gasifier [2]. Most of these reported studies focused on the main components of the producer gas (H_2, CO, CO_2, and CH_4) [2, 3, 5, 13, 16-18, 20-22] and on the tar concentrations [3, 5, 13, 15-17, 19, 21, 22]. However, only a few studies have been reported on concentrations of NH_3 and/or H_2S [3, 8, 13, 14, 19] in the producer gas from co-gasification and very limited information of NH_3 and H_2S can be found from co-gasification in the DFB steam gasifier [3]. The study of Aigner et al. [3] found that NH_3 and H_2S concentrations increased linearly with the increase of coal-to-wood energy ratio in

the feed, where coal and wood were pre-mixed before feeding into to the DFB steam gasifier. Such linearly relationships may not be applicable when pelletised fuel is used.

Recently, Saw and Pang [5] reported that a synergetic effect was observed in co-gasification of blended lignite and wood pellets in terms of producer gas yield, producer gas composition, tar yield, and tar concentrations. This effect was believed to be due to the changes of microstructure of the blended lignite and wood char which influenced the mass transfer and reaction rates [5]. However, no information on the influence of pellet fuels on the NH_3 and H_2S concentrations in the producer gas is reported elsewhere. In the present study, therefore, it was aimed to investigate the influence of L/F mass ratio on the NH_3 and H_2S concentrations in the producer gas from gasification of blended lignite and wood pellets in the DFB steam gasifier. The conversions of fuel-N and fuel-S in the feed to NH_3 and H_2S (also called NH_3 and H_2S conversions) during the co-gasification of the blended lignite and wood pellets are also discussed.

7.2 Experiments and materials

7.2.1 Equipment setup

In this study, a DFB steam gasifier with steam as the gasification agent was used and the schematic diagram is shown in Figure 7.1. The DFB steam gasifier consists of two main parts: a bubbling fluidised bed (BFB) reactor for gasification of the feedstock and a fast fluidised bed (FFB) reactor for combustion of derived char transported from the BFB reactor. In operation, the circulating bed materials are heated by the exothermic combustion reactions of solid char as well as supplementary liquefied petroleum gas (LPG) in the FFB reactor, and then provide heat for the endothermic gasification reactions in the BFB reactor. More details of the gasifier configurations and operations can be found in Saw and Pang [5].

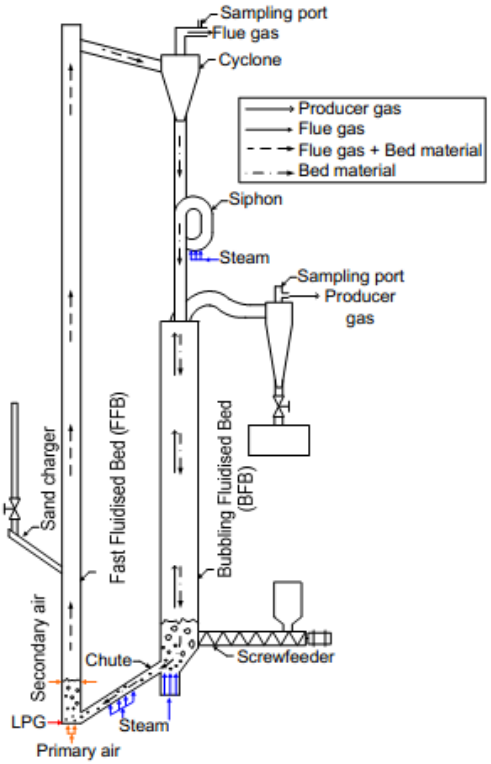

Figure 7.1 Schematic diagram of the DFB steam gasifier used in this study [5]

7.2.2 Materials and operation conditions

Blended lignite and radiata pine wood with the lignite to fuel (L/F) mass ratio ranging from 0% to 100% were tested in the present study. Five feedstocks used include: (1) pure radiata pine wood pellets (0% L/F); (2) pellets of blended lignite and wood at mass ratio of 40:60 (40% L/F); (3) pellets of blended lignite and wood at mass ratio of 70:30 (70% L/F); (4) pellets of blended lignite and wood at mass ratio of 80:20 (80% L/F); and (5) pure lignite particles (100% L/F). The pure wood pellets (0% L/F) with dimensions of 6 mm (diameter) by 15 mm (length) were supplied from a wood pellet plant near Christchurch, New Zealand. The pure lignite particles with particle sizes of 1-8 mm (100% L/F) were obtained from Southland of New Zealand. The pellets of blended lignite and wood with dimensions of 7 mm (diameter) by 20 mm (length) were manufactured and supplied by CRL Energy Ltd., New Zealand. To manufacture pellets of blended lignite and wood, the wood chips sourced from a local wood processing plant near Lower Hutt and the lignite particles from Southland were first dried to a moisture content of 10% which were then ground to fine particles of around 450 μm. After this, the wood sawdust and lignite fine particles were

compounded at required mass ratio to pellets using a pelletizing machine. In the pelletizing machine, the blended lignite and sawdust were firstly mixed with addition of a 2% binding agent of starch, then the blend was heated and pressed to flow out through a screen. This process is the similar to pure wood pelletizing which is operated at a commercial plant.

Before the experiments, feed materials were analysed and the proximate and ultimate analysis results are given in Table 7.1. The XRF analysis results of major elements present in the ash for each fuel are provided in Table 7.2.

The gasifier operation conditions are summarized in Table 7.3. Silica sand was used as the circulating bed material. During the experiments, the temperature in the BFB bed was controlled at the set point, and temperatures both in the BFB reactor and in the FFB reactor at four different height locations were monitored. The average value and maximum deviation over four temperature measurements in BFB are 800±10°C and those in the FFB reactor are 850±15°C as given in Table 7.3. In the experiments, N_2 gas of 5 L/min was purged into the feed hopper to prevent undesired back flow of the producer gas to the feed hopper.

In the experiments, the steam to fuel (S/F) ratio, which is defined as the ratio of a mass flow rate of the feeding steam and moisture in the fuel to a mass flow rate of the dry fuel feedstock, was set within 1.0-1.1 kg/kg_{dry}. The total steam feed rate was controlled at 10 kg/h including steam fed at the BFB base (6 kg/h) as the gasification agent, and steam fed to chute (2 kg/h) and siphon (2 kg/h) for fluidisation. The pre-set S/F ratio was achieved by changing the fuel feed rate within a range of 11-13 kg_{dry}/h while maintaining the steam feeding rate at constant. In the gasification of pure lignite particles, the fuel feed rate was set at 13 kg_{dry}/h which was the maximum limit for the screw-feeding system due to the high moisture content of the lignite. Therefore, the total steam feed rate was reduced from 10 to 8 kg/h for only the test of pure lignite particles, by reducing steam fed at the BFB base from 6 to 4 kg/h, to maintain the S/F ratio of 1.1.

Table 7.1 Proximate and ultimate analysis results of each fuel with different L/F ratios

	Analysis (wt%)	**Method**	**L/F ratio (wt%)**				
			0% L/F	**40% L/F**	**70% L/F**	**80% L/F**	**100% L/F**
Proximate analysis (as-received basis)	Moisture	ISO 5068 or ASTM E871	7.0	20.2	24.3	21.5	34.6
	Ash	ISO 1171 or ASTM D1102	0.6	1.9	3.3	4.0	4.2
	Volatile matter	ISO 562	78.4	59.0	48.5	47.7	32.9
	Fixed carbon	By difference	14.0	18.9	23.9	26.8	28.3
Ultimate analysis (dry and ash free, daf)	C	ISO 12902	51.2	55.4	58.7	60.1	68.4
	H	ISO 12902	6.1	5.8	5.4	5.3	4.9
	N	ISO 12902	0.05	0.41	0.47	0.51	0.72
	S	ASTM D4239	0.01	0.24	0.47	0.55	0.80
	O	By difference	42.6	38.1	35.0	33.6	25.2

Table 7.2 XRF analysis based on ASTM D4326 method of major elements presented in the ash for each fuel with different L/F ratios

Analysis (wt%)	**0% L**	**40% L**	**70% L**	**80% L**	**100% L**
SiO_2	40.7	30.9	36.3	37.4	24.8
Al_2O_3	9.1	1.9	2.0	1.7	3.7
Fe_2O_3	3.1	23.5	16.2	16.4	15.1
CaO	14.4	20.3	22.3	22.1	30.1
MgO	5.6	3.2	3.4	3.2	4.3
Na_2O	3.7	1.0	0.7	0.6	0.4
K_2O	14.0	1.6	1.7	1.2	0.1
TiO_2	0.4	0.2	0.1	0.1	0.2
Mn_3O_4	0.8	0.4	0.3	0.3	0.4
SO_3	1.6	15.6	15.3	15.8	20.3
P_2O_5	2.1	1.0	1.0	0.8	0.03

Table 7.3 DFB steam gasifier operation conditions

Fuel feed rate (kg_{dry}/h)	11-13
Bed material type	Silica sand
Bed material particle size (μm)	180-300
Bed material particle density (kg/m^3)	2,600
Total amount of bed material in the DFB steam gasifier (kg)	30
Average FFB temperature (°C)	850±15
Average BFB temperature (°C)	800±10
Steam feed rate (kg/h)	10
Steam to fuel (S/F) ratio (kg/kg_{dry})	1.0-1.1

7.2.3 Sampling and analysis of NH_3 and H_2S in the producer gas

Details of the sampling and analysis method of NH_3 and H_2S in the producer gas can be found in Chapter 4 (Sections 4.2-4.4).

7.3 Results and discussion

In this study, co-gasification experiments were conducted on the DFB steam gasifier using pellets of blended lignite and wood with different mass ratios of lignite to fuel (L/F) of 0%, 40%, 70%, 80% and 100% (pure lignite particles). The temperature in the BFB gasification reactor was controlled at 800°C and the steam to fuel (S/F) ratio was controlled at 1.0-1.1 kg/kgdry. In the experiments, the concentrations of NH_3 and H_2S in the producer gas were measured. The conversion of N in the fuel to N as NH_3 (or called NH_3 conversion) and the conversion of S in the fuel to S as H_2S (or called H_2S conversion) in the producer gas was calculated based on the experimental results. The results of NH_3 and H_2S concentrations and conversions present in this study were averaged from two or three repeated measurements. The error bars represent the standard deviations.

7.3.1 Influence of L/F ratio on the NH_3 and H_2S concentrations

As the lignite contains much higher N and S than the wood, the N and S contents in the fuel were expected to vary with the L/F ratio. Consequently, the NH_3 and H_2S concentrations in the producer gas were also affected by the L/F ratio which can be confirmed by the experimental results as shown in Figure 7.2 and Figure 7.3. The experimental results for 100% L/F ratio are included in Figure 7.2 and Figure 7.3 as a reference for the pure lignite, because the particles for the 100% L/F ratio feed fuel were different from those of blended lignite and wood in pellets. From Figure 7.2, it can be seen that the N content in the feeding fuel, read from the right-hand side y-axis, was increased linearly with the L/F ratio, whereas the NH_3 concentration in the producer gas was increased exponentially from 525 to 5,590 ppmv when the L/F ratio increased from 0% to 80%. However, the NH_3 concentration in the producer gas for the 100% L/F ratio or pure lignite was measured to be 4,415 ppmv which was close to that of the 70% L/F ratio at 3,983 ppmv. The increase of NH_3 concentration in the producer gas with the L/F ratio from 0% to 80% was due to the increase of N content in the fuel.

The NH_3 concentration with the 80% L/F ratio fuel was found to be higher than that of the 100% L/F ratio fuel which is believed to be due to the higher volatile content and reactivity in the 80% L/F ratio fuel than that in the 100% L/F ratio fuel, which released more volatile-N gases to be thermally cracked and/or reacted with steam to form NH_3. The thermal cracking and steam reforming of volatile-N is an important route of NH_3 formation during the steam gasification of biomass while this route is negligible for the gasification of coal [23, 24]. In addition, the chars generated from the blend pellets are more porous than those of pure lignite particles [25], thus the diffusion of gases, steam, and H radicals is increased within the pellet chars, enhancing the hydrogenation and steam reactions of N in the char to form NH_3 [23, 26].

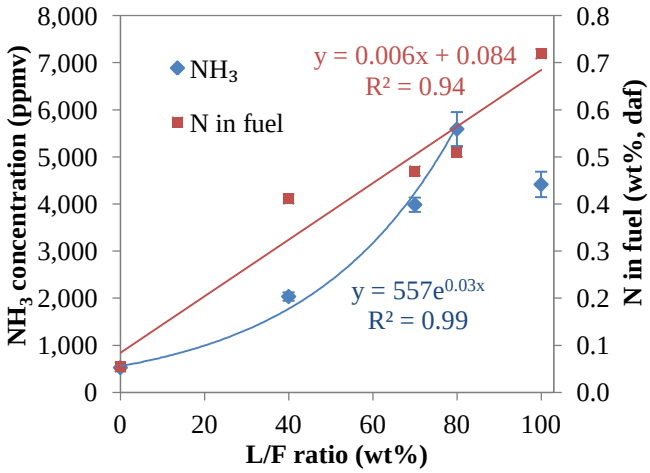

Figure 7.2 Influence of L/F ratio on the NH_3 concentration in the producer gas

The S content in the feed fuel and the H_2S concentration in the producer gas were also affected by the L/F ratio as shown in Figure 7.3. In Figure 7.3, it can be seen that the S content in the fuel was increased linearly with the L/F ratio while the H_2S concentration increased exponentially from 104 to 2,175 ppmv with the L/F ratio increased from 0% to 80%. However, the H_2S concentration in the producer gas for the 100% L/F ratio was found to be similar to that of 80% L/F ratio. The increase of H_2S concentration in the producer gas with the L/F ratio from 0% to 80% was due to the increase of S content in the fuel. Similar explanation of the higher NH_3 concentration of 80% L/F ratio than that of 100% L/F ratio can be deduced for the H_2S concentration.

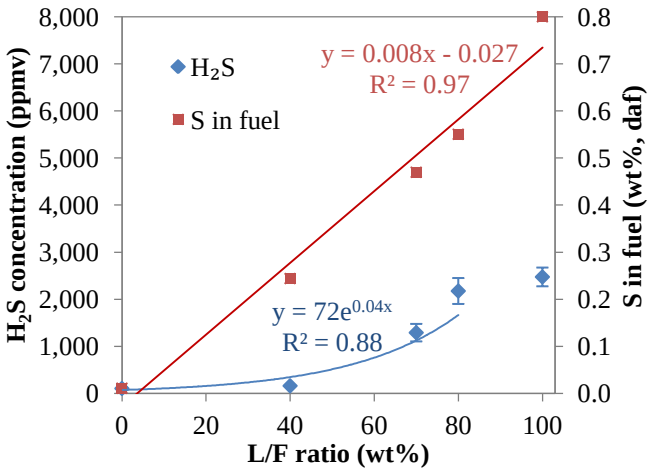

Figure 7.3 Influence of L/F ratio on the H_2S concentration in the producer gas

The results from the present study are consistent with the study of Pinto et al. [8, 13, 14] on co-gasification of low-grade high-ash coal from Puertollano and Colombian and different wastes (pine wood, olive oil bagasse, refuse-derived fuel, and polyethylene) with a mixture of steam and oxygen or a mixture of steam and air being used as gasifying agent in a BFB gasifier. The experiments in the study of Pinto et al. [8, 13, 14] were operated at 850-900°C and atmospheric pressure. They found that the concentrations of NH_3 and H_2S in the producer gas were increased with the coal content in the feed fuel mixture due to its higher N and S contents. They also found a positive trend between the NH_3 and H_2S concentrations in the producer gas and the N and S contents in fuel regardless of the types of tested fuels [8, 13, 14].

However, the correlations between NH_3 and H_2S concentrations based on N and S contents in the fuel may not be generalized as the formation of NH_3 and H_2S relied on a variety of parameters such as gasification operation conditions, gasification agent, N- and S-binding structures of the fuel, and metal or mineral matte present in the fuel, which may act as a catalyst for formation or destruction of NH_3 and H_2S [8, 13]. Moreover, based on experimental results from the present study, it was found that the blending method of the fuels by pelletisation also affected the formation of NH_3 and H_2S in the producer gas.

The results obtained in this study show synergetic effect between coal and wood with pelletizing of the blended fuel, which is confirmed by the non-linear relationship. The blended lignite and wood by pelletisation has changed the microstructure of the blends to differ from those of pure biomass char or pure coal char and this resulted in the changes of the reaction rate of the overall gasification process [25]. Without the synergetic effect between coal and wood, the trends of NH_3 and H_2S concentrations would be linearly correlated to the L/F ratio in the fuel (or the N and S contents) as observed when the coal and wood were non-pelletised [3, 27, 28]. However, this is not the case in the present study as shown in Figure 7.2 and Figure 7.3 when the coal and biomass were pelletised.

The above observations can be verified by literature data as shown In Figure 7.4, in which the results obtained from the present study are compared with those of Aigner et al. [3]. Aigner et al. [3] conducted co-gasification experiments in a DFB steam gasifier at 870°C using non-pelletised mixtures of coal and wood. The calculation of N and S in fuel (wt%, daf) was based on data of fuel properties obtained from Aigner et al. [3] and fuel mass flow obtained from Kern et al. [29]. The concentrations of NH_3 and H_2S measured in the present study were in the same range as those obtained from Aigner et al [3] when N and S contents in the feed are below 0.2%. The pelletised fuel used in the present study showed a negative effect as higher NH_3 concentration was measured than that of the non-pelletised fuel [3] when N content in fuel was increased from 0.4% to 0.7%. However, the pelletised fuel showed a positive effect on H_2S concentration as the H_2S concentration was found to be lower than that of the non-pelletised fuel when S content in fuel was in the range from 0.2% to 0.5%. The different trends between those observed from this study and those obtained from the study of Aigner et al. [3] could be due to various factors including: (1) the difference in coal-biomass interaction between pelletised and physically mixed (non-pelletised) coal and wood; (2) the difference in mass transfer resistance with different particle sizes of the feed fuel [25, 30]; and (3) the difference in structural properties of feedstocks, bed materials, gasification operations, and gasifier configurations.

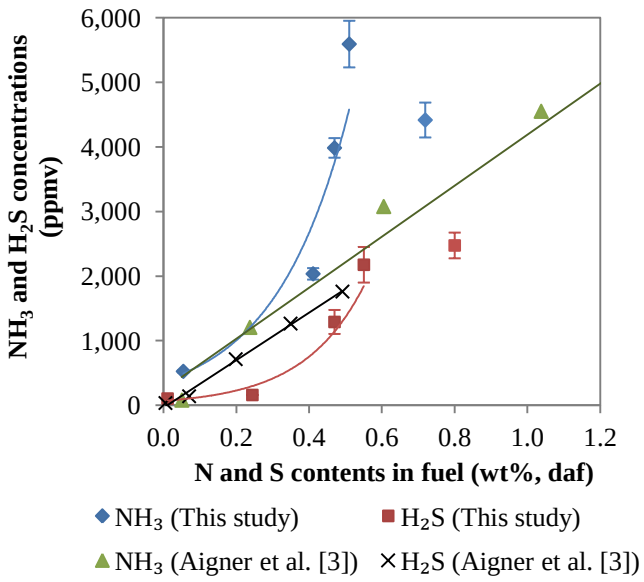

Figure 7.4 Influence of N and S in fuel (wt%, daf) on NH_3 and H_2S concentrations

7.3.2 Influence of L/F ratio on the NH_3 and H_2S conversions

In the DFB steam gasification process, the conversions of fuel-N and fuel-S in the solid feed can occur both in a BFB gasification reactor and a FFB combustion reactor. In the BFB gasification reactor, fuel-N and fuel-S are converted to: (1) N-based gases including NH_3, N_2, and HCN, and S-based gases including H_2S, COS, and CS_2 (2) N-tar and S-tar compounds, and (3) N-char and S-char. In the FFB combustion reactor, NO and SO_2 were formed in the flue gas which were attributed to the oxidation of N and S in the un-gasified char transported from the BFB gasification reactor [3, 31]. In this study, only the NH_3 and H_2S conversions were analysed and defined according to Equations 7.1 and 7.2, respectively. The NH_3 and H_2S conversions are independent of the producer gas flow rate and producer gas yield and thus they can be used for basic estimation of the NH_3 and H_2S yield, respectively, produced from a specific fuel under tested conditions.

NH_3 conversion (wt%) = [N in NH_3 (g/h) × 100] / N in fuel (g/h) (7.1)

H_2S conversion (wt%) = [S in H_2S (g/h) × 100] / S in fuel (g/h) (7.2)

The influence of L/F ratio on the NH_3 and H_2S conversions in the DFB steam gasification process is shown in Figure 7.5. It was found that the NH_3 conversion was decreased from 45% to 25% with the L/F ratio increasing from 0% to 40%. Interestingly, the NH_3 conversion increased linearly as the L/F ratio was increased from 40% to 80%. The NH_3 conversion was then reduced to 42% for the 100% L/F ratio. The NH_3 conversion of 0% L/F ratio or 100% wood obtained in the present study was in the same range as that of Wilk and Hofbauer [31], who studied the conversion of fuel-N in a DFB steam gasification at 850°C of various feedstocks including bark pellets, waste woods, and a mixture of waste plastics with wood pellets. From their experimental results, the NH_3 conversion was found to be 56% for bark pellets with N content of 0.6 wt% (daf).

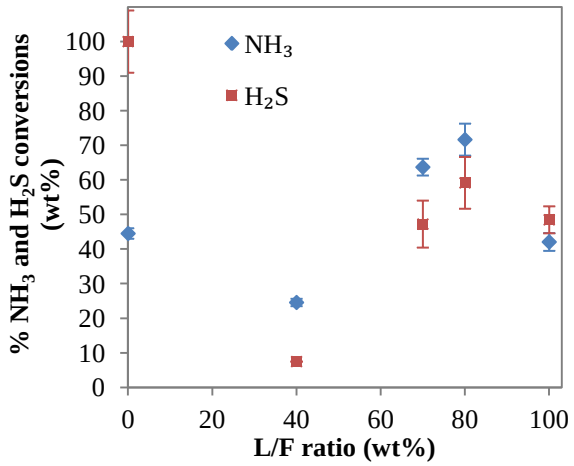

Figure 7.5 Influence of L/F ratio (wt%) on the NH_3 and H_2S conversions

The trend of H_2S conversion with L/F ratio is similar to that of the NH_3 conversion. The H_2S conversion was reduced with the addition of 40% lignite into the wood, and it increased with a further increase in the L/F ratio to 80%. The H_2S conversion of almost 100% for 0% L/F ratio in this study is consistent with the results obtained by Gulyurtlu et al.[27] and Dias and Gulyurtlu [28].

From Figure 7.5, no clear relationships between the NH_3 or H_2S conversion and the L/F ratio are found and this could be due to the synergetic effect of pelletising of the blended fuel.

Without the synergetic effect from the co-gasification of refuse-derived fuel and coal mixtures in an atmospheric BFB gasifier at 850°C, the H_2S conversion was found to decrease with an increment of coal in the feed fuel which could be due to the higher amount of volatile-S in refuse-derived fuel than that in coal [27, 28]. Also, the results of the NH_3 conversion from the present work are inconsistent with those obtained by Sjöström [19], who studied the co-gasification of coal and Swedish birch wood in a pressurised fluidised bed gasifier at 700 and 900°C in which the solid fuel was fed from the top of the gasifier. Sjöström [19] found the synergy from the co-gasification of non-pelletised coal and wood in which the NH_3 conversion was lower than what would be expected from a linear relationship between the NH_3 conversion and the coal to wood mass ratio.

The degree of NH_3 and H_2S conversions in this study not only depended on the L/F ratio or the N and S contents in the feed, but also depended on other parameters including: (1) gasification operation conditions; (2) N- and S-binding structures of the fuel; and (3) mineral matter present in the fuel. Gasification operation conditions, such as fuel feeding position and particle sizes of the fuel, were found to have influenced on the NH_3 and H_2S conversions which affected the contact between the fuel and gasifying agent [31, 32]. For the N- and S-binding structures of the fuel, wood and coal contain N and S in different structures. N in wood is mainly in the form of proteins while N in coal exists as pyrrolic and pyridinic forms [7]. On the other hand, S in wood is in the form of organic phase while S in coal occurs in both the form of pyrites and organic sulphur [33]. The differences or changes of N- and S-binding structures in the blended fuel pellets also affected the NH_3 and H_2S conversions [7, 33]. Moreover, mineral matter in the coal such as Fe, Ca, and Mg can react with H_2S in the gas and form the corresponding sulphides, which are retained in the char [33] as well as they can catalyse the NH_3 decomposition reaction [13, 34]. The mineral matter in the fuel lead to the reduction of NH_3 and H_2S conversions in the producer gas. Finally, from the results obtained in the present study (Figure 7.5), it was discovered that the blending method of the fuels by pelletisation also affected the NH_3 and H_2S conversions due to the synergetic effect of the blends.

7.4 Conclusions

Experiments of co-gasification of blended lignite and radiata pine wood pellets were conducted in the DFB steam gasifier. The influence of lignite to fuel (L/F) ratio on NH_3 and H_2S concentrations and conversions in the producer gas was investigated with the L/F ratio ranging from 0 to 100 wt%. The synergetic effect of blended lignite and wood pellets was found from the results that the NH_3 and H_2S concentrations increased exponentially with the L/F ratio, and the NH_3 and H_2S conversions changed non-linearly with the L/F ratio. The pelletised fuel showed a positive effect on H_2S concentration, when S content of the fuel was from 0.2% to 0.5%, and a negative effect on NH_3 concentration, when N content of the fuel was between 0.4% and 0.7%. Lower H_2S concentration and higher NH_3 concentration were obtained in the producer gas compared to those from co-gasification of non-pelletised fuel.

The optimisation of the L/F ratio in the co-gasification process can be conducted to reduce the concentrations of NH_3 and H_2S in the producer gas. The selection of the optimal L/F ratio will need to consider the availability and price of the fuel feedstock, the energy and cost used for pelletisation of the feed fuel, the composition of the producer gas required, and the downstream application of the producer gas.

7.5 References

[1] National Energy Technology Laboratory (NETL), Gasification 2010 Worldwide Database, in: U.S. Department of Energy, 2010.

[2] J.J. Hernández, G. Aranda-Almansa, C. Serrano, Co-gasification of biomass wastes and coal−coke blends in an entrained flow gasifier: An experimental study, Energy & Fuels, 24 (2010) 2479-2488.

[3] I. Aigner, C. Pfeifer, H. Hofbauer, Co-gasification of coal and wood in a dual fluidized bed gasifier, Fuel, 90 (2011) 2404-2412.

[4] K. Kumabe, T. Hanaoka, S. Fujimoto, T. Minowa, K. Sakanishi, Co-gasification of woody biomass and coal with air and steam, Fuel, 86 (2007) 684-689.

[5] W.L. Saw, S. Pang, Co-gasification of blended lignite and wood pellets in a 100 kW dual fluidised bed steam gasifier: The influence of lignite ratio on producer gas composition and tar content, Fuel, 112 (2013) 117–124.

[6] T. Chmielniak, M. Sciazko, Co-gasification of biomass and coal for methanol synthesis, Applied Energy, 74 (2003) 393-403.

[7] J. Leppälahti, T. Koljonen, Nitrogen evolution from coal, peat and wood during gasification: literature review, Fuel Processing Technology, 43 (1995) 1-45.

[8] F. Pinto, R.N. André, C. Franco, H. Lopes, C. Carolino, R. Costa, I. Gulyurtlu, Co-gasification of coal and wastes in a pilot-scale installation. 2: Effect of catalysts in syngas treatment to achieve sulphur and nitrogen compounds abatement, Fuel, 89 (2010) 3340-3351.

[9] J. Hongrapipat, W.-L. Saw, S. Pang, Removal of ammonia from producer gas in biomass gasification: integration of gasification optimisation and hot catalytic gas cleaning, Biomass Conversion and Biorefinery, 2 (2012) 327-348.

[10] D.J. Stevens, Hot gas conditioning: Recent progress with larger-scale biomass gasification systems, in: National Renewable Energy Laboratory, the U.S. Department of Energy Laboratory, report no: NREL/SR-510-29952, 2001.

[11] H. Boerrigter, H.P. Calis, D.J. Slort, H. Bodenstaff, A.J. Kaandorp, H. den Uil, L.P.L.M. Rabou, Gas cleaning for integrated biomass gasification (BG) and Fischer-Tropsch (FT) systems: Experimental demonstration of two BG-FT systems ("Proof-of-Principle"), in: the Energy research Centre of the Netherlands (ECN), the Netherlands, report no: ECN-C--04-056, 2004.

[12] G. Hoogers, Chapter 8. Stationary power generation, in: Fuel Cell Technology Handbook, CRC Press LLC, 2003.

[13] F. Pinto, H. Lopes, R.N. André, I. Gulyurtlu, I. Cabrita, Effect of catalysts in the quality of syngas and by-products obtained by co-gasification of coal and wastes. 1. Tars and nitrogen compounds abatement, Fuel, 86 (2007) 2052-2063.

[14] F. Pinto, H. Lopes, R.N. André, I. Gulyurtlu, I. Cabrita, Effect of catalysts in the quality of syngas and by-products obtained by co-gasification of coal and wastes. 2: Heavy metals, sulphur and halogen compounds abatement, Fuel, 87 (2008) 1050-1062.

[15] A.G. Collot, Y. Zhuo, D.R. Dugwell, R. Kandiyoti, Co-pyrolysis and co-gasification of coal and biomass in bench-scale fixed-bed and fluidised bed reactors, Fuel, 78 (1999) 667-679.

[16] F. Pinto, R.N. André, C. Franco, H. Lopes, I. Gulyurtlu, I. Cabrita, Co-gasification of coal and wastes in a pilot-scale installation 1: Effect of catalysts in syngas treatment to achieve tar abatement, Fuel, 88 (2009) 2392-2402.

[17] R.N. André, F. Pinto, C. Franco, M. Dias, I. Gulyurtlu, M.A.A. Matos, I. Cabrita, Fluidised bed co-gasification of coal and olive oil industry wastes, Fuel, 84 (2005) 1635-1644.

[18] Y.G. Pan, E. Velo, X. Roca, J.J. Manyà, L. Puigjaner, Fluidized-bed co-gasification of residual biomass/poor coal blends for fuel gas production, Fuel, 79 (2000) 1317-1326.

[19] K. Sjöström, G. Chen, Q. Yu, C. Brage, C. Rosén, Promoted reactivity of char in co-gasification of biomass and coal: synergies in the thermochemical process, Fuel, 78 (1999) 1189-1194.

[20] M.W. Seo, J.H. Goo, S.D. Kim, S.H. Lee, Y.C. Choi, Gasification characteristics of coal/biomass blend in a dual circulating fluidized bed reactor, Energy & Fuels, 24 (2010) 3108-3118.

[21] S. Kern, C. Pfeifer, H. Hofbauer, Co-gasification of wood and lignite in a dual fluidized bed gasifier, Energy & Fuels, 27 (2013) 919-931.

[22] F. Miccio, G. Ruoppolo, S. Kalisz, L. Andersen, T.J. Morgan, D. Baxter, Combined gasification of coal and biomass in internal circulating fluidized bed, Fuel Processing Technology, 95 (2012) 45-54.

[23] F.-J. Tian, J.-l. Yu, L.J. McKenzie, J.-i. Hayashi, T. Chiba, C.-Z. Li, Formation of NOx precursors during the pyrolysis of coal and biomass. Part VII. Pyrolysis and gasification of cane trash with steam, Fuel, 84 (2005) 371-376.

[24] F.-J. Tian, J. Yu, L.J. McKenzie, J.-i. Hayashi, C.-Z. Li, Conversion of Fuel-N into HCN and NH_3 during the pyrolysis and gasification in steam: A comparative study of coal and biomass, Energy & Fuels, 21 (2007) 517-521.

[25] Q. Xu, S. Pang, T. Levi, Reaction kinetics and producer gas compositions of steam gasification of coal and biomass blend chars, part 1: Experimental investigation, Chemical Engineering Science, 66 (2011) 2141-2148.

[26] C.-Z. Li, L.L. Tan, Formation of NOx and SOx precursors during the pyrolysis of coal and biomass. Part III. Further discussion on the formation of HCN and NH_3 during pyrolysis, Fuel, 79 (2000) 1899-1906.

[27] I. Gulyurtlu, F. Pinto, H. Lopes, R.N. André, M. Dias, I. Cabrita, Prediction of H_2S and HCl formation during RDF and co-gasification in fluidized bed, in: Proceedings of the 16th European Biomass Conference and Exhibition, Valencia, Spain, 2008.

[28] M. Dias, I. Gulyurtlu, H_2S and HCl formation during RDF and coal co-gasification: a comparison between the predictions and experimental results, in: Proceedings of the biomass gasification technologies workshop MRC Gebze Campus-Türkiye, 2008.

[29] S. Kern, C. Pfeifer, H. Hofbauer, Dual fluidized-bed steam gasification of solid feedstock: Matching syngas requirements with fuel mixtures, in: Proceedings of the Industrial Fluidization South Africa (IFSA 2011), Johannesburg, South Africa, 2011.

[30] F. Paviet, O. Bals, G. Antonini, The effects of diffusional resistance on wood char gasification, Process Safety and Environmental Protection, 86 (2008) 131-140.

[31] V. Wilk, H. Hofbauer, Conversion of fuel nitrogen in a dual fluidized bed steam gasifier, Fuel, 106 (2013) 793-801.

[32] P. Vriesman, E. Heginuz, K. Sjöström, Biomass gasification in a laboratory-scale AFBG: influence of the location of the feeding point on the fuel-N conversion, Fuel, 79 (2000) 1371-1378.

[33] A. Attar, Chemistry, thermodynamics and kinetics of reactions of sulphur in coal-gas reactions: A review, Fuel, 57 (1978) 201-212.

[34] J. Leppälahti, Formation and behaviour of nitrogen compounds in an IGCC process, Bioresource Technology, 46 (1993) 65-70.

8. Conclusions and recommendations

8.1 Conclusions

Removal of NH_3 and H_2S from biomass gasification producer gas for Fischer-Tropsch liquid fuel synthesis was performed in this research by using primary and secondary measures. The primary measures studied included: (1) optimisation of the operation conditions in the DFB steam gasifier including gasification temperature in the BFB reactor, steam to fuel (S/F) ratio, and mean gas residence time (τ_f); and (2) application of bed materials in the DFB steam gasifier for catalytic NH_3 decomposition and H_2S adsorption, and these included silica sand, iron sand (ilmenite), and calcined olivine sand. The influence of feedstock type or lignite to fuel (L/F) ratio, which is categorised as the optimisation of the operation conditions, was also investigated in the experiments on co-gasification of blended lignite and wood pellets. In the secondary measures, a combined hot catalytic reactor and adsorber was designed, constructed, and studied using titanomagnetite for simultaneous removal of NH_3 by decomposition reaction and removal of H_2S by adsorption reaction. In addition, the dedicated sampling and analysis of NH_3 and H_2S was designed and developed in this research for measuring the concentrations of NH_3 and H_2S in the producer gas.

From the first part of the study on the primary measures, it is found that gasification temperature in the BFB reactor, S/F ratio, and τ_f significantly influenced the NH_3 and H_2S concentrations and conversions. With the use of silica sand as a bed material, the NH_3 and H_2S concentrations and conversions increased with the gasification temperature (in the range of 750-850°C) and the S/F ratio (in the range of 0.6-1.4). However, the increase of τ_f from 0.19 to 0.25 s resulted in the increase in NH_3 concentration and conversion, whereas the H_2S concentration and conversion were slightly decreased. The optimal operation conditions of the wood gasification in the DFB steam gasifier using the silica sand were identified at the BFB reactor of 800°C, S/F ratio of 0.6, and τ_f of 0.19, which resulted in the low NH_3 and H_2S concentrations of 200 and 30 ppmv, respectively.

Based on the results with different bed materials, it is found that ilmenite and calcined olivine sands can reduce the NH_3 and H_2S concentrations and conversions when compared with silica sand, which could be due to their much higher Fe, Ca, Mg, and Mn contents than that of silica sand. In addition, the NH_3 and H_2S concentrations and conversions were reduced by decreasing the S/F ratio irrespective of the bed material types. With the use of ilmenite and calcined olivine sands, the lowest concentrations of NH_3 and H_2S of about 80-120 ppmv and 15-25 ppmv, respectively, have been achieved when the BFB reactor was operated at 800°C and the S/F ratio at 0.6. Overall, minimisation of NH_3 and H_2S concentrations and conversions in the producer gas can be performed by operating the BFB reactor at low temperature, low S/F ratio, and low τ_f when silica sand is used as a bed material. When ilmenite and calcined olivine sands are used at 800°C, the low S/F ratio should be used to achieve the lowest concentrations of NH_3 and H_2S in the producer gas.

The investigation into the L/F ratio in co-gasification of blended lignite and radiata pine wood pellets showed that the NH_3 and H_2S concentrations in the producer gas increased with the L/F ratio due to the increase of N and S contents, respectively, in the fuel. A synergetic effect of pelletised lignite and wood was found on the NH_3 and H_2S concentrations and the NH_3 and H_2S conversions. This effect could be due to the changes of the microstructure of the blends to differ from those of pure biomass char or pure coal char and this led to the changes of the mass transfer and reaction rates of the overall gasification process.

The primary measures by the optimisation of the operation conditions and the application of bed materials in the DFB steam gasifier are very effective for the removal of NH_3 and H_2S concentrations in the producer gas. The selection of the optimal operation conditions and the types of bed material will also need to consider the main gas composition (H_2 and CO) of the producer gas required for the FT liquid fuel synthesis.

In the secondary measures, the H_2-reduced titanomagnetite in the form of ferrite (α-Fe) was tested with three different gas streams, 2,000 ppmv NH_3 in Ar gas, 230 ppmv H_2S in Ar gas, and 2,000 ppmv NH_3 and 230 ppmv H_2S in simulated biomass producer gas. It is found that

the H_2-reduced titanomagnetite achieved 100% NH_3 decomposition of 2,000 ppmv NH_3 in Ar gas at 700 and 800°C. The addition of 230 H_2S into the 2,000 ppmv NH_3 in Ar gas stream led to a small reduction of NH_3 decomposition to >96% and H_2S adsorption of >98% was obtained at 700 and 800°C. Finally, the reduced titanomagnetite in the simulated biomass producer gas achieved 60% NH_3 decomposition and 9% H_2S adsorption at 800°C as well as 40% NH_3 decomposition and an 80% H_2S adsorption at 500°C. The integration of two hot gas reactors operated at 500 and 800°C, respectively or vice versa, will result in the overall removal efficiencies of 76% NH_3 and 82% H_2S in the simulated biomass producer gas.

8.2 Recommendations

The evolution of the fuel-N and fuel-S in the solid fuel in the DFB steam gasifier is a complex issue. In the DFB steam gasification process, the conversions of fuel-N and fuel-S in the solid fuel occur both in the BFB gasification reactor and the FFB combustion reactor. In the BFB gasification reactor, fuel-N and fuel-S are converted to N-based gases (NH_3, N_2, and HCN) and S-based gases (H_2S, COS, and CS_2), N-tar and S-tar compounds, and N-char and S-char. In the FFB combustion reactor, NO and SO_2 are formed in the flue gas. To fully understand the effect of the operation conditions and bed materials used in the DFB steam gasifier, the measurement of all the N and S species in the DFB steam gasifier is necessary. Therefore, the sampling and analysis of all the above-mentioned N and S species should be developed and the measurement of all their concentrations should be conducted as future work.

For the secondary measures to remove NH_3 and H_2S in the hot gas cleaning reactor, the improvement of the performance of titanomagnetite in the simulated producer gas should be conducted by optimisation of the reaction temperature. It is expected that the NH_3 decomposition could be enhanced by using temperatures higher than 800°C due to the endothermic nature of the NH_3 decomposition reaction. In contrast, temperatures lower than 500°C might be required for the improvement of the H_2S adsorption. The experimental results from the temperature optimisation will demonstrate the significant potential of titanomagnetite in commercial applications for the removal of NH_3 and H_2S by the operation of two hot gas cleaning reactors, one reactor operated at a high temperature (≥ 800°C) for NH_3 decomposition

and the other reactor operated at a lower temperature (≤ 500°C) mainly for the adsorption of H_2S.

Further studies on the effect of the simulated biomass producer gas on the performance of titanomagnetite should be conducted by testing the titanomagnetite with individual gases and mixtures of gas components in the producer gas. In addtion, morphological characterisation of the titanomagnetite, both before and after the reaction experiments, shoud be performed by using scanning electron microscopy (SEM) coupled with energy-dispersive X-ray spectroscopy (EDS), and/or transmission electron microscopy (TEM). The iron particle size, size distribution, and iron surface area can be determined from these measurments. The morphology of the titanomagnetite could help explain the effect of the gases on the titanomagnetite efficiency. Insight into these fundamental studies would lead to measures toward improving the performance of titanomagnetite for simultaneous NH_3 and H_2S removal in the simulated biomass producer gas by using only one reactor. Once these additional studies have been conducted and the improvement of the performance of titanomagnetite in the simulated biomass producer gas has been realised, the hot gas reactor for simultaneous removal of NH_3 and H_2S will be integrated into the DFB steam gasifier system and tested for the FT liquid fuel synthesis.

Appendix A. Hazard and Operability (HAZOP) study for a lab-scale reactor for NH_3 and H_2S removal

A.1 Glossary and abbreviations

Hazard and Operability Study (HAZOP)	One of the risk assessment tools for examination of the process and engineering intentions of new or existing facilities to identify and assess potential hazards, consequential effects, and protective and corrective actions.
Hazard	Potential source of harm. Deviations from design or operational intent may constitute or produce a hazard. Hazards are the focus of HAZOP studies, and it should be noted that a single hazard could potentially lead to multiple forms of harm.
Harm	Physical injury or damage to the health of people or damage to property or the environment. Harm is the consequence of a hazard occurring and may take many forms: patient or user safety, employee safety, business risks, regulatory risks, environmental risks, etc.
Risk	Combination of probability of occurrence of harm and the severity of that harm. In a strict sense, "risk" is not always explicitly identified in HAZOP studies since the core methodology does not require identification (also referred to as rating) of the probability or severity of harm. However, risk assessment teams may choose to rate these factors in order to further quantify and prioritize risks if needed
Deviation	A departure from the design and operating intentions

Guide Words	Key supporting elements used to identify deviations from the design and operating intentions in which they guide and stimulate creative thinking towards appropriate deviations.
Score O	Score rated for probability of **O**ccurrence
Score E	Score rated for **E**nvironmental impact
Score P	Score rated for impact on **P**eople
Score SG	Score rated for probability of **S**afe**g**uard Failure
Risk rating score	Final score rated for risk assessment which is calculated from Score O + Score E + Score P - Score SG

A.2 HAZOP methodology

The HAZOP analysis process is divided into four phases as illustrated in Figure A.1 [1]:

A.3 HAZOP team members

The HAZOP team members are chosen to include experts in all relevant areas from design to commissioning and operation of the lab-scale reactor for removal of NH_3 and H_2S. The team members include:

1. Prof. Shusheng Pang	Supervisor
2. Dr. Woei Saw	Associate Supervisor
3. Dr. Alex Yip	Lecturer/Catalyst expert
4. Mr. Leigh Richardson	Technician at Mechanical Workshop
5. Mr. Tim Moore	Technician at Electrical and Electronics Workshop
6. Mr. David Brown	Departmental Safety Officer
7. Mr. Michael Sandridge	Analytical Technician
8. Miss Janjira Hongrapipat	PhD student

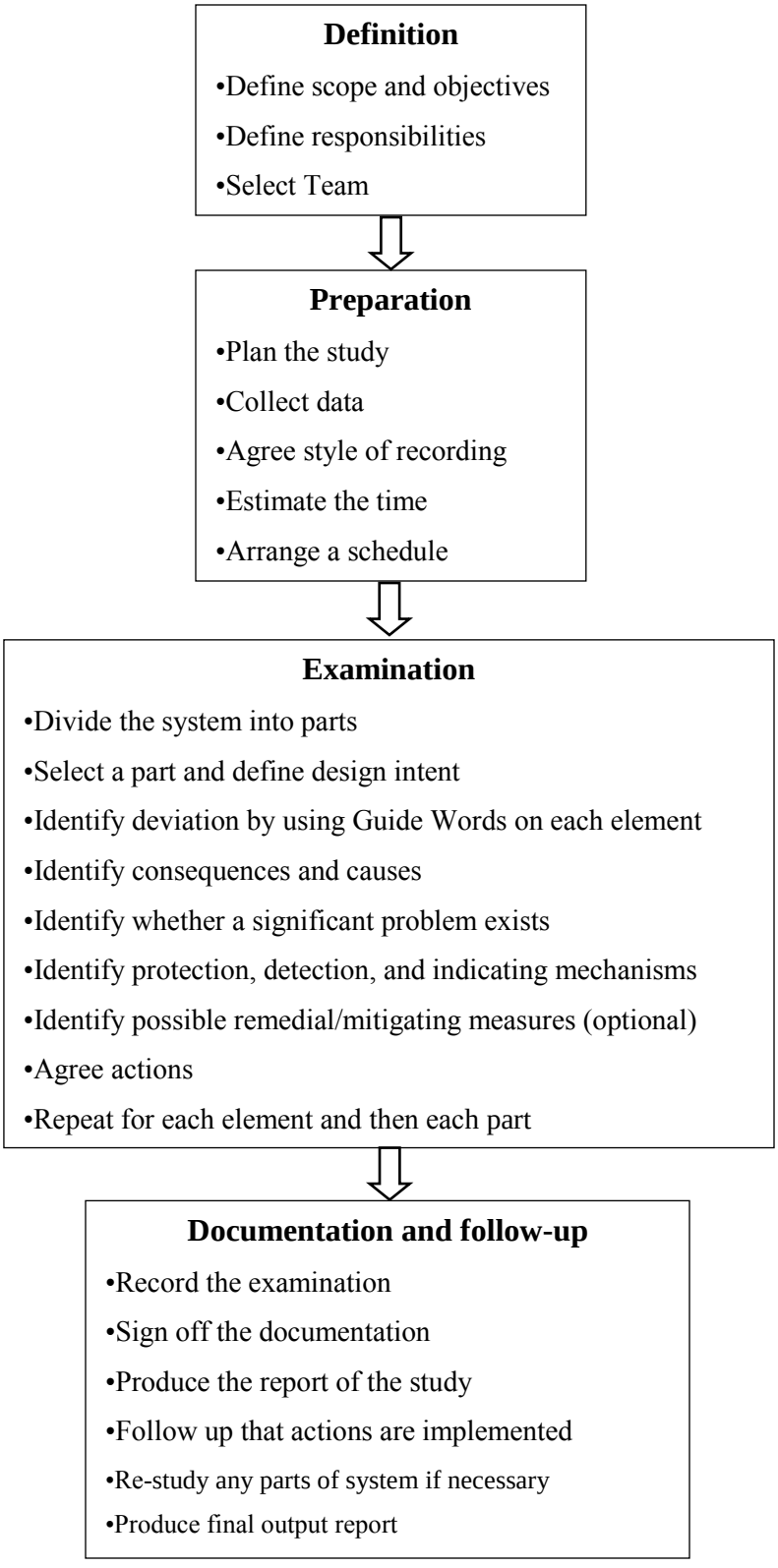

Figure A.1 Diagram of HAZOP methodology

A.4 HAZOP study boundaries

This HAZOP study covers a review of a lab-scale reactor for removal of NH_3 and H_2S, all equipment and operations of the reactor in order to identify possible deviations from normal operation conditions which could lead to potential hazards and operational problems. Causes, consequences, and safeguards of the possible deviations are determined. Consequently, probability and impact of the possible deviations as well as probability of safeguard failure are rated to quantify and prioritize the risks. Finally, risk control measures and additional protective measures are arranged if necessary.

A.5 Description of the lab-scale reactor for removal of NH_3 and H_2S

In the reactor, NH_3 is eliminated by hot catalytic decomposition reaction while H_2S is adsorbed into the adsorbent. Several catalysts and adsorbents including natural substances abundantly achievable in New Zealand, modified catalysts, and combinations of these materials, will be placed in the reactor to investigate their activity towards the removal of NH_3 and H_2S in the simulated producer gas. The simulated producer gas consists of 45 vol% H_2, 20 vol% CO, 20 vol% CO_2, and 15 vol% CH_4. Concentrations of NH_3 and H_2S used will be in a range of 200-2,000 ppmv and 50-200 ppmv, respectively. The design of the lab-scale reactor is shown in Figure A.2. The reactor will be operated in fixed-bed and bubbling fluidised bed regimes. Operating parameters affecting the efficiency of the NH_3 and H_2S removal will be studied, and they are bed temperature and space time or residence time. Space time or residence time is defined as the division of length of the bed (cm) by gas velocity (cm/s), and therefore the unit is second. Several catalysts and adsorbents including olivine/calcined olivine, dolomite/calcined dolomite, calcite, Ni-based catalysts, Fe-based catalysts, biomass char, and coal char will be tested in the lab-scale reactor to investigate their efficiency for the removal of NH_3 and H_2S. Additionally, modified catalysts such as Ni-based and Fe-based catalysts may be developed and tested in the lab-scale reactor.

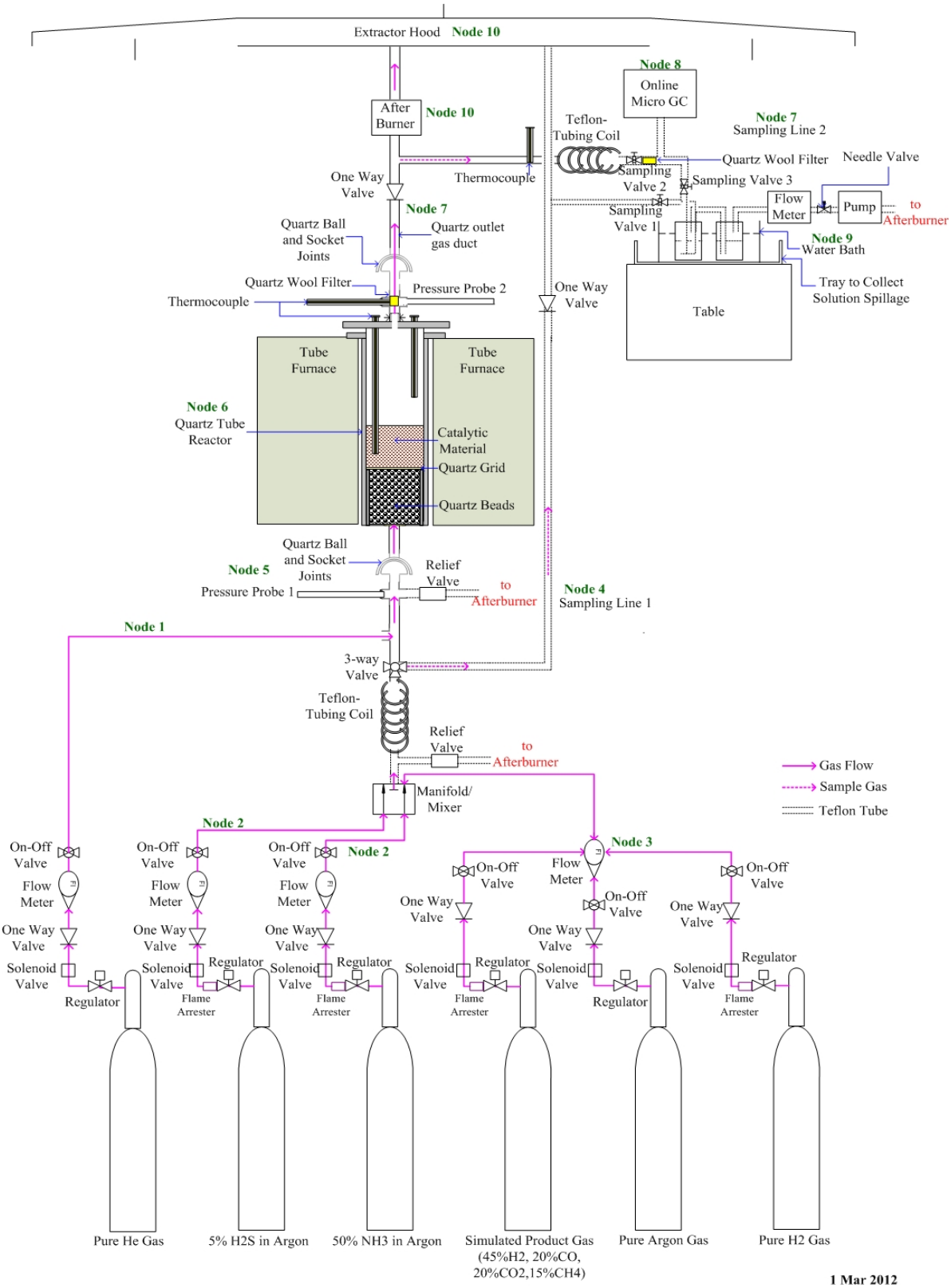

Figure A.2 Schematic diagram of a lab-scale reactor for NH_3 and H_2S removal

A.6 All equipment and parts used

Table A.1 List of all equipment and parts

No.	Description	Dimension/Size/ Characteristic	Intended operational condition	Total number
1	Simulated producer gas cylinder comprises H_2 (45 vol%), CO (20 vol%), CO_2 (20 vol%), and CH_4 (15 vol%)	Size G Volume: 6.1 m^3 Pressure: 13,700 kPa Grade: Beta	Atmospheric pressure Room temperature Flow rate is about 5 L/min	1
2	50 vol% NH_3 in Ar gas cylinder	Size G Volume: 0.4 m^3 Pressure: 750 kPa Grade: Spectra seal	Atmospheric pressure Room temperature Flow rate is 0.002-0.02 L/min	1
3	5 vol% H_2S in Ar gas cylinder	Size G Volume: 7.1 m^3 Pressure: 13,700 kPa Grade: Spectra seal	Atmospheric pressure Room temperature Flow rate is 0.005-0.02 L/min	1
4	Pure He gas cylinder	Size G	Atmospheric pressure Room temperature Flow rate is 0.15-0.25 L/min	1
5	Pure Ar gas cylinder	Size G	Atmospheric pressure Room temperature Flow rate is about 5 L/min	1
6	Pure H_2 gas cylinder	Size G	Atmospheric pressure Room temperature Flow rate is about 5 L/min	1
7	Regulator for simulated producer gas cylinder	Maximum pressure of 3.5 bar gauge outlet	Outlet pressure below 3.5 bar gauge (350 kPa) Room temperature	1
8	Regulator for 50 vol% NH_3 in Ar gas cylinder	Maximum pressure of 3.5 bar gauge outlet		1

Table A.1 List of all equipment and parts (continued)

No.	Description	Dimension/Size/ Characteristic	Intended operational condition	Total number
9	Regulator for 5 vol% H_2S in Ar gas cylinder	Maximum pressure of 3.5 bar gauge outlet	Outlet pressure below 3.5 bar gauge (350 kPa) Room temperature	1
10	Regulator for pure He gas cylinder	Maximum pressure of 17 bar gauge outlet		1
11	Regulator for pure Ar gas cylinder	Maximum pressure of 17 bar gauge outlet		1
12	Regulator for pure H_2 gas cylinder	Maximum pressure of 3.5 bar gauge outlet		1
13	One way valve or check valve	Size 1/4" Cracking pressure 0.07 bar	Pressure higher than 0.07 bar Room temperature	6
14	Flow meter	Triflat Tubes Scale 5"	Outlet gas pressure of the gas cylinder at 0 bar gauge Room temperature	4
15	On-off valve	Glove valve 1/4"	Atmospheric pressure Room temperature	4
16	Manifold or Mixer			1
17	Pressure probe		- Before a reactor: Atmospheric pressure Room temperature - After a reactor: Atmospheric pressure High temperature (300-1,000°C)	2
18	Quartz cross	Made from quartz tube sizes 4 mm (i.d.) x 8 mm (o.d.)		2
19	Quartz ball and socket joints	5 mm (i.d.) x 8 mm (o.d.)		2
20	Sampling line 1	Made from quartz tube, Teflon valve, and Teflon tube		1
21	Sampling line 2			1

Table A.1 List of all equipment and parts (continued)

No.	Description	Dimension/Size/ Characteristic	Intended operational condition	Total number
22	Furnace	3 Zone tube furnace Heated length: 610 mm Internal diameter: 50 mm Max temp: 1,200°C Max continuous temp : 1,150 °C	Atmospheric pressure High temperature (300-1,000°C) Atmospheric pressure High temperature (300-1,000°C)	1
23	Costumed made of quartz cylindrical tube reactor	40 mm (i.d.) x 46 mm (o.d.), 710 mm long		1
24	Quartz grid			1
25	Quartz beads			Height < 200 mm
26	Catalysts			
27	After burner		Atmospheric pressure High temperature Atmospheric pressure High temperature	1
28	Extractor hood			1

A.7 Experimental procedure for the lab-scale reactor for NH_3 and H_2S removal

A.7.1 Experimental procedure for the lab-scale reactor

As shown in Figure A.2, the setup of the experimental system is relatively simple. However, the material aspect is of primary concern because H_2S is selectively adsorbed on glass or metal surfaces [2, 3] and NH_3 can be catalytically or non-catalytically reacted with some reactive materials [4]. Therefore, all inner surfaces of all components and reactor that contact with NH_3 and H_2S gases are made of inert material. Poly-tetrafluoroethylene (PTFE, commonly known

as Teflon) and stainless steel are used when the gas temperature is less than 200°C, whereas quartz material is used with hot gas temperature over 200°C. Therefore, the design of the reactor and all components need careful consideration because the gas will be heated up to high temperature (300-1,000°C).

The experimental procedure for the scrubber and stripper can be divided into three phases: start up or heating up phase, continuous and steady state operation, and shutdown. Brief description of the procedure is given below.

In the start up phase, pure argon (Ar) gas is used to purge N_2 gas in the system to lower detection limit of N_2 by the micro GC. The quartz reactor containing granular catalyst and/or adsorbent is then heated with the electriclal furnace to the temperature set point. Ar gas is also used to fluidise the bed material in the quartz reactor and prevent overheating of the bed material. In the case of catalyst preparation process by H_2 reduction, H_2 gas is flowed through the reactor at set temperature for specified period of time. After the catalyst reduction, Ar gas is restored and the bed is heated to the required temperature. At constant bed temperature, NH_3 gas, H_2S gas, and simulated producer gas are passed through the bed of the catalyst and/or adsorbent. The flow rate of the simulated gas depends on the flow characteristic regime either fixed or fluidised bed. At steady state, gas samples at the inlet and outlet of the reactor are collected and operation conditions (bed temperature, gas temperature, and pressure) are recorded. The sampling and analysis for NH_3 and H_2S are explained in section 5.2.4.3. The main simulated producer gas (H_2, CO, CO_2, CH_4) are measured online via the micro GC. Since the experiment is finished, the furnace is shut off and all the gas bottles are closed.

A.7.2 Measurement of NH_3 and H_2S

The two methods proposed for NH_3 and H_2S measurement are the impinger method and the gas detector tube. The impinger method is the absorption of NH_3 in acid solution and H_2S in basic solution. In this study, weak sulphuric acid (H_2SO_4) of 0.05 molar is used to absorb NH_3 while weak basic sodium hydroxide (NaOH) solution is used with H_2S. As shown in Figure A.2, gas with known volume is drawn into the impingers, where NH_3 or H_2S is absorbed and reacted

with absorbing solution either acid or basic solvent. The absorbing solution is then analysed potentiometrically using ion-selective electrode (ISE) according to ASTM standard method. Analysis of NH_3 is based on ASTM: D 1426 – 08 (Standard Test Methods for Ammonia Nitrogen in Water) and H_2S is based on ASTM: D 4658 – 09 (Standard Test Method for Sulphide Ion in Water).

For the gas detector tube, Drager tubes from Drager Company are used. The Drager tubes are small glass vials filled with a reactive chemical that reacts with a specific gas species and changes its colour [5]. A specified volume of sample gas is drawn through the Drager tubes with a Drager pump enabling determination of NH_3 or H_2S concentration by reading the end of colour change on the scaled tube. The standard deviation of results from the tubes for NH_3 and H_2S is about ± 5-15%. The accuracy of the results from Drager tubes might be lowered caused by high temperature and humidity of the sampled gas. It is therefore a long quartz tube and Teflon tube are used to cool down the gas temperature at sampling port 2.

A.8 HAZOP study

Details of parameters, Guide Words, score O, score E, score P, score SG, and final risk rating and prioritisation are shown in Table A.2-A.7. The HAZOP analysis of all nodes or streams as assigned in Figure A.2 is shown in Table A.8.

Table A.2 Parameters and guide words used in the HAZOP

Parameter	**Guide Words**
Flow rate	Zero, Too High, Too Low, Reverse, Other than = Other gases flow to
Temperature	Too high, Too low
Pressure	Too high, Too low
Level	Zero, Too High, Too Low
Start-up/Shut-down	Too fast, Too slow
Reaction	Zero, Too fast, Too slow, Other than = unwanted reaction
Utility failure (power)	Failure

Table A.3 Probability of occurrence score (Score O)

Score	Order of magnitude Frequency or Likelihood	Qualitative
+1	About once per month (10^{1})	Expected to occur frequently or regularly
0	Once per year (10^{0})	Likely to occur occasionally/several times during plant lifetime
-1	10% chance per year (10^{-1}) (once every 10 years)	Probably will happen more than once during plant lifetime
-2	1% chance per year (10^{-2}) (once every 100 years) (100 plant, once/year)	Not expected to occur but could occur during plant lifetime
-3	1 in 1,000 chance per year (10^{-3})	Would be very surprising if happened during plant lifetime
-4	1 in 10,000 chance per year (10^{-4})	Extremely remote, or not expected to be possible

Table A.4 Environmental impact score (Score E)

Score	Effects expected to occur exclusively On-Site	Effects expected to occur Off-site
6		• Catastrophic release to environment • Long term effects • Substantial fines/penalties expected
5	• Catastrophic release to facility • Long term effects • Substantial fines/penalties expected	• Major release to environment • Long term impact likely • Fines/penalties likely
4	• Major release to facility • Long term impact likely • Fines/penalties likely	• Minor release to environment/outside help needed • Short term impact likely • Legal/public relation consequences

Table A.4 Environmental impact score (Score E) (continued)

Score	Effects expected to occur exclusively On-Site	Effects expected to occur Off-site
3	• Minor release to facility/outside help needed • Short term impact likely • Legal/public relation consequences	• Major release handled with internal resources • No legal/public relation consequences
2	• Major release handled with internal resources • No legal/public relation consequences	• Minor release handled with internal resources • No legal/public relation consequences
1	• Minor release handled with internal resources • No legal/public relation consequences	• Environmental impact unlikely
0	• Environmental impact unlikely	none

Table A.5 Impact on people score (Score P)

Score	Unlikely but might affect one person On-site (10% of time)	Likely to affect 1-2 people On-site	Likely to affect 5-20 people On-site or Off-site
6			Fatality
5		Fatality	Immediate impairment, Permanent health effects
4	Fatality	Immediate impairment, Permanent health effects	Severe injury, Lost time
3	Immediate impairment, Permanent health effects	Severe injury, Lost time	Injury requiring medical treatment
2	Severe injury, Lost time	Injury requiring medical treatment	Minor injury
1	Injury requiring medical treatment	Minor injury	Probably none
0	Minor injury	Probably none	None

Table A.6 Probability of safeguard failure score (Score SG)

Score	Probability of safeguard failure	Example
0	100%	• No safeguards • Operator in difficult position
1	10%	• Single operator with adequate time (> 5 min) fails to do correct thing 1 out of 10 times
2	1%	• Single set of hardware, functionally tested • Automatic shutdown procedure
3	0.1%	• Passive protection (explosion disk) • Combination of Score 1 & 2
4	0.01%	• Two independent sets of hardware

Table A.7 Risk rating and prioritisation

Risk level	Risk rating score	Descriptions
1	-8 to -1	Low risk, existing safeguards are adequate
2	0 to 3	Low risk, but risk control measures are required
3	4 to 8	High risk, risk control measures and additional protective measures are needed
4	9 to 13	Very high risk, this part or process cannot be operated unless risk control measures and additional protective measures have been conducted to reduce the risk and hazard

Table A.8 Hazard and Operability (HAZOP) study

Node/ Stream	**Parameter**	**Guide Word**	**Deviation**	**Causes**	**Score O[1]**	**Consequences**	**Score E[2]**	**Score P[3]**	**Safeguards**	**Score SG[4]**	**Risk Rating[5]**	**Risk level**	**Actions**
Assign each entry a unique tracking number	Describe parameter that the guide word pertains to	Insert deviat-ion guide word used	Describe the deviation	Describe how the deviation may occur	Key in score from Table A.3	Describe what may happen if the deviation occurs	Key in score from Table A.4	Key in score from Table A.5	List controls (preventive or reactive) that reduce deviation likelihood or severity	Key in score from Table A.6	Calcul-ate from equation	Key in level from Table A.7	Identify any hazard mitigation or control actions required
1. He gas cylinder to the connec-tor after 3-way valve	1.1 Flow rate	Zero	No He gas flows to the connector after 3-way valve	Empty cylinder	0	No He gas for measurement of total gas flow rate	0	0	Have checklist to check pressure of gas cylinder before each run	1	-1	1	- Prepare checklist for testing all these parts before each run and checklist during the run. - Ensure all checklists are used (keep the filled checklists for record) - Ensure ventilation system is adequate
				Regulator failure	-1	No He gas flows	0	0	Test regulator before each run	1	-2	1	
				Regulator is closed	1	No He gas flows	0	0	Have checklist for opening regulator during the run	1	0	2	
				One way valve failure closed or gas pressure is below cracking pressure	-1	No He gas flows	0	0	Test a valve before each run if it is failed or gas pressure is too low	1	-2	1	

[1]Score O is for probability of **O**ccurrence
[2]Score E is for **E**nvironmental impact
[3]Score P is for impact on **P**eople
[4]Score SG is for probability of **S**afe**g**uard Failure
[5]Risk rating score is calculated from Score O + Score E + Score P - Score SG

Table A.8 Hazard and Operability (HAZOP) study (continued)

Node/ Stream	Parameter	Guide Word	Deviation	Causes	Score O[1]	Consequences	Score E[2]	Score P[3]	Safeguards	Score SG[4]	Risk Rating[5]	Risk level	Actions
1. He gas cylinder to the connec-tor after 3-way valve	1.1 Flow rate	Zero	No He gas flows to the connector after 3-way valve	One way valve failure opened	-1	Backflow of other gases	0	1	Gas detectors must be used before replacing the He bottle and ventilation must be turned on	2	-2	1	- Checklist is required for Leigh
				Flow meter failure or blockage	-2	No He gas flows	0	0	Test flow meter before each run	2	-4	1	
				On-off valve is off	1	No He gas flows	0	0	Have checklist for opening valve during the run	1	0	2	
				Pipe breakage or loose (not properly tightened or disconnect due to a big aftershock)	0	He gas leaks to the lab	0	0	- Test leaks with liquid soap every 3 months - Ventilation must be turned on	0	0	2	Installation of solenoid valve
	1.1 Flow rate	Too high	He gas flow rate is too high	Regulator failure	-1	Gas flow rate to a reactor is too high and could blow catalysts out of the reactor	0	0	Test regulator before each run	1	-2	1	- Pressure relief valve after Node 1 - Gases will be vented through the bypass line
				Regulator setting is too high	1	Same as above	0	0	Record pressure during the run	1	0	2	
				Flow meter failure	-1	Same as above	0	0	Test flow meter before each run	1	-2	1	
				Flow meter setting is too high	1	Same as above	0	0	Record level during the run	1	0	2	

Table A.8 Hazard and Operability (HAZOP) study (continued)

Node/ Stream	Parameter	Guide Word	Deviation	Causes	Score O[1]	Consequences	Score E[2]	Score P[3]	Safeguards	Score SG[4]	Risk Rating[5]	Risk level	Actions
1. He gas cylinder to the connec-tor after 3-way valve	1.1 Flow rate	Too low	He gas flow rate is too low	Gas in cylinder is almost empty	0	- Gas flow rate to a reactor is too low - No He gas flows due to too low pressure to crack the one-way valve	0	0	Have checklist to Check pressure of gas cylinder before each run	1	-1	1	
				Regulator failure (same as no flow)	-1	Same as above	0	0	Test regulator before each run	1	-2	1	
				Regulator setting is too low (same as no flow – regulator is closed)	1	Same as above	0	0	Record pressure during the run	1	0	2	
				On-off valve is not fully opened	1	Same as above	0	0	Have checklist for opening valve during the run	1	0	2	
				Pipe breakage or loose (not properly tightened or disconnect due to a big aftershock)	0	He gas leaks to the lab	0	0	- Test leaks with liquid soap before each run - Adequate ventilation system is installed	0	0	2	
	1.1 Flow rate	Rever-se	He gas flows in the reverse direction	One way valve failure closed or gas pressure is below cracking pressure	-1	No He gas for measurement of total gas flow rate	0	1	Test a valve before each run if it is failed or gas pressure is too low	1	-1	1	

Table A.8 Hazard and Operability (HAZOP) study (continued)

Node/ Stream	Parameter	Guide Word	Deviation	Causes	Score O[1]	Consequences	Score E[2]	Score P[3]	Safeguards	Score SG[4]	Risk Rating[5]	Risk level	Actions
1. He gas cylinder to the connec-tor after 3-way valve	1.1 Flow rate	Other than	Other gases flow into this node	One way valve failure (Same as above– one way valve failure opened)	-1	He gas in a cylinder could be contaminated from backflow of other gases	0	1	Test a valve before each run if it is failed	1	-1	1	
	1.2 Tempera-ture	Too high & too low	Not a concern										
	1.3 Pressure	Too high (Sam e as high flow)	Gas pressure in this stream is too high	Regulator failure	-1	- Potential of Pipe breakage or loose and then He gas leaks to the lab - Gas flow rate to a reactor is too high and could blow catalysts out of the reactor	0	0	- Test regulator before each run - Adequate ventilation system is installed - Relief valve is installed	1	-2	1	
				Regulator setting is too high	1	Same as above	0	0	Record pressure during the run	1	0	2	
	1.3 Pressure	Too low (Same as low flow)	Gas pressure in this stream is too low	Regulator failure	-1	- Gas flow rate to a reactor is too low - No He gas flows due to too low pressure to crack the one-way valve	0	0	Test regulator before each run	1	-2	1	
				Regulator setting is too low	1	Same as above	0	0	Record pressure during the run	1	0	2	

Table A.8 Hazard and Operability (HAZOP) study (continued)

Node/ Stream	Parameter	Guide Word	Deviation	Causes	Score O[1]	Consequences	Score E[2]	Score P[3]	Safeguards	Score SG[4]	Risk Rating[5]	Risk level	Actions
2. NH_3 and H_2S gas cylinders to manifold	2.1 Flow rate	Zero	No NH_3 and/or H_2S gas flows to manifold	Empty cylinder	0	No NH_3 and/or H_2S gas for test	0	0	Have checklist to Check pressure of gas cylinder before each run	1	-1	1	- Prepare checklist for testing all these parts before each run and checklist during the run. - Ensure all checklists are used (keep the filled checklists for record) - Ensure ventilation is adequate - Ensure sensors work properly - Gas detectors are required
				Regulator failure	-1	No NH_3 and/or H_2S gas flows	0	0	Test regulator before each run	1	-2	1	
				Regulator is closed	1	No NH_3 and/or H_2S gas flows	0	0	Have checklist for opening regulator during the run	1	0	2	
				One way valve failure (closed) or gas pressure is below cracking pressure	-1	No NH_3 and/or H_2S gas flows	0	0	Test a valve before each run if it is failed or gas pressure is too low	1	-2	1	
				One way valve failure (opened)	-1		0	1		2	-2	1	
				Flow meter failure or blockage	-2	No NH_3 and/or H_2S gas flows	0	1	Test flow meter before each run	2	-3	1	
				On-off valve is off	1	No NH_3 and/or H_2S gas flows	0	1	Have checklist for opening valve during the run	2	0	2	
				Pipe breakage or loose (not properly tightened or disconnect due to a big aftershock)	0	NH_3 and/or H_2S gas leaks to the lab	3	3	- Test leaks with liquid soap before each run - Adequate ventilation is installed - NH_3 and H_2S sensors for monitoring are required	3	3	2	Installation of solenoid valve

Table A.8 Hazard and Operability (HAZOP) study (continued)

Node/ Stream	Parameter	Guide Word	Deviation	Causes	Score O[1]	Consequences	Score E[2]	Score P[3]	Safeguards	Score SG[4]	Risk Rating[5]	Risk level	Actions
2. NH_3 and H_2S gas cylinders to manifold	2.1 Flow rate	Too high	NH_3 and/or H_2S gas flow rate is too high	Regulator failure	-1	Gas flow rate to a reactor is too high and could blow catalysts out of the reactor	1	0	Test regulator before each run	1	-1	1	- Pressure relief valve after the manifold - Gases will be vented through the bypass line
				Regulator setting is too high	1	Same as above	1	0	Record pressure during the run	1	1	2	
				Flow meter failure	-1	Same as above	1	0	Test flow meter before each run	1	-1	1	
				Flow meter setting is too high	1	Same as above	1	0	Record level during the run	1	1	2	
	2.1 Flow rate	Too low	NH_3 and/or H_2S gas flow rate is too low	Gas in cylinder is almost empty (same as no flow)	0	- Gas flow rate to a reactor is too low - No NH_3 and/or H_2S gas flows due to too low pressure to crack the one-way valve	0	0	Have checklist to Check pressure of gas cylinder before each run	1	-1	1	
				Regulator failure (same as no flow)	-1	Same as above	0	0	Test regulator before each run	1	-2	1	
				Regulator setting is too low (same as no flow)	1	Same as above	0	0	Record pressure during the run	1	0	2	
				On-off valve is not fully opened (same as no flow)	1	Same as above	0	1	Have checklist for opening valve during the run	2	0	2	

Table A.8 Hazard and Operability (HAZOP) study (continued)

Node/ Stream	Parameter	Guide Word	Deviation	Causes	Score O[1]	Consequences	Score E[2]	Score P[3]	Safeguards	Score SG[4]	Risk Rating[5]	Risk level	Actions
2. NH_3 and H_2S gas cylinders to manifold	2.1 Flow rate	Too low	NH_3 and/or H_2S gas flow rate is too low	Pipe breakage or loose (not properly tightened or disconnect due to a big aftershock)	0	NH_3 and/or H_2S gas leaks to the lab	3	3	- Test leaks with liquid soap before each run - Adequate ventilation is installed - NH_3 and H_2S sensors for monitoring are required	3	3	2	Installation of solenoid valve
	2.1 Flow rate	Rever-se	NH_3 and/or H_2S gas flows in the reverse direction	One way valve failure or gas pressure is below cracking pressure (same as backflow)	-1	No NH_3 and/or H_2S gas for test	0	1	Test a valve before each run if it is failed or gas pressure is too low	1	-1	1	
	2.1 Flow rate	Other than	Other gases flow into this node	One way valve failure (same as He)	-1	NH_3 and/or H_2S gas in a cylinder can be contaminated	0	1	Test a valve before each run if it is failed	1	-1	1	
	2.2 Tempera-ture	Too high & too low	Not a concern										
	2.3 Pressure	Too high	Gas pressure in this stream is too high	Regulator failure (same as high flow)	-1	- Potential of Pipe breakage or loose and NH_3 and/or H_2S gas leaks - Gas flow rate to a reactor is too high and could blow catalysts out of the reactor	1	0	- Test regulator before each run - Adequate ventilation is installed - NH_3 and H_2S sensors for monitoring are required	1	-1	1	

Table A.8 Hazard and Operability (HAZOP) study (continued)

Node/ Stream	Parameter	Guide Word	Deviation	Causes	Score O[1]	Consequences	Score E[2]	Score P[3]	Safeguards	Score SG[4]	Risk Rating[5]	Risk level	Actions
2. NH_3 and H_2S gas cylinders to manifold	2.3 Pressure	Too high	Gas pressure in this stream is too high	Regulator setting is too high	1	Same as above	1	0	Record pressure during the run	1	1	2	
	2.3 Pressure	Too low	Gas pressure in this stream is too low	Regulator failure (same as low flow)	-1	- Gas flow rate to a reactor is too low - No NH_3 and/or H_2S gas flows due to too low pressure to crack the one-way valve	0	0	Test regulator before each run	1	-2	1	
				Regulator setting is too low	1	Same as above	0	0	Record pressure during the run	1	0	2	
3. Syngas, Ar, and H_2 gas cylinders to manifold	3.1 Flow rate	Zero	No syngas, Ar, and/or H_2 gas flows to manifold	Empty cylinder	0	No syngas, Ar, and/or H_2 gas for test	0	0	Have checklist to Check pressure of gas cylinder before each run	1	-1	1	- Prepare checklist for testing all these parts before and during each run and checklist the run. - Ensure all checklists are used. - Ensure ventilation is adequate - Ensure sensors work properly
				Regulator failure	-1	No syngas, Ar, and/or H_2 gas flows	0	0	Test regulator before each run	1	-2	1	
				Regulator is closed	1	No syngas, Ar, and/or H_2 gas flows	0	0	Have checklist for opening regulator during the run	1	0	2	

Table A.8 Hazard and Operability (HAZOP) study (continued)

Node/ Stream	Parameter	Guide Word	Deviation	Causes	Score O[1]	Consequences	Score E[2]	Score P[3]	Safeguards	Score SG[4]	Risk Rating[5]	Risk level	Actions
3. Syngas, Ar, and H_2 gas cylinders to manifold	3.1 Flow rate	Zero	No syngas, Ar, and/or H_2 gas flows to manifold	One way valve failure (closed) or gas pressure is below cracking pressure	-1	No syngas, Ar, and/or H_2 gas flows	0	0	Test a valve before each run if it is failed or gas pressure is too low	1	-2	1	
				One way valve failure (opened)	-1		0	1		2	-2	1	
				Flow meter failure or blockage	-2	No syngas, Ar, and/or H_2 gas flows	0	0	Test flow meter before each run	1	-3	1	
				On-off valve is off	1	No syngas, Ar, and/or H_2 gas flows	0	0	Have checklist for opening valve during the run	1	0	2	
				Pipe breakage or loose (not properly tightened or disconnect due to a big aftershock)	0	Syngas, Ar, and/or H_2 gas leaks to the lab	3	3	- Test leaks with liquid soap before each run - Adequate ventilation is installed - H_2 and CO sensors for monitoring are required	3	3	2	Installation of solenoid valve
	3.1 Flow rate	Too high	Syngas, Ar, and/or H_2 gas flow rate is too high	Regulator failure	-1	Gas flow rate to a reactor is too high and could blow catalysts out of the reactor	1	0	Test regulator before each run	1	-1	1	
				Regulator setting is too high	1	Same as above	1	0	Record pressure during the run	1	1	2	

Table A.8 Hazard and Operability (HAZOP) study (continued)

Node/ Stream	Parameter	Guide Word	Deviation	Causes	Score O[1]	Consequences	Score E[2]	Score P[3]	Safeguards	Score SG[4]	Risk Rating[5]	Risk level	Actions
3. Syngas, Ar, and H_2 gas cylinders to manifold	3.1 Flow rate	Too high	Syngas, Ar, and/or H_2 gas flow rate is too high	Flow meter failure	-1	Same as above	1	0	Test flow meter before each run	1	-1	1	
				Flow meter setting is too high	1	Same as above	1	0	Record level during the run	1	1	2	
	3.1 Flow rate	Too low	Syngas, Ar, and/or H_2 gas flow rate is too low	Gas in cylinder is almost empty	0	- Gas flow rate to a reactor is too low - No NH_3 and/or H_2S gas flows due to too low pressure to crack the one-way valve	0	0	Have checklist to check pressure of gas cylinder before each run	1	-1	1	
				Regulator failure	-1	Same as above	0	0	Test regulator before each run	1	-2	1	
				Regulator setting is too low	1	Same as above	0	0	Record pressure during the run	1	0	2	
				On-off valve is not fully opened	1	Same as above	0	0	Have checklist for opening valve during the run	1	0	2	
				Pipe breakage or loose (not properly tightened or disconnect due to a big aftershock)	0	Syngas, Ar, and/or H_2 gas leaks to the lab	3	3	- Test leaks with liquid soap before each run - Adequate ventilation is installed - H_2 and CO sensors for monitoring are required	3	3	2	Installation of solenoid valve

Table A.8 Hazard and Operability (HAZOP) study (continued)

Node/ Stream	Parameter	Guide Word	Deviation	Causes	Score O[1]	Consequences	Score E[2]	Score P[3]	Safeguards	Score SG[4]	Risk Rating[5]	Risk level	Actions
3. Syngas, Ar, and H_2 gas cylinders to manifold	3.1 Flow rate	Rever-se	Syngas, Ar, and/or H_2 gas flows in the reverse direction	One way valve failure or gas pressure is below cracking pressure	-1	No syngas, Ar, and/or H_2 gas for test	0	1	Test a valve before each run if it is failed or gas pressure is too low	1	-1	1	
	3.1 Flow rate	Other than	Other gases flow into this node	One way valve failure	-1	Syngas, Ar, and/or H_2 gas in a cylinder could be contaminated	0	1	Test a valve before each run if it is failed	1	-1	1	
	3.2 Tempera-ture	Too high	Not a concern										
	3.2 Tempera-ture	Too low	Not a concern										
	3.3 Pressure	Too high	Gas pressure in this stream is too high	Regulator failure	-1	- Potential of Pipe breakage or loose and then syngas, Ar, and/or H_2 gas leaks to the lab - Gas flow rate to a reactor is too high and could blow catalysts out of the reactor	1	0	- Test regulator before each run - Adequate ventilation system is installed - H_2 and CO sensors for monitoring are required	1	-1	1	
				Regulator setting is too high	1	Same as above	1	0	Record pressure during the run	1	1	2	

Table A.8 Hazard and Operability (HAZOP) study (continued)

Node/ Stream	Parameter	Guide Word	Deviation	Causes	Score O[1]	Consequences	Score E[2]	Score P[3]	Safeguards	Score SG[4]	Risk Rating[5]	Risk level	Actions
3. Syngas, Ar, and H_2 gas cylinders to manifold	3.3 Pressure	Too low	Gas pressure in this stream is too low	Regulator failure	-1	- Gas flow rate to a reactor is too low - No syngas, Ar, and/or H_2 gas flows due to too low pressure to crack the one-way valve	1	0	Test regulator before each run	1	-1	1	
				Regulator setting is too low	1	Same as above	1	0	Record pressure during the run	1	1	2	
4. From mixer through tubing coil, one way valve also cover the line before water bath	4.1 Flow rate	Zero	No gas flow into a reactor and sampling line 1	At least one or all of Node 1-3 failure	0	No gas for sampling	0	0	Same as Node 1-3 for no gas flow	0	0	1	- Ensure all fittings are tightened - Prepare checklist for leak test before each run and checklist during the run. - Ensure all checklists are used (keep the filled checklists for record)

Table A.8 Hazard and Operability (HAZOP) study (continued)

Node/ Stream	Parameter	Guide Word	Deviation	Causes	Score O[1]	Consequences	Score E[2]	Score P[3]	Safeguards	Score SG[4]	Risk Rating[5]	Risk level	Actions
4. From mixer through tubing coil, one way valve also cover the line before water bath	4.1 Flow rate	Zero	No gas flow into sampling line 1	Pipe breakage or loose (not properly tightened or disconnect due to a big aftershock)	0	Syngas, NH_3, H_2S, Ar, He and/or H_2 gas leaks to the lab	3	3	Same as Node 1-3 for no gas flow	3	3	2	- Same as Node 1-3 - Extraction system -Solenoid valve to shut off the gases with an emergency button (similar to power shortage) -Enclosed the whole system -2 operators are required
	4.1 Flow rate	Too high	Gas flow rate into sampling line 1 is too high	Gas flow rate from one or more of Node 1-3 is too high (due to the setting is too high)	1	Potential of Teflon fittings loose and then gas leaks to the lab	1	0	Same as Node 1-3 for too high flow rate	1	1	2	
	4.1 Flow rate	Too low	Gas flow rate into sampling line 1 is too low	Gas flow rate from one or more of Node 1-3 is too low (due to the setting is too low)	1	Gas flow rate to a sampling line 1 is too low for analysis	1	0	Same as Node 1-3 for too low flow rate	1	1	2	
	4.1 Flow rate	Rever-se	Gas flow in the reverse direction back to manifold	One way valve failure and 3-way valve partially open to both sides, sampling valves 2 and 3 are opened and sampling rate higher than the inlet flow rate	-2	Explosion in the reactor from air is drawn from the lab through sampling line 2 to reactor	4	2	Operating procedure is required so that this does not occurred	3	1	2	

Table A.8 Hazard and Operability (HAZOP) study (continued)

Node/ Stream	Parameter	Guide Word	Deviation	Causes	Score O[1]	Consequences	Score E[2]	Score P[3]	Safeguards	Score SG[4]	Risk Rating[5]	Risk level	Actions
4. From mixer through tubing coil, one way valve also cover the line before water bath	4.1 Flow rate	Other than	No case of other than										
	4.2 Tempera-ture	Too high & too low	Not a concern										
	4.3 Pressure	Too high	Gas pressure in this stream is too high	Blockage at 3-way valve	-1		1	0	Relief valve is at the top of the mixer	3	-3	1	
				Relief valve failure		Not a concern							
	4.3 Pressure	Too low	Gas pressure in this stream is too low	Not a concern									
5. 3-way valve to the furnace	5.1 Flow rate	Zero	Not a concern										
	5.1 Flow rate	Too high	Gas flow rate is too high	Gas flow rate from one or more of Node 1-3 is too high (due to the setting is too high)	1	- Potential of quartz fittings breakage or loose and then gas leaks - Gas flow rate to a reactor is too high and could blow catalysts out of the reactor	1	0	Same as Node 1-3 for too high flow rate	1	1	2	
	5.1 Flow rate	Too low	Gas flow rate into sampling line 1 is too low	Gas flow rate from one or more of Node 1-3 is too low (due to the setting is too low)	1	- Gas flow rate to a sampling line 1 is too low for analysis	1	0	Same as Node 1-3 for too low flow rate	1	1	2	

Table A.8 Hazard and Operability (HAZOP) study (continued)

Node/ Stream	Parameter	Guide Word	Deviation	Causes	Score O[1]	Consequences	Score E[2]	Score P[3]	Safeguards	Score SG[4]	Risk Rating[5]	Risk level	Actions
5. 3-way valve to the furnace	5.1 Flow rate	Rever-se	Gas flow in reverse direction	Catalyst bed length is too long	0	- No gas into the reactor for experiment	0	1		1	0	2	
	5.1 Flow rate	Other than	No case of other than										
	5.2 Tempera-ture	Too high	Not a concern										
	5.2 Tempera-ture	Too low	Not a concern										
	5.3 Pressure	Too high	Not a concern										
	5.3 Pressure	Too low	Not a concern										
6. Quartz tube reactor and furnace	6.1 Flow rate	Zero	No gas in the reactor	At least one or all of Node 1-5 failure	0	No gas for test	0	0	Same as Node 1-5 for no gas flow	1	-1	1	- Same as Node 1-5
				Pipe breakage or loose (not properly tightened or disconnect due to a big aftershock)	0	Syngas, NH_3, H_2S, Ar, He and/or H_2 gas leaks to the lab	3	3	Same as Node 1-5 for no gas flow	3	3	2	- Same as Node 1-5 - Extraction system -Solenoid valve to shut off the gases with emergency button (similar to power shortage) -Enclosed the whole system

Table A.8 Hazard and Operability (HAZOP) study (continued)

Node/ Stream	Parameter	Guide Word	Deviation	Causes	Score O[1]	Consequences	Score E[2]	Score P[3]	Safeguards	Score SG[4]	Risk Rating[5]	Risk level	Actions
6. Quartz tube reactor and furnace	6.1 Flow rate	Too high (same as Node 2 high flow)	Gas flow rate in the reactor is too high	Gas flow rate from one or more of Node 1-5 is too high (due to the setting is too high)	1	- Potential of quartz fittings breakage or loose and then gas leaks - Gas flow rate to the reactor is too high and could blow catalysts out of the reactor	1	0	Same as Node 1-5 for too high flow rate	1	1	2	
	6.1 Flow rate	Too low (same as Node 2)	Gas flow rate in a reactor is too low	Gas flow rate from one or more of Node 1-5 is too low (the setting is too low)	1	- Gas flow rate to a reactor is too low	1	0	Same as Node 1-5 for too low flow rate	1	1	2	
	6.1 Flow rate	Rever-se	Gas flow back to Node 5	Catalyst bed length is too long	0		0	1		1	0	2	
	6.2 Tempera-ture	Too high	Furnace temperature is too high	Furnace temperature controllers failure	-1	- Damage to heating elements and insulation - Gas temperature is too high - Potential of catalyst melting	2	2		3	0	2	Data logging system with alarm
				Furnace setting temperatures are too high	0	Same as above	2	2	Record setting temperature and actual temperature during the run	3	1	2	Temperature limit will be set and use checklist

Table A.8 Hazard and Operability (HAZOP) study (continued)

Node/ Stream	Parameter	Guide Word	Deviation	Causes	Score O[1]	Consequences	Score E[2]	Score P[3]	Safeguards	Score SG[4]	Risk Rating[5]	Risk level	Actions
6. Quartz tube reactor and furnace	6.2 Tempera-ture	Too low	Furnace temperature is too low	Furnace temperature controllers failure	-1	Experiment failure	0	0		3	-4	1	
				Furnace setting temperatures are too low	0		0	0	Record setting temperature and actual temperature during the run	3	-3	1	
	6.3 Pressure	Too high	Gas pressure in the reactor is too high	Catalysts block in the afterburner	0		2	2		3	1	2	-Pressure relief valve -Pressure sensor
	6.3 Pressure	Too low	Gas pressure in the reactor is too low	Air entering the furnace may cause explosion if H_2 is in the reactor	0		2	3		1	4	3	-During sampling initial concentrations of NH_3 and H_2S, He will be used to purge the gas in the reactor. -Ensure the sampling flow rate is always lower than the total flow rate
	6.4 Start-up	Too fast	Furnace heating up is too fast	Furnace temperature controllers failure	-3	Damage to heating elements and insulation	0	0		2	-5	1	-Check the temperature controller and the limit heating rate

Table A.8 Hazard and Operability (HAZOP) study (continued)

Node/ Stream	Parameter	Guide Word	Deviation	Causes	Score O[1]	Consequences	Score E[2]	Score P[3]	Safeguards	Score SG[4]	Risk Rating[5]	Risk level	Actions
6. Quartz tube reactor and furnace	6.4 Start-up	Too fast	Furnace heating up is too fast	Heating rate of furnace temperature controllers is too fast	-3	Same as above	0	0	Record controller set up parameters and check before each run	1	-4	1	
	6.4 Start-up	Too slow	Furnace heating up is too slow	Not a concern									
	6.5 Reaction	No	No reaction occurs	Not a concern									
	6.5 Reaction	Too fast	H_2 reduction reaction is too fast	Not a concern									- Monitor with thermocou-ple - Low H_2 concentra-tion (5vol%) will be used and operated at below 600°C - Operating procedure
	6.5 Reaction	Too slow	H_2 reduction reaction is too slow	Not a concern									
	6.5 Reaction	Other than	Unwanted reactions occur	Not a concern									
	6.6 Utility failure (power)	Failure	Power cut	- Power cut from power supply failure - Power cut from emergency	0	Experiment failure	0	0		2	-2	1	Not a concern

Table A.8 Hazard and Operability (HAZOP) study (continued)

Node/ Stream	Parameter	Guide Word	Deviation	Causes	Score O[1]	Consequences	Score E[2]	Score P[3]	Safeguards	Score SG[4]	Risk Rating[5]	Risk level	Actions
7. Quartz tube connects with reactor outlet port to quartz socket joint including pressure probe, sampling line 2, pump, and flow meter	7.1 Flow rate	Zero	No gas flow out of the reactor and into sampling line 2	At least one or all of Node 1-6 failure	0	No gas for sampling	0	0	Same as Node 1-6 for no gas flow	1	-1	1	- Ensure all quartz fittings are tightened - Prepare checklist for leak test before each run and checklist during the run. - Ensure all checklists are used (keep the filled checklists for record)
				Pipe breakage or loose (not properly tightened or disconnect due to a big aftershock)	-1	Syngas, NH_3, H_2S, Ar, He and/or H_2 gas leaks to the lab	2	2	Same as Node 1-6 for no gas flow	1	3	2	
			Not a concern	Pump failure		No gas for sampling			Test pumps before each run				
			Not a concern	Pump is off		Same as above			Have checklist for turning on the pump during the run				
			Not a concern	Flow meter failure or blockage from catalyst flows to the flow meter		Same as above			Test flow meter before each run				

Table A.8 Hazard and Operability (HAZOP) study (continued)

Node/ Stream	Parameter	Guide Word	Deviation	Causes	Score O[1]	Consequences	Score E[2]	Score P[3]	Safeguards	Score SG[4]	Risk Rating[5]	Risk level	Actions
7. Quartz tube connects with reactor outlet port to quartz socket joint including pressure probe, sampling line 2, pump, and flow meter	7.1 Flow rate	Too high	Gas flow rate in sampling line 2 is too high	Gas flow rate from one or more of Node 1-6 is too high (due to the setting is too high)	1	- Potential of quartz fittings breakage or loose and then gas leaks to the lab - Gas flow rate to a reactor is too high and could blow catalysts out of the reactor	1	0	Same as Node 1-6 for too high flow rate	1	1	2	
				Flow meter setting is too high	1	Gas flow rate for sampling is too high	2	2	Record level during the run	3	2	2	- Relief valve will take care of it. - Operating procedure will be used
			Same as air entering into the system (above)	Sampling flow rate is higher than the total flow rate of the system into sampling train	1	-Air entering the system, -Water in the washing bottles entering into the system and pump	2	2		3	2	2	One way valve is installed to avoid air from lab flows into the system

Table A.8 Hazard and Operability (HAZOP) study (continued)

Node/ Stream	Parameter	Guide Word	Deviation	Causes	Score O[1]	Consequences	Score E[2]	Score P[3]	Safeguards	Score SG[4]	Risk Rating[5]	Risk level	Actions
7. Quartz tube connects with reactor outlet port to quartz socket joint including pressure probe, sampling line 2, pump, and flow meter	7.1 Flow rate	Too low	Not a concern	Gas flow rate from one or more of Node 1-6 is too low		Gas flow rate for sampling is too low			Same as Node 1-6 for too low flow rate				
			Not a concern	1 or 2 flow meters setting is too low		Gas flow rate for sampling is too low			Record level during the run				
	7.1 Flow rate	Rever-se	Gas flow in reverse direction	Catalyst bed length is too long	0	- No gas into the reactor for experiment	0	1		1	0	2	
	7.2 Tempera-ture	Too high	Gas temperature is too high	Furnace temperature is too high	-1	- Melt Teflon tubing - Gas leakage	2	2		1	2	2	
	7.2 Tempera-ture	Too low	Not a concern										
	7.3 Pressure	Too high	Gas pressure is too high	Blockage of quartz filter (pressure is too high in the line before the filter)	1	-Glass breakage	2	2		3	2	2	Relief valve will take care of it.
	7.3 Pressure	Too low	Not a concern										

Table A.8 Hazard and Operability (HAZOP) study (continued)

Node/ Stream	Parameter	Guide Word	Deviation	Causes	Score O[1]	Consequences	Score E[2]	Score P[3]	Safeguards	Score SG[4]	Risk Rating[5]	Risk level	Actions
8. GC	8.1 Tempera-ture	Too high	Temperature of GC is too high	Not a concern									- Prepare checklist - Ensure the checklist is used (keep the filled checklist for record)
			Gas temperature to GC is too high	Not a concern									
	8.1 Tempera-ture	Too low	Temperature of GC is too low	Not a concern									
			Gas temperature to GC is too low	Not a concern									
	8.2 Utility failure (power)	Failure	Power cut	- Power cut from power supply failure - Power cut from emergency case or a big aftershock		Not a concern							
9. Water bath, and washing bottles	9.1 Tempera-ture	Too high	Temperature of water bath is too high	Water bath failure		Not a concern							- Prepare checklist - Ensure the checklist is used (keep the filled checklist for record)
				Water bath setting temperature is too high		Not a concern			Record setting temperature and actual temperature during the run				
			Gas temperature to washing bottles is too high	Temperature of solutions (H_2SO_4 or NaOH) is too high		Unwanted reactions could occur			Not a concern				

Table A.8 Hazard and Operability (HAZOP) study (continued)

Node/ Stream	Parameter	Guide Word	Deviation	Causes	Score O[1]	Consequences	Score E[2]	Score P[3]	Safeguards	Score SG[4]	Risk Rating[5]	Risk level	Actions
9. Water bath, and washing bottles	9.1 Tempera-ture	Too low	Temperature of water bath is too low	Water bath failure		Not a concern							
				Water bath setting temperature is too high		Not a concern			Record setting temperature and actual temperature during the run				
			Gas temperature to washing bottles is too low			Not a concern							
	9.2 Pressure	Too high				Not a concern							
	9.2 Pressure	Too low				Not a concern							
	9.3 Level	Zero	No water in the water bath	Human mistakes					Not a concern				
	9.3 Level	Too high	Water level in water bath is too high	Human mistakes		Potential of water overflow from water bath			Not a concern				
	9.3 Level	Too low	Water level in water bath is too low	Human mistakes		Temperature of solution in washing bottles does not reach 20°C and is not constant.			Not a concern				

Table A.8 Hazard and Operability (HAZOP) study (continued)

Node/ Stream	Parameter	Guide Word	Deviation	Causes	Score O[1]	Consequences	Score E[2]	Score P[3]	Safeguards	Score SG[4]	Risk Rating[5]	Risk level	Actions
9. Water bath, and washing bottles	9.4 Utility failure (power)	Failure	Power cut	- Power cut from power supply failure - Power cut from emergency case or a big aftershock		Not a concern							
10. After burner and extractor hood	10.1 Flow rate	Too high	Gas flow rate to afterburner is too high	Not a concern									
	10.1 Flow rate	Too low	Gas flow rate to afterburner is too low	Not a concern									
	10.1 Flow rate	Rever-se	Gas flows in reverse direction	One way valve failure and vacuum in the furnace	-2	explosion	4	2		3	1	2	
	10.2 Tempera-ture	Too high	Gas temperature to afterburner is too high	Not a concern									
			Gas temperature to extractor hood is too high	Not a concern									
	10.2 Tempera-ture	Too low	Gas temperature to afterburner is too low	Not a concern									

Table A.8 Hazard and Operability (HAZOP) study (continued)

Node/ Stream	Parameter	Guide Word	Deviation	Causes	Score O[1]	Consequences	Score E[2]	Score P[3]	Safeguards	Score SG[4]	Risk Rating[5]	Risk level	Actions
10. After burner and extractor hood	10.2 Tempera-ture	Too low	Gas temperature to extractor hood is too low	Not a concern									
	10.3 Utility failure (power)	Failure	Power cut	- Power cut from power supply failure - Power cut from emergency case or a big aftershock	0	Extractor hood stops	0	0		3	-3	1	
	10.4 Failure	Failure	Afterburner failure	Gas bottle empty	0	Syngas or NH_3 or H_2S to vent	2	2		3	1	2	Check LPG bottle before the experiment
			Afterburner flame off		0	Syngas or NH_3 or H_2S to vent	2	2		3	1	2	Use flame detector

A.9 References

[1] Product Quality Research Institute, Hazard & Operability Analysis (HAZOP), 2011, from: http://www.pqri.org/pdfs/MTC/HAZOP_Training_Guide.pdf.

[2] R.C. Brown, J. Smeenk, G. Norton, Development of analytical techniques and scrubbing options for contaminants in gasifier streams intended for use in fuel cells, in: Center for Sustainable Environmental Technologies at Iowa State University, 2001.

[3] P. Ståhlberg, M. Lappi, E. Kurkela, P. Simell, P. Oesch, M. Nieminen, Sampling of contaminants from product gases of biomass gasifiers, in: VTT Technical Research Centre of Finland, report no: VTT Research Notes 1903, 1998.

[4] C. Li, P. Nelson, Interactions of quartz, zircon sand and stainless steel with ammonia: implications for the measurement of ammonia at high temperatures, Fuel, 75 (1996) 525-526.

[5] Dräger Safety AG & Co. KGaA, Dräger-Tubes & CMS-Handbook, 16th edition, 2011.

Appendix B. Experimental checklist for a lab-scale reactor for NH_3 and H_2S removal

There are 5 Checklists for this experiment which can be divided to:

Checklists in Table B.1 and Table B.2 for testing all equipment and instrument, and these checklists will be used occasionally.

Checklists in Tables B.3, B.4, and B.5 for all instructions in the experiment

Table B.1 Checklist for testing all regulators, air operated valves, a solenoid valve, one way valves, on-off valves, flow meters, relief valves, an extraction hood, an afterburner, and emergency stops

Procedures	**Date**		
1	Turn on extraction hood and check if it work properly (Extractor hood is always for Chris Penniall's rig)		
2	Measure flow rate of the extraction hood by flow meter		
3	Test if all regulators work properly and no gas leaks		
4	Test if all air operated valves work properly and no gas leaks		
5	Test if a solenoid valve works properly		
6	Test if all one way valves (check valves) work properly and no gas leaks		
7	Test if all on-off valves work properly and no gas leaks		
8	Test if all flow meters work properly and no gas leaks		
9	Test if there is no leak at manifold		
10	Test if all relief valves work properly		
11	Test if the afterburner works properly		
12	Test if the emergency stops work properly		
13	Test interlock for fume hood system 13.1 Fume hood off = everything is off (fume hood, gas bottle and power) 13.2 power cut = fume hood is still on but gas bottles and power are off		
14	Ensure all gas cylinders and on-off valves are off after testing		
15	Do not release or change the regulator pressure (always set at 100 kPa for Ar and He and 40 kPa for NH_3 and H_2S)		
16	Put on sign at door to warn people		
17	Email everyone before running H_2 overnight		

Table B.2 Checklist for testing a GC, a PID gas instrument for NH_3 and H_2S, and an NH_3 gas detector

Procedures	**Date**		
1	Test if the GC is working properly with air or Ar gas		
2	Check if He gas in the GC is enough for the experiment		
3	Test if NH_3 gas detector (ToxiRAE Pro) for safety works properly		
4	Test if Area RAE multigas detectors for H_2S monitoring works properly		
5	Ensure two CO detectors are available		

Table B.3 Checklist for preparation before the experiment

Procedures	**Date**		
1	Check if the extractor hood is working		
2	Check if the GC is available		
3	Bake out the GC overnight (>12 hr) only if the GC is used before by other people		
4	Check gas in all cylinders is enough for a day run to be completed satisfactorily 4.1 Pressure of Ar instrument grade = 4.2 Pressure of Ar welding grade for H_2 reduction = 4.3 Pressure of Ar welding grade for purging after run = 4.4 Pressure of NH_3 bottle = 4.5 Pressure of H_2S bottle = 4.6 Pressure of H_2 bottle = 4.7 Pressure of Syngas bottle =		
5	Add catalyst into the reactor and place the reactor into the furnace		
6	Assemble all quartz fittings		
7	Check the connection of all quartz fittings are tight by: 7.1 Test leak by turning on Ar gas and using liquid soap 7.2 Ensure an Ar gas cylinder and all on-off valves are off after testing 7.3 Do not release or change the regulator pressure (always set at 100 kPa for Ar gas bottle)		
8	Ensure 2 sampling valves (SV1 & SV3) are closed and OV 7 is open (Ar purge into the reactor is the first thing to do after heating up the furnace)		
9	Ensure the sampling valve (SV4) is closed		
10	Ensure 3 sampling valves (SV2 & SV5 & SV6) are opened for GC analysis		
11	SV5 has to be opened all the time except when sampling outlet gas by impinge method		
12	Check the setting of the furnace temperature controller are correct		
13	Check if time of 2 laptops are the same		
14	Open the on-off valve between the H2 flow meter and manifold		
15	Turn on water bath for ISE mehod		

Table B.4 Checklist for normal experimental operation

Procedures	**Date**		
1	Ensure all gas detector for ambient are ON		
2	Locate the web-cam		
3	Turn on the computer and start data logging for thermocouples and pressure transducer		
4	Bake out the GC for about 1 hr or longer (It takes about 20 min to cool down the GC after bake out and start first sample)		
5	Ensure on-off valve (OV 7) of gas line to reactor is fully opened		
6	6.1 Ensure 4 sampling valves (SV1 – SV4) are closed 6.2 Ensure 2 sampling valves (SV5 & SV6) are opened for GC analysis 6.3 SV5 has to be opened all the time except when sampling outlet gas by impinge method		
7	Turn on the Ar gas welding grade cylinder (bottle 2)		
8	Check if the Ar gas regulator is set at 100 kPa		
9	Turn on "on-off valve" (OV 4) of the Ar gas		
10	Check if the Ar flow meter is set at level 8 (about 2.35 L/min)		
11	Check again the sampling valve (SV 5 & SV6) are opened (that are connected with the GC) and start data logging to: 11.1 test the GC (takes 20 min to cool down to start 1st sample) 11.2 measure N_2 and O_2 concentrations in the outlet gas to ensure that there are no N_2 and O_2 in the system 11.3 ensure no gas leakage out of the system before the reaction/experiment is started		
12	H_2 reduction process: - Ensure no N_2 and O_2 in the outlet gas - Turn on the H_2 gas cylinder and on-off valve (OV 1), where the regulator (100 kPa) is pre-set and adjust the flow meter to level 3 (about 1.35 L/min) (H_2 concentration in Ar is about 36.5%)		
13	Start logging samples by GC and set it runs automatically Use GC method "Jan_H2 reduction" 18 March 2013 12:44:07 p.m."		
14	Turn the furnace on after flowing H_2 gas for 15 min (5 GC samples) Check if the area count of H_2 is 365,000, then turn on furnace		
15	Check the ramping rate of 3 zone heating controller of the furnace If they are 10°C/min		
16	Set 3 temperature controllers of 3 zone heating elements to 810-820°C, and then set the temperature alarm at 840°C		
17	Monitor furnace temperature, catalytic bed temperature and pressure		
18	Monitor the H_2 concentration in the outlet gas by the GC to find out the H_2 consumption		
19	Maintain furnace temperature at 810-820°C overnight or until H_2 concentration of outlet equal to that of the inlet (area count of $H_2 \approx$ 365,000)		

Table B.4 Checklist for normal experimental operation (continued)

Procedures	**Date**		
20	After the catalyst reduction, close on-off valve (OV 1) and H_2 gas cylinder		
21	Close the on-off valve between the H_2 flow meter and manifold		
22	Swap between Ar welding grade and Ar instrument grade: 22.1 Turn on Ar instrument grade (bottle 1) and adjust pressure to 100 kPa 22.2 Close OV 4 and open OV 5 immediately 22.3 Adjust F 4 to level 11 22.4 Turn the Ar welding grade cylinder off (bottle 2)		
23	Reduce furnace temperature to 700°C and let the Ar instrument grade gas cool down reactor to 700°C until see H_2 area count at about 1,000 (take about 30-40 min) Use GC method "Jan_NH3_new" 20 March 2013 11:30:43 a.m."		
24	Start NH_3 decomposition reaction: Turn on the NH_3 gas cylinder and on-off valve (OV 3), where the regulator (40 kPa) and flow meter (level 5, about 0.015 L/min)		
25	Start logging samples by GC and set it runs automatically Use GC method "Jan_NH3_new" 20 March 2013 11:30:43 a.m."		
26	Check if reactor temperatures (T1 & T2) reach set point and steady		
27	Note the pressure drop at steady temperatures		
28	When the % NH_3 removal is steady $\rightarrow$ Measure NH_3 outlet gas		
29	Stop GC auto-sampling first Use GC to find out N_2 and H_2, and then go to step 30 immediately		
30	Use NH_3 ToxiRAE and Area RAE VOC to read NH_3 - Detect the outlet gas in air by putting the detector near the gas flowing into the fume hood (wear mask!!!) - Detect the outlet gas in Ar by setting up the detector with vent and 3-way valve and then go to step 31 immediately		
31	Use ISE method to sample the NH_3 (mostly 200 ml 1 bottle) + (a few of 200 ml + 200 ml in series) sampling no more than 6 min for 200 ml 1 bottle or 8-10 min if % NH_3 removal $\geq$ 90%		
32	Repeat step 29-31		
33	Start H_2S adsorption in NH_3+Ar gas: Turn on the H_2S gas cylinder and on-off valve (OV 2), where the regulator (40 kPa) and flow meter (level 6, about 0.017 L/min)		
34	Use GC to find out N_2 and H_2 and when the % NH_3 removal is steady (maybe about 20-30 min) then go to step 35 immediately		
35	Use NH_3 ToxiRAE and Area RAE VOC&EC to read NH_3 & H_2S - Detect the outlet gas in air by putting the detector near the gas flowing into the fume hood (wear mask!!!) - Detect the outlet gas in Ar by setting up the detector with vent and 3-way valve		
36	Use ISE method to sample the NH_3 (mostly 200 ml 1 bottle) + (a few of 200 ml + 100 ml in series)		

Table B.4 Checklist for normal experimental operation (continued)

Procedures	**Date**		
37	Use ISE method to sample the H_2S (mostly 200 ml 1 bottle) + (a few of 200 ml + 200 ml in series) sampling no more than 6 min for 200 ml 1 bottle or 8-10 min if $H_2 > N_2$ about 10%		
38	Repeat step 34-37		
39	Stop H_2S and close H_2S gas bottle (to see if the activity of the sand for NH_3 cracking resumes after H_2S exposure) NH_3 and Ar are still running into the reactor		
40	Use GC to find out N_2 and H_2 and when the % NH_3 removal is steady (maybe about 20-30 min) then go to step 41 immediately		
41	Use NH_3 ToxiRAE and Area RAE VOC to read NH_3 - Detect the outlet gas in air by putting the detector near the gas flowing into the fume hood (wear mask!!!) - Detect the outlet gas in Ar by setting up the detector with vent and 3-way valve and then go to step 31 immediately		
42	Use ISE method to sample the NH_3 (mostly 200 ml 1 bottle) + (a few of 200 ml + 100 ml in series)		
43	Repeat step 40-42		

Table B.5 Checklist for shut down

Procedures	**Date**		
1	Set the 3 heating zone controllers to 20°C and turn furnace OFF		
2	Turn NH_3 gas cylinders OFF		
3	Swap between Ar instrument grade and Ar welding grade: 3.1 Turn on Ar welding grade (bottle 2) and adjust pressure to 100 kPa and leave the Ar flows overnight 3.2 Close OV 5 and open OV 4 immediately 3.3 Adjust F 4 to level 2 (0.22 L/min) or 4 (0.84 L/min) or 4.5 (1 L/min) or 5 (1.2 L/min) 3.4 Turn the Ar instrument grade cylinder off (bottle 1)		
4	Turn the main power supply to the furnace off		
5	Leave GC ON and log samples every 20 min to find out if there is air in the system when flow Ar at low flow rate		
6	Leave 2 gas detectors for ambient ON		
7	Leave the extraction hood ON		
8	Leave the computer for temperature and pressure measurement ON		
9	Turn water bath off		
10	Cool down the GC (it takes about 1 hr) and turn off the GC		
11	Turn off all gas detectors for ambient		
12	To remove the catalyst in the reactor: - Check if T1 & T2 are at about room temperature - Remove the catalyst and keep it in the closed container filled with silica gel		

Appendix C. Instructions for quartz reactor cleaning

1. Wear proper protective equipment, i.e. nitrile gloves and a top layer of elbow length rubber gloves, lab coat and PVC apron on top, goggles, face shield, or acid protection half face respirator. A full face respirator is highly recommended to avoid contact of acid or vapour to facial skin, where it is not covered. When full face respirator is used, goggles, face shield, acid protection half face respirator are not required.
2. Clean the reactor in the fume hood.
3. Clamp the tube on two stands to hold the reactor tube about 30 degree on the x-axis in the fume hood.
4. Put a red Teflon cap rubber at the bottom end.
5. Mix some fresh aqua regia approximately 80 ml in total: 1 part volume of concentrated nitric acid (HNO_3) + 3 parts volume of concentrated hydrochloric acid (HCl). Always add the nitric acid to the hydrochloric acid slowly.
6. Pour acid into the reactor tube with care by using the funnel (the acids are corrosive).
7. Turn around the acid to soak the dirty part in the middle part of the reactor.
8. Apply the heat (60°C) evenly and gradually to the quartz distributor area with a heat gun. Move the reactor tube all around for even heating. Leave the heat gun on for 2 hours. It was found that with the heat applied at 60°C, the sand inside the quartz distributor came off.
9. The acids will turn red or brown as it cleaned the distributor and also any staining further up the tube.
10. Leave the aqua regia solution overnight. In the next day, pour the old aqua regia into the beaker filled with water for dilution and dispose via the drain in the fume hood, followed by flushing with large amounts of water.
11. Repeat step 5-10 for at least 8 times minimum.
12. Then, rinse acid out of the reactor tube with water sprayed in with a rubber hose.
13. Add hydrogen peroxide about 40 ml into the reactor by using the funnel, and then add very small amount of potassium hydroxide pellets into the hydrogen peroxide. Wait until reaction finished and then add more of potassium hydroxide pellets. Use very small amount of potassium hydroxide pellets each time. The reaction of hydrogen peroxide and potassium hydroxide is highly exothermic, so care must be taken.

14. Dispose the hydrogen peroxide and potassium hydroxide solution by pouring into the beaker filled with water for dilution and dispose via the drain in the fume hood, followed by flushing with large amounts of water.
15. Repeat step 13-14 for one more time.
16. It was found that the reaction of hydrogen peroxide and potassium hydroxide removes all the trace sand inside the quartz distributor.
17. Rinse solution out of the reactor tube with water sprayed in with a rubber hose. Rinse several times and let run down sink with plenty of hot water.
18. Rinse again with distilled or deionized water.
19. Dry the reactor with the tube furnace at about 200-300°C (the furnace temperature is higher than boiling point of all solutions used as shown in Table C.1).

Table C.1 Properties of chemicals used for reactor cleaning

No.	**Chemical**	**Assay (%)**	**Boiling Point (°C)**
1	Nitric acid	70%	119.9 (from bottle label)
2	Hydrochloric acid	37-38%	>100 (from MSDS Hydrochloric acid)
3	Hydrogen peroxide	34-35%	150 (from MSDS - Hydrogen peroxide solution - Chemwatch)
4	Potassium hydroxide	85% pellet form	1,320 (from MSDS - Potassium hydroxide)

Appendix D. Experimental checklist for sampling of NH_3 and H_2S in the producer gas from the DFB steam gasifier

Table D.1 Checklist for all experimental operations

Procedures	**Date**		
1	**Preparation before the experiment** 1.1 Remove the sampling line from the gasifier sampling port. 1.2 Dismantle 2 filter housings for cleaning without taking apart of the heating elements otherwise it may damage the heating elements. 1.3 Remove the quartz wool and quartz microfiber thimble. 1.4 Use hexane, iso-propanol (IPA) or Dichloromethane (DCM) to clean the inner surface of the 2 filter housings. 1.5 Fill the 1st filter housing (equipped with thermocouple T1) with quartz wool (5-15 μm) and the 2nd filter housing equipped with quartz microfiber thimble and quartz wool. 1.6 Ensure the stainless steel mesh is attached to the 1st filter housing 1.7 Assemble the filter housings and install with the gasifier sampling port.		
2	**Setting up the sampling system** 2.1 Connect the heating elements with the controller. 2.2 Connect thermocouples T1 – T4 with the data logging box and computer and start data logging (use Tracer DAQ software). 2.3 Set the controller for 1st heating element at 150°C and the 2nd heating element at 110°C. The controlled temperatures (T1 and T2) should be below the tar dew point and higher than the water dew point of the producer gas. 2.4 Turn on the water bath and set the controller at 1°C to control T4 at 4°C. 2.5 For NH_3 sampling, 3 washing bottles filled with 200 ml 0.05 M H_2SO_4 solution are used and the 4th washing bottle is empty. 2.6 For H_2S sampling, 3 washing bottles filled with 200 ml 0.05 M NaOH solution are used and 4th washing bottle is empty. 2.7 Absorbing solutions from 2.5 and 2.6 will be transferred for analysis by Ion Selective Electrode (ISE) method based on ASTM standard.		

Table D.1 Checklist for all experimental operations (continued)

Procedures	**Date**		
3	**Sampling of the procedure gas** 3.1 Set the float of ABB flow meter (Tube: FP-1/4-10-G-5 and Float: FP-CD-14 (Glass)) at level 7 (about 3 L/min) before sampling. 3.2 Set up the sampling train as shown in the picture. The PVC tubes are use to connect the washing bottles together. 3.3 To start sampling, open fully the glove valve in between the 2 filter housings. Then turn on the pump and start timing. For the wood gasification, minimum sampling time is 6 minutes. For higher NH_3 and H_2S concentrations, sampling time is 3 minutes. 3.4 To stop sampling, turn off the pump and then close fully the glove valve. 3.5 The NH_3 or sulphide samples in the solutions will be preserved according to ASTM standard as below. 3.6 T3 of gas outlet temperature and 4 main producer gas concentrations are used to calculate the actual producer gas flow rate from the ABB calculator software.		
4	**Shut down** 4.1 Turn off the controller of heating elements. 4.2 Stop the data logging and turn off the computer. 4.3 Turn off the water bath.		